Process Systems Engineering of Microgrid Energy Networks: Design, Scheduling, and Supervisory Control

A THESIS
SUBMITTED TO THE FACULTY OF THE GRADUATE SCHOOL
OF THE UNIVERSITY OF MINNESOTA
BY

Michael J. Zachar

IN PARTIAL FULFILLMENT OF THE REQUIREMENTS
FOR THE DEGREE OF
DOCTOR OF PHILOSOPHY

Advised by Prodromos Daoutidis

May, 2017

Acknowledgements

I would like to thank my adviser, Professor Prodromos Daoutidis, for giving me the opportunity to work on these exciting research projects, and for giving me the freedom to take the project in interesting directions. His advice and teaching over the years has helped me to grow as a researcher/scientist and honed my communication skills. I would also like to thank Professor Daniel Resasco at the University of Oklahoma with who I did my undergraduate research. Without his insistence, I never would have considered going to grad school.

A special thanks goes my Daoutidis group office-mates over the years: Dr. Milana Trifkovic, Dr. Ana Torres, Dr. Dimitris Georgis, Dr. Srinivas Rangarajan, Dr. Seongmin Heo, Dr. Alex Marvin, Dr. Adam Kelloway, Dr. Abdulla Malek, Dr. Nahla Al Amoodi, Udit Gupta, Mustafa Caglayan, Andrew Allman, Nitish Mittal, Manjiri Moharir, Matt Palys, and Wentao Tang. Their company has made the long hours in the office over the past 5 years enjoyable, and I will miss the coffee runs with Udit and Adam (though not the coffee itself). I've had the great pleasure and privilege to work with Milana, Andrew, and Matt on several collaborative projects. I would be remiss if I did not also thank the undergraduate students who worked with me on some small projects: Brooke Jaunich, Ryan Chan, and Rohan Pitre.

And last, I would like to thank my family and all of my friends in CEMS department who have been an important part of my life over the past 5 year. In particular, I would

like to thank my parents, Laura and Steve, for supporting my science and engineering education (especially back in high school when I joined the Texas Bioscience Institute program which ultimately lead to me pursuing chemical engineering). Most of all I would like to thank my wife Ami who shared this adventure with me. She was a constant source of love and support through both the good times and the bad.

To my wife, for sharing in my stress

Abstract

Proliferation of small, distributed power generation has the potential to reduce losses from electricity transportation, alleviate congestion, enable high efficiency cogeneration systems, and serve as a way to harvest inherently dispersed renewable feedstocks. Unfortunately, relative to traditional power plants, distributed generation tends to have high capital costs, and the power output of distributed renewable generation (i.e. based on wind and solar) is inherently stochastic and intermittent. Multiple distributed generation technologies can be combined into a single system (i.e. a microgrid) to take advantage of synergies and improve the overall performance. However, this introduces a challenging design problem with a wide variety of generation and storage technology alternatives to choose from. In addition, distributed generation systems must be designed and operated so there is no disruptive impact on the existing infrastructure. Nonetheless, distributed generation can be an important part of an overall strategy to improve the sustainability and efficiency of power supply.

This thesis addresses important practical problems related to the integration of distributed generation in the form of microgrid power systems using techniques from the Process Systems Engineering field. The problem of optimal microgrid design is investigated to (i) determine how public policy can drive microgrid adoption, (ii) quantify how geographic location and customer type impact microgrid efficacy and technology selection, and (iii) identify recurring motifs/trends in the technology selection and unit sizing. Then, the problem of optimal scheduling and supervisory control of a microgrid is considered to develop a framework for non-disruptive interaction with the existing electrical infrastructure. In particular, (i) a novel market structure for microgrids is formulated, (ii) a hierarchical supervisory control system is developed which utilizes stochastic optimization, and (iii) this control system is tested using a detailed, virtual microgrid simulation.

Optimal microgrid system design was addressed with the application of mathematical optimization, specifically mixed integer linear programming. The problem considered was designing a system which provides both power and heat. Technologies considered include renewable generation, fuel-based cogeneration, and storage. In addition,

the microgrid was assumed to be connected to the existing electrical infrastructure (i.e. power can be imported). This design problem was solved for a variety of policy scenarios, in different geographic locations, and for different types of customers (i.e. different load profiles). Important design parameters that were studied include the cost of energy supply, the integration of renewable power, the emissions associated with energy supply, and the optimal level of self-generation. The design results for different geographic locations and load profiles were then used to develop and train a heuristic procedure that can serve as a surrogate for detailed optimization. This heuristic procedure is used to clearly identify and quantify underlying trends in the results.

Optimal microgrid operation was addressed using a hierarchical control structure based on the Economic Model Predictive Control paradigm. The operational problem was divided into an hourly stochastic scheduling problem, and a more frequent deterministic unit dispatch problem. This supervisory controller is used to comply with a proposed novel market structure which explicitly limits uncertainty and variability in the energy exchange between the microgrid and the utility company. The formulation was initially developed for a power-only microgrid, but was then extended to a cogeneration microgrid which also regulates building temperature. The performance of the proposed control system was studied by implementing it on a detailed dynamic simulation in the Simulink software environment.

Contents

Acknowledgements **i**

Dedication **iii**

Abstract **iv**

List of Tables **xi**

List of Figures **xv**

1 Introduction **1**

1.1 The Energy Landscape 1

1.2 Distributed Generation 4

1.3 Thesis Scope and Organization 8

2 Policy Effects on Microgrid Economics, Technology Selection, and Environmental Impact **11**

2.1 Introduction 11

2.2 Model Formulation 14

2.2.1 Model Equations 15

2.2.2 Linearization of Capital Costs 16

2.2.3 Heat Load . . . 17
2.2.4 Microturbines . . . 19
2.2.5 PV Array . . . 20
2.2.6 Wind Turbine . . . 21
2.2.7 Boilers . . . 23
2.2.8 Battery Bank . . . 23
2.3 Policy Considerations . . . 24
2.4 Results and Discussion . . . 25
2.4.1 Reference Case . . . 25
2.4.2 Minimum Autonomy Scenario . . . 26
2.4.3 Emission Tax Scenario . . . 28
2.4.4 Economic Incentives Scenario . . . 30
2.4.5 Emissions Cap Scenario . . . 32
2.4.6 Minimum Renewables Scenario . . . 35
2.4.7 Capital Cost Uncertainty . . . 37
2.5 Conclusions . . . 39
2.6 Nomenclature . . . 41

3 Understanding and Predicting the Impact of Location and Load on Microgrid Design 44
3.1 Introduction . . . 44
3.2 Model Formulation . . . 47
3.2.1 Unit Modeling . . . 49
3.2.2 Energy Balances . . . 56
3.2.3 Locations and Load Shapes Considered . . . 56
3.3 Microgrid Design Optimization Results . . . 58
3.3.1 Reference Case . . . 58
3.3.2 Impacts of Location Selection . . . 59
3.3.3 Impacts of Load Shape . . . 65
3.4 ANN Method for Predicting Design Results . . . 71
3.4.1 Proposed Method . . . 71
3.4.2 Performance . . . 72

3.4.3 Predictions over Parameter Space . . . 76
3.4.4 Validation Case . . . 81
3.5 Conclusions . . . 86
3.6 Nomenclature . . . 88
3.7 Supporting Information . . . 92
3.7.1 Reference Case Values . . . 92
3.7.2 Additional Plots . . . 94

4 Microgrid/Macrogrid Energy Exchange: A Novel Market Structure and Stochastic Scheduling 97
4.1 Introduction . . . 97
4.2 Literature Review . . . 100
4.3 Proposed Market . . . 104
4.4 Model Formulation . . . 107
4.4.1 Macrogrid Exchange . . . 109
4.4.2 Microturbines . . . 111
4.4.3 Battery Bank . . . 112
4.4.4 Photovoltaic Power . . . 113
4.4.5 Power Balance . . . 113
4.4.6 Objective Function . . . 116
4.4.7 Scheduling Formulations . . . 117
4.5 Case Study . . . 118
4.5.1 Calculation of Realized Second Stage Variables . . . 119
4.6 Results and Discussion . . . 119
4.6.1 Power Exchange with the Macrogrid . . . 119
4.6.2 Operating Cost . . . 123
4.6.3 Utilization of Renewables . . . 124
4.6.4 Local Fuel Efficiency . . . 125
4.7 Conclusion . . . 125
4.8 Nomenclature . . . 127

5 Scheduling and Supervisory Control for Cost Effective Load Shaping of Microgrids with Flexible Demands 129
5.1 Introduction . . . 129
5.2 Model Formulation . . . 131
5.2.1 Market Structure . . . 133
5.2.2 Microturbines . . . 134
5.2.3 Photovoltaic Panel . . . 135
5.2.4 Battery . . . 136
5.2.5 Building Thermal Model . . . 137
5.2.6 Cooling System . . . 142
5.2.7 Incorporation of Uncertainty . . . 143
5.2.8 Optimization Formulations . . . 145
5.3 Dynamic System Model . . . 146
5.3.1 Other Considerations . . . 148
5.4 Case Study . . . 149
5.5 Results . . . 152
5.6 Conclusions . . . 158
5.7 Nomenclature . . . 160
5.8 Supporting Information . . . 166
5.8.1 Scheduling Layer Formulation . . . 166
5.8.2 Dispatch Layer Formulation . . . 171
5.8.3 Case Study Parameter Values . . . 174
5.8.4 Online Forecast Updates . . . 183

6 Energy Management and Load Shaping for Commercial Microgrids Coupled with Flexible Building Environmental Control 185
6.1 Introduction . . . 185
6.2 Model Formulation . . . 186
6.2.1 Market Structure . . . 187
6.2.2 Microturbines . . . 188
6.2.3 Photovoltaic Panel . . . 189
6.2.4 Battery . . . 189

6.2.5 Building Thermal Model . . . 190
6.2.6 HVAC System . . . 193
6.2.7 Energy Balances . . . 196
6.2.8 Objective Functions . . . 197
6.2.9 Dynamic System Model . . . 198
6.3 Case Study . . . 199
6.4 Results . . . 202
6.5 Conclusions . . . 211
6.6 Nomenclature . . . 213
6.7 Supporting Information . . . 221
6.7.1 Scheduling Layer Formulation . . . 221
6.7.2 Dispatch Layer Formulation . . . 227
6.7.3 Building Layouts . . . 230
6.7.4 Case Study Parameter Values . . . 231

7 Conclusion and Future Directions **238**
7.1 Conclusions . . . 238
7.2 Future Directions . . . 240
7.2.1 Operation of Non-Commercial Systems . . . 240
7.2.2 Development of Rich Simulation Testbed . . . 241
7.2.3 On-Line Model Identification . . . 241
7.2.4 Integration of Design and Non-Disruptive Operations . . . 242
7.2.5 Quantification of Operational Benefits to Utilities . . . 243
7.2.6 Applications to Utility Expansion Planning . . . 243

Bibliography **245**

A Glossary and Acronyms **259**
A.1 Glossary . . . 259
A.2 Acronyms . . . 260
A.3 Piecewise Linearization . . . 262

List of Tables

2.1 Objective function parameters 17
2.2 Parameters used to find optimal linear capital cost 18
2.3 Microturbine model parameters 21
2.4 Wind turbine model parameters 22
2.5 Computational statistics of the scenarios considered. CPU time reported is the mean for all runs in a scenario. In all cases, a 1% relative optimality gap is used. 25
2.6 Reference case optimization results 26
2.7 Nomenclature - Indices/Sets 41
2.8 Nomenclature - Parameters 41
2.9 Nomenclature - Binary Variables ($1 \implies$ True) 42
2.10 Nomenclature - Continuous Variables 43
3.1 Photovoltaic piecewise linearization 51
3.2 Microturbine parameter values 53
3.3 Wind turbine piecewise linearization 53
3.4 Boiler parameters 54
3.5 Battery parameters 55
3.6 Thermal storage parameters 56

3.7 Comparison of cities considered in the MILP optimization study. Cooling and heating degree days based on a 65 ^{o}F basis. Mean insolation given for a horizontal plane. Mean wind speed given for 10-m above ground level. 57
3.8 Comparison of energy demands in load shapes considered. Values shown are for Albuquerque, NM. 58
3.9 Optimal autonomy level for all cities considered (mean over all load shapes). 61
3.10 Size and performance of ANNs used in the prediction procedure. The values in parenthesis show the RMS error when predicted relative cost and renewables contribution are used rather than true values. 75
3.11 MILP design results for the validation case at minimum autonomy levels of 20%, 55%, and 90%. Continuous variables have been rounded to the nearest 5 kW or kWh. 84
3.12 Comparison of MILP, HOMER, and RETScreen results for Design 1. . . 85
3.13 Comparison of MILP, HOMER, and RETScreen results for Design 2. . . 85
3.14 Comparison of MILP, HOMER, and RETScreen results for Design 3. . . 85
3.15 Nomenclature - Sets/Indices 88
3.16 Nomenclature - Parameters 88
3.17 Nomenclature - Binary Variables ($1 \implies$ True) 90
3.18 Nomenclature - Integer Variables ($\in \{0, 1, 2, ...\}$) 90
3.19 Nomenclature - Continuous Variables 91
3.20 Net present cost of energy supply in million $ for the reference case for each location and load shape. 92
3.21 Expected annual CO_2 emissions in tons for the reference case for each location and load shape. 93
4.1 First- and Second-Stage Variables in the Scheduling Problem 108
4.2 Microturbine Model Parameters 118
4.3 Battery Model Parameters 119
4.4 Time-of-Use Pricing Scheme 119
4.5 Nomenclature - Sets/Indicies 127
4.6 Nomenclature - Parameters 127

4.7 Nomenclature - Binary Variables (1 $\implies$ True) 127
4.8 Nomenclature - Integer Variables ($\in$ {0, 1, 2, ...}) 128
4.9 Nomenclature - Continuous Variables 128
5.1 Case study market parameters 149
5.2 Time-of-Use Pricing Scheme 150
5.3 Terminal Storage Values 151
5.4 Constant Cost Values 151
5.5 Energy Exchange Results 154
5.6 Economic Results 155
5.7 Nomenclature - Sets/Indicies 160
5.8 Nomenclature - Parameters 160
5.9 Nomenclature - Binary Variables (1 $\implies$ True) 163
5.10 Nomenclature - Integer Variables ($\in$ {0, 1, 2, ...}) 163
5.11 Nomenclature - Continuous Variables 164
5.12 Scalar Case Study Values 175
6.1 Market Parameters 202
6.2 Unit sizing 202
6.3 Energy supply cost (relative to base case). 203
6.4 Cumulative commitment violations (kWh). The value in parenthesis shows this cumulative commitment violations scaled by the allowed elasticity to facilitate easier comparison among the load shapes. 204
6.5 Characteristic time scales for heat losses in each building in units of hours. 206
6.6 Mean load factor. The value in parenthesis shows the improvement relative to the base case. 211
6.7 Load variability in units of kW. The value in parenthesis shows the change relative to the base case. 211
6.8 Utilization of available solar power. 212
6.9 Nomenclature - Sets/Indicies 213
6.10 Nomenclature - Parameters 213
6.11 Nomenclature - Binary Variables (1 $\implies$ True) 217
6.12 Nomenclature - Integer Variables ($\in$ {0, 1, 2, ...}) 217
6.13 Nomenclature - Continuous Variables 217

6.14 Scalar Case Study Values 232
6.15 Time-of-Use Values 233
6.16 Load-Shape Dependent Values 237
A.1 Acronyms 260

List of Figures

1.1 Traditional electricity delivery system [3]. 2
1.2 A microgrid which utilizes a variety of distributed generation and storage technologies to satisfy local cooling, heating, and power demands. 7
1.3 Increased solar generation can lead to steep ramping needs and overgeneration risk [13]. 8
2.1 Energy flow diagram of the microgrid considered. 14
2.2 Hot water heating load scaled by the peak load. 18
2.3 Effective internal temperature used for calculating heat load. 19
2.4 Wind turbine power factor versus wind speed at hub height. 22
2.5 Relative cost and environmental impact of microgrid solutions in the minimum autonomy scenario. 27
2.6 Power production breakdown by source for the minimum autonomy scenario. The balance not shown is made up of power purchased from the macrogrid. Numerals indicate the number of microturbines installed in each regime. 28
2.7 Net present cost breakdown by source for the minimum autonomy scenario. 29
2.8 Overall cost and expected environmental impact of microgrid designs in the minimum autonomy and the emission tax scenarios. 30

2.9 Power supply breakdown of optimal microgrids without a tax (left) and with a \$30/ton CO_2 tax (right). The balance not shown is made up of power purchased from the macrogrid. 30
2.10 Net present cost (left) and annual emissions (right) in the economic incentives scenario. Values shown are relative to the reference case. 31
2.11 Power production breakdown in the economic incentives scenario. The balance not shown is made up of power purchased from the macrogrid. Numerals indicate the number of microturbines installed in each regime. 32
2.12 Relative net present cost of emissions reduction. 33
2.13 Power supply breakdown of optimal microgrids in independent (left) and economy-wide (right) emission reduction scenarios. The balance not shown is made up of power purchased from the macrogrid. 34
2.14 Heat supply breakdown of optimal microgrids in independent (left) and economy-wide (right) emission reduction scenarios. 34
2.15 Cost breakdown for the minimum renewables scenario (left) and environmental impact compared to minimum autonomy scenario (right). 36
2.16 Heat and power breakdown by technology in the minimum renewables scenario. The balance not shown on left is made up of power purchased from the macrogrid. 36
2.17 Comparison of cost vs. environmental impact in minimum renewables and independent emission cap scenarios. 37
3.1 Energy flow diagram of the microgrid system considered. Not all possible technologies will be included in every optimal design. 48
3.2 Relative cost vs. autonomy level for the hospital load in all cities considered. 60
3.3 Mean utilization of renewables for each city across all load shapes and minimum autonomy levels considered. 62
3.4 Power supply breakdown for a large office in Baltimore showing total microturbines installed capacity. 63
3.5 Relative emissions versus renewables usage across all optimization results. 64
3.6 Relative CO_2 emissions for a large office in Baltimore. 65

3.7 Comparison of relative emission levels (left) and dedicated natural gas heating (right) for the hospital load in Houston and Duluth. 66
3.8 Comparisson of the autonomy level at which the minimum emissions are observed versus the ratio of average heat demand to average power demand across all optimization results. 67
3.9 Relative cost versus autonomy level for all load shapes in Albuquerque, NM. 68
3.10 Mean utilization of renewables for each load shape. 69
3.11 (a) Mean utilization of renewables versus the ratio of heat to power demands in Miami and Atlanta, and (b) renewable utilization versus autonomy level for 3 load shapes in Atlanta. 69
3.12 Relative emissions versus autonomy level for all load shapes (mean over all cities for each minimum autonomy level). 70
3.13 Prediction process for relative cost, relative emissions, and renewables penetration in microgrid designs. 73
3.14 Parity plot of ANN output versus true optimization results for (a) optimal autonomy level, (b) relative cost, (c) renewables penetration, and (d) relative emissions. 74
3.15 Optimization results (symbols) and ANN prediction (lines) of autonomy level vs. relative cost for Albuquerque (left) and Fairbanks (right). . . 76
3.16 Surface plots showing predictions for relative cost. All values not shown on the X, Y axes are held at the nominal values for a hospital in Albuquerque, NM. 77
3.17 Surface plots showing predictions for renewables contribution. All values not shown on the X, Y axes are held at the nominal values for a hospital in Albuquerque, NM. 79
3.18 Ternary surface plots showing predictions for relative emissions. Axes show the contribution of different sources to total power production. All parameters not shown are held at nominal values for a hospital in Albuquerque, NM. 80
3.19 Comparison of the MILP results and heuristic procedure prediction for (a) relative cost and (b) renewables contribution in the validation case. . 81

3.20 Comparison of the MILP results and heuristic procedure prediction for relative emissions. Since there were significant errors in the prediction of renewables contribution, the results of the heuristic procedure using the interpolated MILP renewables contribution is shown as well. 82
3.21 Surface plots showing predictions for relative cost. All values not shown on the X, Y axes are held at the nominal values for a supermarket in Seattle, WA. 94
3.22 Contour plots showing predictions for renewables contribution. Values not shown on the axes are held at the nominal values for a supermarket in Seattle, WA. 95
3.23 Ternary surface plots showing predictions for relative emissions. Axes show the contribution of different sources to total power production. All parameters not shown are held at nominal values for a supermarket in Seattle, WA. 96
4.1 Energy flow diagram of the microgrid system considered. 108
4.2 Duration curves for aggregate (a) power demand and (b) PV power in the case study considered. Data obtained from Pecan Street Inc. Dataport. 117
4.3 Complimentary empirical cumulative distribution function of commitment violations when schedule adpatability is 30 kWh. 120
4.4 Complimentary empirical cumulative distribution function of commitment violations when schedule elasticity is 30 kWh. 121
4.5 Distribution of step sizes in energy exchange with the macrogrid for the unmodified load, load minus all available renewable power, chance-constrained scheduling results, and deterministic scheduling results. Load and PV data obtained from Pecan Street Inc. Dataport. 121
4.6 Annual peak load vs. market parameters. 122
4.7 Realized operating cost vs. schedule adaptability. 122
4.8 Curtailed PV power vs. schedule adaptability. 124
4.9 Local fuel efficiency for the chance-constrained scheduling approach. . . 125
5.1 System considered. 132
5.2 Overview of information flow in the proposed hierarchical control approach. 133

5.3 Sample building model. Internal building elements (e.g. internal walls, ceilings, etc.) are shown in light yellow, external building elements (i.e. external walls, roofs) are shown in blue, conditioned thermal zones are shown in white, and plenum spaces are shown in red. Black arrows indicate air flow for the ventillation system. 138
5.4 True and forecasted value for inflexible power demand. 150
5.5 True and forecasted value for outdoor air temperature. 151
5.6 True and forecasted value for global solar radiation on a horizontal plane. 152
5.7 Microgrid residual load in Case 1 with maximum and minimum bounds based on the day-ahead commitments. Time less than zero indicates the burn-in period. 153
5.8 Comparison of residual load in Case 1 and Case 4 over first 3 days. . . . 154
5.9 Battery state of charge in Case 1 and Case 4. Time less than zero indicates the burn-in period. 156
5.10 Average temperature in core zones and perimeter zones in Case 1. The shaded region indicates the target temperature range. Time less than zero indicates the burn-in period. 157
5.11 Zone average and total building average temperatures in Case 1. The shaded regions indicate times of On-Peak and Off-Peak pricing. Time less than zero indicates the burn-in period. 158
5.12 Frequency and magnitude of temperature violations. 159
6.1 Energy flow diagram of the microgrid system considered. 186
6.2 Illustrative thermal model example. 192
6.3 Power demand and heat generation profiles for each customer type. . . . 200
6.4 Solar radiation profiles and forecasts for each season. 201
6.5 Breakdown of cost factors in each scenario. Values are shown in terms of relative cost (i.e. scaled by the total cost in the base case). 203
6.6 Residual load profile for each load shape in the summer season. Maximum and minimum bounds result from the day-ahead commitments. 205
6.7 Temperature profiles for each load shape in the summer season. The comfort range varies by load shape due to the differences in occupancy patterns. 207

6.8 Residual load profile for the office building in each season. Maximum and minimum bounds result from the day-ahead commitments. 209
6.9 Temperature profiles for the office building in each season. 210
6.10 Office building layout. 230
6.11 Stand-alone retail building layout. 230
6.12 School building layout. 230
6.13 Hospital building layout. 231
A.1 Piecewise linear approximation for nonlinear function y=f(x) 262

CHAPTER 1

Introduction

The objective of this chapter is to provide a motivational background to the thesis. A brief summary of recent trends and future directions in the power infrastructure is presented, along with some basic terminology for power systems and microgrids. Special attention is paid to the integration of distributed power sources and to the microgrid paradigm. The merits and challenges of incorporating distributed generation in microgrids to address needs in the power system are identified. The challenges motivate the application of mathematical optimization techniques rooted in the Process Systems Engineering field to these microgrid energy systems. These Process Systems Engineering approaches allow one to systematically approach complex, interconnected systems with conflicting objectives, such as balancing economic and environmental objectives, which are intrinsic to such problems.

1.1 The Energy Landscape

Access to affordable and reliable electricity is a critical component to economic development and human health in the modern era [1, 2]. Electricity is ubiquitously used by

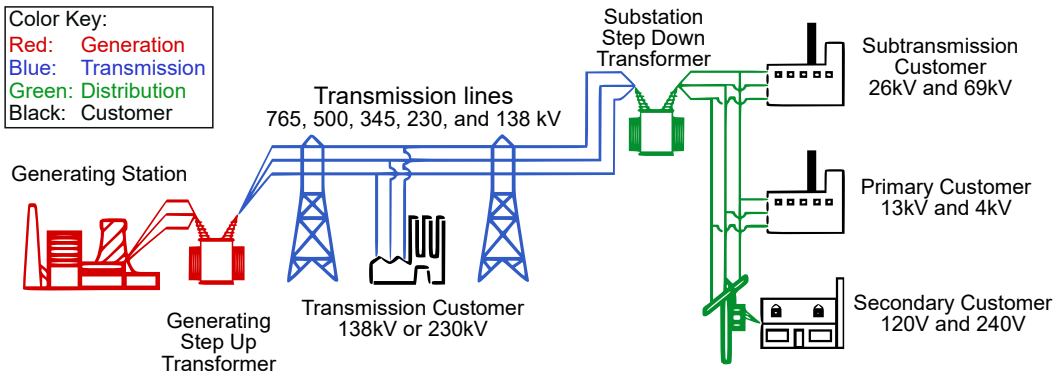

Figure 1.1: Traditional electricity delivery system [3].

residential, commercial, and industrial customers. In addition, many other vital infrastructures (e.g. water, communication, and emergency response) all depend on the power infrastructure to function. Traditionally, the electricity generation and supply has been characterized by a top-down paradigm wherein a few large, centralized power plants generate electricity which is then transmitted to consumers over a wide region. Within this paradigm, the vast majority of power consumers are passive participants. A small number of large industrial customers have participated in *demand response* programs in which they modify their power conumption level to support system-wide stability or economics. This large, interconnected system of power plants, transmission and distribution infrastructure, and consumers is termed *the macrogrid*. The basic architecture of this macrogrid infrastructure is shown in Figure 1.1.

However, the traditional macrogrid paradigm must be revisited in light of 21st century challenges and concerns. In particular, aging of existing infrastructure, rising global energy demand, and changes to traditional business models and demand patterns jeopardize our ability to ensure sufficient and sustainable power supply [3, 4]. Moreover, innovation is needed considering societal goals to increase fuel efficiency, decrease energy costs, reduce environmental impact of energy supply, and improve the resiliency of the electrical infrastructure (e.g. to extreme weather events and malicious attacks) [5, 6]. These myriad challenges can only be adequately addressed through transformational changes to the current energy supply infrastructure. No single approach is sufficient to tackle these complex, monumental challenges alone; rather a balanced combination of strategies focused on modernizing the macrogrid infrastructure, changing the role and

behavior of consumers, and deploying novel technologies will be required.

On the supply-side, grid modernization is enabled by evolution of the generation mix (i.e. the types of technologies used to generate power at the macrogrid-scale) and by investments in the electrical transmission and distribution infrastructure. Significant changes in the generation mix are driven primarily by economic factors such as the abundance of cheap natural gas in the U.S. (leading to a shift from coal to gas-fired power plants) and the decreasing cost of wind and solar power (due to the technology maturation). In the longer term, public policy constraints and current research and development (R&D) may enable the use of some novel technologies (e.g. power plants with carbon capture, next-generation nuclear power plants, or wave/tidal-based renewables), but these are expected to have relatively little impact over the next several decades [7]. Underinvestment in the transmission and distribution infrastructure can lead to increasing congestion and lower efficiency within the macrogrid [8]. However, many nations have made significant efforts to begin to renovate their transmission network in recent years, particularly as they consider increasing the penetration of renewables (i.e. wind and solar) which may need to be transmitted over long distances during periods of favorable weather [9, 10]. Improvements in transmission and distribution will reduce transport losses, alleviate congestion, and prevent stranded/spilled power.[1] These investments not only enable increased integration of renewables, but also improve the efficiency of the current fossil fuel-based infrastructure.

On the demand-side, changes in behavior and roles of consumers, emerging market paradigms, and technology advances help to support grid modernization. Continued progress in end-use efficiency (driven by public policy regulations and utility-sponsored programs) helps to reduce the environmental impact of electricity use, though this is largely offset by an overall increase in the total demand [7]. Recent advances in metering and communication technologies also enable consumers to move beyond the traditional passive role they have played in the power market. In particular, the ability for utility companies to send time-varying price signals and to measure consumption with a finer temporal granularity enables individual residential and commercial customers to participate in demand response activities. These demand response initiatives encourage end-users to leverage latent sources of flexibility/storage within their existing energy

[1] I.e. power which is wasted or unable to be used due to transportation bottlenecks

loads. By responding to dynamic market prices, end-users are able to decrease their own electricity costs, and the overall market becomes more efficient and less waste is incurred (e.g. by lowering peak demands when inefficient power plants would otherwise be utilized). Importantly, a higher level of demand response also facilitates renewable power integration, as customers are encouraged to shift loads to hours of high renewables availability when prices are lower. This trend towards closing the feedback loop between macrogrid operations and consumers is a key part of the *smart grid* paradigm, which seeks to use changes in business models and advances in communication, metering, and automation technologies to create a more efficient and reliable power infrastructure [11, 12].

A third strategy, and the topic of thesis, is to reexamine the traditional, centralized generation paradigm, and explore how distributed generation can be integrated into the power infrastructure to improve sustainability, efficiency, and resiliency.

1.2 Distributed Generation

Distributed generation (DG) refers to the production of electricity in close proximity to the end-use, and at a much smaller capacity than traditional power plants (i.e. distributed generation units typically have a capacity of ∼1-1000 kW as compared to utility-scale power plants which have an output of ∼100-1000 MW). A variety of technologies can be used for distributed generation, both renewable (e.g. wind turbines and solar photovoltaics) and non-renewable (e.g. diesel generators, gas-fired microturbines, and internal combustion engines). In addition, distributed energy storage technologies (e.g. batteries) can be incorporated into the power system to complement distributed generation or enable load leveling. These distributed generation and distributed storage process are referred to as *distributed energy resources* (DERs).

Non-renewable distributed generation relies on fuel feeds (typically fossil fuels like natural gas) for power generation. Fuel-fired generation offers several benefits:

- Waste heat can be recovered to provide low-grade thermal loads such as space heating and hot water supply.
- Power generation can be increased or decreased in response to electricity prices to enable economic savings.

- Power generation can be increased during periods of high demand to enables peak shaving (i.e. reducing the maximum power import).
- The DG unit can serve as a source of backup power for enhanced reliability.
- The DG unit can perform local power quality regulation[2].

However, distributed fuel-fired generation is not without its challenges. For one, when generating electricity only, DG units typically have a lower fuel efficiency as compared to traditional power plants. In addition, due to their small characteristic size, DG units face adverse economies of scale as compared to utility-scale power plants.

Renewable-based distributed generation generates power based on stochastic weather inputs. Since their available power is dependent on the weather, they cannot fill the same role as fuel-fired DG (e.g. changing output in response to electricity prices). However, renewable-based generation offers several benefits:

- The feedstocks have no cost (e.g. wind and solar are freely available).
- Power is generated without any operating emissions.
- Power can be generated at remote locations without any need for fuel supply infrastructure.

Obviously, the inherent stochasticity in renewable availability is a significant challenge. In addition, the capital cost of renewable DG units is higher than traditional fuel-fired generation.

In addition, some benefits are common to all types of distributed generation:

- Short project lead times allow DG to be deployed to quickly meet needs.
- Power generation close to the end-user alleviates congestion and avoids losses associated with transmission and distribution.
- Distributed generation enables self-determination in power supply (i.e. individual users can select what types of technologies/feedstocks they invest in).

[2] e.g. minimizing deviations from the nominal voltage

A particular paradigm in the area of distributed generation is the *microgrid*, which is a system consisting of multiple distributed generation units, energy storage units, and/or flexible loads whose net generation/consumption is aggregated. These systems may be grid-tied wherein they interact with the larger power system (i.e. the macrogrid) by importing and exporting power, or they may exist as stand-alone systems with no external power connections. By integrating multiple devices into a single system, one can exploit synergies between availability of different renewable feedstocks, coordinate scheduling to ensure efficient fuel consumption, and utilize controllable assets to balance out inherent renewable intermittancy. In addition, microgrids can provide enhanced reliability to local consumers by using distributed generation and storage units to continue partial power supply during macrogrid outages (i.e. blackouts). Microgrids with flexible loads offer a natural case where integrated supply-and-demand planning can be used to achieve improved fuel-efficiency and utilization of renewables. Figure 1.2 showcases a microgrid system which employs a variety of potential distributed generation and storage technologies.

There are several critical challenges associated with integration of distributed generation into the power system which must be addressed. Microgrid system design is a complex task due to the wide variety of technologies to choose from and desire to enable effective operational synergies. This challenge is exacerbated by the uncertainty in future public policy which may impact such systems. Moreover, the high upfront cost of distributed generation units (particularly renewables like wind and solar) makes poor investments particularly punitive. Distributed generation may also have a disruptive impact on operations of the surrounding macrogrid. Currently, in the scheduling and operation of the macrogrid, distributed generation is treated like a stochastic, negative "demand". Thus, distributed generation increases the uncertainty in power demand, making it harder for utility companies to effectively schedule and dispatch power plants. In addition, a significant increase in distributed renewable power can have an adverse effect on the net power consumption profile (referred to as the load shape). For example, deep penetration of solar power can lead to the load shape in Figure 1.3. Such demand profiles are difficult for utility companies to supply due to constraints on the flexibility and agility of large power plants. These challenges must be addressed before microgrids can become a prolific alternative to centralized power generation and not one limited

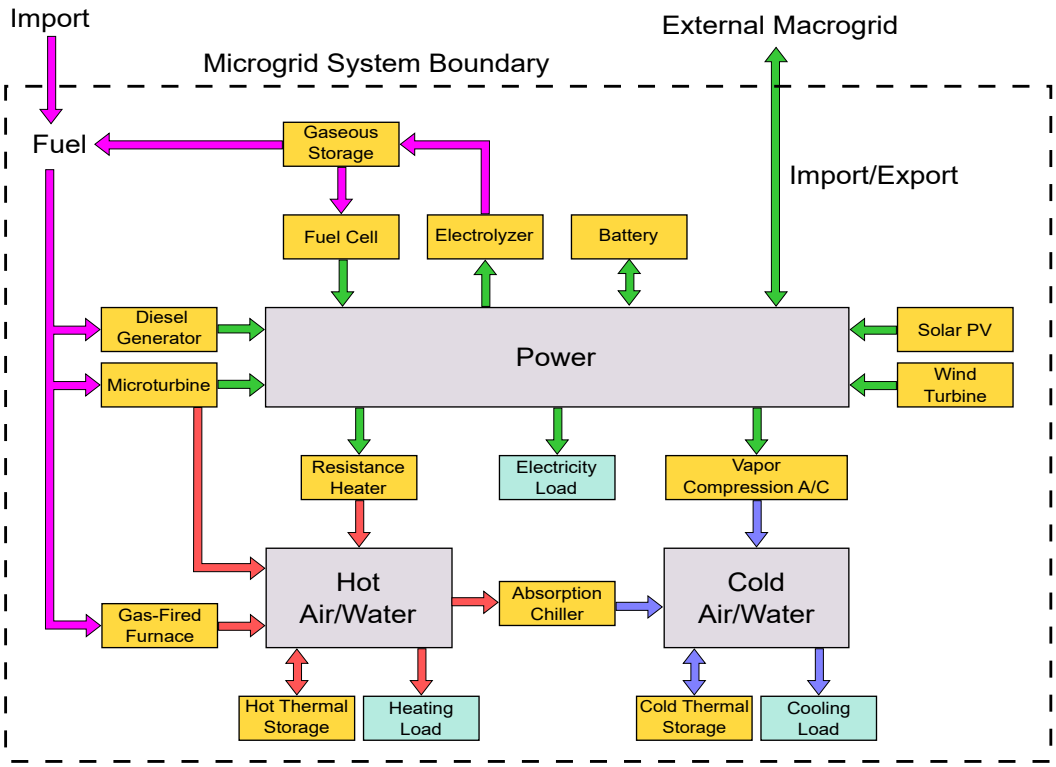

Figure 1.2: A microgrid which utilizes a variety of distributed generation and storage technologies to satisfy local cooling, heating, and power demands.

to niche customers or early adopters.

Now is an opportune time to address these challenges as distributed generation is still a small fraction of total capacity, but it is growing swiftly. Widespread adoption of ineffective or impractical system designs could lead to higher electricity costs or the need for expensive retrofits given the long lifespan and high investment costs of distributed energy resources. Inefficient systems would also lead to significantly increased environmental impacts (e.g. due to significant spillage or curtailment of available renewable power). Finally, issues related to integration of distributed power into the macrogrid should be addressed before DG reaches a penetration which could be disruptive to macrogrid stability or market operations.

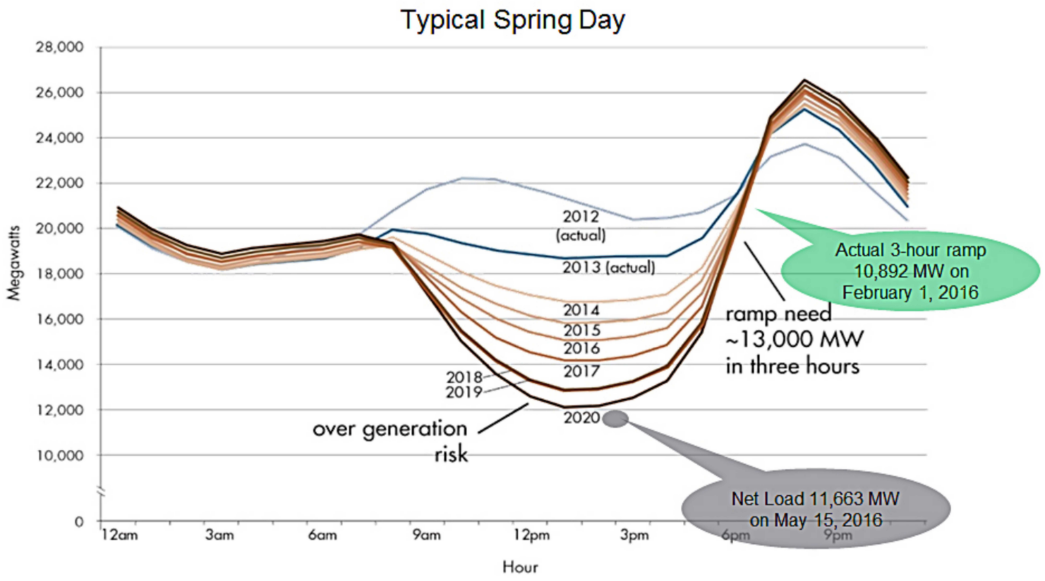

Figure 1.3: Increased solar generation can lead to steep ramping needs and overgeneration risk [13].

1.3 Thesis Scope and Organization

The unifying theme of the research presented in this thesis is the application of optimization techniques from the field of process systems engineering to address challenges related to the adoption of microgrids. Two broad topics are addressed: the optimal microgrid system design/technology selection, and the optimal scheduling/supervisory control of a microgrid system. In the design research, optimization is used to systematically study the impact of public policy, geographic location, and customer type on microgrid design trends. In the scheduling and operation research, a novel market structure for grid-tied microgrids is proposed which minimizes potentially disruptive interactions with the macrogrid, and a hierarchical scheduling/control framework is developed for effective economic operation and load shaping of microgrid.

Chapters 2 and 3 focus on the optimization of microgrid design (i.e. technology selection and unit sizing). Chapter 2 is reprinted with permission from [14] with an expanded background section on microgrid design optimization. This chapter studies the impact of public policy decisions on optimal microgrid design. Candidate technologies for selection in the microgrid design include both renewables (i.e. solar photovoltaics and

small wind turbines) and non-renewable technologies (e.g. gas-fueled microturbines and batteries). The microgrid considered supplies both some portion of the power demand and the low grade heat for space heating and hot water supply. Particular attention is paid to how policy decisions can change the optimal generation mix of a microgrid, and what kind of policy landscape is necessary to encourage microgrid proliferation and renewables integration.

Chapter 3 is reprinted with permission from [15]; the introduction is modified to highlight the differences and expansions from Chapter 2, and the model formulation section is modified to incorporate details originally included in the appendix and to minimize repetition of details described in Chapter 2. This chapter studies the impact of geographic location and load shape on optimal microgrid design. The model from Chapter 2 is extended to consider thermal storage and multiple types of microturbines. The microgrid design problem is solved for 16 different geographic locations and 6 distinct load shapes. The results are analyzed to identify important underlying trends in microgrid design and recurring motifs. Finally, a predictive procedure is proposed to estimate some basic microgrid design metrics using only a parsimonious set of inputs.

Chapters 4, 5, and 6 focus on the optimal scheduling and control of microgrids with a high penetration of stochastic renewable power. In particular, the objective is to not only minimize energy supply costs, but also to ensure non-disruptive interactions with the external macrogrid. Chapter 4 is reprinted with permission from [16] with an expanded background. This chapter includes a proposed novel market structure that explicitly limits the uncertainty and variability in energy exchange between a microgrid system and the surrounding macrogrid. A stochastic scheduling approach is formulated for operation of a microgrid in this environment. A 1-year case study demonstrates that the proposed market structure can be used to significantly reduce the burden imposed on utility companies by distributed renewables, and showcases the value of utilizing a stochastic optimization formulation for scheduling.

Chapter 5 expands the system considered in Chapter 4 to also include flexible loads (i.e. a controllable air conditioning system and the associated thermal dynamics of a building). Furthermore, a hierarchical control structure is formulated which encompasses not only the hourly scheduling of such a system, but also more frequent recourse optimization and methods to ensure effective coordination between the decision making

at different time scales. This hierarchical control approach is implemented into a dynamic Simulink simulation over a 1-week case study. The results show that leveraging flexible loads is a practical way to achieve the load shaping required under the proposed market structure at little opportunity cost.

Chapter 6 focuses on exploring how the proposed approach works across a wider case study. In particular, the formulation in Chapter 5 is extended to consider a more generic building model and flexible space heating dynamics in addition to flexible cooling. A case study shows that load shaping can be achieved across a broad range of commercial load shapes and in seasons throughout the year without any impact on end-user comfort. Importantly, this demonstrates the ubiquity of mollifying distributed renewables via microgrids with flexible thermal loads, and highlights potential challenges that might lead to higher costs.

As a note, some notation in the reprinted papers has been altered to improve consistency throughout the thesis. A nomenclature section is included at the end of each chapter for the reader's convenience.

CHAPTER 2

Policy Effects on Microgrid Economics, Technology Selection, and Environmental Impact*

2.1 Introduction

Today's power supply infrastructure is rapidly evolving in response to aging infrastructure, changing feedstock and technology costs, and environmental concerns. A variety of technologies and operational strategies have been proposed to modernize the power grid while maintaining a low electricity selling price and high reliability. A renewed interest in distributed generation has stemmed from this desire for more robust and environmentally friendly power supply [17, 18]. Distributed fuel-fired units can be sited closer to consumers than traditional power plants to reduce transmission losses, reduce congestion during peak hours, and so that waste heat can be recovered to meet local heating demand [18]. Finally, distributed renewables can be used to harvest inherently dispersed wind and solar feedstocks to provide power with little operating cost or emissions. In the area of distributed generation, microgrids are particularly interesting as they offer peripheral benefits that can further reduce environmental impact or increase

*Reprinted (adapted) with permission from Michael Zachar, Milana Trifkovic, and Prodromos Daoutids, *Computers and Chemical Engineering*, 81:364-375, 2015 [14]. Copyright

end-user satisfaction.

A microgrid is an autonomous or semi-autonomous energy system containing distributed power generation units and loads [19]. The aggregation of multiple DERs helps to better match local supply with demand by exploiting synergies in different renewable technologies (i.e. the availability of wind and solar are relatively decoupled), using storage devices to shift excess renewable output, and operating dispatchable generators to complement intermittent DERs [20, 21]. By locally complementing renewables, the microgrid architecture insulates the macrogrid from the negative effects of intermittent renewable power production. Microgrids also allow for effective harvesting of waste heat from thermal units due it close proximity to the ultimate load [18]. These systems may also be desirable for their ability to continue power supply during macrogrid blackouts or brownouts in a process known as "islanding" [22]. Thus, microgrids can be used to achieve a level of uptime and power quality that may not be available from the macrogrid. Lastly, microgrids give consumers the freedom to choose their energy supply technologies, fuel sources, and environmental impact.

Proper sizing of units in these microgrids is important as the upfront cost of DERs can be quite significant. This is especially true in the case of renewables technologies, where the capital costs are the vast majority of the total cost. In addition, due to the non-dispatchable nature of wind and solar, improper sizing of units may limit operational flexibility, leading to a higher dependence on the macrogrid as an energy buffer and negating some of the potential microgrid benefits. Optimal system design (i.e. in terms of technology selection and unit sizing) is a problem that must be addressed in order to encourage adoption of microgrids.

There have been some previous papers that have considered the optimal design of microgrid power systems [23–28]. Some early work in this area focused on the modeling and design of fuel-fired cogeneration systems for improved overall energy efficiency and reduced environmental impact (e.g. [29]). Other early works focused on the design of stand-alone renewable energy systems for power supply in locations without convenient grid access [30–32]. As the economics of renewables have continued to improve, analysis of the design for hybrid systems including fuel-fired units and renewable technologies has been carried out using approaches including mixed integer linear programming [33, 34], metaheuristic algorithms [25, 35, 36], enumerative models like NREL's HOMER [23, 37],

and stochastic programming [38]. Recent work has focused on integrating uncertainty into microgrid design [39], utilizing measured data for demand and renewables output rather than representative models [40], and providing experimental feedback of actual operational performance of DERs to improve modeling and assumptions at the design level [41].

In this chapter, we focus on the interplay between public policy and microgrid design. Public policy can play an important role in the design and technology selection for energy systems. Government programs (e.g. the U.S. Business Investment Tax Credit [42]) have been instrumental in driving the early adoption of wind and solar. However, future public policy is quite uncertain and volatile, especially as countries strive to meet increasingly stringent environmental goals. In particular, current concerns about greenhouse gas (GHG) emissions associated with power supply and their potential role in anthropogenic climate change play an important role in shaping energy policy. Many countries have made pledges to reduce GHG emissions in order to limit the potential increase in global average temperature. Nonetheless, projections show that the emission levels in 2020 will exceed target levels by 18-37% in the business-as-usual scenario and by 7-16% if countries meet their highest ambition pledges established in the Copenhagen Accord [43]. Thus, it is likely that energy policy will undergo further refinement and changes in the future in response to evolving environmental goals, ongoing successes or failures, and technology development. It is important to consider how these potential policy changes will impact microgrid adoption, both to ensure sound investments are made by end-users and to identify how policy decisions can effectively evoke the intended responses in the energy landscape.

Yet, relatively few studies have examined ways in which public policy changes may impact factors in the optimal microgrid design such as technology selection, economics, and environmental impact [26–28]. Even in these cases, only a single particular policy of interest was examined. Due to differences in model formulation, assumptions, and input data between authors, general comparisons about the differences under various policy scenarios are difficult or impossible to draw. In order to achieve widespread adoption, investors will need to be assured that their microgrid design will not become obsolete or hugely more expensive to operate part way through its lifetime due to public policy changes. Thus, it is necessary to compare the impacts of likely public policy constraints

to identify promising designs and robust cost estimates.

In this chapter, several leading candidate policies proposed for transformational change in power supply (emission taxation, investment tax credits, and emission caps) are analyzed. In addition, these results are compared to the results from increasing autonomy, reducing emissions, and increasing renewable power production via a microgrid without public policy constraints.

2.2 Model Formulation

In order to explore the impact of policy constraints on microgrid economic potential, environmental performance, and technology selection, a case study was carried out using weather and load data from Sarnia, ON. The total annual electric load was 3.65 GWh (average load of 417 kW). The energy supply problem considered includes both heat and power supply.

A mixed integer linear program (MILP) is formulated to find the optimal unit sizes and hourly set points over a one year period in order to minimize the net present value of energy supply costs over the microgrid lifespan (20 years). The objective function and constraints of this program are modified to represent the various policy scenarios considered.

Local units must supply all of the heat demand of the system. Electrical demand may either be satisfied through local units or through power purchased from the macrogrid. Technologies included in this optimization include microturbines, photovoltaics, wind

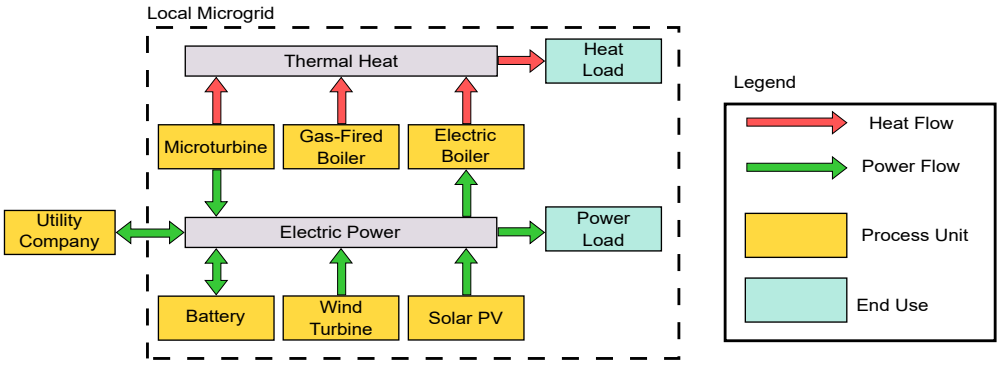

Figure 2.1: Energy flow diagram of the microgrid considered.

turbines, lead-acid batteries, electric boilers, and gas-fired boilers. The largest possible energy flow diagram of the microgrid is shown in Fig. 2.1, but most solutions will not employ all possible technologies. Key optimization design variables are the number of microturbines to include, the capacity of the battery, and the rated outputs of the PV array, wind turbine, and boilers. The assumptions and modeling for each individual unit type are described in more detail in the following sections.

2.2.1 Model Equations

The objective function, the net present value of energy supply costs (NPC), can be described as the sum of capital and operating expenditures:

$$NPC = Capex + Opex \tag{2.1}$$

where:

$$\begin{aligned} Capex = &\sum_m I_m \kappa_m \theta_m + P_{w,rated} \kappa_w \theta_w + P_{s,rated} \kappa_s \theta_s \\ &+ Q_{e,rated} \kappa_e \theta_e + Q_{n,rated} \kappa_n \theta_n + E_{b,max} \kappa_b \theta_b \end{aligned} \tag{2.2}$$

$$\begin{aligned} Opex = &P_{s,rated} \zeta_s \phi_s + \sum_k \Bigg[\sum_m \big(P_m(k) \zeta_m + y_m(k) \zeta_{start} \big) \phi_m \\ &+ P_w(k) \zeta_w \phi_w + Q_n(k) \zeta_n \phi_n + Q_e(k) \zeta_e \phi_e + P_d(k) \zeta_b \phi_b \\ &+ \Bigg(\sum_m F_m(k) + F_n(k) \Bigg) \zeta_{gas} \phi_{gas} + P_{grid}(k) \zeta_{grid} \phi_{grid} \Bigg] \end{aligned} \tag{2.3}$$

where $Capex$ is the sum of initial capital and replacement costs for each unit, and $Opex$ is the sum of annual maintenance costs for each unit, the cost of purchased fuel, and the cost of power purchased from the utility company. A comprehensive nomenclature for this chapter is included in Section 2.6. Note that although export of power to the macrogrid is allowed, no positive economic value is assigned to it to limit the impact of distributed generation on macrogrid control and stability.

At each hour over the design year the heat and power loads must be satisfied. These

give rise to the following constraints:

$$\sum_m P_m(k) + P_s(k) + P_w(k) + P_d(k) + P_{grid}(k) = P_\ell(k) + P_c(k) + P_e(k) + P_{spill}(k) \quad (2.4)$$

$$\sum_m Q_m(k) + Q_e(k) + Q_n(k) = Q_\ell(k) + Q_{spill}(k) \quad (2.5)$$

The non-negative dump load P_{spill} is the power exported to the macrogrid at no economic gain. Similarly, Q_{spill} is a non-negative heat dump load which represents excess heat that is rejected to the environment.

A constant annual tariff is used for both power purchased from the macrogrid and natural gas consumed. The costs for electricity and natural gas in the first year are \$0.108/kWh and \$8.4/1000 cu. ft. (\$0.30/m^3), respectively. These prices and maintenance costs are expected to rise at the rate of inflation, taken to be 2.5% per annum. A discount rate of 8.3% is used for calculating the present value of costs after the first year.

2.2.2 Linearization of Capital Costs

Table 2.1 shows the capital cost and maintenance cost values used for each unit in the objective function. Capital costs are assumed to be linearly related to the sizing variable to improve computational tractability of the optimization problem. In reality, the capital cost of many industrial units can be described by a power law relationship:

$$\frac{\delta}{\delta_{ref}} = \left(\frac{\chi}{\chi_{ref}}\right)^\alpha \quad (2.6)$$

where δ is the capital cost, χ is some generalized unit size/capacity, and α is a scaling coefficient typically less than 1.

In order to select a fair linear capital cost coefficient, the square error between the power law cost and linear cost prediction is minimized over some size range of interest ($\chi \in [\chi_L, \chi_U]$):

$$\text{minimize}_\kappa \int_{\chi_L}^{\chi_U} \left(\delta_{ref}\left(\frac{\chi}{\chi_{ref}}\right)^\alpha - \kappa\chi\right)^2 d\chi \quad (2.7)$$

where κ is the linear capital cost coefficient of interest. The solution to this problem

Table 2.1: Objective function parameters

Unit Type	Capital Cost	Maintenance Cost	Lifetime
Microturbines	\$594,000/turbine (\$3,600/rated kW)	\$0.02/kWh + \$10/startup	20 years
PV	\$5,000/rated kW	\$52/rated kW	20 years
Wind Turbine	\$3,400/rated kW	\$0.008/kWh	20 years
Electric Boiler	\$60/rated kW	\$0.0075/kWh	16 years
Gas-Fired Boiler	\$60/rated kW	\$0.0075/kWh	16 years
Battery Bank	\$132/kWh capacity	\$0.00143/kWh	5 years

can easily be shown to be:

$$\kappa = \frac{3\delta_{ref}}{\chi_{ref}^{\alpha}(2+\alpha)} \frac{\chi_U^{2+\alpha} - \chi_L^{2+\alpha}}{\chi_U^3 - \chi_L^3} \tag{2.8}$$

Table 2.2 shows the reference size, reference cost, scaling coefficient, and size range used to obtain these linear capital costs for each unit considered. The scaling coefficient is very close to 1 for batteries and PV due to their modular nature. Linearization is not performed for the microturbines because they are installed as individual units with a fixed capacity and cost.

There is significant uncertainty in the cost of distributed renewable units due to the quantity of available data, continuing technological advancement, site-specific installation costs, and a wide variety of reported costs for units of a similar capacity. For example, the installed cost of small (<100 kW) distributed wind towers has been reported to vary from 5,000-10,000 \$/kW [44]. The range of reported costs tends to narrow as the capacity increases, but site-specific factors like permitting and foundation costs can still vary significantly. The other units are more established technologies, but advancements in alternative technologies, e.g. lithium-based batteries, could provide a disruptive force in the marketplace. The potential impact of these uncertainties and assumptions is revisited in the discussion for this chapter.

2.2.3 Heat Load

Historical hourly heat load corresponding to the weather and power load dataset was not available, so it is instead synthetically generated. The microgrid's total heat demand

Table 2.2: Parameters used to find optimal linear capital cost

Unit Type	Reference Size	Reference Cost	Scaling Coefficient	Size Range
PV	300 kW	$1,620,000	0.94	0-2000 kW
Wind Turbine	300 kW	$1,380,000	0.80	0-2000 kW
Electric Boiler	180 kW	$21,600	0.60	0-1500 kW
Gas-Fired Boiler	180 kW	$21,600	0.60	0-1500 kW
Battery Bank	150 kWh	$45,000	0.95	0-5000 kWh

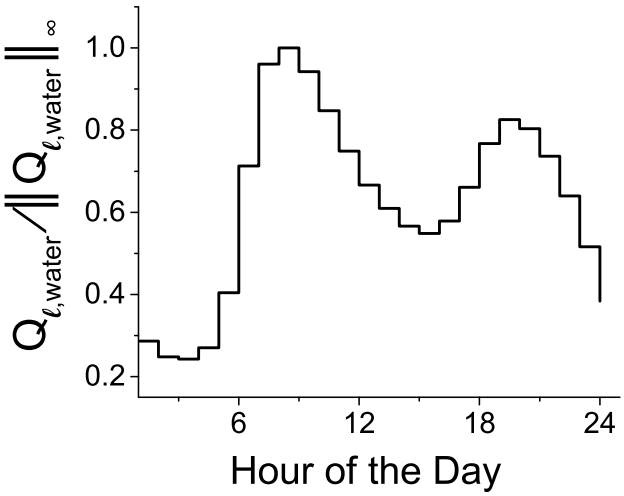

Figure 2.2: Hot water heating load scaled by the peak load.

is assumed to be the sum of space heating and hot water heating demands. Hot water heating load, $Q_{\ell,water}$, is assumed to be independent of the weather and season. The daily pattern of $Q_{\ell,water}$ is shown in Fig. 2.2. The values in this figure are scaled by the peak hot water heating load, i.e. $||Q_{\ell,water}||_\infty$.

The space heating load, $Q_{\ell,space}$, was assumed to be directly proportional to the temperature difference between building interiors and the outside air:

$$\Delta T(k) = T_{interior}(k) - T_{ambient}(k) \tag{2.9}$$

$$Q_{\ell,space}(k) = max(0, k\Delta T(k)) \tag{2.10}$$

where k is a constant proportionality constant.

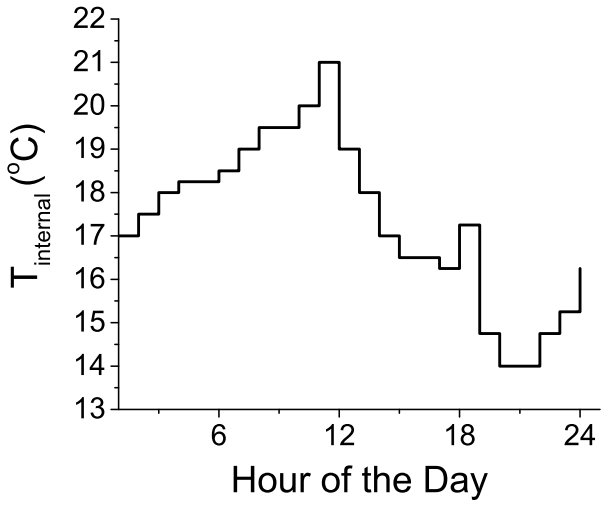

Figure 2.3: Effective internal temperature used for calculating heat load.

Instead of assuming a constant value for $T_{interior}$, a value dependent on the time of day is used to account for effects such as hourly variance in internal heat generation and occupancy. This effective $T_{interior}$ is shown in Fig. 2.3.

These heat loads are scaled so that hot water heating and space heating account for 15% and 34% of total energy annual demand, respectively. This results in a proportionality constant, k, of 32.6 kW/^{o}C, and a peak hot water heating load of 195 kW.

2.2.4 Microturbines

Microturbines were selected as a source of dispatchable generation due to their low number of moving parts (less maintenance burden on the operators), their ability to cogenerate heat and power for high fuel efficiency, and their flexibility with respect to fuel [18].

Due to decreasing efficiency at low set points, microturbines were constrained to operate above 50% rated power when on:

$$0.5x_m(k)P_{m,rated} \leq P_m(k) \leq x_m(k)P_{m,rated} \tag{2.11}$$

where x_m is a binary on/off state.

The electrical efficiency and heat recovery ratio are assumed to be constant in this range for computational simplicity. Thus, the useful heat generated and fuel consumption are directly proportional to power output:

$$Q_m(k) = P_m(k)\lambda_m \tag{2.12}$$

$$F_m(k) = P_m(k)/\eta_m \tag{2.13}$$

This fixed electrical efficiency was chosen to minimize the square error between η_m and the true efficiency given by a typical partial load curve with a maximum efficiency of 28.5% [45]. The heat-to-power ratio, λ_m, has been shown to be almost constant over the operational range considered [46].

Obviously, microturbines can only be turned on if they are installed. In addition, startup events are tracked since a startup cost is added to the annual maintenance cost of microturbines to account for fuel usage and additional unit wear that occurs during these events. These constraints can be described by:

$$x_m(k) \leq I_m \tag{2.14}$$

$$y_m(k) \geq x_m(k) - x_m(k-1) \tag{2.15}$$

where I_m is a binary variable equal to 1 only if the microturbine is installed, and y_m is a binary variable equal to 1 in time periods when the microturbine is started.

Due to commercial availability in only a limited number of fixed capacities, the number of microturbines installed in the system was a variable in the optimization rather than the rated power. Relevant technical parameters assumed for the microturbines are summarized in Table 2.3. Note that all microturbines were considered to be identical.

2.2.5 PV Array

A single PV array is used to harvest solar energy. A maximum power point tracker is assumed to keep the array operating at optimal voltage and current. Thus, the power

Table 2.3: Microturbine model parameters

Parameter	**Value**
$P_{m,rated}$ (kW)	165
λ_m	1.5
η_m	0.27

production of the PV array is directly proportional to the incident solar radiation:

$$P_s(k) = P_{s,rated}\frac{H(k)}{H_{rated}} \tag{2.16}$$

The rated power of the array refers to the power output at 1000 W/m^2 and 25^{o}C. Temperature dependence of panel efficiency has been neglected.

2.2.6 Wind Turbine

A single variable speed wind turbine is used to harvest available wind energy. Between the wind turbine's cut-in and rated speed, the power output is a cubic function of wind speed. Between the rated speed and cut-out speed, the power output is equal to the rated power. Below the cut-in speed and above the cut-out speed there is no power production due to insufficient wind energy and to prevent turbine damage, respectively. Since the input wind speed is known *a priori*, this dependence on wind speed can be converted into a fractional availability of the rated power, f_w. The wind power power output is therefore a linear equation:

$$P_w(k) = f_w(k)P_{w,rated} \tag{2.17}$$

where f_w is calculated before the optimization using simple if-statements:

$$f_w(k) = \begin{cases} 0, & v(k) < v_{ci} \text{ or } v(k) > v_{co} \\ \frac{v(k)^3 - v_{ci}^3}{v_r^3 - v_{ci}^3}, & v_{ci} \leq v(k) \leq v_r \\ 1, & v_r < v(k) \leq v_{co} \end{cases} \tag{2.18}$$

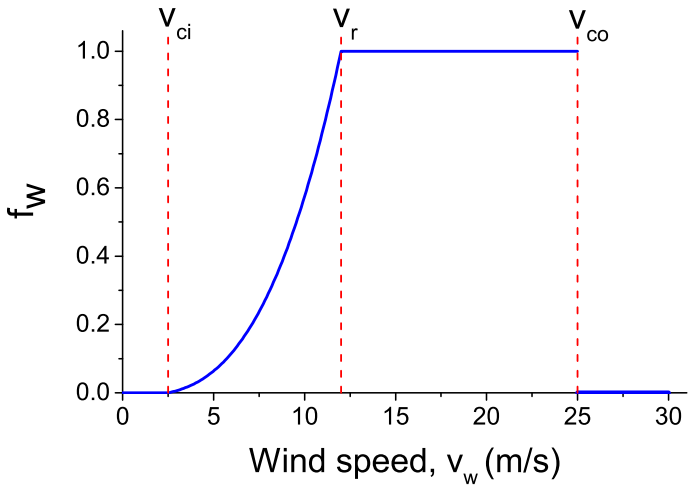

Figure 2.4: Wind turbine power factor versus wind speed at hub height.

Table 2.4: Wind turbine model parameters

Parameter	**Value**	**Parameter**	**Value**
h (m)	30	v_{ci} (m/s)	3
v_r (m/s)	12	v_{co} (m/s)	25

This fractional availability curve is shown graphically in Figure 2.4

Wind speed data collected at 10-m was extrapolated to turbine hub height using a power law relationship with a scaling coefficient of 1/7 based on recommended values for flat, open areas [47]:

$$v(k) = v_{ref}(k)\left(\frac{h}{h_{ref}}\right)^{1/7} \tag{2.19}$$

Model parameters for the wind turbine are summarized in Table 2.4.

2.2.7 Boilers

The electric and fuel-fired boilers are modeled as simple energy conversion units that provide heat to satisfy thermal loads. In general, the energy efficiency of boilers decreases when operated below their maximum output. However, these boilers can be efficiently cycled on a sub-hour scale, so they are assumed to always be operating at their nominal conditions (e.g. to achieve an effective heat output of 50%, they are turned on to 100% for half of the time period and off for the other half).

Thus, the heat production and power/fuel consumption can be described by:

$$0 \leq Q_e(k) \leq Q_{e,rated} \tag{2.20}$$

$$0 \leq Q_n(k) \leq Q_{n,rated} \tag{2.21}$$

$$P_e(k) = Q_e(k)/\eta_e \tag{2.22}$$

$$F_n(t) = Q_n(k)/\eta_n \tag{2.23}$$

where the conversion efficiencies η_e and η_n are the nominal efficiencies of 0.9 and 0.85, respectively.

2.2.8 Battery Bank

A lead-acid battery bank is used to store excess electrical energy produced and dispatch it later as needed. Other types of batteries, i.e. nickel-cadmium or lithium-based batteries, are not considered due to higher cost, fragility with respect to operating conditions, and more intensive maintenance requirements [48].

In general, the energy storage level in a battery can be calculated using a simple energy balance:

$$\frac{dE_b}{dt} = P_c(k)\eta_c - P_d(k)/\eta_d \tag{2.24}$$

When considering discrete time intervals of 1 hour with power measured in kW and energy in kWh, along with the assumptions of constant efficiencies (90% when charging and 95% when discharging) and constant power setpoints in each time interval, one can simplify this to the linear equation:

$$E_b(k) = E_b(k-1) + P_c(k)\eta_c - P_d(k)/\eta_d \tag{2.25}$$

The storage level is also limited by its capacity and maximum discharge level:

$$0.2E_{b,max} \leq E_b(k) \leq E_{b,max} \tag{2.26}$$

The battery bank is not allowed to discharge below 20% of capacity due to the adverse affect on battery lifespan and the potential for causing permenant damage. Cycling of the batteries is not explicitly tracked in order to limit the number of binary variables in the problem. Instead, a low end value for lifespan is assumed to account for the expected behavior of one charge/discharge cycle per day.

2.3 Policy Considerations

In addition to the overall cost of energy supply, the level of autonomy and environmental impact of design solutions are studied. In this work, the environmental impact of heat and power supply is quantified via expected annual CO_2 emissions. Over the past decade, CO_2 has been responsible for >80% of the increase in radiative forcing from long-lasting GHGs [49]. The emissions from microturbines and gas-fired boilers are found using their conversion efficiency and an assumed heating value for natural gas of 950 BTU/ft^3 (35.4 MJ/m^3). The macrogrid is assumed to produce CO_2 at a rate of 0.575 ton/MWh (based on an average of 37% coal-fired and 30% natural gas-fired power plants [50]).

The level of autonomy from the macrogrid is quantified by the fraction of power produced by local units annually. Mathematically, the autonomy level, $\mathcal{A}$, is given by:

$$\mathcal{A} = \frac{\sum_k \left(\sum_m P_m(k) + P_s(k) + P_w(k) \right)}{\sum_k \left(\sum_m P_m(k) + P_s(k) + P_w(k) + P_{grid}(k) \right)}$$

This autonomy may be desirable as it allows for some level of continued power during macrogrid outages. No benefit is assigned to autonomy in the objective function since the economic value of such energy independence would vary greatly depending on the end user. Instead, a constraint is added in some scenarios to enforce a minimum level

Table 2.5: Computational statistics of the scenarios considered. CPU time reported is the mean for all runs in a scenario. In all cases, a 1% relative optimality gap is used.

Scenario	**Number of Equations**	**Number of Variables**		**CPU Time (sec)**
		Continuous	**Binary**	
Reference Case	113,885	96,370	17,521	39.3
Minimum Autonomy	113,889	96,373	17,521	222.4
Emission Tax	113,889	96,373	17,521	187.1
Economic Incentives	113,885	96,370	17,521	202.2
Emissions Cap	113,886	96,370	17,521	173.6
Minimum Renewables	113,889	96,373	17,521	155.5

of autonomy:

$$\sum_k \left(\sum_m P_m(k) + P_s(k) + P_w(k) \right) \geq \mathcal{A}_{min} \sum_k \left(\sum_m P_m(k) + P_s(k) + P_w(k) + P_{grid}(k) \right)$$

where $\mathcal{A}_{min}$ is the minimum autonomy level parameter.

Sending power into the macrogrid is not economically rewarded due to concerns that these reverse flows from distributed generation sites to the macrogrid may have detrimental effects on power quality regulation and macrogrid infrastructure [17]. Cases in which there is significant flow of power back into the surrounding macrogrid are explicitly discussed in the results.

2.4 Results and Discussion

The resulting MILP is formulated in GAMS and the optimization solved using the CPLEX 12 solver to a relative optimality gap of 1%. The model statistics for the various scenarios considered are shown in Table 2.5.

2.4.1 Reference Case

A reference case is used to normalize the results among the various scenarios examined. In this reference case, there are no public policy initiatives/constraints and no minimum autonomy level for the microgrid. The optimization results are shown in Table 2.6.

Table 2.6: Reference case optimization results

Variable	**Value**	**Variable**	**Value**
Microturbines Installed	0	$P_{w,rated}$ (kW_e)	0
$P_{s,rated}$ (kW_e)	0	$E_{b,max}$ (kWh_e)	0
$Q_{e,rated}$ (kW_h)	0	$Q_{n,rated}$ (kW_h)	1340
NPC (million \$)	6.91	CO_2 emissions (t/a)	2910

Unsurprisingly, these results indicate that the NPC is minimized when power is supplied solely through macrogrid and heat solely through combustion of natural gas. In the following results, relative cost and relative emissions will refer to the net present cost and annual CO_2 emissions divided by the reference case values, respectively.

2.4.2 Minimum Autonomy Scenario

In this scenario, no public policy constraints are added to the optimization, but a minimum autonomy level is required. The optimization results are analyzed as the minimum autonomy level is increased in 5% increments.

Fig. 2.5 shows the Pareto frontiers for NPC and annual emissions as the autonomy level is increased. Fig. 2.6 shows that the system is almost entirely reliant on microturbines for local power production. These results indicate that the use of limited local thermal generation (microturbines) may not be significantly more expensive than traditional energy supply.

The discontinuities seen in Fig. 2.5 result from changes in technology selection which can be seen in Fig. 2.6. When one microturbine is installed, the annual emissions are reduced by about 7% relative to the reference case due to the cogeneration of heat and power. This single microturbine is operated consistently at or near its rated power with all available heat used to satisfy demand. When the required autonomy level rises above 40%, another microturbine is installed. The emissions drop again, but not as significantly. This is because microturbines are now required to operate at times when heat demand is low, resulting in excess heat production and lower fuel efficiency. Operation of these microturbines in suboptimal time periods becomes more frequent as the autonomy level rises, leading to the gradual increase of emissions levels seen in

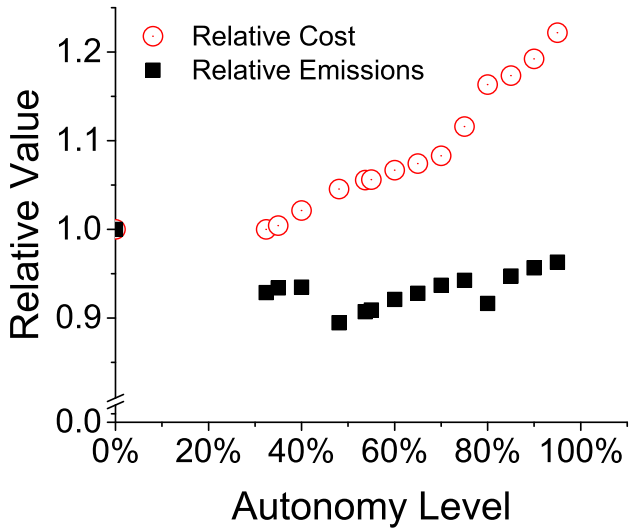

Figure 2.5: Relative cost and environmental impact of microgrid solutions in the minimum autonomy scenario.

Fig. 2.5. The slight deviation in this trend corresponds to the case in which a small amount of wind power was installed. In addition, the relative cost increases steadily with the autonomy level (since local generation is more expensive than traditional power supply) with discontinuities when the number of microturbines or renewables capacity is increased.

Wind and solar are not generally selected by the optimization due to the high relative cost of small capacity renewables. Therefore, power from the macrogrid (which is predominately thermal generation) is being replaced with microturbines (another form of thermal generation), so the annual CO_2 emissions are not dramatically reduced in this scenario. The public policies in the following sections will explore under what scenarios one sees a departure from this reliance on fossil fuels, and what the impacts are on system costs.

Fig. 2.7 shows the contribution of various economic factors to the overall NPC. It is important to note that all of these solutions represent a much higher upfront cost relative to the reference case (capital cost expenditures >6x the reference case). This large initial investment represents a significant economic risk, and is likely to inhibit the adoption

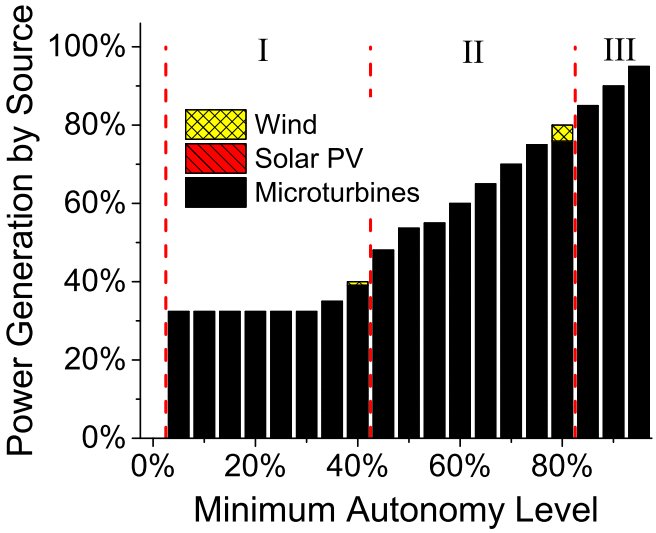

Figure 2.6: Power production breakdown by source for the minimum autonomy scenario. The balance not shown is made up of power purchased from the macrogrid. Numerals indicate the number of microturbines installed in each regime.

of such systems unless local generation is also desired for its ability to maintain critical systems during blackouts. Again, the discontinuities in the various economic factors correspond with changes in the number of microturbines or renewables capacity.

2.4.3 Emission Tax Scenario

In this scenario, a tax of \$30 per ton CO_2 emitted is implemented. Every year, this tax grows at a rate equal to inflation. This level of emission taxation is similar to what has been proposed and implemented in OECD countries [51, 52]. Due to the large capacity and long lifespan of utility scale power plants, macrogrid infrastructure is assumed to remain the same over the design horizon. The emission cost incurred by utility companies is passed on to the end consumer. Thus, consumers may want to invest in local power generation to reduce their dependence on this now more expensive macrogrid power.

Fig. 2.8 shows that this emission tax raises the optimal NPC by a relatively constant amount and has negligible effect on the system's annual emissions. Fig. 2.9 shows that

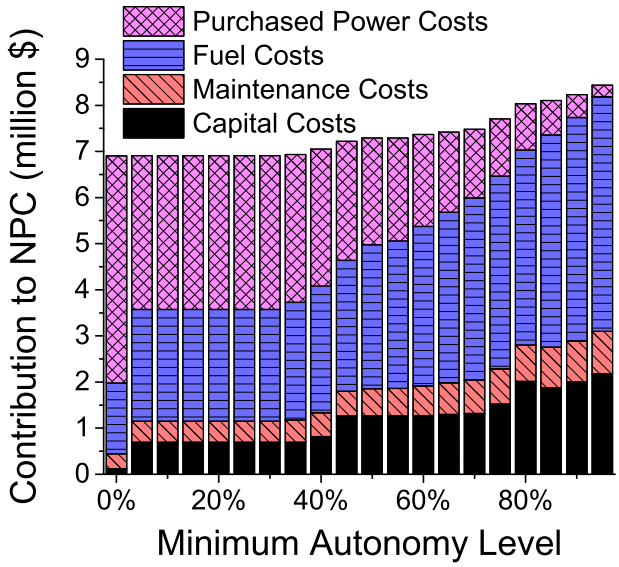

Figure 2.7: Net present cost breakdown by source for the minimum autonomy scenario.

the power technology utilization in this scenario is almost identical to the minimum autonomy scenario. The same can be shown for heat generation technology (not shown). Since no appreciable change in technology selection or dispatch has occurred, there is practically no change in the environmental impact of these microgrid systems due to emission taxation. Again, the discontinuities in relative cost and emissions can be explained by a change in the number of microturbines installed or the sudden addition or removal of renewable power capacity.

With or without emission taxation, microgrids reliant on combined heat and power reduce overall emissions by 5-15%. The small amount saved in emission taxation does not offset the higher overall cost of local thermal power supply, so reasonable carbon taxation is not predicted to have any significant positive or negative impact on microgrid economics. Microgrids with a high penetration of wind and solar are also unlikely to be helped by such a tax since the high relative capital cost of small capacity renewables is much more than the emission taxation cost.

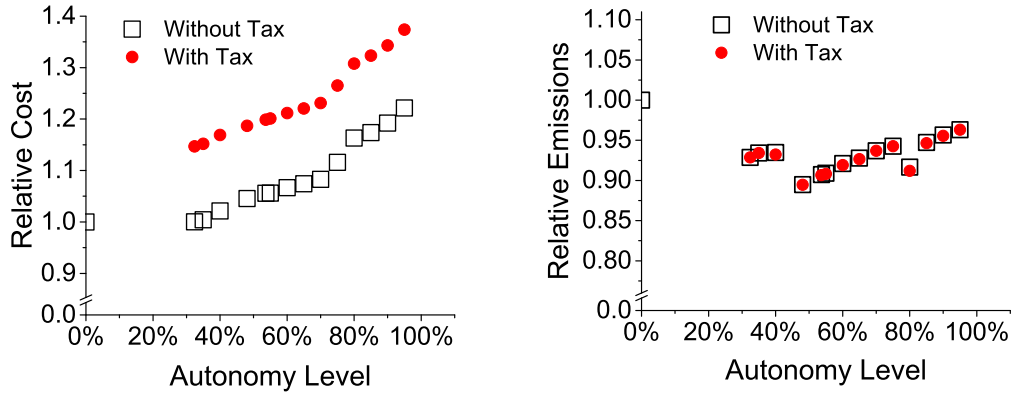

Figure 2.8: Overall cost and expected environmental impact of microgrid designs in the minimum autonomy and the emission tax scenarios.

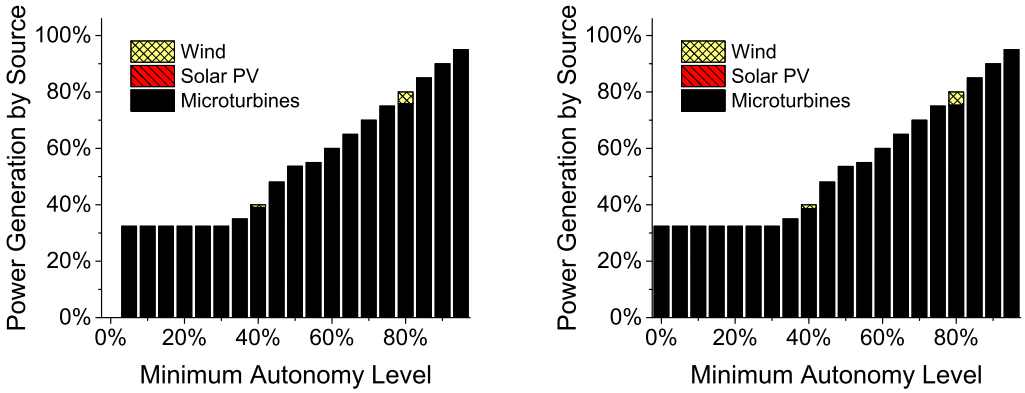

Figure 2.9: Power supply breakdown of optimal microgrids without a tax (left) and with a \$30/ton CO_2 tax (right). The balance not shown is made up of power purchased from the macrogrid.

2.4.4 Economic Incentives Scenario

In this scenario, economic incentives are used to encourage the use of less carbon intensive power technologies. In particular, the case of tax incentives to reduce the cost of wind and solar power systems is examined. Tax incentives equal to 30% and 50% of the total installed cost of renewable power technologies are considered.

Similar tax incentives already exist in certain areas (e.g. the U.S. Business Energy Investment Tax Credit [42]), but they have varying restrictions on eligible technologies,

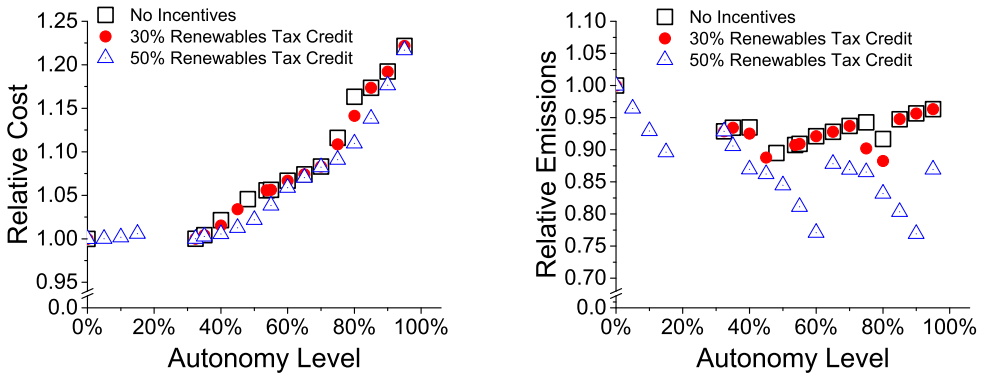

Figure 2.10: Net present cost (left) and annual emissions (right) in the economic incentives scenario. Values shown are relative to the reference case.

systems capacities, etc. In this scenario, economic incentives are available to microgrid scale renewable energy systems, but not to utility scale systems (order of 100 MW). Thus, the effective cost of local wind and solar is reduced, but macrogrid infrastructure and selling price remain unchanged.

Fig. 2.10 shows that neither level of incentives is sufficient to significantly lower the cost of supplying power locally. However, strong economic incentives do have an effect on the environmental impact and technology selection of microgrids. At 30% tax credits, the relative emissions remain close to the levels observed in the minimum autonomy scenario (where renewable power usage was insignificant), but at 50%, there is a noticeable departure from this trend.

Fig. 2.11 shows the technology selection in terms of contribution to power supply. Wind is the dominant form of renewable power selected due to its lower capital cost. Even in the case of 50% effective capital cost reduction, renewables are not economically viable as the primary source of power supply due to their intermittent nature and thus the need for expensive electrical storage technologies or oversizing of power generation. Instead, renewable power is used to supplement the microturbines and the macrogrid, providing at most 25% of the overall power supply. Whenever another microturbine is added, there is a significant reduction in the installed renewables capacity and a discontinuous jump in the relative emissions as seen in Fig. 2.10. In both tax incentive cases, heat supply remains dependent upon fuel-fired sources (gas boiler and microturbine heat recovery).

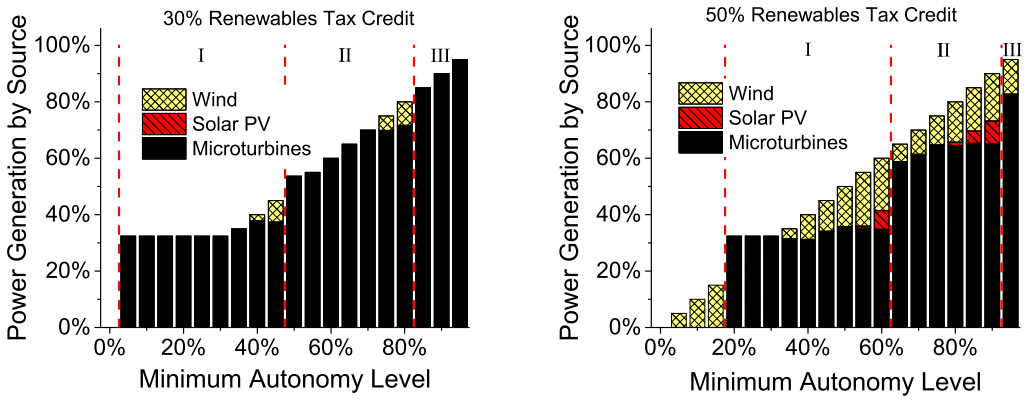

Figure 2.11: Power production breakdown in the economic incentives scenario. The balance not shown is made up of power purchased from the macrogrid. Numerals indicate the number of microturbines installed in each regime.

2.4.5 Emissions Cap Scenario

In this scenario, a cap on the total annual CO_2 emissions is implemented. The emissions from both heat and power supply, including any emissions associated with power purchased from the macrogrid, are included in this cap. Two limiting cases are explored, referred to as the independent emissions reduction case and the economy-wide emission reduction scenario. The independent emission reduction scenario reflects the case in which the end user elects to limit their carbon emissions in the absence of governmental pressure. In this case, macrogrid emission levels and electricity price remain the same.

In the economy-wide reduction scenario, macrogrid emission levels decrease with the emissions cap but electricity price increases, reflecting a broad transition in the economy to greener but more expensive fuel sources or technologies. The reduction in macrogrid emission rate is set to be proportional to the reduction in total allowed annual emissions of the energy supply optimization. Therefore, when optimization is constrained to have annual emissions below 50% of the reference case, the macrogrid emission rate is 50% of the reference case value. Using the electrical generation technology split proposed in [53] and the near-future levelized cost of energy from various technologies estimated in the 2014 Annual Energy Outlook [54], a ∼95% reduction in the carbon intensity of electricity generation would result in a ∼25% increase in cost. The relation between macrogrid emission reduction and electricity selling price is assumed to be linear.

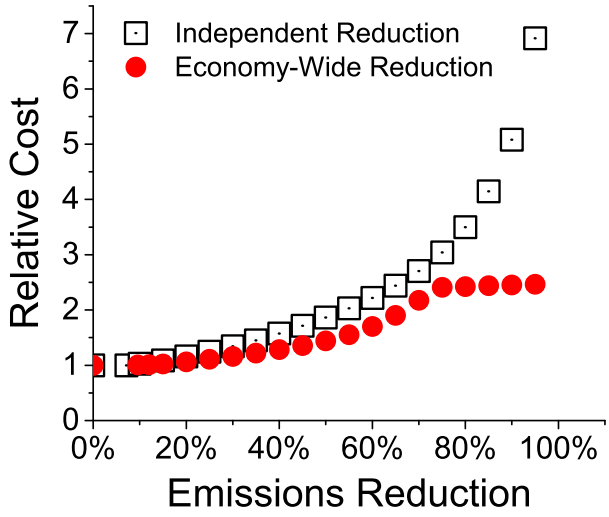

Figure 2.12: Relative net present cost of emissions reduction.

Fig. 2.12 shows the change in NPC for these two limiting cases as the emission cap is decreased. The relative cost of the two cases is somewhat close for low emission reduction points, but independent reduction becomes much more expensive at high emission reduction levels.

Figs. 2.13 and 2.14 show the progression of technology selection in the two scenarios as the emission cap is decreased. For the independent reduction scenario, initial emission reduction is attained through a switch to local combined heat and power. For further emission reduction, renewable power is added to replace carbon intensive power from the macrogrid. Eventually, local microturbines begin to be underutilized and electric heating (powered with more renewables) is used to continue emission reduction. As the annual emissions become very small, the optimal microgrid relies entirely on wind and solar power (with a sizable battery), and primarily electric heating with cheaper gas-fired heating used only as much as the emission cap will allow.

The progression of optimal technology selection is different in the economy-wide emission reduction scenario. Again, initial emission reduction is achieved through use of combined heat and power. However, once emission reduction is pushed above 35%, the optimal microgrid no longer uses microturbines. Instead, a combination of the

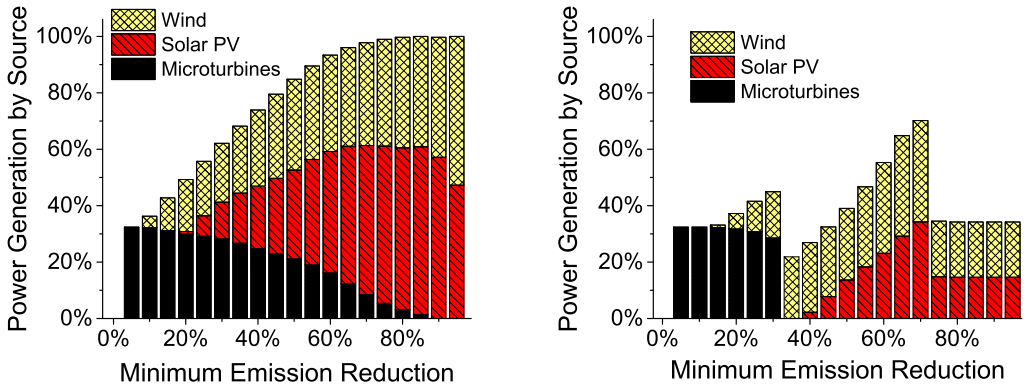

Figure 2.13: Power supply breakdown of optimal microgrids in independent (left) and economy-wide (right) emission reduction scenarios. The balance not shown is made up of power purchased from the macrogrid.

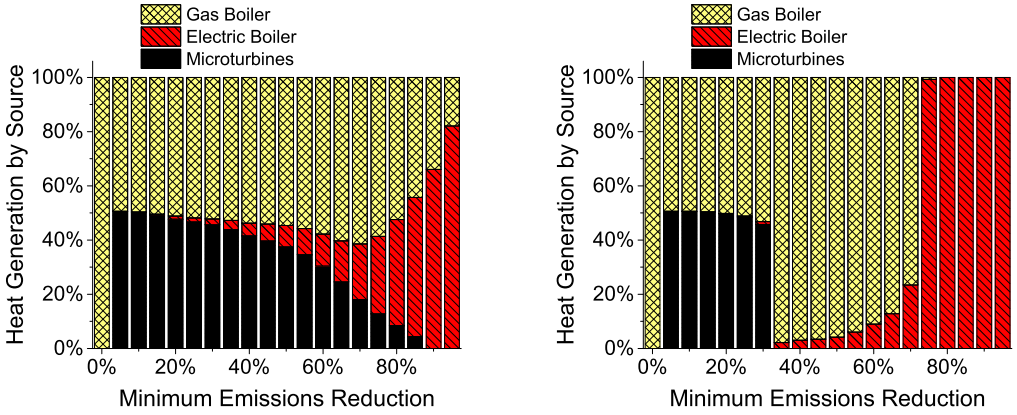

Figure 2.14: Heat supply breakdown of optimal microgrids in independent (left) and economy-wide (right) emission reduction scenarios.

macrogrid and local renewables is used to supply power with heat primarily supplied through dedicated natural gas combustion. Above 75% emission reduction another technology regime is observed. In this regime, the unit sizing is constant with 34% of the power supplied via renewables and all heat supplied by electric heating. This constant sizing and dispatch leads to the linear cost profile observed in the high emission reduction range.

In both emission reduction scenarios, significant excess power is shed to the macrogrid as emission reduction increases. In the independent reduction scenario total excess power remains small (less than 2% of annual demand) until emission reduction is pushed to 50% and above. As emission reduction increases past the 50% point, excess power is seen to rise exponentially, reaching 70% of annual demand at 90% emission reduction and 120% at 95% emission reduction. This would place a very large strain on the macrogrid, meaning that renewable power production would likely need to be curtailed frequently or local energy storage capacity increased. In the economy wide emission reduction case, excess electricity production remains small when emission reduction is below 60%. After this point, excess electricity production is 3-8% of total annual demand, stabilizing at 5.3% in the fixed design observed in the tail end of cases. These values, while significant, may be feasible so long as renewable energy production is forecasted ahead of time, especially considering that the macrogrid would have adapted to handle significant utility scale renewable generation in these cases.

2.4.6 Minimum Renewables Scenario

In this scenario, a minimum fraction of the power must be generated through local renewable power systems. Fig. 2.15 shows that the major cost factor in this scenario is the capital cost investment for the renewables and battery storage systems. This figure also shows the environmental performance in this scenario versus the minimum autonomy scenario where no restriction was placed on how local power was to be produced. The annual CO_2 emission levels drop approximately linearly with the renewables penetration, but reach a minimum at around 25% of the reference case value.

Fig. 2.16 shows the contribution of the various technologies to heat and power supply. As previously observed, wind power is selected first due to its lower cost, but at higher levels of renewables penetration/emission reduction a combination of wind and solar power is preferred. This combination of wind and solar technology helps to spread the renewables power output over time so that less overall battery capacity is necessary. The relative emissions observed in Fig. 2.15 do not go to zero since the heat supply is still primarily reliant upon the gas-fired boiler.

Fig. 2.17 shows that the relative cost and relative emission values from this scenario are very close to the Pareto front established in the independent emission reduction

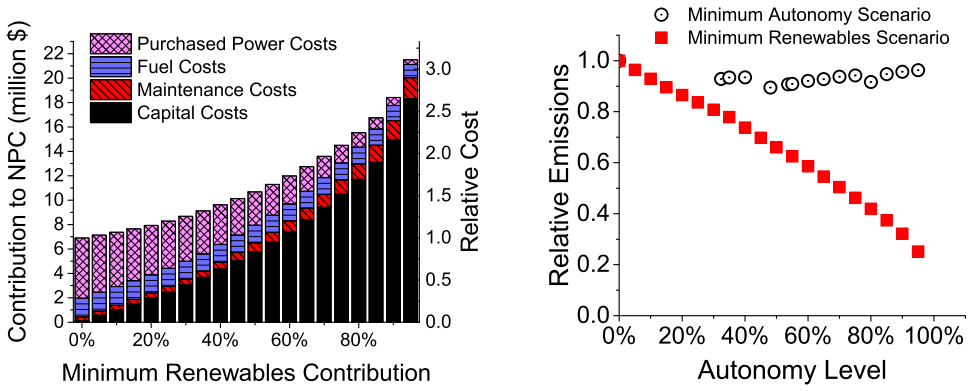

Figure 2.15: Cost breakdown for the minimum renewables scenario (left) and environmental impact compared to minimum autonomy scenario (right).

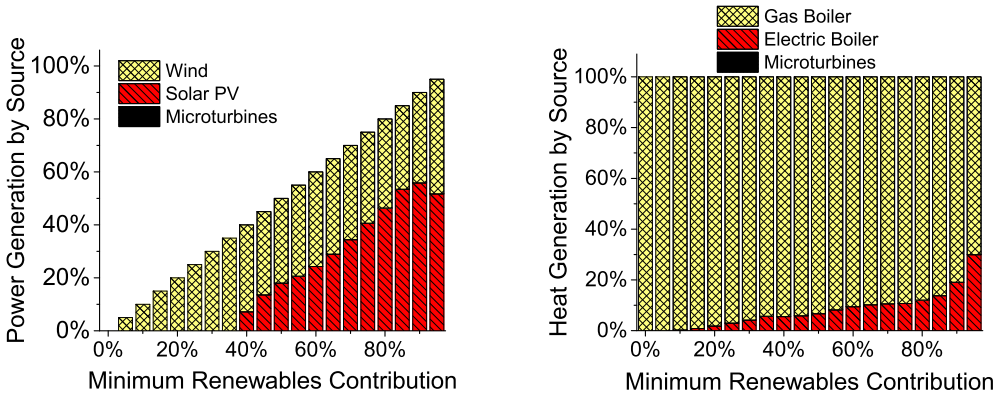

Figure 2.16: Heat and power breakdown by technology in the minimum renewables scenario. The balance not shown on left is made up of power purchased from the macrogrid.

scenario even though the technology selection is significantly different with respect to utilization of microturbines. Thus, this renewables-only approach to local power supply could be an alternative way to achieve moderate emission reduction when local fuel supply for the microturbines would be expensive or difficult to achieve. However, in general the superstructures proposed in the emission reduction scenario would be preferred since microturbines are dispatchable (more reliable for critical power supply).

In almost all cases of this minimum renewables scenario, the overall amount of power fed back into the macrogrid is less than 5% of the annual power demand. Above 85% renewables penetration, this back flow of power rises dramatically, reaching over

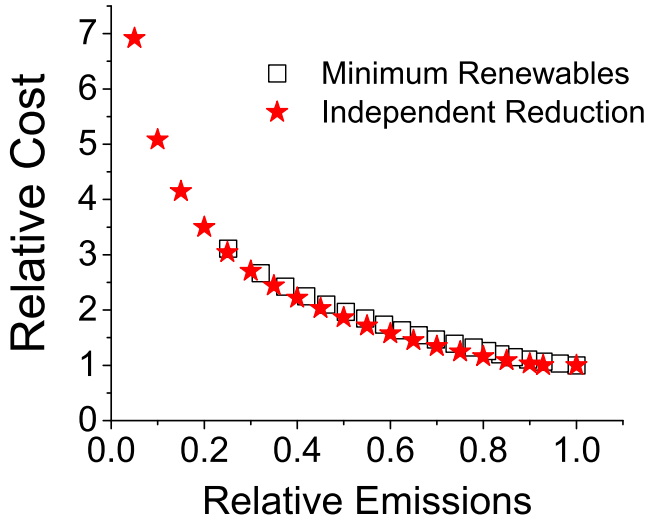

Figure 2.17: Comparison of cost vs. environmental impact in minimum renewables and independent emission cap scenarios.

16% of average demand at 95% renewables penetration. There is negligible excess heat produced since the optimal designs in this scenario do not utilize local thermal power generation.

2.4.7 Capital Cost Uncertainty

The proposed microgrid design method uses deterministic capital costs for the various units. As mentioned, there is uncertainty in these costs, especially for distributed renewables like wind and PV. Fortunately, the CPU time for the MILP is on the order of 3-4 min., so one could easily explore a number of different cost scenarios or do a full sensitivity analysis within a reasonable amount of time. Full sensitivity analysis with respect to each units capital cost in each scenario has not been performed here for the sake of brevity, but some observations about the impact of the assumed costs can be made.

Uncertainty in the installed cost of microturbines and boilers is expected to have little impact on the observed results. These technologies, particularly the boilers, are

widely commercially available, established technologies, so the magnitude of this uncertainty is small. Moreover, the cost associated with these units comes primarily from operational expenditures, in particular the fuel/electricity required to run them, and not from capital expenditures. Thus, uncertainty in the capital cost of these units is unlikely to affect design choices or the overall cost of heat and power supply.

Lead acid batteries are the primary form of electrical storage employed in distributed power systems and a well matured technology. However, continuing research into alternative battery chemistries and alternative technologies introduces uncertainty in the future cost of electrical storage. In the near future, this would affect the results in the emission cap and minimum renewables scenarios where renewable power and batteries are heavily used. However, even in these cases the batteries accounted for at most 27% (and typically 10-15%) of the capital expenditures, with PV and wind power accounting for most of the balance. Thus, the high cost in these scenarios will ultimately be more influenced by uncertainty in the capital cost of distributed renewables. In all other scenarios, the capital expenditures on batteries accounts for less than 6% of the total energy supply cost.

The units with the largest uncertainty in their capital cost are the wind and PV. The installed cost of distributed renewable technology has a standard deviation of around 1,000 $/kW, with further uncertainty about future cost reductions due to public policy changes or technological advancements. The impact of a 30% and 50% reduction in the total installed cost of renewables technologies can be seen in the economic incentives scenario (Section 2.4.4). This section was motivated with the discussion of tax credits that are in place, but the effective reduction of the renewables' capital cost could also be achieved through other means (e.g. improvements in PV panel technology). It was shown that renewables were still little used under a 30% reduction in installed cost. Considering that some portion of this installed cost is independent of such technology advancements (e.g. permitting fees and labor costs), near-future improvements in technology alone are unlikely to significantly improve the attractiveness of microgrids with high renewables usage. These improvements would decrease the cost seen in the emission reduction and minimum renewables scenarios, but they would still be much more expensive than fossil fuel-based energy supply.

The combined effect of capital cost reductions with other policies considered (e.g.

CO2 taxation) could certainly be considered through a model like this, but the analysis of such heterogeneous policy scenarios is neglected in favor of discussing the considered scenarios in sufficient detail.

2.5 Conclusions

Microgrids reliant on local thermal power generation with coupled heat recovery were seen to be the optimal design choice in the absence of public policy incentives. Through the cogeneration of heat and power, these microgrids could potentially lower the annual CO_2 emission levels by 5-10%, but renewables or electric based heating technologies are required to further reduce emissions. Both emission taxation and moderate economic incentives on renewables had little effect on the overall economics and optimal technology for microgrids. This is primarily due to the additional cost of peripherals (in this case battery storage) that are needed to cope with the intermittancy in renewable power production. When wind and solar technology were discounted more than 30%, there was a noticeable increase in renewables usage and reduction in emissions, but power supply was still primarily reliant on microturbines and the macrogrid. In addition to immediate tax incentives, government support of renewable technology research will help to reduce their cost, and make renewables a more attractive alternative.

High penetration of renewable power was observed primarily in the emission reduction scenarios and when an explicit fraction of renewable power was required. However, these scenarios were projected to be significantly more expensive than the reference case, to the point where they would not be currently economically practical when a connection to the macrogrid is available.

Simplifications in heat and power production (e.g. not accounting for temperature effects, using constant conversion efficiencies) are expected to have little overall effect on unit sizes and annual operating cost. Thus, these assumptions should have small impact on the trends observed under the policies considered. The capital cost estimates used for renewables technologies reflect their high cost for small capacity systems. However, using lower values to reflect a larger system or continued technology maturation should increase their penetration in low emission reduction scenarios (potentially supplanting

microturbines entirely), lower the threshold at which economic incentives become effective, and lower the overall cost of the emission reduction and minimum renewables scenarios.

This type of policy-based analysis can be used to identify robust microgrid superstructures given the inherent uncertainty in future public policy decisions. For example, similar sizing decisions were made by the optimization under the autonomy, emission taxation, and moderate economic incentives scenarios. The number of microturbines installed versus the microgrid power contribution was almost identical across these scenarios. With heavy economic incentives (50% renewables tax credit) more utilization of renewables was observed, but the number of microturbines installed was similar. In this case, the renewable power capacity could always be installed later when the tax credits or other forms of incentives are introduced and the dispatch strategy modified to favor using renewable power.

This approach can also serve to highlight potential risks with a given microgrid design. For example, a change in public policy to significantly cap emissions would hamper a microgrid design primarily reliant on microturbines (note the disappearance of microgrid power in the emission reduction scenario). This information, along with analysis of the likelihood of future public policies, can be used to make informed decisions about system design.

The results observed in this work are expected to be generalizable to North American locations of a similar climate. Using the DOE identified climate zones, this corresponds to most of the U.S. Midwest, Northeast, and high plains regions. The extent to which location dependent parameters (e.g. the ratio between heat and power demands, climate, and local pricing of natural gas and utility power) affect the optimal microgrid design results is explored in the next chapter.

2.6 Nomenclature

Table 2.7: Nomenclature - Indices/Sets

k	Time periods	m	Microturbines

Table 2.8: Nomenclature - Parameters

ζ_b	Battery maintenance cost
ζ_e	Electric boiler maintenance cost
ζ_{gas}	Natural gas cost
ζ_{grid}	Power purchase cost
ζ_m	Microturbine maintenance cost
ζ_n	Gas boiler maintenance cost
ζ_s	Solar PV maintenance cost
ζ_{start}	Microturbine startup cost
ζ_w	Wind turbine maintenance cost
η_c	Battery charging efficiency
η_d	Battery discharging efficiency
η_e	Electric boiler efficiency
η_n	Gas boiler efficiency
θ_b	NPV factor for battery capital cost
θ_e	NPV factor for electric boiler capital cost
θ_m	NPV factor for microturbine capital cost
θ_n	NPV factor for gas boiler capital cost
θ_s	NPV factor for solar PV capital cost
θ_w	NPV factor for wind turbine capital cost
κ_b	Battery capital cost
κ_e	Electric boiler capital cost
κ_m	Microturbine capital cost
κ_n	Gas boiler capital cost
κ_s	Solar PV capital cost

Continued on next page

Table 2.8 – continued from previous page

κ_w	Wind turbine capital cost
λ_m	Microturbine heat-to-power ratio
ϕ_b	NPV factor for battery maintenance
ϕ_e	NPV factor for electric boiler maintenance
ϕ_{gas}	NPV factor for natural gas purchases
ϕ_{grid}	NPV factor for power purchases
ϕ_m	NPV factor for microturbine maintenance
ϕ_n	NPV factor for gas boiler maintenance
ϕ_s	NPV factor for solar maintenance
ϕ_w	NPV factor for wind turbine maintenance
f_w	Wind power fractional availability
h	Height
h_{ref}	Reference height
H	Solar irradiance
H_{rated}	Rated solar irradiance
P_ℓ	Power demand
Q_ℓ	Heat demand
v	Wind speed
v_{ci}	Cut-in wind speed
v_{co}	Cut-out wind speed
v_r	Rated wind speed
v_{ref}	Wind speed at reference height

Table 2.9: Nomenclature - Binary Variables ($1 \implies$ True)

I_m	Is microturbine installed	y_m	Is microturbine started up
x_m	Is microturbine on		

Table 2.10: Nomenclature - Continuous Variables

$Capex$	Capital costs (present value)	P_s	Power from solar PV
E_b	Battery storage level	$P_{s,rated}$	Solar PV rated power
$E_{b,max}$	Battery storage capacity	P_{spill}	Power spilled
F_m	Microturbine fuel consumption	P_w	Power from wind turbine
F_n	Gas boiler fuel consumption	$P_{w,rated}$	Wind turbine rated power
NPC	Project net present cost	Q_e	Heat from electric boiler
$OPEX$	Operational cost (present value)	$Q_{e,rated}$	Electric boiler rated heat
P_c	Power charged to the battery	Q_m	Heat from microturbines
P_d	Power discharged from the battery	Q_n	Heat from gas boiler
P_e	Power used by the electric boiler	$Q_{n,rated}$	Gas boiler rated heat
P_{grid}	Power imported from the utility	Q_{spill}	Heat spilled
P_m	Power from microturbines		

CHAPTER 3

Understanding and Predicting the Impact of Location and Load on Microgrid Design*

3.1 Introduction

In Chaper 2, the optimization of microgrid design and technology selection was analyzed particularly with respect to public policy decisions. This chapter expands upon that idea, but with a focus on elucidating the impact of geographic location and load shape on design results. Geographic location is obviously closely tied to the typical weather, and has a strong impact on the productivity of renewable technologies as well as the magnitude of heating and cooling demands. In addition, differences in energy prices (i.e. electricity and natural gas) between different locations may make certain microgrid design motifs more or less attractive. Different types of customers can also exhibit significant differences in their energy demand patterns (i.e. their load shape). These difference manifest in terms of the magnitude of energy demands, the ratio between demands for different forms of energy (e.g. heat and power), and the relative volatility in the demand profiles over time. All of these effects can have a profound impact on

*Reprinted (adapted) with permission from Michael Zachar and Prodromos Daoutids, *Energy*, 90:1005-1023, 2015 [15]. Copyright ©2015 Elsevier Ltd.

the optimal microgrid design and technology selection.

Understanding the impact of these local parameters on the optimal microgrid design is vital to identifying the strengths and weakness of competing DER technologies, rationally directing future research endeavors, and informing future public policy discussions. Despite this fact, most microgrid design studies in literature present case studies for a single location and load shape. Moreover, the selection of these case study parameters is often driven by incidental factors like availability of data or academic affiliation.

There has been some past work which partially addressed this research need. In [55], sensitivity analysis was performed for the design of a combined cooling, heat, and power (CCHP) system serving a hospital load. The authors analyzed how the optimal design changed with respect to several input parameters (i.e. DER capital cost, DER performance, and energy tariffs). They found that reduction in electricity tariff had little effect on the design, but reduction in natural gas tariff resulted in significant increase in DER capacity. However, renewable technologies were not considered, and the sensitivity with respect to other important factors (such as magnitude of thermal loads) was not analyzed. In [56], the differences in system design, energy supply cost, and environmental performance for a CCHP system across 5 different climate zones in China is presented. However, the authors did not consider renewable technologies or storage units in their design, and the comparison of results made is largely qualitative. In [57], the design of a CCHP system is considered for 5 different climate zones and 3 different load shapes. The authors consider both fuel-fired units and photovoltaics, but do not consider energy storage units and did not allow power sales to the macrogrid. Perhaps for this reason, they observed only dispatchable cogeneration units in their optimal designs. No minimum contribution of DERs was enforced, but the authors did analyze the results for fixed renewable DER capacity and for the case of CO_2 taxation. They observed that gas fired units were much more economical than renewables unless significant taxation was imposed. In addition, they did not examine alternative renewable technologies (e.g. wind) or the potential benefit of energy storage for enabling effective renewables utilization.

The objective of this chapter is two-fold: to provide a comprehensive assessment of the trends in microgrid design over a wide range of locations and load shapes, and to propose a heuristic procedure to quantify these trends. This work improves on

previous contributions in the field by expanding the scope to include a wider variety of locations and load shapes while at the same time providing an approach to quantitatively evaluating the trends given the design results at these disparate conditions. In the first part, mixed integer linear programming is used to find the optimal microgrid design. The formulation from Chapter 2 is extended to consider new units (i.e. thermal storage and new sizes of microturbines). In addition, the modeling of some units is improved, for example by considering piecewise linear cost function for renewables, temperature effects on renewable availability, and lower part-load efficiency of microturbines. In the second part of the chapter, a heuristic procedure for fitting design trends is proposed.

An interesting technical contribution of this chapter is the use of artificial neural networks (ANNs) as a surrogate for detailed design optimization. This is detailed later in Section 3.4, but in essence the results from MILP optimization at various conditions are used to develop and train a heuristic procedure which predicts key microgrid design characteristics based on only a parsimonious set of inputs. Once trained, this heuristic procedure can then act as a surrogate for future time-intensive optimization runs. In this chapter, it is shown that this can serve as a valuable way to identify underlying trends in a high-volume study such as this. In addition, it can serve as a predictive tool when a broad parameter space is of interest as shown in Section 3.4.3. Important limitations in this procedure are also identified. The ability of other publicly available software tools to fill this role as a surrogate for formal optimization is also examined in 3.4.4.

In Section 3.2 the mixed integer linear program used for microgrid design is introduced. In Section 3.3, the results of this optimization problem over different locations, load shapes, and microgrid penetration levels are discussed. Input parameters that serve as good predictors of microgrid design and performance (i.e. the optimal microgrid penetration level, cost of energy supply, annual emission levels, and utilization of renewable power) are identified. Finally, in Section 3.4, a procedure for fitting these design results using a series of artificial neural networks is introduced and the performance of this method is analyzed. For the reader's convenience a comprehensive nomenclature for this chapter is included in Section 3.6.

3.2 Model Formulation

In order to properly isolate the effects of location and load shape selection on microgrid optimal design, a consistent model formulation and methodology for input data generation must be used. In this chapter, the Typical Meteorological Year version 3 (TMY3) datasets from NREL are used for input weather values (wind, insolation, and air temperature) [58]. Load data for various commercial reference buildings was generated using the DOE's EnergyPlus simulation software with TMY3 weather files as input. These data sets are publicly available on the National Solar Radiation Data Base website[2] and the Open Energy Information website[3].

A mixed integer linear program (MILP) is formulated to find the optimal unit sizes that minimize the total present cost of energy supply over the microgrid lifespan (taken to be 20 years). Units considered include PV, wind turbine, battery bank, electric and natural gas boilers, microturbines, and a thermal storage unit. The microgrid supplies both heat and power. A connection to the external utility can be used to exchange power. The import or export of heat is not considered due to the high transmission and distribution losses that would occur. The energy flow diagram showing all potential DER units is shown in Fig. 3.1.

The energy supply cost is taken to be:

$$NPC = Capex + Opex$$

where $Capex$ is the present value of unit capital costs (including any necessary replacements) and and $Opex$ is the present value of the expected unit maintenance, fuel, and purchased power costs over the system lifetime. The capital costs are given by:

$$\begin{aligned} Capex = &\sum_{m} N_m \kappa_m \theta_m + Q_{e,rated} \kappa_e \theta_e + Q_{n,rated} \kappa_n \theta_n + E_{b,max} \kappa_b \theta_b + E_{h,max} \kappa_h \theta_h \\ &+ \sum_{w} \left(P_{w,rated} \kappa_{w,var} + I_w \kappa_{w,fix} \right) \theta_w + \sum_{s} \left(P_{s,rated} \kappa_{s,var} + I_s \kappa_{s,fix} \right) \theta_s \end{aligned}$$

In addition to the term related to the thermal storage unit, there are two important

[2] http://rredc.nrel.gov/solar/old_data/nsrdb/1991-2005/tmy3/

[3] http://en.openei.org/doe-opendata/dataset/commercial-and-residential-hourly-load-profiles-for-all-tmy3-locations-in-the-united-states

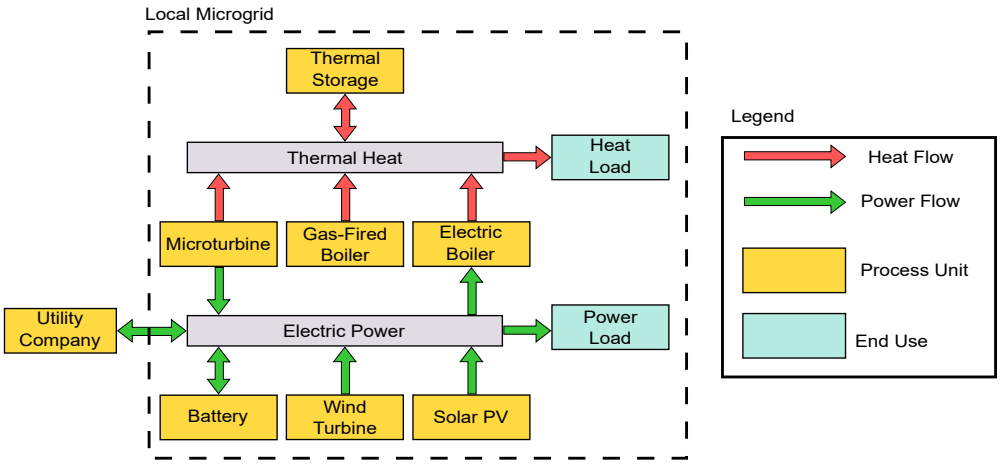

Figure 3.1: Energy flow diagram of the microgrid system considered. Not all possible technologies will be included in every optimal design.

differences from the formulation in Chapter 2:

- Different classes (i.e. capacities) of microturbines are now considered, and microturbines of the same class are treated as indistinguishable
- The capital cost of wind and solar units are now described by piecewise linear functions

In this chapter, m is an index which refers to a classes of microturbines rather than to an individual unit. The integer variable N_m indicates the number of microturbines of class m installed. For wind and solar power, the indicies s and w represent different characteristic size ranges, and binary variables (i.e. I_s and I_w) are used to indicate which size range is active. In particular, this is enforced by the introduction of two additional constraints:

$$I_s P_{s,lo} \leq P_{s,rated} \leq I_s P_{s,up} \qquad \forall s$$
$$I_w P_{w,lo} \leq P_{w,rated} \leq I_w P_{w,up} \qquad \forall w$$

where $P_{s,lo}$ and $P_{w,lo}$ denote the lower bounds of size ranges, and $P_{s,up}$ and $P_{w,up}$ denote the upper bounds of size ranges. The solar cost curve is divided into 3 subdomains and the wind cost curve is divided into 6 subdomains. Additional details on piecewise

linearization can be found in Appendix A.3.

The operational costs are given by:

$$\begin{aligned} Opex = & \sum_{s} P_{s,rated}\zeta_s\phi_s + \sum_{w} P_{w,rated}\zeta_w\phi_w \\ & + \sum_{k}\Bigg[\sum_{m}\big(P_m(k)\zeta_m + y_m(k)\zeta_{m,start}\big)\phi_m + Q_n(k)\zeta_n\phi_n + Q_e(k)\zeta_e\phi_e \\ & + P_d(k)\zeta_b\phi_b + Q_{h,in}(k)\zeta_h\phi_h + \Bigg(\sum_{m} F_m(k) + F_n(k)\Bigg)\zeta_{gas}\phi_{gas} + P_{grid}(k)\zeta_{grid}\phi_{grid}\Bigg] \end{aligned}$$

A discount rate of 8.3% is used to calculate the present value of costs in future years. The electricity tariff and maintenance costs are assumed to escalate at a rate of 2.5%/annum, and the cost of natural gas is assumed to escalate at a slightly higher rate of 3.7%/annum. Though the optimal design is selected based only on the overall cost, other factors like CO_2 emission levels and incorporation of renewable technologies are also analyzed.

3.2.1 Unit Modeling

A brief description of the modeling of each unit is given here focusing in particular on any differences from the previous chapter.

Microturbines

Microturbines are used as a local source of dispatchable heat and power. Three different size of microturbines are modeled based on the commercially available C30-LP, C65, and C200-LP units from the Capstone Microturbine Co. [59]. Power output of the microturbines is described by:

$$0 \leq P_m(k) \leq x_m(k)P_{m,rated} \qquad \forall\, k, m$$

$$x_m(k) \leq N_m \qquad \forall\, k, m$$

where x_m is the number of microturbines of class m turned on.

Since a wider range of operation is considered than in Chapter 2, constant efficiency cannot be assumed. Indeed, fuel efficiency drops when the microturbines are operated

at partial load. An explicit calculation of the part-load fuel efficiency would lead to a non-linear equation for fuel consumption given by:

$$F_m(k) = P_m(k)/\eta_m(k) \qquad \forall k, m$$

To preserve the linearity of the model, the fuel consumption is instead calculated as an affine function of power setpoint and on/off status:

$$F_m(k) = F_{m,fixed} x_m(k) + F_{m,var} P_m(k) \qquad \forall\, k, m$$

where the parameters $F_{m,fixed}$ and $F_{m,var}$ are fitted using the part load efficiency curve given in [45] and the manufacturer's specifications for electrical efficiency at rated power [59].

As in Chapter 2, startups are tracked, and microturbines are used for cogeneration of heat:

$$y_m(k) \geq x_m(k) - x_m(k-1) \qquad \forall\, k, m$$

$$Q_m(k) = P_m(k)\lambda_m \qquad \forall\, k, m$$

Specific parameters values for the 3 types of microturbines are shown in Table 3.2.

PV Array

Fixed-angle solar photovoltaics are used to harvest freely available solar energy for local power production. A maximum power point tracker is assumed to be used, and panel tilt angle is set equal to the location's latitude. The power output of the PV is described by:

$$P_s(k) = \eta_s(k) P_{s,rated} \frac{H(k)}{H_{ref}} \qquad \forall\, k, s$$

where η_s is a cell temperature dependent efficiency given by:

$$\eta_s(k) = 1 - 0.0045(T_s(k) - 25) \qquad \forall\, k, s$$

Cell temperature, T_s, is approximated as an affine function of the weather[60]:

$$T_s(k) = 0.943T(k) + 0.28H(k) - 1.528v(k) + 4.3 \qquad \forall\, k, s$$

where $T(k)$ is the ambient air temperature, and the units are specified as ^{o}C for temperatures, m/s for the wind speed, and W/m^2 for the insolation. The total insolation on the panels is given by:

$$H(k) = DNI(k)cos(\Theta(k)) + DHI(k) \qquad \forall\, k$$

where DNI is the direct normal insolation, Θ is the angle of incidence between the direct sunlight and the panels, and DHI is the diffuse horizontal insolation.

Parameter values for the PV array are shown in Table 3.1. Capital costs in each size regieme were derived based on a power law cost model with a scaling exponent of 0.944 and a reference cost of $340,000 for a 100 kW system [61]. Only uses 3 size regimes were used since the capital cost is nearly linear due to the modular nature of photovoltaics.

Table 3.1: Photovoltaic piecewise linearization

s	$P_{s,lo}$ (kW)	$P_{s,up}$ (kW)	$\kappa_{s,fixed}$ ($)	$\kappa_{s,var}$ ($/kW)	$\theta_s{}^*$	ζ_s ($/kW)	ϕ_s
s_1	0	100	0	3400	1	52	12.5
s_2	100	400	33,862	3061	1	52	12.5
s_3	400	∞	135,572	2807	1	52	12.5

*Based on a lifespan of 20 years.

Wind Turbines

A variable speed wind turbine is used to harvest wind kinetic energy for onsite power production. The power output of the wind turbine is described by:

$$P_w(k) = f_w(k)P_{w,rated}\frac{\rho(k)}{\rho_{ref}} \qquad \forall\, k$$

where ρ is density of air as a function of temperature, ρ_{ref} is the density of air at 25^{o}C, and f_w is a fractional availability factor dependent upon the wind speed at the turbine's hub height. The air densities are found using the ideal gas law as this is a

good approximation over the relevant temperature range.

The fractional availability is described as a function of wind speed in the same way as Chapter 2. I.e., f_w is taken to be 0 below the cut-in wind speed and above the cut-out speed due to insufficient wind power available and to protect the turbine and generator equipment, respectively. f_w is a cubic function of wind speed between the cut-in and rated wind speeds, and is equal to 1 between the rated and cut-out wind speeds. The wind speed data in the TMY3 data is given at a height of 10-m. The wind speeds at the relevant wind turbine hub heights are then found using the common wind power law approximation:

$$v_w(k) = v_{ref}(k) \left(\frac{h_w}{h_{ref}} \right)^{1/7} \qquad \forall\, k$$

where the 1/7 scaling exponent is a good assumption when the topography around the turbine is not known in detail.

Parameter values for the wind turbine are shown in Table 3.3. Capital costs were derived based on a power law cost model with a scaling exponent of 0.8035 and a reference cost of $414,326 for a 100 kW system [44]. Note that larger wind turbines are associated with taller towers (and thus a higher hub height and faster wind speeds).

Table 3.2: Microturbine parameter values

m	Reference Unit	$P_{m,rated}$ (kW)	κ_m ($)	θ_m*	ζ_m ($/kW)	$\zeta_{m,start}$ ($)	ϕ_m	λ_m	$F_{m,fixed}$ (kW)	$F_{m,var}$
m_1	C30-LP	28	96,600	1	0.2	5	12.5	1.82	16.6	3.41
m_2	C65	62	164,775	1	0.2	10	12.5	1.72	33.2	3.08
m_3	C200-LP	190	484,400	1	0.2	30	12.5	1.45	90.7	2.75

*Based on a lifespan of 20 years.

Table 3.3: Wind turbine piecewise linearization

w	$P_{w,lo}$ (kW)	$P_{w,up}$ (kW)	$\kappa_{w,fixed}$ ($)	$\kappa_{w,var}$ ($/kW)	θ_w*	ζ_w ($/kW)	ϕ_w	h_w (m)	v_{ci} (m/s)	v_r (m/s)	v_{co} (m/s)
w_1	0	50	0	4748	1	55	12.5	30	3	12	25
w_2	50	100	60,456	3539	1	35	12.5	40	3	12	25
w_3	100	200	105,516	3088	1	30	12.5	50	3	12	25
w_4	200	400	184,160	2695	1	30	12.5	60	3	12	25
w_5	400	1000	346,602	2289	1	30	12.5	70	3	12	25
w_6	1000	∞	671,150	1964	1	30	12.5	80	3	12	25

*Based on a lifespan of 20 years.

Table 3.4: Boiler parameters

Parameter	**Value**	**Parameter**	**Value**
κ_e (\$/kW)	70	κ_n (\$/kW)	70
${\theta_e}^*$	1.3	${\theta_n}^*$	1.3
ζ_e (\$/kWh)	0.0075	ζ_n (\$/kWh)	0.0075
ϕ_e	12.5	ϕ_n	12.5
η_e	0.9	η_n	0.85

*Based on a lifespan of 16 years.

Boilers

As before, electric and gas-fired boilers are modeled as simple, constant efficiency energy conversion units:

$$0 \leq Q_e(t) \leq Q_{e,rated} \qquad \forall\, k$$

$$P_e(k) = Q_e(k)/\eta_e \qquad \forall\, k$$

$$0 \leq Q_n(k) \leq Q_{n,rated} \qquad \forall\, k$$

$$F_n(k) = Q_n(k)/\eta_n \qquad \forall\, k$$

The parameter values for the boilers are shown in Table 3.4.

Battery Bank

A lead-acid battery bank is used to shift excess electricity production to times when it is needed. The storage level propagation of the battery is given by:

$$E_b(k) = E_b(k-1) + \eta_c P_c(k) - P_d(k)/\eta_d \qquad \forall\, k$$

$$0.2E_{b,max} \leq E_b(k) \leq E_{b,max} \qquad \forall\, k$$

where the storage level in the battery is constrained to stay between 20% and 100% of the capacity since deep discharges can damage battery lifespan. In addition, charge and discharge rates are now constrained to be below 10% of the battery capacity per hour

Table 3.5: Battery parameters

Parameter	**Value**	**Parameter**	**Value**
κ_b (\$/kWh)	150	ζ_b (\$/kWh)	0.00143
${\theta_b}^*$	1.43	ϕ_b	12.5
η_c	0.9	η_d	0.95

*Based on a lifespan of 5 years.

to prevent temperatures spikes which could damage the battery bank:

$$P_c(k) \leq 0.1 E_{b,max} \qquad \forall\, k$$

$$P_d(k) \leq 0.1 E_{b,max} \qquad \forall\, k$$

Nonlinearities in battery efficiency due to rapid charging and discharging are not accounted for since the rate of power exchange is kept low. Similarly, nonlinearity in the discharging efficiency at low capacity is not accounted for since the battery level is constrained to stay above 20% of the rated capacity.

Thermal Storage

Thermal storage is used to shift excess heat production to times when it is needed. The unit is modeled based on a generic hot water storage tank. The storage level of the thermal storage is given by:

$$E_h(k) = E_h(k-1) + Q_{h,in}(k) - Q_{h,out}(k)/\eta_h \qquad \forall\, k$$

$$0 \leq E_h(k) \leq E_{h,max} \qquad \forall\, k$$

The parameter values for thermal storage unit are shown in Table 3.6. A constant roundtrip efficiency is used for this unit since fluid dynamics modeling to capture the degree of thermal stratification across the tank as a function of time would render the optimization problem computationally intractable.

Table 3.6: Thermal storage parameters

Parameter	**Value**	**Parameter**	**Value**
κ_h (\$/kWh)	10	ζ_h (\$/kWh)	0.0137
${\theta_h}^*$	1	ϕ_h	12.5
η_h	0.6		

*Based on a lifespan of 20 years.

3.2.2 Energy Balances

At each hour, supply and demand from both heat and power must be matched through DER generation, energy transfers to and from local storage, power transfers to and from the macrogrid, and exhausting of heat to the surrounding environment. These energy balance requirements can be expressed as:

$$\sum_m P_m(k) + \sum_s P_s(k) + \sum_w P_w(k) + P_d(k) + P_{grid}(k) = P_\ell(k) + P_c(k) + P_e(k) + P_{spill}(k) \qquad \forall\, k$$

$$\sum_m Q_m(k) + Q_e(k) + Q_n(k) + Q_{h,out}(k) = Q_\ell(k) + Q_{h,in}(k) + Q_{spill}(k) \qquad \forall\, k$$

In addition, as in Chapter 2, a minimum autonomy level may be enforced:

$$\sum_k \left(\sum_m P_m(k) + \sum_s P_s(k) + \sum_w P_w(k) \right) \geq \mathcal{A}_{min} \sum_k \left(\sum_m P_m(k) + \sum_s P_s(k) + \sum_w P_w(k) + P_{grid}(k) \right)$$

where $\mathcal{A}_{min}$ is the minimum autonomy level parameter. The optimization results are analyzed for different locations, load shapes, and values of the $\mathcal{A}_{min}$ parameter.

3.2.3 Locations and Load Shapes Considered

The design optimization is performed for combinations of 16 different locations and 6 different load shapes. The 16 different locations considered are representative cities in the U.S. for various climate zones used in building simulations. The cities used are shown

Table 3.7: Comparison of cities considered in the MILP optimization study. Cooling and heating degree days based on a 65 ^{o}F basis. Mean insolation given for a horizontal plane. Mean wind speed given for 10-m above ground level.

City	Cooling Degree Days (^{o}F)	Heating Degree Days (^{o}F)	Mean Insolation (W/m^2)	Mean Wind Speed (m/s)	Electricity Tariff (¢/kWh)	Natural Gas Tariff (¢/kWh)
Miami, FL	4292	236	200	4.12	10.25	3.97
Houston, TX	3017	1686	185	3.44	8.00	2.60
Phoenix, AZ	4847	1254	239	2.76	9.55	3.03
Atlanta, GA	1930	3034	192	4.04	10.47	3.37
Los Angeles, CA	506	1489	208	3.36	13.57	2.53
Las Vegas, NV	3469	2482	231	4.46	8.86	2.37
San Francisco, CA	209	3191	196	4.67	13.57	2.53
Baltimore, MD	1368	4735	169	3.92	12.32	3.59
Albuquerque, NM	1449	4509	226	3.90	9.94	2.40
Seattle, WA	290	4950	141	3.75	8.01	3.53
Chicago, IL	1014	6497	161	4.56	8.69	2.79
Boulder, CO	938	6216	189	3.71	9.75	2.61
Minneapolis, MN	891	7856	160	4.59	9.50	2.45
Helena, MT	559	7898	167	3.25	9.21	2.92
Duluth, MN	307	9710	153	4.63	9.50	2.45
Fairbanks, AK	156	13145	108	2.46	16.73	3.02

in Table 3.7 along with basic climatological data and the prices used for electricity and natural gas. The cooling degree days and heating degree days are representative of the annual cooling and heating energy loads, respectively. True heating and cooling loads are affected by other variables, such as occupancy and internal heat generation, but these values show the relative difference in HVAC loads between the various locations. The average insolation and wind speed give an indication of the relative abundance of renewable fuel sources for each location.

The 6 load shapes considered are shown in Table 3.8. These different load shapes represent 6 out of the 16 DOE commercial reference buildings. The different building types vary both in the magnitude and consistency of their energy demands. Some buildings exhibit strong seasonal, weekly, and diurnal patterns in power load (e.g. the secondary school), while others have a more constant load profile (e.g. the hospital). Rather than

Table 3.8: Comparison of energy demands in load shapes considered. Values shown are for Albuquerque, NM.

Load Type	Mean Power Demand (kW)	Power Demand Coefficient of Variation	Mean Heat Demand (kW)	Heat Demand Coefficient of Variation
Hospital	987	0.22	311	0.38
Large Office	670	0.60	51	2.62
Secondary School	328	0.76	131	2.40
Large Hotel	270	0.28	246	0.59
Supermarket	184	0.40	66	1.43
Outpatient Healthcare	163	0.42	87	0.38

try to quantify these phenomena occurring at different time scales, a simplified metric, the coefficient of variation (CV), is shown in Table 3.8. A higher coefficient of variation indicates that the load profile will exhibit larger peaks or larger seasonal variation which might impact the sizing of DER units. In addition, the various building types exhibit different ratios between their heat and power demands which could effect the performance of different DER technologies, especially those that rely on cogeneration.

3.3 Microgrid Design Optimization Results

The resulting MILP was formulated in GAMS and solved with CPLEX 12 to within a relative optimality gap of 1%. The model consists of 271588 equations, 210262 continuous variables, and 52572 integer/binary variables. First, reference case values were determined based on the energy supply cost without local power generation. Then, the full MILP design problem was solved for each pair of location and load shape at minimum autonomy levels ranging from 0 to 100% in 5% increments.

3.3.1 Reference Case

A reference case is used to normalize the energy supply cost and annual CO_2 emissions to make comparisons among the various locations and load shapes easier. In this reference case, all power is purchased from the macrogrid and heat is only generated by the

natural gas boiler. Annual CO_2 emissions are calculated based on the amount of power purchased from the macrogrid and the amount of natural gas consumed by the boiler. The macrogrid is assumed to have constant efficiency and an emission rate of 0.575 tons CO_2/MWh. Each MWh of natural gas consumed locally contributes 0.202 tons of CO_2 (based on assumptions of complete combustion and a heating value of 9.83 kWh/m^3).

The numerical results for energy supply cost and annual emissions in this reference case are available in 3.7.1. In the following sections, energy supply cost and annual emissions are normalized by the reference case values:

$$\text{Relative cost } = \frac{Capex + Opex}{Capex_{ref} + Opex_{ref}} = \frac{Cost}{Cost_{ref}}$$

$$\text{Relative emissions } = \frac{\text{Annual emissions}}{\text{Annual emissions}_{ref}}$$

Annual emissions are calculated in the same way, but natural gas is consumed by microturbines as well as the gas-fired boiler. This normalization is performed so that the interpretation of results is not skewed by the fact that locations and load shapes with higher demands inherently have higher costs and emission levels.

3.3.2 Impacts of Location Selection

Relative Cost

Fig. 3.2 shows the relative cost vs. autonomy level results for the hospital load in all the cities. Note that not all of the curves extend all the way to 0% autonomy. In these cases, even when there is no minimum autonomy required, some level of local power generation is able to achieve a lower energy supply cost than the reference case. This level of local power generation which results in the lowest possible cost is referred to as the optimal autonomy level, $\mathcal{A}_{opt}$.

For each location, the average value of $\mathcal{A}_{opt}$ over all load shapes is shown in Table 3.9. There is a general trend that as the heating requirements of the location increase (more heating degree days), the optimal autonomy level increases. This is because locations with high heating requirements are able to effectively use cogeneration from microturbines. In climates with relatively low heating requirements, the microturbines' value is based primarily on their power production since the amount of heat recovered exceeds

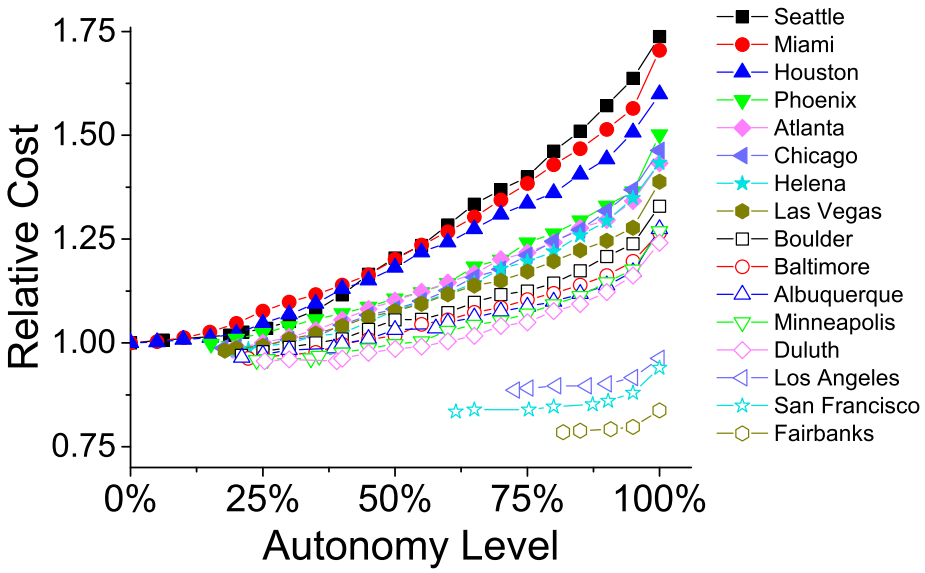

Figure 3.2: Relative cost vs. autonomy level for the hospital load in all cities considered.

local demand. This is not cost competitive since large utility plants have economies of scale working in their favor. Even in cold climates, as the usage of microturbines rises, much of their usable heat output is wasted (due to mismatches between the magnitude and timing of heat and power demands) and the relative cost increases. Distributed wind and PV are not used as the primary source of power since they are still more expensive than thermal generation.

Another important factor is the regional pricing of electricity and natural gas. For example, the two California locations exhibit a high $\mathcal{A}_{opt}$ and low relative cost despite their relatively low heating requirements because the cost of electricity relative to natural gas is substantially higher than other locations. Thus, even though the utilization of microturbine heat output is very low, it can be cheaper to generate electricity locally via natural gas combustion than to buy it from the macrogrid. Similarly, Seattle and Chicago exhibit a lower than expected $\mathcal{A}_{opt}$ since the electricity tariff is relatively low. In these cases, the heating cost saved through cogeneration does not offset the increased cost of local power generation. Miami and Seattle exhibit the highest relative cost since they have the largest ratios of natural gas tariff to electricity tariff. As a final note,

Table 3.9: Optimal autonomy level for all cities considered (mean over all load shapes).

City	Mean $\mathcal{A}_{opt}$ (%)	City	Mean $\mathcal{A}_{opt}$ (%)
Miami	2.8	Albuquerque	20
Houston	0	Seattle	0
Phoenix	5.4	Chicago	6.6
Atlanta	6.7	Boulder	20
Los Angeles	51	Minneapolis	22
Las Vegas	6.5	Helena	21
San Francisco	60	Duluth	22
Baltimore	19	Fairbanks	85

there is no strong correlation observed between the amount of renewable fuel sources (wind and insolation) and the relative cost or optimal autonomy level.

Incorporation of Renewables

Fig. 3.3 shows the mean contribution of renewable power in each city considered. When natural gas is cheaply available, microturbines are favored over renewables for providing local power. This can be easily seen by comparing Miami and Albuquerque. There is only a ∼3% difference in the price of electricity in the two cities and Albuquerque actually has a higher mean insolation. However, Miami uses more than 3x more solar power than Albuquerque in the optimization results. Albuquerque relies primarily on microturbines for satisfying the required local power production since its natural gas tariff is substantially lower (about 40% less than Miami's).

In general, the utilization of wind and solar power remains very low due to the high cost of distributed renewables. In many cases, renewables are used to provide a small increase in local power production to satisfy the minimum autonomy constraint. Microturbines are not well suited to this task since they are only available in discrete capacities which may exceed the amount needed. If the $\mathcal{A}_{min}$ parameter is increased further, it often becomes economical to forgo renewables in favor of the microturbine (as the full capacity will now be utilized). This can be seen in Fig. 3.4 which shows the technology selection and microturbine capacity of the optimal design as a function of the $\mathcal{A}_{min}$ parameter. Note the discontinuities in renewables contribution which correspond to an increase in installed microturbine capacity.

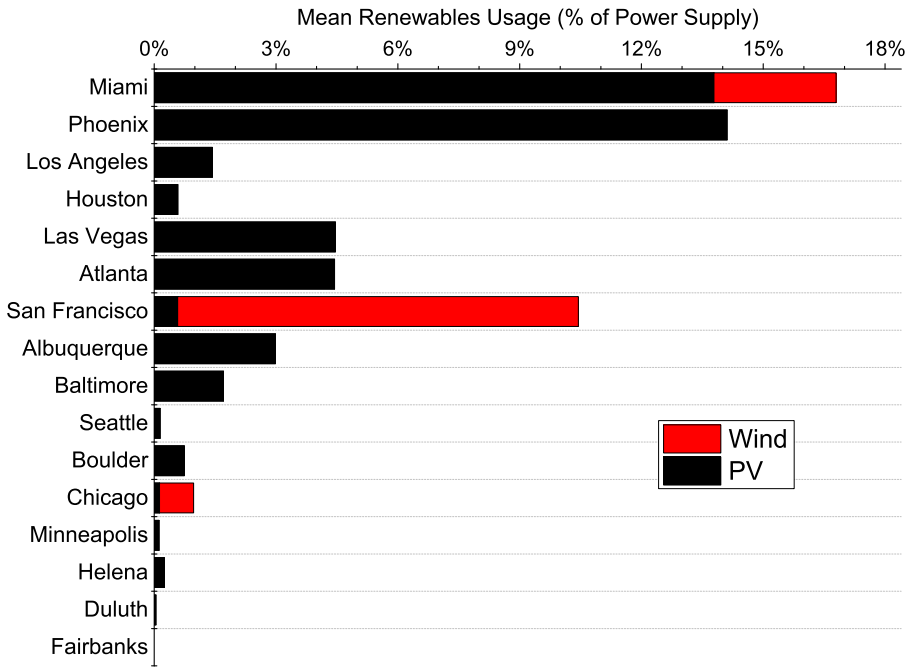

Figure 3.3: Mean utilization of renewables for each city across all load shapes and minimum autonomy levels considered.

Moreover, small capacities of renewables are generally favored because their power can be entirely used when it is generated. At higher rated powers, the excess output must either be wasted or shifted to other time periods through the use of expensive battery storage. In 95% of the cases considered, the battery capacity was less than 300 kWh due to this high cost. In such cases, less than 30 kWh of excess energy can be stored each hour due to the charging rate constraints.

San Francisco is the only city where incorporation of renewable power is selected when there is no minimum autonomy requirement. For the hospital and large office loads in San Francisco, wind power is used to satisfy about 28% of the power supply. This preference for renewable power is due to the high cost of purchasing electricity in California and the relative abundance of wind energy in San Francisco. Usage of renewable power is not optimal in other locations with similar wind potential (e.g. Minneapolis, Chicago, and Las Vegas) since the cost of electricity is at least 30% lower. In addition, wind power is not used in Los Angeles (where electricity prices used are

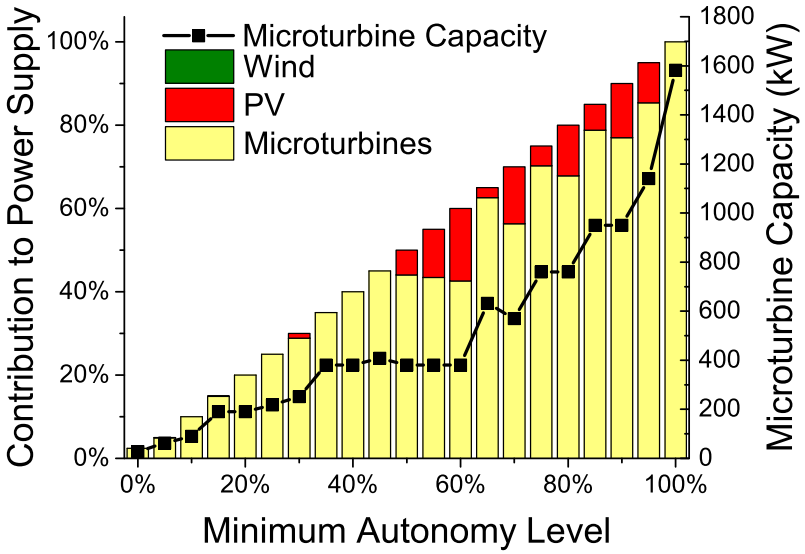

Figure 3.4: Power supply breakdown for a large office in Baltimore showing total microturbines installed capacity.

identical to San Francisco) due to its lower wind speeds. Despite the generally sunny climate of California, wind power is favored over PV in this case since its capital cost is 8-10% cheaper at the relevant capacities (750-1000 kW).

No public policy initiatives or constraints have been considered in this chapter since they vary significantly with location. The introduction of public policy measures such as emissions taxation, renewables incentives, and emission reduction requirements can affect the utilization of renewables and overall economics of microgrids as was discussed in Chapter 2.

Emission Levels

The strong correlation between renewables utilization and relative emissions level is shown in Fig. 3.5. However, as noted in the previous section, the utilization of renewables is often a discontinuous function of the minimum autonomy level for a given location. This naturally results in discontinuous patterns in relative emissions, as shown in Fig. 3.6. These discontinuities make it difficult to identify other trends, for example

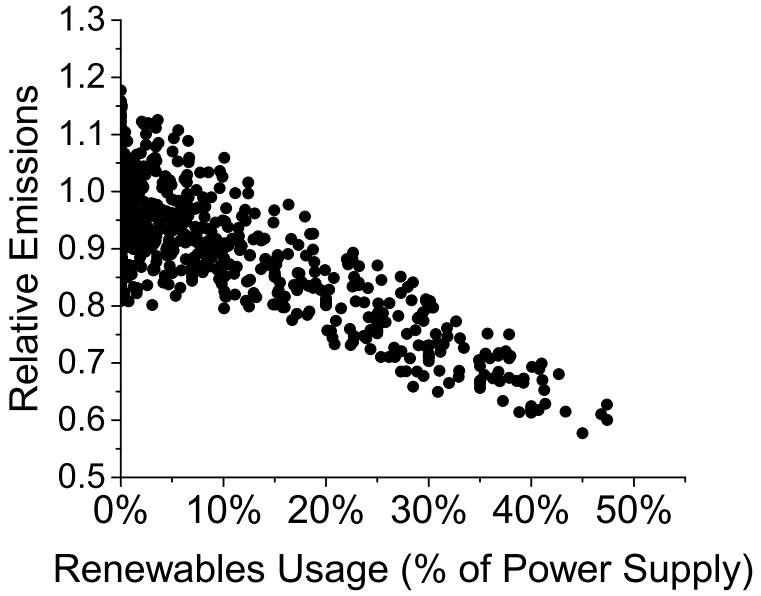

Figure 3.5: Relative emissions versus renewables usage across all optimization results.

the impact of microturbine usage on emissions levels.

Locations where there is little incorporation of renewables, such as Houston and Duluth, can be used to help analyze these other trends. Fig. 3.7 compares the relative emission results versus autonomy level for a hospital load in these two cities (note: the contribution or renewables did not exceed 2% in any of the results shown in this graph). In both cases there is an initial decrease in the CO_2 emissions as combined heat and power output of the microturbines is fully utilized. Above some critical autonomy level, the emissions begin to rise as additional heat output is no longer utilized (note the absence of dedicated natural gas boilers at high autonomy levels). As observed by other authors (e.g. [56]), cogeneration is able to reduce environmental impact more in colder climates due to the presence of larger heating loads. However, the inferred relationship between thermal demands and environmental impact cannot be blindly relied on. Fig. 3.8 shows the relative heat demand versus the autonomy level at which minimum emissions are achieved for all the locations and load shapes considered. One would expect a strong positive correlation in this data based on the above arguments, but this does not generally hold due to the complex relationship between optimization

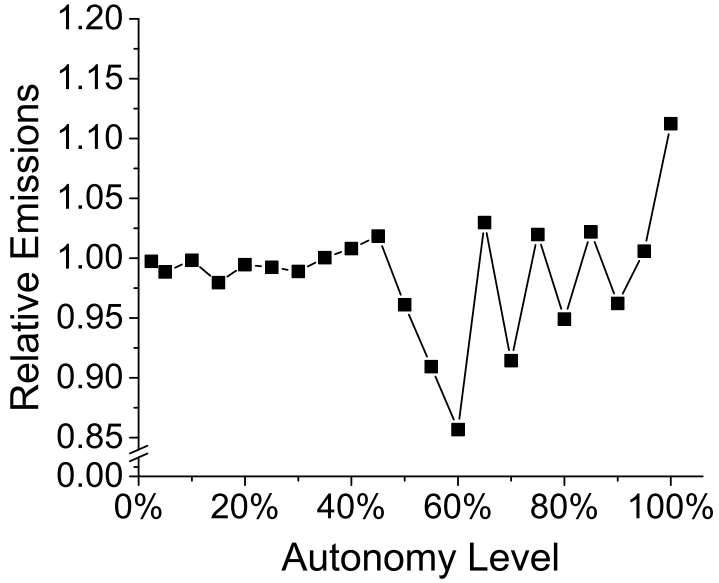

Figure 3.6: Relative CO_2 emissions for a large office in Baltimore.

inputs and resulting design. These potential pitfalls are hard to observe in previous works due to their limited scope.

3.3.3 Impacts of Load Shape

Relative Cost

Fig. 3.9 shows the relative cost curves for all 6 loads shapes in Albuquerque, NM. The cost is lowest for the large hotel as it has the highest ratio of heat to power demand as well as low variability in both heat and power loads. This allows the microgrid to use microturbines as a cheap and effective alternative to grid power. The hospital and outpatient facility also have a non-zero optimal autonomy level and lower cost due to the low variability in the power load, but are not as cheap as the hotel since they do not have large heat loads.

The supermarket and outpatient facility have a similar CV in power loads, but for the supermarket has a higher relative cost at low autonomy levels since the heat load CV is higher. This variability makes it difficult to coordinate microturbine cogeneration with

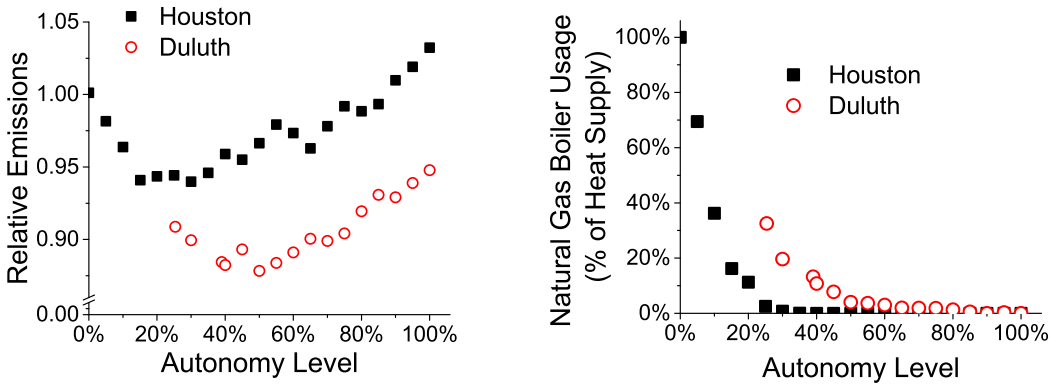

Figure 3.7: Comparison of relative emission levels (left) and dedicated natural gas heating (right) for the hospital load in Houston and Duluth.

both heat and power loads, so they are not as effective in offsetting heat demand and the relative cost is higher. As the autonomy level approaches 100%, the microturbines produce a significant excess amount of usable heat and coordination of heat and power generation is no longer an issue. At this limit, the relative cost for the supermarket and outpatient facility are very close.

The relative cost is highest for the large office and secondary school since they have a large CV for both demands, so DERs must be have a much larger capacity to cover the resulting peaks in heat and power loads. Similar results are observed in the other locations considered.

Incorporation of Renewables

Fig. 3.10 shows the average incorporation of renewables for each load shape. The utilization of renewable power tends to be higher when the ratio of heat demand to power demand is low (since cogeneration is not advantageous). Indeed, the order of heat-to-power ratios for the different load shapes is:

Hotel > Outpatient Facility > Secondary School > Supermarket > Hospital > Office

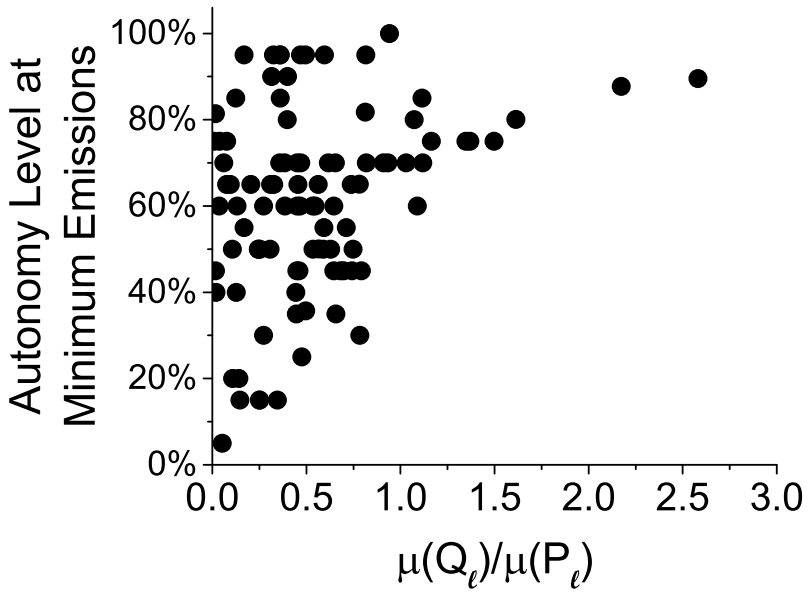

Figure 3.8: Comparisson of the autonomy level at which the minimum emissions are observed versus the ratio of average heat demand to average power demand across all optimization results.

and the order of mean renewables usage is:

Hotel < Outpatient Facility < Supermarket < Secondary School < Hospital < Office

This relationship can be explored further by examining the results for the different load shapes in a couple of cities as shown in Fig. 3.11a. The relationship between mean renewables usage and relative heat load appears to be approximately linear, but the slope and intercept are affected by other inputs such as climate and natural gas pricing. While this trend works well for describing the average utilization of renewables over multiple autonomy levels, it breaks down for individual optimization results due other factors (e.g. discrete microturbine capacities). For example, see Fig. 3.11b which shows the renewables contribution at multiple autonomy levels for 3 of the load shapes in Atlanta.

Wind power is only used in the two load shapes with the largest annual power demands (the hospital and large office). This is due to the use of piecewise linear cost

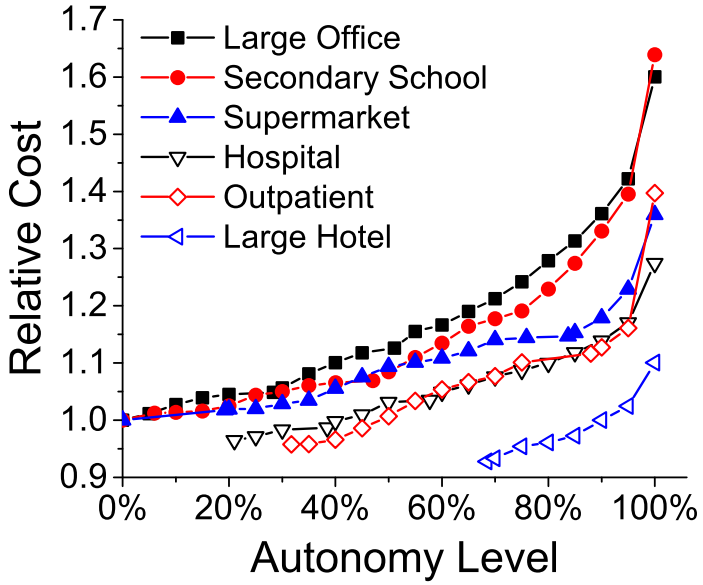

Figure 3.9: Relative cost versus autonomy level for all load shapes in Albuquerque, NM.

functions for the renewable units. Solar photovoltaics have a lower marginal capital cost (per rated kW) than wind turbines at small capacities. However, due to their modularity, PV does not benefit much from economies of scale, and the marginal cost does not go down significantly at large unit sizes. Wind turbines, on the other hand, do benefit from economies of scale at large unit sizes, and thus are more economical at high rated powers. Wind turbines with high rated powers also tend to utilize higher towers and therefore experience a higher average wind speed. These phenomena result in PV being used across a broad range of unit sizes, but wind only being installed at capacities above 550 kW in the optimization results. Thus, wind power is better suited to serve loads with larger power demands, such as the hospital and large office. As an aside, other parameters (such as the availability of renewable fuel sources and correlation between renewable availability and electrical load) also affect which, if any, renewable technology is selected in the microgrid optimal design.

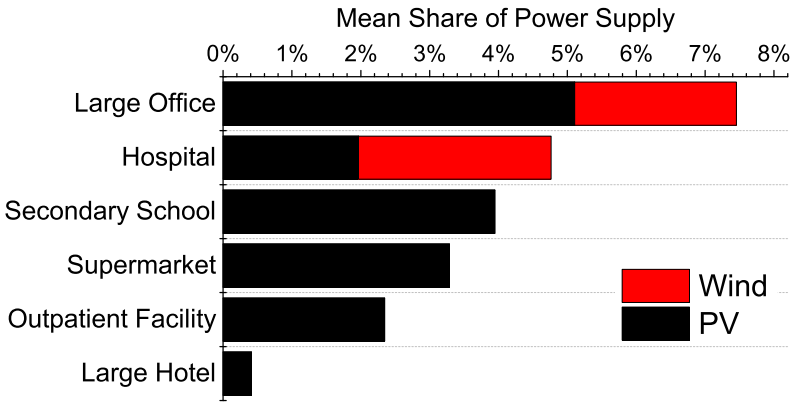

Figure 3.10: Mean utilization of renewables for each load shape.

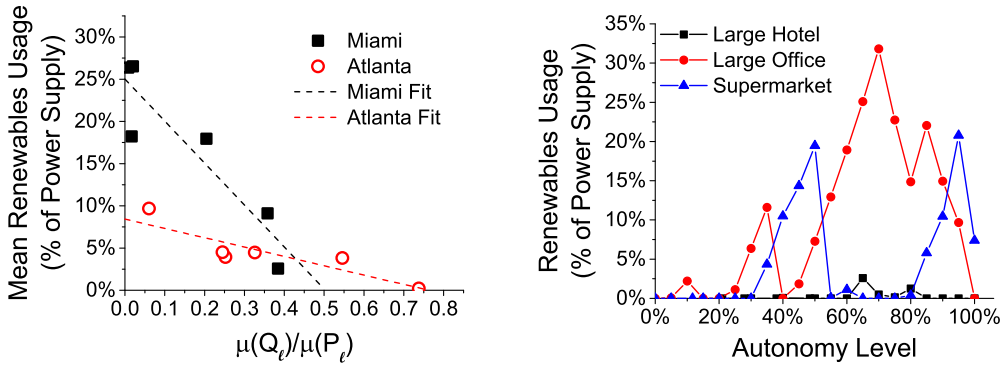

(a) (b)

Figure 3.11: (a) Mean utilization of renewables versus the ratio of heat to power demands in Miami and Atlanta, and (b) renewable utilization versus autonomy level for 3 load shapes in Atlanta.

Emissions Levels

Fig. 3.12 shows how the relative emissions vs. autonomy level curves vary for the 6 loads considered. The curves in this figure show the average results over all 16 cities. The hotel has the lowest emission levels and the large office, supermarket, and secondary school have the highest emission levels. This is largely due to the differences in the

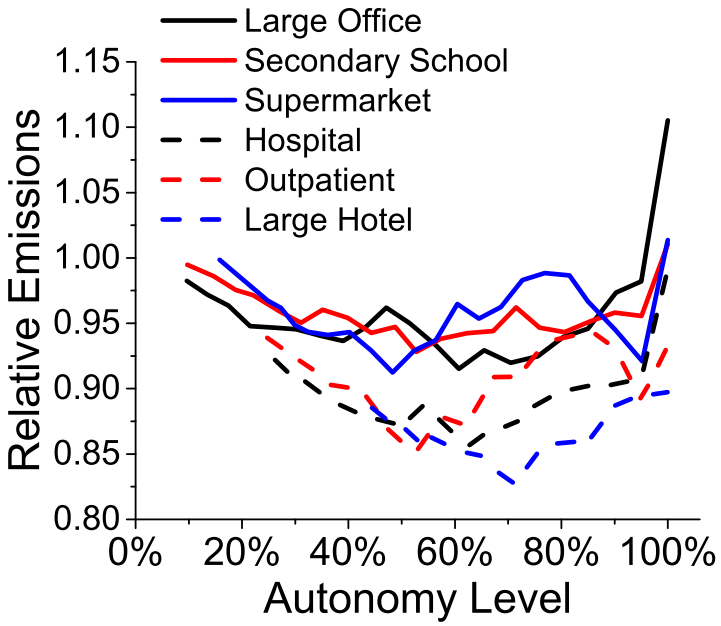

Figure 3.12: Relative emissions versus autonomy level for all load shapes (mean over all cities for each minimum autonomy level).

consistency of heat and power demands. When demand levels are relatively constant, microturbines can be more easily operated close to their rated power where they have a higher fuel efficiency. The ratio between heat and power demands also plays a role in emission levels as discussed previously. Thus, the large hotel, which has the largest ratio of heat to power demand, has the lowest relative emissions.

The trends in emission levels are not nearly as smooth as the trends in relative cost due to the discontinuities in installed renewable capacity as discussed in Section 3.3.2. The results are even noisier when examining the results for a particular location rather than the averaged results shown in Fig. 3.12. Therefore, it is very difficult to come up with an analytical relationship describing how these emission levels depend on the location and load shape chosen.

3.4 ANN Method for Predicting Design Results

3.4.1 Proposed Method

Parameters that depend on location and load shape (such as natural gas price) have a strong impact on microgrid optimal design. The results and analysis in the previous section provide a more complete investigation of these trends than any previous work. However, quantification of the trends is difficult due to the number of inputs and constraints in the optimization. This quantification is of interest as it allows one to make predictions about microgrid optimal design, determine dominant factors in the design, and quickly identify interesting parameter spaces for future research endeavors. To this end, machine learning techniques have been used to analyze the results and fit the relationship between the optimization inputs and the resulting design. In particular, the remainder of this chapter will focus on using ANNs to predict the optimal autonomy level, relative cost, relative emissions, and renewables contribution.

The following parameters are used to predict the optimal design values:

- Average wind speed
- Average insolation
- Electricity tariff
- Natural gas tariff
- Coefficient of variation in power load
- Coefficient of variation in heat load
- Ratio of overall heat to power demand

This approach reduces the microgrid design problem from one with ∼10,000 inputs to one with ∼10 inputs. A heuristic process which can accurately relate these 7 inputs to microgrid design results should be able to solve much faster than traditional optimization techniques like MILP and genetic algorithms. In addition, this allows microgrid design and performance to be predicted when detailed inputs (e.g. hourly load values) are not readily available. This is particullarly useful as many situations where microgrids would

be most useful (e.g. remote regions or developing nations) are also cases where detailed hourly data is unlikely to be available.

The proposed prediction procedure is shown in Fig. 3.13. This can be described briefly as a sequence of 5 steps:

1. The optimal autonomy level is predicted based on the 7 inputs listed above.
   (a) This $\mathcal{A}_{opt}$ value is saturated to the feasible region of 0-100% since there will inherently be imprecisions in the heuristic fitting.
   (b) This $\mathcal{A}_{opt}$ value is reduced if the relative cost is predicted to ¿1.
   (c) If the proposed $\mathcal{A}_{opt}$ is sufficiently small, it is simply set to 0 (i.e. the reference case is economically optimal).
2. The specifies an autonomy level (or vector of autonomy levels) between $\mathcal{A}_{opt}$ and 100%.
3. The relative cost is predicted based on 7 design inputs and the specified autonomy level.[4]
4. The contribution of renewable power is predicted based on the autonomy level, relative cost, and design inputs.
5. The relative emissions are predicted based on the autonomy level, renewables contribution, and a few of the design inputs.

An ANN is used for each prediction in the procedure described. The size of the various ANNs and the RMS error between the true optimization output and the predicted values are shown in Table 3.10. All ANNs were trained using Bayesian regulation backpropagation and the number of neurons was kept small to prevent the ANNs from overtraining so that results would generalize well without overfitting of the sample points [62].

3.4.2 Performance

Since the prediction process is sequential (cost is used in the prediction of renewables contribution, and renewables contribution is used in the prediction of emissions) an

[4]Note that the same ANN is used for this step and when checking the relative cost at $\mathcal{A}_{opt}$ in step 1.

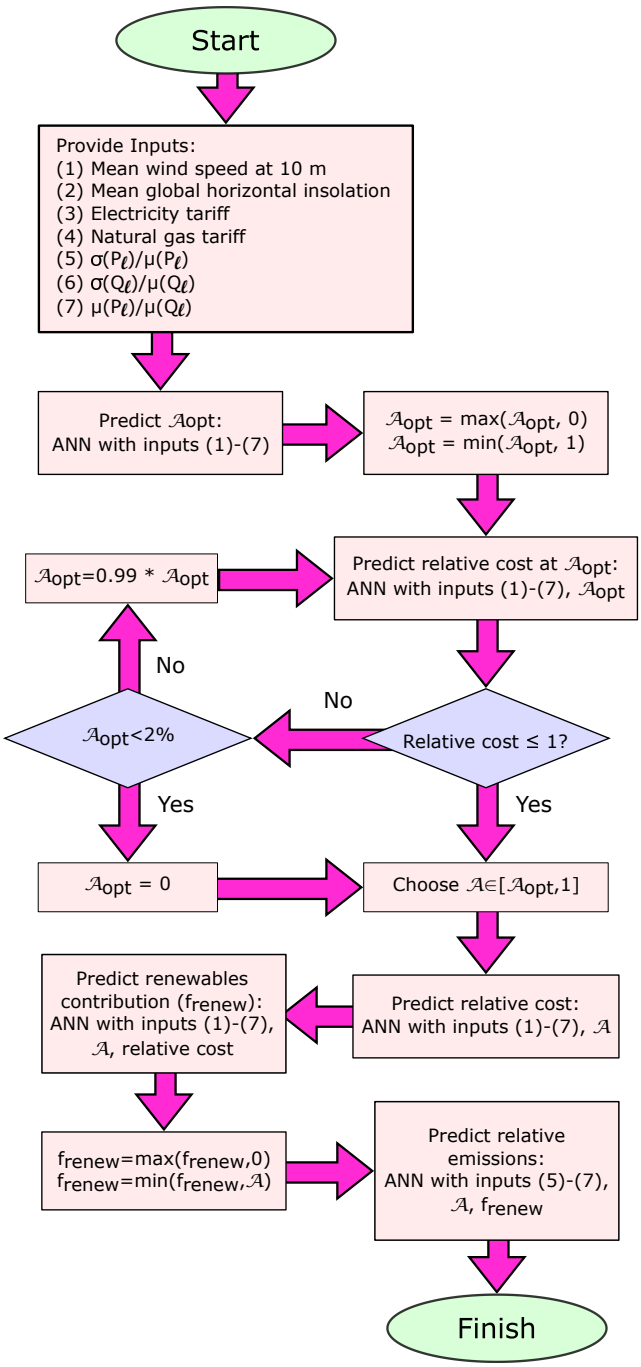

Figure 3.13: Prediction process for relative cost, relative emissions, and renewables penetration in microgrid designs.

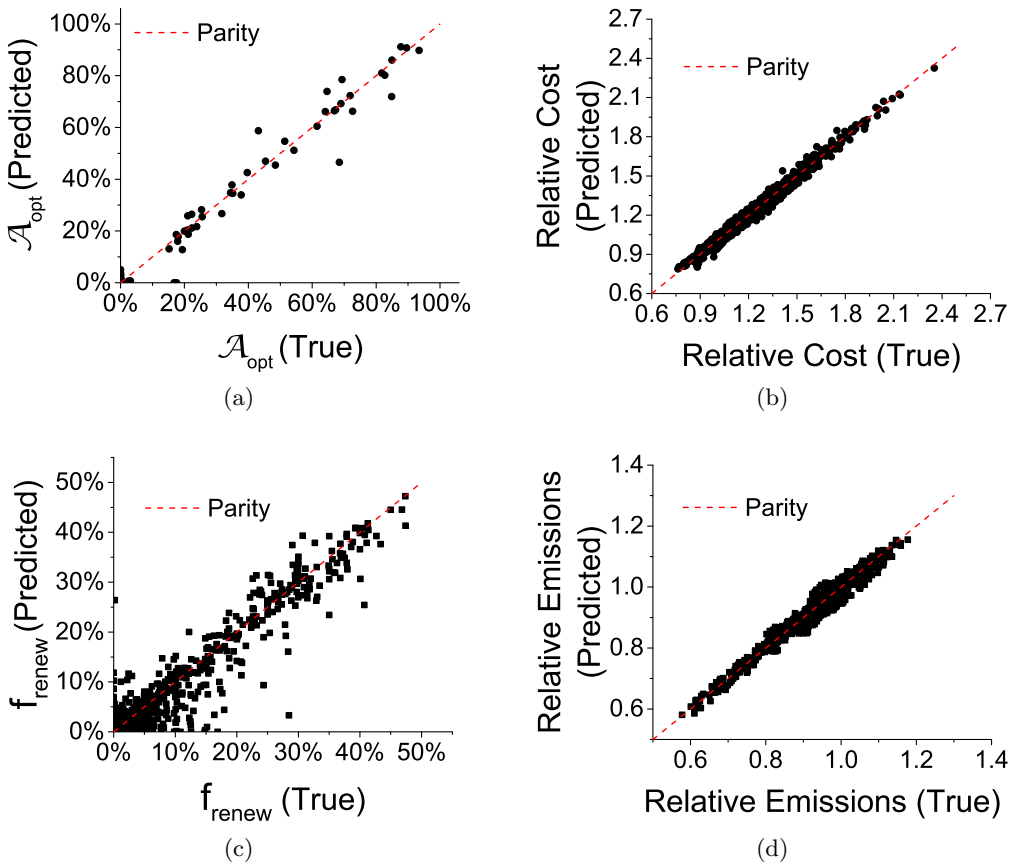

Figure 3.14: Parity plot of ANN output versus true optimization results for (a) optimal autonomy level, (b) relative cost, (c) renewables penetration, and (d) relative emissions.

error in an early step will be propagated forward. Fig. 3.14 shows the accuracy of each individual step in the process. For this figure, the true values (MILP results) are used as inputs to the ANN for predicting renewables contribution. Similarly, the true values of renewables contribution are used as inputs to the ANN for predicting relative emissions. As the figure shows, the largest errors are introduced when predicting the optimal autonomy level and the amount of power that is generated via renewables.

The difficulty in accurately predicting the optimal autonomy level is primarily due to the small dataset available for training (since there is only one optimal autonomy level for each pair of location and load shape). An ANN trained using this small dataset

Table 3.10: Size and performance of ANNs used in the prediction procedure. The values in parenthesis show the RMS error when predicted relative cost and renewables contribution are used rather than true values.

Value Predicted	# of Hidden Layers	# of Neurons per Hidden Layer	RMS Error	
Optimal Autonomy Level	2	3	0.046	
Relative Cost	2	3	0.026	
Renewables Contribution	2	10	0.023	(0.036)
Relative Emissions	1	3	0.018	(0.040)

is not able to fully capture the complexity of the MILP design problem, but there is a strong correlation between the MILP results and predicted values, indicating that it is able to describe the trends. Another potential factor in these errors is the shallowness of the relative cost versus autonomy curve close to the optimal autonomy level. This shallowness means that the optimal cost is relatively insensitive to the optimal autonomy level, allowing significant error in a heuristic fitting procedure such as this one.

The failure of the ANNs to adequately forecast the contribution of renewables is due to the discontinuities in installed renewables capacity and the small number of optimization samples with a significant renewables contribution. In 66% of the optimization results there is no utilization of renewable power and in an additional 21% of the results renewables contributed less than 10% of the annual power. One way to tackle these challenges would be to simply use a larger data set to train the ANNs. Alternatively, one could consider a different objective function (e.g. a multiobjective optimization to minimize cost and emissions) which would result in considerably more sample results that use renewables and lead to a better ANN for such predictions.

Fig. 3.15 shows the relative cost curve generated by the heuristic process and the true optimization results for Albuquerque and Fairbanks. In most cases, the ANN prediction matches very well with the true optimization results as seen in Albuquerque. One may note the discrepancy between the optimal autonomy level predicted by the heuristic process (lines) and the optimal autonomy level found by the MILP (symbols). Even when there are errors in this value, the heuristic process accurately predicts the trends in optimal autonomy level, the shape of the autonomy versus cost curve, and the optimal

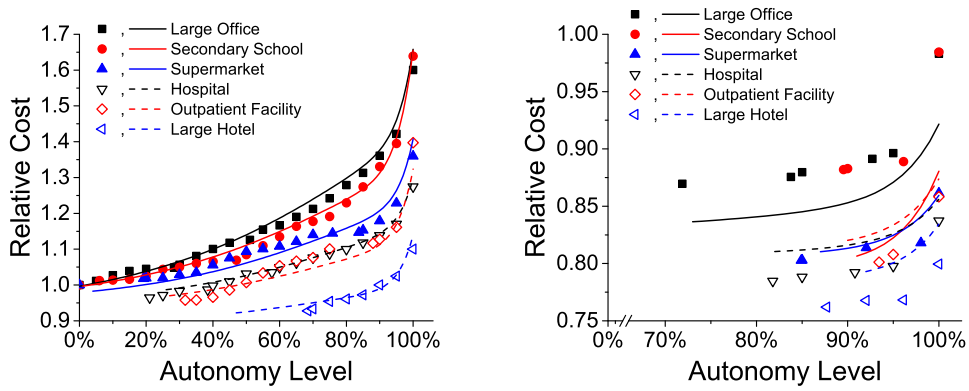

Figure 3.15: Optimization results (symbols) and ANN prediction (lines) of autonomy level vs. relative cost for Albuquerque (left) and Fairbanks (right).

cost. Fairbanks is an exception and showcases a poor fit due to the limited number of sample data points in the nearby parameter space. Fairbanks has substantially different location specific parameters than the other cities considered (e.g. electricity tariff 23% higher than next highest location, 35% more heating degree days than next highest location, etc.) since it is geographically isolated from the lower 48 states. In addition, the optimal autonomy level is very high for all loads in Fairbanks due to the expensive grid electricity and ample opportunity to utilize CHP in the cold climate. This leads to few actual data points ($\leq$7 for each load shape) for Fairbanks itself. Such problems can be mitigated through a rational choice of the locations and load shapes used in the sample optimizations. This ANN technique is useful for generalizing design parameters within the parameter space considered, but not reliable when extrapolating outside of the parameter space that was used for ANN training.

3.4.3 Predictions over Parameter Space

Figs. 3.16, 3.17, and 3.18 show plots for ANN predictions of relative cost, renewables utilization, and relative emissions, respectively. The input parameters for a hospital in Albuquerque, NM were used as nominal values when generating these figures. Further surface plots showing similar results expanded around other nominal values are available in Section 3.7.2. Note that Figs. 3.16 and 3.17 are only extended to the predicted optimal autonomy level, which may be $> 0\%$.

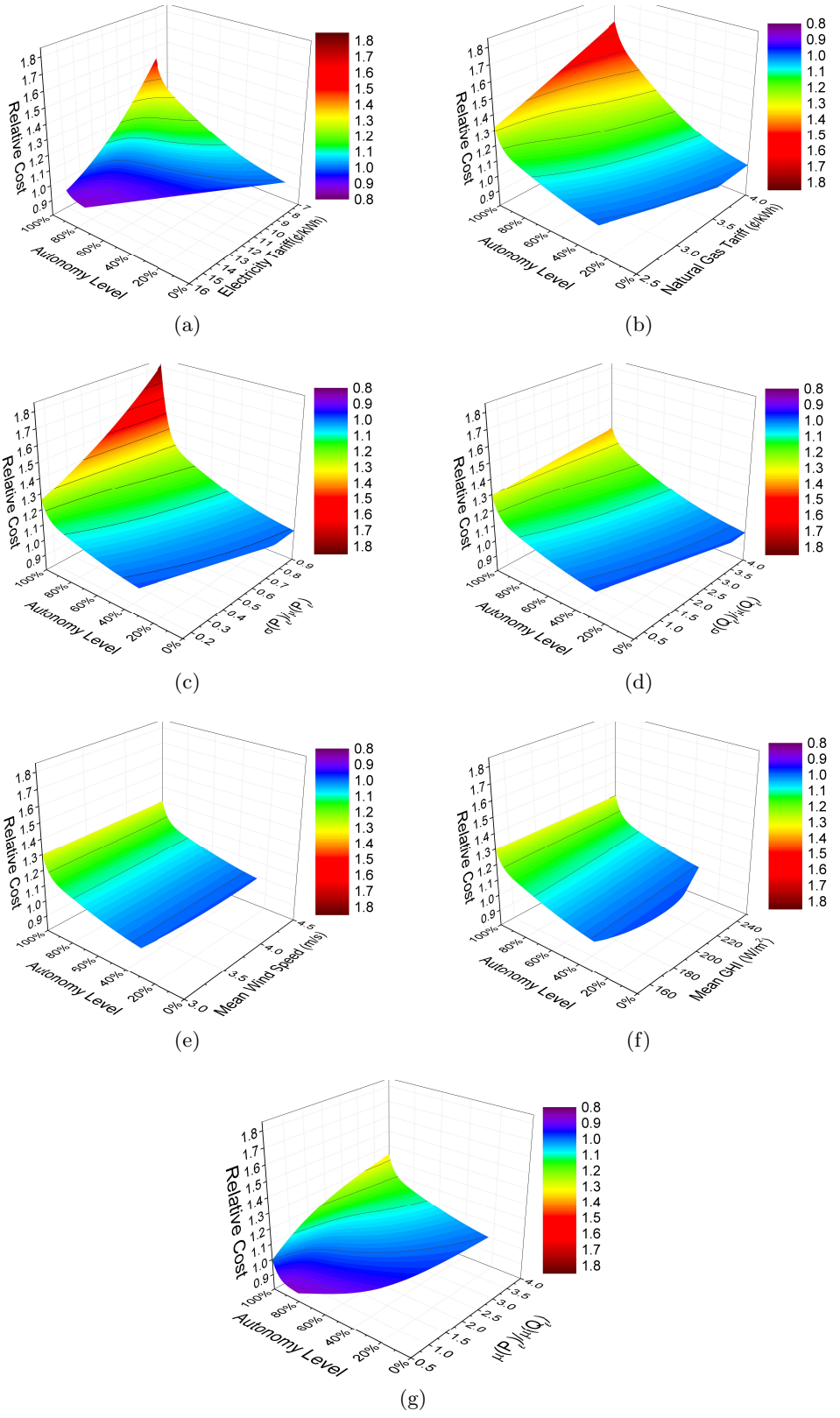

Figure 3.16: Surface plots showing predictions for relative cost. All values not shown on the X, Y axes are held at the nominal values for a hospital in Albuquerque, NM.

Fig. 3.16 shows that the electricity tariff, natural gas tariff, power load CV, autonomy level, and overall ratio of heat to power loads are the most important factors in determining the relative cost. The heat load CV has a more mild effect on relative cost, but is important in determining the optimal autonomy level. Meteorological parameters, i.e. average wind and insolation, are seen to have little impact on the shape of the relative cost surface. The availability of renewable fuel sources has such a small impact on this surface since distributed renewables are still relatively expensive and thus not likely to be able to minimize the energy supply cost when used as the primary source of local power. There is generally a sharp increase in the relative cost as the autonomy level approaches 100% due to the need for a large increase in local power and/or battery capacities to cover all of the peaks in the power load curve. This cost increase is of course worst when the coefficient of variation in the power load is very high as seen in the figure.

Fig. 3.17 shows contours of the projected contribution of renewables to the power supply. There are broad regions where the contribution of renewables is expected to be 0% with the occasional peak or plateau where it spikes up to 20-30% of total power generation. There is significant uncertainty in these predictions, again due to the sparsity of sample data with significant renewables incorporation, but one may note several promising trends in the predictions. Increased availability of wind and sun is seen to be positively correlated with predicted renewables usage. In addition, the usage of renewables is seen to taper off sharply as the autonomy level approaches 100%. This is also observed in the optimization results and is due to the enormous battery capacities that would be needed to shift power from times of peak renewable production to times of peak demand. It is much more economical to use a combination of dispatchable generation and smaller batteries to cover these peaks.

Fig. 3.18 shows contours of the projected relative annual emissions versus the contribution of the macrogrid, microturbines, and renewables to the power supply. As expected, the emissions level is most strongly dependent on the level of renewables incorporation. However, this heuristic procedure has also captured and disaggregated other trends observed in the optimization results. For example, when the magnitude of thermal loads is low, increasing the microturbine contribution (at constant renewables contribution) increases emissions, and vice versa. In addition, a more consistent

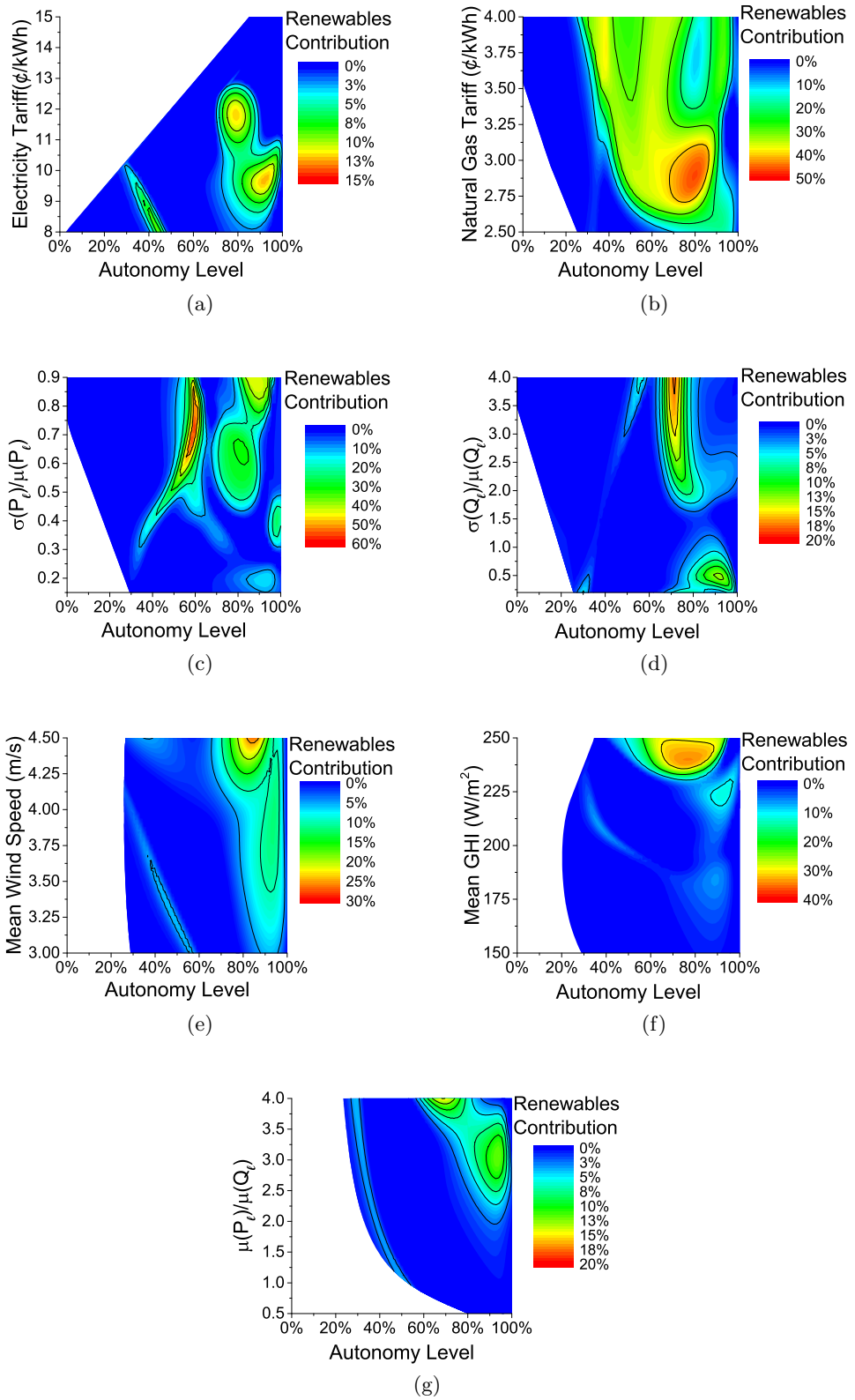

Figure 3.17: Surface plots showing predictions for renewables contribution. All values not shown on the X, Y axes are held at the nominal values for a hospital in Albuquerque, NM.

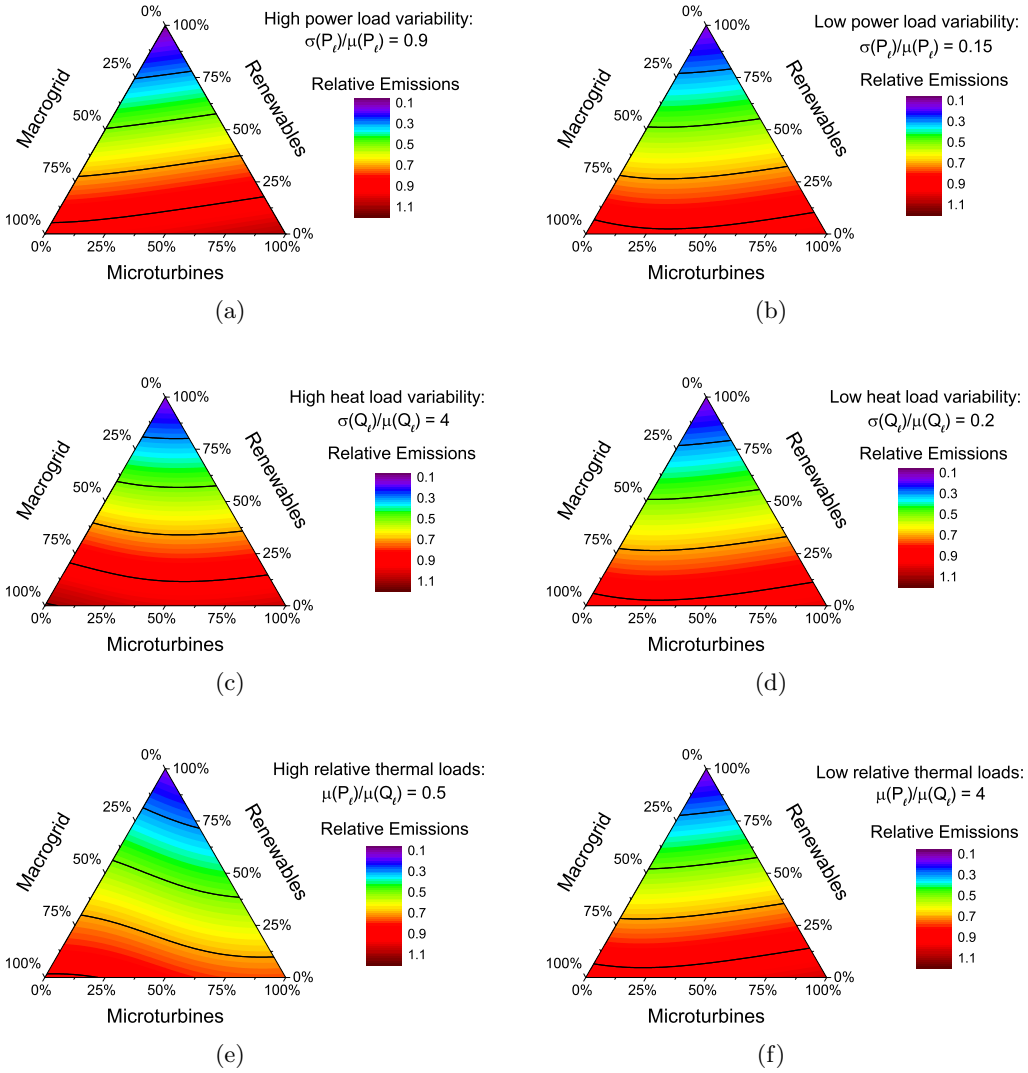

Figure 3.18: Ternary surface plots showing predictions for relative emissions. Axes show the contribution of different sources to total power production. All parameters not shown are held at nominal values for a hospital in Albuquerque, NM.

power loads leads to lower emissions at high microturbine penetration. This is because a consistent power demand allows microturbines to be operated continuously at a high efficiency setpoint. When the demand profile has more variability, either microturbines must be operated sometimes at inefficient setpoints or energy storage must be used to

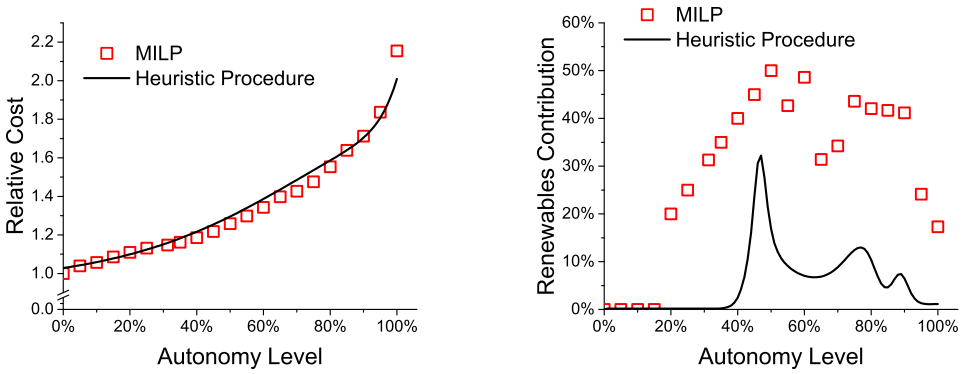

(a) (b)

Figure 3.19: Comparison of the MILP results and heuristic procedure prediction for (a) relative cost and (b) renewables contribution in the validation case.

shift power production (which involves round-trip losses), both of which decrease the overall system efficiency.

3.4.4 Validation Case

In order to verify that the heuristic procedure performs well for locations and load shapes outside of the training set and that the RMS errors observed were not due to overfitting, a short validation case is performed. In this validation case, a microgrid is considered which supplies heat and power for 3 medium office buildings and 3 stand-alone retail buildings located in Oklahoma City, OK. Fig. 3.19 compares the results of the MILP and heuristic procedure for relative cost and renewables incorporation. The heuristic procedure provides a very good fit for the overall cost. There is significant difference in the incorporation of renewables, but the heuristic procedure does capture the trend observed. This error is not unexpected based on the results observed in Fig. 3.14c and the discussion in Section 3.4.2. This error is propogated forward into the prediction of relative emissions shown in Fig. 3.20. If interpolated values of the MILP results for renewable contribution are used instead, there is very little error in the predicted emissions.

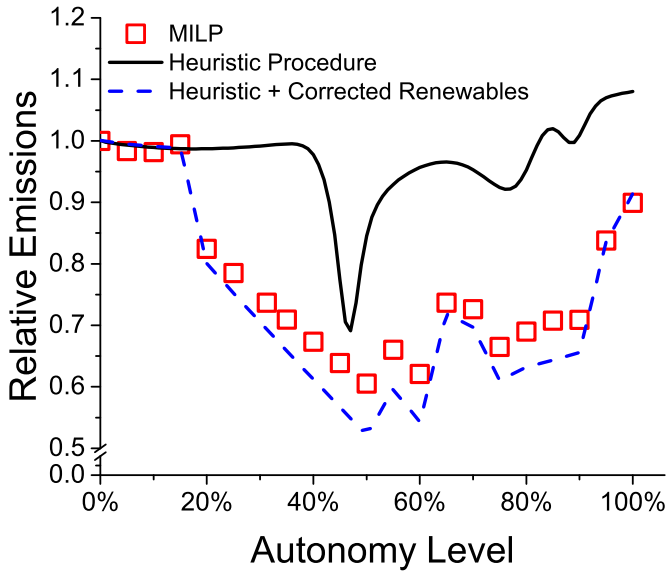

Figure 3.20: Comparison of the MILP results and heuristic procedure prediction for relative emissions. Since there were significant errors in the prediction of renewables contribution, the results of the heuristic procedure using the interpolated MILP renewables contribution is shown as well.

Comparison to Established Methods

There are several publicly available software tools for the analysis of hybrid energy systems. The results from 2 of the most popular programs, HOMER [63] and RETScreen [64], have been compared to the MILP results as an external validation.

HOMER is a simulation and design optimization tool that allows for the incorporation of a variety of renewable, thermal, and storage technologies. The systems simulated can include power, heat, and hydrogen loads. HOMER requires that users specify discrete sizes to be considered for all units. It then determines the optimal design by enumerating all the possible configurations and evaluating their feasibility and cost. The program is convenient for inexperienced modelers because it can synthesize load curves based on average values and contains a variety of built-in unit models that can be selected (with the option to create custom ones as well). In addition, HOMER generates a ranked list of alternative configurations which may be of interest to decision

makers, and it provides easy implementation of sensitivity analysis. However, the types of technologies and loads that can be considered in HOMER are limited. For example, common aspects of CCHP systems, such as explicit cooling loads and absorption chillers, cannot be considered. In contrast, a generic optimization model, like the one presented in Section 3.2, can easily be expanded to include new units and load types.

An exact match of the model presented here cannot be created in HOMER since it does not have the capability to include thermal storage units. Furthermore, HOMER cannot directly account for the capital costs or maintenance costs of boilers, though these values are usually relatively small. A constraint on the maximum amount of imported power is used analogously to the minimum autonomy constraint in the MILP formulation. It was observed that when HOMER is allowed to optimize the dispatch of microturbines it may identify designs with this maximum import constraint as infeasible. However, when the microturbines are forced to be on at some minimum setpoint, HOMER is able to find a feasible solution. This approach requires *a priori* knowledge of when generators should be operated, and results in suboptimal operational costs since the minimum setpoint is enforced throughout the year. For these reasons, HOMER could not be relied on to accurately identify alternative microgrid designs. However, for a fixed design, one can compare design parameters such as cost and emission levels between the MILP and HOMER.

RETScreen is an Excel-based tool which evaluates the environmental and economic performance of energy systems. RETScreen does not perform design optimization, but is a popular tool for the economic and environmental analysis of proposed microgrid designs. Like HOMER, RETScreen is useful because it contains a number of built-in unit models, it can retrieve climate data, and it can synthesize load data based on average values. However, unlike HOMER, detailed load and weather data cannot be manually imported, and the user must rely on the data synthesized based on monthly values. RETScreen is particularly useful since it has a number of built-in financial modules such as risk analysis and sensitivity analysis. RETScreen also explicitly accounts for the spacial layout, heat losses, and capital cost of the heat distribution network in combined heat and power systems. Since this tool evaluates a user-specified design, it can be used to analyze the designs proposed by the MILP, but cannot be used to search for alternative designs. For combined heat and power analysis, RETScreen can only

Table 3.11: MILP design results for the validation case at minimum autonomy levels of 20%, 55%, and 90%. Continuous variables have been rounded to the nearest 5 kW or kWh.

	Design 1	Design 2	Design 3
Number of C30-LP microturbines	0	0	0
Number of C65 microturbines	0	1	0
Number of C200-LP microturbines	0	0	2
Wind turbine rated power (kW)	260	580	560
PV array rated power (kW)	0	0	0
Gas-fired boiler rated heat output (kW)	1160	770	280
Electric boiler rated heat output (kW)	75	255	240
Battery capacity (kWh)	0	0	200
Thermal storage capacity (kWh)	955	1650	2135

consider up to two power systems (e.g. a wind turbine and a microturbine). This is sufficient for most of the results, but the MILP can in general select designs that include more than two power systems.

To compare the results from the MILP, HOMER, and RETScreen, 3 of the designs from the validation case were selected. The unit sizing of these 3 designs are shown in Table 3.11. Tables 3.12, 3.13, and 3.14 show the MILP, HOMER, and RETScreen results for these designs. Battery storage could not be modeled in RETScreen, and thermal storage could not be modeled in either RETScreen or HOMER.

HOMER predicts a significantly lower cost for Design 1 since the capital and maintenance costs boilers are not taken into account during simulation, but an *a posteri* calculation of these values would bring the net present cost up to $3.98 MM. To obtain the HOMER results for Designs 2 and 3, the microturbines were forced on for the full year with a minimum setpoint of 94% and 85%, respectively. Without these constraints, HOMER identified it as impossible to meet the desired autonomy level. However, because this forced suboptimal usage of the microturbines (particularly in the case of Design 3), the natural gas consumption, annual emissions, and cost predicted by HOMER are higher.

RETScreen and the MILP predict similar results for both Design 1 and 2. In Design 3, RETScreen predicts a lower cost and higher autonomy level than the MILP. This is due to the simplified load data input used in RETScreen. RETScreen only allows the

Table 3.12: Comparison of MILP, HOMER, and RETScreen results for Design 1.

	MILP	HOMER	RETScreen
Net present cost (MM $)	3.97	3.80	3.99
Annual CO_2 emissions (tons)	1611	1634	1632
Autonomy level	20%	19%	17%
Renewable contribution	20%	19%	17%
Annual natural gas consumption (MWh)	816	817	824

Table 3.13: Comparison of MILP, HOMER, and RETScreen results for Design 2.

	MILP	HOMER	RETScreen
Net present cost (MM $)	4.65	4.69	4.52
Annual CO_2 emissions (tons)	1290	1394	1154
Autonomy level	55%	57%	58%
Renewable contribution	43%	42%	41%
Annual natural gas consumption (MWh)	1965	2326	2207

Table 3.14: Comparison of MILP, HOMER, and RETScreen results for Design 3.

	MILP	HOMER	RETScreen
Net present cost (MM $)	6.13	7.87	5.35
Annual CO_2 emissions (tons)	1386	2310	1118
Autonomy level	90%	90%	98%
Renewable contribution	41%	29%	39%
Annual natural gas consumption (MWh)	5863	9438	6017

user to specify monthly average power loads and the annual peak. This method offers little ability to distinguish between loads that have a strong diurnal pattern (such as offices) versus loads that have a weak diurnal pattern (like hospitals), so RETScreen may underestimate the variability in power load demands. This does not significantly affect the results at low autonomy levels since DER units supply base power and imported power covers the peaks in demand. However, at high autonomy levels like Design 3, these peak demands must be satisfied by DERs, and underestimating the variability in the load can lead to over-prediction of the performance of dispatchable units.

The results between the proposed MILP and available software programs matches

very well at low autonomy levels (as long as all of the same cost factors can be taken into account). However, the underlying assumptions, solution methods, and simplified data input of these software programs leads to inaccurate results at high autonomy levels. In general, the proposed MILP method offers more flexibility in the problem formulation (since any arbitrary unit, energy balance, or system constraint could easily be added to the problem) at the expense of placing a larger burden on the user (since they must input accurate load data and unit models).

3.5 Conclusions

The optimal design of microgrids varies greatly depending upon the geographic location and load data used. These differences can be seen in design values like total cost, environmental impact, incorporation of renewable power technologies, optimal microgrid penetration, etc. Understanding and predicting the impact of location and load on microgrid design results is vitally important in developing effective public policy and in directing future research endeavors. The optimization results in this work show how these design results vary for microgrids serving commercial loads in locations across the continental U.S. Incorporation of renewable power in the optimal design is primarily dependent on the local cost of natural gas and the ratio of heat to power demands since renewables are competing with the gas-fired microturbines. The level of annual CO_2 emissions is primarily dependent on the penetration of renewable power. In the absence of renewables, these emission levels are dependent on the fraction of load served by microturbines, the ratio of heat to power demands, and the variability in heat and power demands. The cost of local energy supply and optimal autonomy level are impacted most by the heating requirements of the system considered, the variability in heat and power loads, and the ratio between electricity and natural gas prices.

While the observed relationships between these location and load input values and optimal design results are reasonable and could be obtained through a logical consideration of the energy supply problem, developing analytical equations that relate these inputs and outputs is onerous and perhaps infeasible. Machine learning techniques like artificial neural networks can be used to capture the input-output relationship of traditional optimization methods in order to predict these microgrid design metrics. A

heuristic procedure is proposed that uses a series of ANNs along with a few simple rules to predict relative cost, emissions, and renewable power penetration in microgrid optimal design. There is a low RMS error between the relative cost from the optimization results and the relative cost predicted by the heuristic process. The RMS error for the other predicted values (optimal autonomy level, relative emissions, and optimal renewables contribution) is slightly higher due to a relatively shallow minimum of the Pareto frontier between autonomy level and cost (in the case of optimal autonomy level), discontinuities in installed capacities of microturbines and renewables (in the case of relative emissions), and sparsity of design results with a high penetration of renewables (in the case of renewables contribution). Even with these difficulties present, the heuristic process is able to capture and quantify trends in the optimal microgrid design.

The heuristic prediction process is ideally suited for studying the design of such systems across a broad range of geographic locations and load shapes and aiding in public policy decision making. Furthermore, the simplified inputs required for the heuristic process allow one to obtain estimates about the optimal design of microgrid power systems in cases where detailed information like hourly weather and load data is not available. This is particularly useful as microgrids are often proposed as an alternative energy supply infrastructure for remote locations or developing regions where there is not a robust macrogrid available.

3.6 Nomenclature

Table 3.15: Nomenclature - Sets/Indices

k	Time periods	m	Microturbine classes
s	Solar PV regimes	w	Wind turbine regimes

Table 3.16: Nomenclature - Parameters

ζ_b	Battery maintenance cost
ζ_e	Electric boiler maintenance cost
ζ_{gas}	Natural gas cost
ζ_{grid}	Power purchase cost
ζ_h	Thermal storage maintenance cost
ζ_m	Microturbine maintenance cost
$\zeta_{m,start}$	Microturbine startup cost
ζ_n	Gas boiler maintenance cost
ζ_s	Solar PV maintenance cost
ζ_w	Wind turbine maintenance cost
η_c	Battery charging efficiency
η_d	Battery discharging efficiency
η_e	Electric boiler efficiency
η_h	Thermal storage efficiency
η_n	Gas boiler efficiency
η_s	PV temperature-dependent efficiency
θ_b	NPV factor for battery capital cost
θ_e	NPV factor for electric boiler capital cost
θ_h	NPV factor for thermal storage capital cost
θ_m	NPV factor for microturbine capital cost
θ_n	NPV factor for gas boiler capital cost
θ_s	NPV factor for solar PV capital cost
θ_w	NPV factor for wind turbine capital cost

Continued on next page

Table 3.16 – continued from previous page

κ_b	Battery capital cost
κ_e	Electric boiler capital cost
κ_h	Thermal storage capital cost
κ_m	Microturbine capital cost
κ_n	Gas boiler capital cost
$\kappa_{s,fix}$	Solar PV fixed capital cost
$\kappa_{s,var}$	Solar PV marginal capital cost
$\kappa_{w,fix}$	Wind turbine fixed capital cost
$\kappa_{w,var}$	Wind turbine marginal capital cost
λ_m	Microturbine heat-to-power ratio
ρ	Air density
ρ_{ref}	Reference air density
ϕ_b	NPV factor for battery maintenance
ϕ_e	NPV factor for electric boiler maintenance
ϕ_h	NPV factor for thermal storage maintenance
ϕ_{gas}	NPV factor for natural gas purchases
ϕ_{grid}	NPV factor for power purchases
ϕ_m	NPV factor for microturbine maintenance
ϕ_n	NPV factor for gas boiler maintenance
ϕ_s	NPV factor for solar maintenance
ϕ_w	NPV factor for wind turbine maintenance
$\mathcal{A}_{min}$	Minimum autonomy level
f_w	Wind power fractional availability
$F_{m,fix}$	Microturbine fixed fuel consumption
$F_{m,var}$	Microturbine marginal fuel consumption
h_w	Wind turbine hub height
h_{ref}	Reference height
H	Solar irradiance
H_{rated}	Rated solar irradiance
P_ℓ	Power demand

Continued on next page

Table 3.16 – continued from previous page

$P_{s,lo}$	Solar PV regime lower bound
$P_{s,up}$	Solar PV regime upper bound
$P_{w,lo}$	Wind turbine regime lower bound
$P_{w,up}$	Wind turbine regime upper bound
Q_ℓ	Heat demand
T	Ambient temperature
T_s	Temperature of PV panel
v	Wind speed
v_w	Wind speed at turbine hub height
v_{ci}	Cut-in wind speed
v_{co}	Cut-out wind speed
v_r	Rated wind speed
v_{ref}	Wind speed at reference height

Table 3.17: Nomenclature - Binary Variables ($1 \implies$ True)

I_s	Is solar regime active	I_w	Is wind regime active

Table 3.18: Nomenclature - Integer Variables ($\in \{0, 1, 2, ...\}$)

N_m	Number of microturbines installed	y_m	Number of microturbines started up
x_m	Number of microturbines on		

Table 3.19: Nomenclature - Continuous Variables

$Capex$	Capital costs (present value)	P_s	Power from solar PV
E_b	Battery storage level	$P_{s,rated}$	Solar PV rated power
$E_{b,max}$	Battery storage capacity	P_{spill}	Power spilled
E_h	Thermal storage level	P_w	Power from wind turbine
$E_{h,max}$	Thermal storage capacity	$P_{w,rated}$	Wind turbine rated power
F_m	Microturbine fuel consumption	Q_e	Heat from electric boiler
F_n	Gas boiler fuel consumption	$Q_{e,rated}$	Electric boiler rated heat
NPC	Project net present cost	$Q_{h,in}$	Heat sent to thermal storage
$OPEX$	Operational cost (present value)	$Q_{h,out}$	Heat from thermal storage
P_c	Power charged to the battery	Q_m	Heat from microturbines
P_d	Power discharged from the battery	Q_n	Heat from gas boiler
P_e	Power used by the electric boiler	$Q_{n,rated}$	Gas boiler rated heat
P_{grid}	Power imported from the utility	Q_{spill}	Heat spilled
P_m	Power from microturbines		

3.7 Supporting Information

3.7.1 Reference Case Values

Table 3.20: Net present cost of energy supply in million $ for the reference case for each location and load shape.

	Hospital	Large Office	Secondary School	Large Hotel	Supermarket	Outpatient Healthcare
Miami, FL	14.9	10.6	7.17	4.48	2.61	2.38
Houston, TX	12.0	7.99	5.04	3.48	2.07	1.81
Phoenix, AZ	13.7	9.33	6.34	4.02	2.34	2.24
Atlanta, GA	15.2	9.52	5.63	4.66	2.63	2.31
Los Angeles, CA	17.2	11.1	5.34	5.14	3.05	2.51
Las Vegas, NV	11.9	7.30	4.64	3.61	2.08	1.96
San Francisco, CA	17.1	10.4	5.06	5.10	3.03	2.46
Baltimore, MA	17.9	11.2	6.59	5.51	3.11	2.68
Albuquerque, NM	12.1	7.59	4.29	4.03	2.31	2.15
Seattle, WA	11.5	6.18	3.53	3.96	2.12	1.78
Chicago, IL	12.3	7.59	4.87	4.24	2.34	1.92
Boulder, CO	11.9	7.46	4.22	4.21	2.36	2.09
Minneapolis, MN	12.8	8.24	5.28	4.46	2.52	2.05
Helena, MT	11.6	7.24	4.43	4.39	2.43	2.01
Duluth, MN	12.4	8.12	5.12	4.61	2.59	2.01
Fairbanks, AK	19.3	13.7	8.26	7.19	4.44	3.28

Table 3.21: Expected annual CO_2 emissions in tons for the reference case for each location and load shape.

	Hospital	Large Office	Secondary School	Large Hotel	Supermarket	Outpatient Healthcare
Miami, FL	6480	4760	3190	1900	1160	1010
Houston, TX	6700	4500	2790	1890	1160	994
Phoenix, AZ	6480	4460	3000	1860	1110	1040
Atlanta, GA	6530	4110	2360	1940	1120	977
Los Angeles, CA	6050	3770	1810	1840	1050	898
Las Vegas, NV	6130	3770	2340	1840	1060	1000
San Francisco, CA	6050	3550	1730	1850	1060	885
Baltimore, MA	6620	4110	2340	2000	1130	981
Albuquerque, NM	5620	3480	1930	1870	1060	1000
Seattle, WA	5990	3360	1710	1900	1090	886
Chicago, IL	6260	3830	2300	2050	1170	959
Boulder, CO	5570	3430	1880	1930	1090	969
Minneapolis, MN	6140	3850	2380	2110	1190	975
Helena, MT	5580	3440	1960	2010	1150	954
Duluth, MN	5960	3800	2300	2180	1220	960
Fairbanks, AK	5720	4000	2590	2300	1340	982

3.7.2 Additional Plots

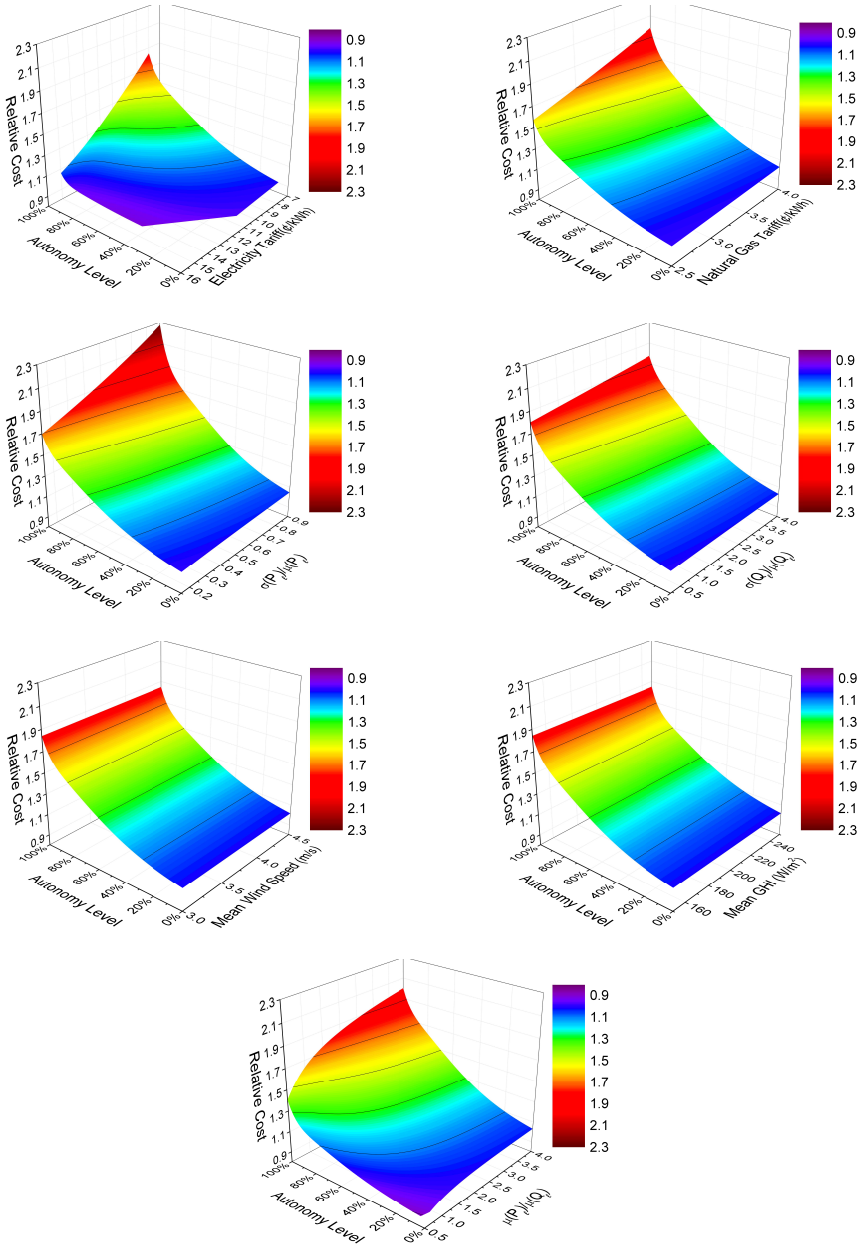

Figure 3.21: Surface plots showing predictions for relative cost. All values not shown on the X, Y axes are held at the nominal values for a supermarket in Seattle, WA.

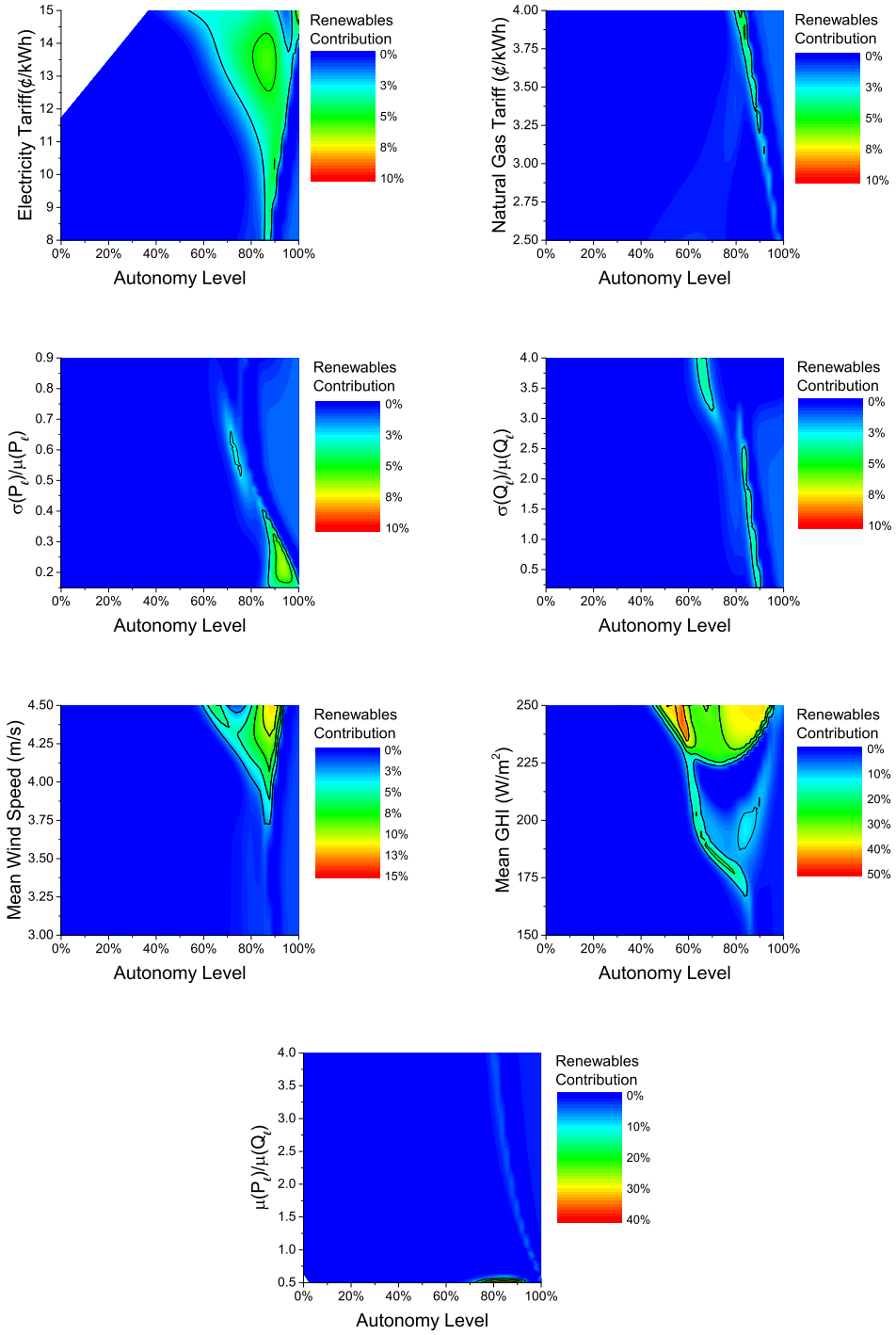

Figure 3.22: Contour plots showing predictions for renewables contribution. Values not shown on the axes are held at the nominal values for a supermarket in Seattle, WA.

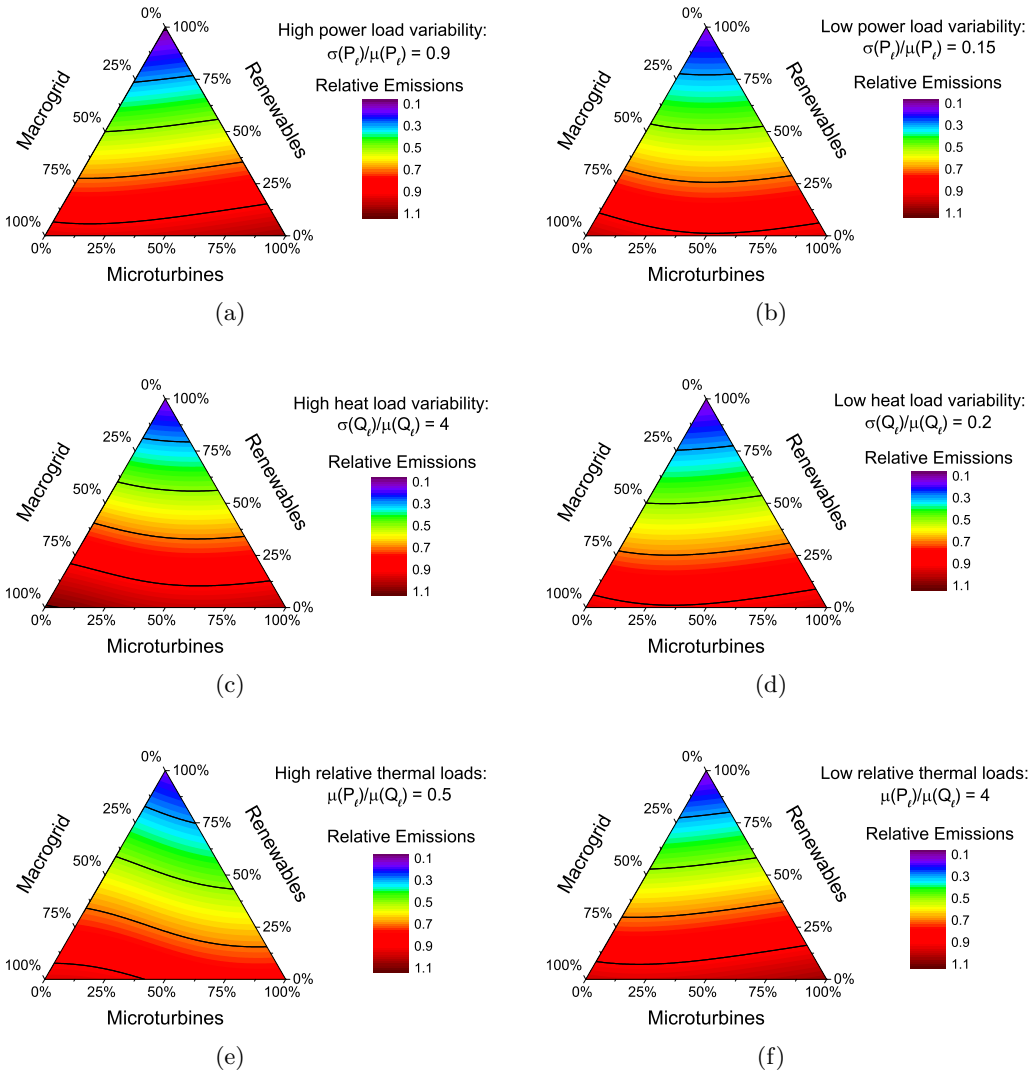

Figure 3.23: Ternary surface plots showing predictions for relative emissions. Axes show the contribution of different sources to total power production. All parameters not shown are held at nominal values for a supermarket in Seattle, WA.

CHAPTER 4

Microgrid/Macrogrid Energy Exchange: A Novel Market Structure and Stochastic Scheduling*

4.1 Introduction

Currently, electricity generation is reliant on a highly centralized infrastructure with only a small amount of distributed generation. However, the penetration of distributed generation (and in particular distributed renewable generation) is already significant in certain locations, and is expected to increase substantially over the coming decades [65]. This proliferation of distributed generation is driven by many potential benefits: a reduction in transmission losses and electrical congestion; recovery of waste heat to serve low-grade thermal needs and improve fuel efficiency; and incorporation of inherently dispersed renewable feedstocks (i.e. wind and solar) [18, 66]. As seen in Chapters 2 and 3, grid-connected microgrids are often very preferable in terms of their economic performance (i.e. achieving a high autonomy level was observed to be expensive). Therefore, there may be special cases where a stand-alone system is preferable (e.g. if the location is remote and one would have to pay to extend power lines from the macrogrid), but

*Reprinted (adapted) with permission from Michael Zachar and Prodromos Daoutids, *IEEE Transactions on Smart Grid*, 8(1):178-189, 2017 [16].

the majority of microgrids will probably import and export power from the macrogrid.

However, increasing the penetration of distributed generation (particularly non-dispatchable renewables) also introduces inherent challenges to the current electrical infrastructure. Utility companies are still expected to supply any and all demands not met by local generation (and to absorb any local generation in excess of demands). The resulting load profile that utility companies must serve is referred to as the *residual load*. Because neither renewable availability nor end user behavior can be predicted perfectly ahead of time, distributed generation increases stochasticity/uncertainty in the residual load. In addition, temporal mismatch between generation and demand may cause deep troughs and sharp ramps in the residual load. These phenomena increase the cost and reduce the fuel efficiency of macrogrid power supply due to operation of power plants at low capacity factors, increased reserve requirements, and increased ramping [67–70]. These disruptions to macrogrid operation are the central problem addressed in this chapter. These issues can be addressed at the macrogrid level by leveraging large, dispatchable loads (e.g. data centers [71]), or by revising the scheduling formulations and procedures for large power plants to better handle renewable uncertainty and stochasticity [72, 73]. Alternatively, demand-side load shaping could perhaps be used to address these challenges in a more efficient manner [74].

The microgrid architecture enables this load shaping, but demand smoothing may not be economically optimal for microgrids under current market structures. In particular, net metering and feed-in tariffs are designed primarily to promote the usage of distributed renewables for environmental reasons, with distributed generation remunerated for exporting power without regard to the impact on the macrogrid. This, combined with other microgrid operating policies, such as heat-following for cogeneration, can exacerbate the aforementioned problems with integration of renewable power [17, 66]. This potentially disruptive behavior has given rise to regulatory and financial barriers to microgrid adoption such as disallowing the export of power to the macrogrid or imposing high fixed costs (e.g. interconnection fees and monthly connection charges) to recoup the cost of maintaining the macrogrid, supplying adequate reserve margins, and servicing these highly uncertain and variable loads [68, 75, 76].

In this chapter, a potential market structure is proposed which seeks to alleviate concerns for both microgrid operators and utility companies. In particular, this market

structure is formulated to allow microgrid operators to exchange (i.e. buy/sell) power with the utility companies at known rates in return for explicitly limiting uncertainty and variability in the residual load. In the market structure proposed, microgrid operators must provide a day-ahead commitment for energy exchange with the macrogrid. Microgrid operators are penalized for deviating too far from commitments to reduce uncertainty, and the hour-to-hour difference between commitment values is limited to reduce variability. Such a market structure can help protect utility companies from the undue burden of renewable stochasticity, but also allows microgrid operators to meet these commitments through a variety of methods (e.g. dispatch of local thermal units and storage devices, curtailing of renewable units, and rescheduling of flexible loads). Moreover, since the residual load is better regulated, utility companies may be more amenable to negotiating better electricity tariffs or lower fixed costs for microgrids.

In this chapter, the feasibility of the proposed market/regulatory structure is evaluated (i.e. whether the commitments can be met with a high degree of satisfaction), and its impact on microgrid performance is studied. To do so, a chance-constrained scheduling problem for microgrid operations is formulated, and it is implemented in a 1-year case study. Results are evaluated in terms of the frequency and magnitude of commitment violations, characteristics of the residual load, cost of energy supply, curtailment of renewable power, and fuel efficiency. Particular attention is paid to how tuning the market parameters changes microgrid performance and energy exchange regulation. To facilitate a straightforward presentation of the optimization problem and results, an electric-only microgrid with inflexible load is considered.

From a technical perspective, the primary contribution of this chapter lies in the approach used for stochastic scheduling of the microgrid. Coping with uncertainty in renewable output and end user demand is one of the primary challenges in scheduling and supervisory control of microgrid systems. This problem has been addressed in past literature by casting the problem as a scenario-based stochastic programming problem (e.g. [77–79]). One challenge with this approach is the supervisory control must have scenario generation capabilities. In addition, it increases the optimization problem size and computational burden. An alternative approach is to formulate a robust optimization problem which considers some "worst case" cost in the objective function (e.g. [80–82]). Robust optimization does not require scenario generation nor

does it significantly increase the problem size. However, it may also be difficult to define a proper "worst case" scenario in such systems. Additionally, since a worst-case cost is considered, it may lead to overly-conservative performance. The chance-constrained scheduling formulation developed in this chapter is an interesting alternative:

- It minimizes the expected cost based on only point forecasts.
- It limits the probability of undesirable or expensive outcomes without explicitly considering their cost.

The former point means that this scheduling approach does not require scenario generation, and it can natively use a variety of publicly available forecasts (e.g. the forecasts from the National Weather Service) which give only hourly expected values. This helps to enable implementation, and keeps the problem size small so it can easily be solved on the hardware available to end users. The latter point helps to reduce the conservativeness of the resulting schedule. This is showcased in the results by comparing the performance to a scheduling approach which assumes forecasts are perfect.

A few previous authors have considered chance-constrained scheduling or control of microgrids, but in a different manner. In [83, 84], a chance-constrained energy balance is used in the microgrid scheduling problem to consider demand and renewables uncertainty. A chance-constrained formulation is also considered in [85] to ensure that maximum and minimum storage levels are not violated with a high level of confidence Unlike these previous approaches, the formulation presented later in this chapter specifically accounts for the recourse action that can be taken after uncertainty is revealed. In essence, it seeks to find a schedule that minimizes the expected cost (i.e. based on the forecasted load/renewable availability) but also ensures that sufficient flexibility is available at the recourse stage to prevent commitment violations.

4.2 Literature Review

Microgrid scheduling and control systems are used to dispatch available local generation units, coordinate the charging and discharging of storage systems, and manage controllable loads. The primary goal is typically ensuring that end user energy demands are met, but other operational objectives are often considered, such as minimizing fuel

usage, operating cost, and environmental impact or maximizing renewables utilization and fuel efficiency.

Several authors have formulated microgrid scheduling and dispatch problems where energy exchange is minimized or not allowed. These formulations avoid the detrimental interactions with the macrogrid, but add operational difficulties as microgrids must be self-reliant. One approach to this problem is to implement a control system which responds almost instantaneously to changing weather and load conditions. For example, rule-based power management algorithms [86] and metaheurisitic approaches like particle swarm optimization [87] offer rapid (but not necessarily optimal) response to any disturbance. Similarly, dynamic programming can be used to quickly reject forecasting errors by redispatching generation or storage units [88]. Dynamic programming works well for microgrids with a small number of dispatchable units, but the number of states which must be considered and computation time grow combinatorially for highly heterogeneous systems. A more common approach is to formulate a traditional scheduling optimization problem which decides unit states and dispatch levels over a $\sim$1 day horizon to ensure long-term economic performance and optimization of storage levels. In particular, receding horizon optimization approaches may be used so that forecasting errors can be rejected [89]. Demand response can be incorporated into the schedule to shed, shift, or otherwise modify the load curve so that it better matches the availability of power [90, 91]. Since there exists a significant amount of stochasticity in both the energy demands and renewable availability in microgrid-scale systems, extensions to stochastic or robust formulations have been proposed to improve performance of these stand-alone systems [79, 92–94]. However, the work in Chapters 2 and 3 has shown that significant energy exchange with the macrogrid is necessary for microgrids to be economically competitive. Therefore, if microgrids are to be widely adopted and not limited to niche applications, it is vital that they exchange energy with the macrogrid, but not in the potentially disruptive ways discussed in the introduction to this chapter.

Many authors have considered the centralized scheduling of microgrids connected to the macrogrid in a simple tariff-based market scheme. In these formulations, the cost/revenue from energy exchange with the macrogrid may be constant, time-of-use (i.e. following a fixed schedule), or real-time. Dynamic programming has also been used for these grid-connected systems and may be used to incorporate a peak shaving

constraint [95]. Scheduling problems which incorporate discrete operating modes and startup/shutdown costs have been formulated using mixed integer linear programming (MILP) [96]. Incorporating controllable loads into microgrid scheduling can be used to further improve the economic performance, and this problem has been addressed using a MILP approach [97]. Stochastic programming has been used for scheduling a microgrid with uncertainty in renewables output, local demand, market prices, and unit availability [77, 79]. Finally, robust optimization has been used for scheduling microgrids considering the worst-case transaction cost resulting from uncertainty in renewables output [80].

Scheduling and dispatch has also been considered for multi-agent microgrids with an active aggregator. This aggregator acts as an autonomous agent which buys power from local generation units, sells power to local customers, and buys/sells power to the upstream macrogrid. Under such a market structure, deterministic optimization has been proposed for the dispatch of local generators and flexible loads [98]. In this formulation, generators and flexible loads are assumed to provide linear bids to the aggregator, and two market policies are investigated, i.e. minimizing overall microgrid cost and maximizing the aggregator's profit. A similar problem has been considered for a multi-agent microgrid where the aggregator may reserve capacity on the day-ahead market [99]. A distributed, iterative solution approach was proposed where consumer agents update their demand forecast in response to a price signal broadcasted by the aggregator. Optimization of the aggregator's profit has also been considered for the case where fixed rates are used for purchasing local renewable capacity and selling power to local users [100]. A hybrid stochastic/robust optimization was proposed where uncertainty in renewables is handled via a stochastic approach and uncertainty in the spot price is handled via a robust approach. A similar market structure is considered in [81]. In this formulation, the aggregator seeks to minimize its expected cost and conditional value at risk using stochastic optimization. Deterministic optimization has also been used to maximize the aggregator's profit when energy can only be purchased on the day-ahead market and recourse actions are limited to updating local generator setpoints and shedding loads [101].

Scheduling of microgrids without an active aggregator has also been considered. For a microgrid with a small number of participants, agents may negotiate billateral energy

contracts with each other or purchase/sell power to the upstream macrogrid. A bidding strategy based on robust optimization for such a microgrid has been proposed [102]. In a microgrid with a larger number of participants, direct negotiation between each agent may not be feasible. Instead, a market structure where each active user must commit to a net energy production/consumption in a day-ahead market is proposed in [103]. An iterative, asynchronous negotiation based on minimizing each users' expected cost was proposed for establishing day-ahead commitments, and recourse optimization was used to minimize the penalty each user incurred due to real-time deviation from their commitment.

Finally, centrally controlled microgrids which participate in the auction process of the power market have been considered. A hybrid stochastic/robust optimization for constructing microgrid bidding curves on the day-ahead wholesale market has been proposed in [82]. In this formulation, day-ahead clearing price and renewables output are treated with a stochastic optimization approach, while expensive purchases on the real-time market are minimized using a robust optimization approach. A market structure where a distribution network operator negotiates energy exchange contracts directly with microgrids has been considered in [93]. An iterative, distributed negotiation process was proposed where the microgrids and network operator each solve a stochastic optimization problem to maximize their own utility and then exchange information about requested energy exchange contracts.

A common weakness in many of these previous scheduling approaches for grid-connected systems is that they result in a residual load which is highly variable and stochastic. Some of the proposed market systems help to mitigate load uncertainty by encouraging microgrids to minimize their real-time energy purchases (e.g. [82, 99, 104]). However, residual load variability is treated only indirectly (e.g. by considering quadratic cost and welfare functions which discourage high peak loads). Moreover, these markets then introduce uncertainty into the volume and revenue of energy exchanges, which exacerbates payback uncertainty and may deter potential microgrid investors. In addition, auction rules must be carefully designed so that participants do not engage in strategic bidding which results in a socially sub-optimal market clearing [105]. Finally, implementation of certain auction-based or multi-agent markets may be impeded by the reluctance of entities to reveal pertinent private information or by the scalability if

iterative negotiations are required. Other approaches have been proposed to explicitly reduce load variability (e.g. [106]), but they do not address the uncertainty.

The proposed market structure seeks to address these issues and explicitly reduce both variability and uncertainty in the residual load. It differs from traditional feed-in tariff or net metering systems primarily due to the day-ahead energy exchange commitments that must be made. Also, unlike previous stochastic and robust scheduling formulations, a chance-constrained scheduling problem is proposed which allows microgrid operators to optimize the expected economic performance based on point forecasts while also ensuring that the likelihood of unexpected commitment violations is very small.

4.3 Proposed Market

In this chapter, the focus is on centrally coordinated, small to medium sized microgrids (e.g. those with a cumulative generation capacity < 1 MW), who are assumed to exchange power with a larger power system (referred to as the macrogrid) operated by a utility company. In order to arrive at a satisfactory market structure, one must first identify the most salient objectives for each shareholder (i.e. the microgrid operator and the utility company). Microgrid operators are primarily concerned with ensuring that their energy demands can be met reliably and economically. Due to the stochasticity in both loads and renewables availability, it is difficult to design a robust self-sufficient microgrid system without significant oversizing of generation or storage, so the ability to exchange power with the macrogrid is vital. In addition, microgrid units are generally capital intensive with the assumption that they will yield economic benefits over their lifespan on the order of years to decades. Therefore, it is important to reduce any possible uncertainty in the design stage so that intelligent and economically efficient investments can be made. On the other hand, the utility is concerned with how the integration of microgrids into their operating area will impact their operations. Specific concerns include the impact on the macrogrid power quality, amount of utility reserve capacity that must be committed, and ramp-rates of utility-scale power plants. In addition, the utility would prefer that microgrid residual load is low during peak hours and high during off-peak hours (to ensure that base-load plants can continue to operate

at a high utilization factor).

From the microgrid operator perspective desirable market characteristics would be:

- The microgrid should be able to import and export power as needed
- Rates for buying and selling power should be known during project planning so that estimates of financial payback can be made

It should be emphasized that this discussion is targeted towards single agent medium and small microgrids, and that larger microgrids may be more willing to participate in auction-based markets since they have less demand/generation uncertainty and more bargaining power.

For the utility, desirable market characteristics would be:

- Power demand/supply from the microgrids should be known sufficiently ahead of time so that utility plants can be committed/ramped appropriately
- The ramp-rates of the macrogrid should be mild
- Microgrid operators should be fined for deviating from the committed schedule as it may require utilities to engage in expensive corrective action
- Microgrids should supply power to the macrogrid during peak hours over non-peak hours

It should also be noted that the utility would likely be connected to many such microgrids as well as their non-microgrid customers. Thus, small deviations from the expected power exchange of an individual microgrid are unlikely to have a significant impact due to the smoothing effect of aggregation. This is especially true if each microgrid's deviation is a Gaussian-like process.

Motivated by this discussion, we propose a market structure which has a fixed tariff structure and requires microgrid operators to supply the utility with day-ahead commitments for net hourly energy exchange. In addition, the maximum difference between energy exchange commitments from hour-to-hour is constrained. The fixed tariff structure may be time-of-use (but not real time) in order to incentivize shifting load away from peak-hours. Finally, microgrid operators are allowed to deviate a small amount

from their energy exchange commitment without penalty, but are heavily penalized outside of this small interval.

This market structure has two important market parameters, namely the *schedule elasticity* and *schedule adaptability*. The schedule elasticity is the maximum deviation from the committed energy exchange before penalties are incurred. The schedule adaptability is the maximum hour-to-hour difference between energy exchange commitments. Thus, residual load variability and uncertainty are explicitly reduced by lowering these schedule elasticity and adaptability values. It is envisioned that these market parameters would be fixed during the microgrid project planning stage, i.e. via a long term contract between the microgrid and utility company. The electricity tariffs, feed-in tariffs, and fixed charges over the contract life would also be agreed to at this time. Therefore, this could be implemented in a manner similar to existing power purchase agreements.

During operation, the microgrid operators communicate a 24-hour-ahead energy exchange commitment to the utility company at the start of every hour. The power exchange is then metered over the subsequent hour, and the microgrid operators billed (or remunerated, if applicable) based on the volume of energy exchange and any potential commitment violation (based on the commitment value that was previously established for that time period).

This proposed market structure has several important advantages over previously considered microgrid market structures. Unlike net metering or simple feed-in tariff schemes, microgrid operators are obligated to provide energy exchange commitments to reduce the uncertainty that the utility must mitigate. In addition, the schedule adaptability can be tuned to reduce the load variability. Unlike auction-based market systems (e.g. [107]), the microgrid operators are provided with stable rates that they can use for financial analysis before initial investment and expansion planning. Moreover, the proposed market system is scalable since there is no iterative negotiation involved to reach a market equilibrium. The framework may also enable microgrid operators to negotiate more attractive electricity rates or lower fixed costs, e.g. in exchange for tighter schedule elasticity or adaptability values, since the residual load is easier to service. Finally, the proposed market structure may be considered similar to some industrial

demand side management programs (e.g. the system in [108]) wherein large, energy-intensive industrial customers negotiate an energy exchange commitment curve with the utility. Important differences in this work are that the load curve is unilaterally decided by the microgrid operators, there is some permissible deviation from commitments, and microgrids have significant generation/storage capacity in addition to load. In addition, there are differences in the inherent challenges in each problem (i.e. load and renewables stochasticity for the microgrid vs. job-shop constraints for industrial customers).

4.4 Model Formulation

The microgrid considered includes photovoltaics (PV), microturbines, a battery, and a bi-directional connection to the macrogrid. The energy flow diagram is shown in Fig. 4.1. The microgrid is operated to minimize the cost of meeting the power demand through local generation, dispatch of storage devices, and power exchange with the macrogrid. This chapter focuses on the scheduling problem which consists of deciding first-stage variables and predicting second-stage variables. Optimal scheduling is needed to ensure that real-time operation is both feasible and economical. The first- and second-stage variables of the problem considered are shown in Table 4.1. Note that even though microturbines can be started very quickly (i.e. order of minutes), the number of committed microturbines is fixed as a first-stage variable to prevent frequent startups and shutdowns during dispatch which would result in excessive unit wear and premature failure. Similarly, the battery charging/discharging state is fixed as a first-stage variable to prevent excessive intra-hour charging and discharging cycles in response to short term demand fluctuations which could increase the battery degradation.

The scheduling problem is formulated as a discrete-time optimization with 1 hour time periods. A receding horizon of 48 hours is used in the optimization. The optimization initiated at the start of time period k_c considers a 48-hour planning horizon identified as:

$$\mathcal{H}(k_c) := \{k_c, k_c + 1, k_c + 2, ..., k_c + 47\} \tag{4.1}$$

In the proposed market structure, microgrid operators must provide an estimate of their hourly net energy exchange with the macrogrid one day ahead of time to allow adequate time for scheduling of large power plants. The optimization horizon is split up

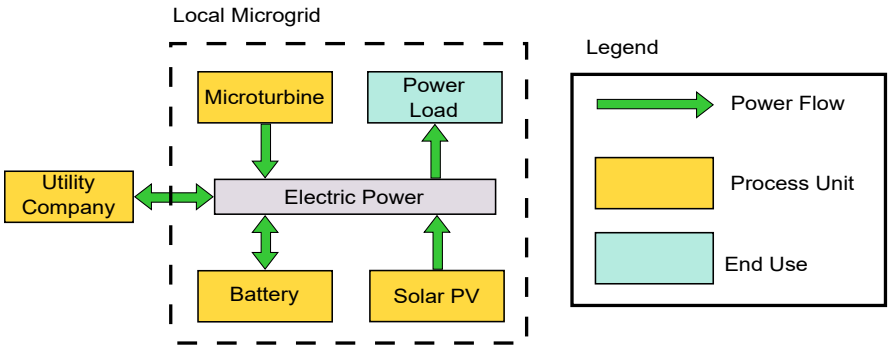

Figure 4.1: Energy flow diagram of the microgrid system considered.

Table 4.1: First- and Second-Stage Variables in the Scheduling Problem

First-Stage Variables	Second-Stage Variables
Microturbine on/off states	Microturbine setpoints
Battery charge/discharge state	Battery setpoint
Energy exchange commitment	Power exchange with the utility
	PV curtailment

into two distinct phases because of this day-ahead commitment. In the first 24 hours, scheduled power exchange must lie close to the previously established commitments. In the latter 24 hours no commitments have been made. Thus, the optimization horizon can be divided into two subsets:

$$\mathcal{H}_1(k_c) := \{k_c, k_c + 1, k_c + 2, ..., k_c + 23\} \tag{4.2}$$

$$\mathcal{H}_2(k_c) := \{k_c + 24, k_c + 25, k_c + 26, ..., k_c + 47\} \tag{4.3}$$

Given that there is significant stochasticity in both microgrid-scale load and renewable availability, the scheduling problem is formulated as a chance-constrained optimization problem. This problem is then transformed into a MILP which can be solved using standard methods.

4.4.1 Macrogrid Exchange

The net power exchange with the macrogrid is given by:

$$P_g(k) = P_{buy}(k) - P_{sell}(k) \qquad \forall k \in \mathcal{H}(k_c) \tag{4.4}$$

where P_{buy} is power bought from the macrogrid, P_{sell} is power sold to the macrogrid, and P_g is the net power exchange with the macrogrid. The scheduling optimization is formulated as a discrete-time problem with a sampling time denoted by Δ_T. The energy exchange with the macrogrid over a single time period is given by $P_g(k)\Delta_T$. Since Δ_T= 1 hour and units of kW and kWh are used in this work, the Δ_T will not be shown when converting between power and energy units in subsequent equations.

In the proposed market structure, energy exchange commitments have some maximum hour-to-hour difference, and microgrids are penalized for large deviations from their commitments. The schedule adaptability, δ, is the maximum hour-to-hour commitment difference:

$$|E_{gc}(k) - E_{gc}(k-1)| \leq \delta \tag{4.5}$$

where E_{gc} is the energy exchange commitment. This equation can be reformulated to remove the absolute value operator:

$$-\delta \leq E_{gc}(k) - E_{gc}(k-1) \leq \delta \tag{4.6}$$

A high adaptability gives microgrid operators more freedom to shape their energy exchange schedule to match forecasted renewables output, while a low adaptability reduces ramping requirements for macrogrid power plants. The schedule elasticity, γ, is the maximum permissible deviation from energy exchange commitments before market penalties are incurred:

$$E_v(k) = max\Big(0, \big|E_{gc}(k) - P_g(k)\big| - \gamma\Big) \tag{4.7}$$

where E_v is the commitment violation, which is penalized at a high rate. A high elasticity allows microgrid operators more freedom to update their energy exchange as uncertain conditions are realized, while a low elasticity reduces the uncertainty in the

hourly residual load. This equation can be reformulated into a set of linear inequalities to remove the *max* and absolute value operators:

$$E_v(k) \geq E_{gc}(k) - P_g(k) - \gamma \quad \forall k \in \mathcal{H}_1(k_c) \tag{4.8}$$

$$E_v(k) \geq P_g(k) - E_{gc}(k) - \gamma \quad \forall k \in \mathcal{H}_1(k_c) \tag{4.9}$$

The schedule adaptability and elasticity are tunable market parameters that would be negotiated at the project planning phase. In the case study presented in Section 4.5, the effect of these parameters on the microgrid performance and energy exchange regulation will be investigated by varying them within a specified range.

The microgrid operator must make a new day-ahead energy exchange commitment each hour. Auxiliary variables, E_{gc}^{exp}, are introduced to represent the microgrid operator's expected energy exchange commitments over the latter 24 hours of the scheduling horizon (i.e. if forced to make commitments for all those hours right now, these would be the best values). After each scheduling optimization, a new energy exchange commitment is submitted to the utility company:

$$E_{gc}(k_c + 24) \leftarrow E_{gc}^{exp}(k_c + 24) \tag{4.10}$$

Once a commitment has been established, it cannot change in future time periods.

These expected commitments are treated with constraints similar to the real commitments. For example, they are constrained to ensure that (4.6) is not violated:

$$-\delta \leq E_{gc}^{exp}(k_c + 24) - E_{gc}(k_c + 23) \leq \delta \tag{4.11}$$

$$-\delta \leq E_{gc}^{exp}(k) - E_{gc}^{exp}(k-1) \leq \delta \qquad \forall\, k \in \mathcal{H}_2(k_c) \setminus k_c + 24 \tag{4.12}$$

They are also used to quantify expected commitment violations in the latter half of the optimization horizon:

$$E_v(k) \geq E_{gc}^{exp}(k) - P_g(k) - \gamma \quad \forall k \in \mathcal{H}_2(k_c) \tag{4.13}$$

$$E_v(k) \geq P_g(k) - E_{gc}^{exp}(k) - \gamma \quad \forall k \in \mathcal{H}_2(k_c) \tag{4.14}$$

Finally, the microgrid operator should make energy exchange commitments which are

both economical and unlikely to be violated. A commitment deviation, Λ, can be defined as the difference between the expected energy exchange and the actual commitment value supplied to the utility:

$$\Lambda = \left| P_g(k_c + 24) - E_{gc}^{exp}(k_c + 24) \right| \tag{4.15}$$

where it is desirable to have a commitment deviation close to zero (i.e. the microgrid operator should not mislead the utility about expected energy exchange). Again, this can be reformulated to remove the absolute value operator:

$$\Lambda \geq P_g(k_c + 24) - E_{gc}^{exp}(k_c + 24) \tag{4.16}$$

$$\Lambda \geq E_{gc}^{exp}(k_c + 24) - P_g(k_c + 24) \tag{4.17}$$

4.4.2 Microturbines

Microturbines serve as a dispatchable power source. For simplicity, only a single model is considered in this paper, and the individual units are considered to be indistinguishable:

$$x_m(k) \in \{0, 1, 2, ..., N_m\} \qquad \forall\, k \in \mathcal{H}(k_c) \tag{4.18}$$

where x_m is the number of microturbines turned on, and N_m is the number of microturbines installed. When on, microturbines must operate at a power, P_m, between some maximum and minimum setpoint to maintain stable operation:

$$x_m(k) P_m^{lo} \leq P_m(k) \leq x_m(k) P_m^{up} \quad \forall\, k \in \mathcal{H}(k_c) \tag{4.19}$$

Fuel usage, F_m, is taken to be an affine function of power output:

$$F_m(k) = P_m(k) F_{m,var} + x_m(k) F_{m,fix} \quad \forall\, k \in \mathcal{H}(k_c) \tag{4.20}$$

where $F_{m,var}$ and $F_{m,fix}$ are constant coefficients.

Startup events are tracked and penalized in the objective function since they contribute extra wear and fuel usage:

$$y_m(k) \geq x_m(k) - x(k-1) \quad \forall\, k \in \mathcal{H}(k_c) \tag{4.21}$$

where y_m is the number of microturbines startups. Note that $x(k_c - 1)$ refers to true current value for the number of turbines on. A similar argument can made for all equations that have coupling over time, but they will not be explicitly stated in the interest of brevity.

4.4.3 Battery Bank

A battery bank is used to store and dispatch power. The storage level in the battery, E_b, is governed by the discretized ordinary differential equation:

$$E_b(k) = E_b(k-1) + P_c(k)\eta_c - \frac{P_d(k)}{\eta_d} \quad \forall\, k \in \mathcal{H}(k_c) \tag{4.22}$$

where P_c and P_d are power charged and discharged, respectively, and η_c and η_d are charging and discharging efficiencies, respectively. The energy level of the battery must lie somewhere between its maximum capacity and minimum capacity ($E_{b,max}$ and $E_{b,min}$, respectively) to prevent deep discharges which shorten battery life. The battery power is also constrained since the battery efficiency is much lower during rapid charing/discharging. This also prevents temperature spikes which could damage the battery. Finally, it is constrained to either be charging or discharging in each time period. The feasible range of battery operation can then be described by:

$$P_d^{max}(k) \leq 0.1 E_{b,max} \chi_b(k) \qquad \forall\, k \in \mathcal{H}(k_c) \tag{4.23}$$

$$P_c^{max}(k) \leq 0.1 E_{b,max}\big(1 - \chi_b(k)\big) \qquad \forall\, k \in \mathcal{H}(k_c) \tag{4.24}$$

$$P_d^{max}(k) \leq \big(E_b(k-1) - E_{b,min}\big)\eta_d \qquad \forall\, k \in \mathcal{H}(k_c) \tag{4.25}$$

$$P_c^{max}(k) \leq \left(E_{b,max} - E_b(k-1)\right)/\eta_c \qquad \forall\, k \in \mathcal{H}(k_c) \tag{4.26}$$

$$0 \leq P_d(k) \leq P_d^{max}(k) \qquad \forall\, k \in \mathcal{H}(k_c) \tag{4.27}$$

$$0 \leq P_c(k) \leq P_c^{max}(k) \qquad \forall\, k \in \mathcal{H}(k_c) \tag{4.28}$$

where χ_b is a binary variable which is equal to 1 when discharging, and P_c^{max} and P_d^{max} are auxiliary variables which describe the maximum feasible setpoints for P_c and P_d, respectively. Like microturbine startups, cycling of the battery bank is tracked and penalized in the objective function:

$$\psi_b(k) \geq \chi_b(k) - \chi_b(k-1) \quad \forall\, k \in \mathcal{H}(k_c) \tag{4.29}$$

where ψ_b is a binary variable indicating cycling.

4.4.4 Photovoltaic Power

PV power can be curtailed if desired:

$$0 \leq P_s(k) \leq P_s^{max}(k) \qquad \forall\, k \in \mathcal{H}(k_c) \tag{4.30}$$

where P_s is the actual PV power generated and P_s^{max} is the forecasted power generation when operating at the maximum power point.

4.4.5 Power Balance

In each time period, the expected generation, consumption, import, and export of power must be balanced based on the expected value of second-stage variables:

$$P_m(k) + P_d(k) - P_c(k) + P_g(k) = P_\ell(k) - P_s(k) \qquad \forall\, k \in \mathcal{H}(k_c) \tag{4.31}$$

where P_ℓ is the forecasted load. However, there are inherent forecasting errors in the load and PV availability values. The first-stage variables should be chosen such that forecasting errors will not lead to an unexpected increase in commitment violations since these are severely penalized. For this purpose, the chance-constrained power balance (4.32) is used:

$$Prob\left[\begin{array}{r|l} \hat{P}_m(k) + \hat{P}_d(k) - \hat{P}_c(k) + \hat{P}_g(k) & \hat{E}_v(k) \leq E_v(k) \\ = \hat{P}_\ell(k) - \hat{P}_s(k) & x_m(k),\ \chi_b(k) \end{array}\right] \geq \alpha \quad \forall\, k \in \mathcal{H}(k_c) \tag{4.32}$$

where the second-stage variables denoted with a circumflex (e.g. $\hat{P_m}$) refer to the realized values after uncertainty has been revealed and recourse action has been taken. This equation states that, after revealing the true values for PV availability and demand, the energy balance can be satisfied without increasing E_v (and without changing discrete unit states) with at least a probability of α, where $1-\alpha$ is a small value. In this chapter, α is chosen to be 0.95.

Chance-constrained equations cannot be directly used in standard optimization solvers, so (4.32) is transformed into a set of linear inequalities based on forecasted values for the stochastic parameters. Full discussion of the forecasting of load and PV output is beyond the scope of this chapter; instead, simple noise corruption of the true load values is used to simulate this forecasting. The forecasted values are given by:

$$P_\ell(k) = \hat{P}_\ell(k) + e_\ell(k) \tag{4.33}$$

$$P_s^{max}(k) = \hat{P}_s^{max}(k) + e_s(k) \tag{4.34}$$

where the forecasting errors, e_ℓ and e_s, are assumed to be zero-mean and normally distributed [109]. The standard deviations are described by :

$$\sigma_\ell(k) = \hat{P}_\ell(k)\left(0.13 + 0.015\frac{k-k_c}{47}\right) \tag{4.35}$$

$$\sigma_s(k) = min\left(\frac{\hat{P}_s^{max}(k)}{3}, P_{s,rated}\left(.17 + .05\frac{k-k_c}{47}\right)\right) \tag{4.36}$$

where the relative uncertainty is assumed to increase further into the future, and the relative PV power uncertainty is higher when solar radiation levels are low (i.e. sunrise, sunset, and cloudy periods) [110, 111]. The magnitude of the uncertainty is based on the errors reported in relevant forecasting literature [111, 112].

In reality, the uncertainty distribution and magnitude will vary depending on the load shape (i.e. type of end-user) and geographic location. Therefore, some numerical values reported later in Section 4.6 (e.g. microgrid operating cost) will depend on the case study specifics. However, the results should be generic in terms of effectiveness of the market structure at reducing residual load uncertainty and variability, and in terms of trends in the microgrid performance. The inherent uncertainty of the microgrid's load

and renewables production should be considered during the negotiation of appropriate values for schedule elasticity and adaptability. Also note that other probability distributions could be used for e_ℓ and e_s. Normal distributions are used here for simplicity and because they are a common assumption.

Eq. (4.32) can be satisfied by ensuring that the probability of over- and under-commitment are both less than $(1-\alpha)/2$. This is captured in (4.37) and (4.38):

$$Prob\left[\begin{array}{r|l}\hat{P}_m(k)+\hat{P}_d(k)-\hat{P}_c(k)+\hat{P}_g(k) & \hat{E}_v(k)\le E_v(k)\\ \ge \hat{P}_\ell(k)-\hat{P}_s(k) & x_m(k),\ \chi_b(k)\end{array}\right]\le\frac{1-\alpha}{2}\quad\forall\, k\in\mathcal{H}(k_c) \tag{4.37}$$

$$Prob\left[\begin{array}{r|l}\hat{P}_m(k)+\hat{P}_d(k)-\hat{P}_c(k)+\hat{P}_g(k) & \hat{E}_v(k)\le E_v(k)\\ \le \hat{P}_\ell(k)-\hat{P}_s(k) & x_m(k),\ \chi_b(k)\end{array}\right]\le\frac{1-\alpha}{2}\quad\forall\, k\in\mathcal{H}(k_c) \tag{4.38}$$

These equations limit commitment violations that occur due to having too much or too little capacity committed, respectively. To avoid commitment violations due to generating excess local power, units can always be operated at their minimum feasible power contributions and all renewable power can be curtailed. Similarly, to avoid commitment violations due to insufficient local generation, units can be operated at their maximum feasible power contributions with no renewable curtailment.

Using these assumptions, (4.37) can be reformulated as (4.39) and (4.40):

$$\begin{aligned}x_m(k)P_m^{lo}-P_c^{max}(k)+E_{gc}(k)-\gamma-E_v(k)&\\ \le P_\ell(k)+\Phi^{-1}\left(\frac{1-\alpha}{2}\right)\sigma_\ell(k)&\quad\forall\, k\in\mathcal{H}_1(k_c)\end{aligned} \tag{4.39}$$

$$\begin{aligned}x_m(k)P_m^{lo}-P_c^{max}(k)+E_{gc}^{exp}(k)-\gamma-E_v(k)&\\ \le P_\ell(k)+\Phi^{-1}\left(\frac{1-\alpha}{2}\right)\sigma_\ell(k)&\quad\forall\, k\in\mathcal{H}_2(k_c)\end{aligned} \tag{4.40}$$

In these equations, $\Phi^{-1}(p)$ is the inverse cumulative distribution function of the standard normal distribution evaluated at probability p. To obtain these equations, the realized values of dispatch decisions are replaced by their minimum value, the uncertainty of the demand is evaluated at the required probability level (note that PV power is curtailed and thus not evaluated), and the equality is replaced by an inequality. In short, these

linear inequalities ensure that there exists a feasible setpoint for second-stage dispatch decisions such that the energy balance is maintained without having to increase E_v when the demand is very low. Similarly, (4.38) can be reformulated as (4.41) and (4.42):

$$\begin{aligned} x_m(k)P_m^{up} + P_d^{max}(k) + E_{gc}(k) + \gamma + E_v(k) \\ \geq P_\ell(k) - P_s^{max}(k) + \Phi^{-1}\left(\frac{1+\alpha}{2}\right)\sqrt{\sigma_\ell^2(k) + \sigma_s^2(k)} \end{aligned} \quad \forall\, k \in \mathcal{H}_1(k_c) \quad (4.41)$$

$$\begin{aligned} x_m(k)P_m^{up} + P_d^{max}(k) + E_{gc}^{exp}(k) + \gamma + E_v(k) \\ \geq P_\ell(k) - P_s^{max}(k) + \Phi^{-1}\left(\frac{1+\alpha}{2}\right)\sqrt{\sigma_\ell^2(k) + \sigma_s^2(k)} \end{aligned} \quad \forall\, k \in \mathcal{H}_2(k_c) \quad (4.42)$$

In these equations, the realized values of dispatch decisions are replaced by their maximum value, and the uncertainty of the net demand minus PV power is evaluated at the required probability level. These equations ensure that there exists a feasible setpoint for second-stage dispatch decisions such that the energy balance is maintained without having increase E_v when the net demand is high and renewables availability is low.

Eqns. (4.39)-(4.42) are used in place of (4.32) in order to obtain a MILP formulation for the scheduling problem.

4.4.6 Objective Function

The objective function to be minimized is the expected cost over the scheduling horizon. The expected operational cost for the horizon starting at time period k_c is given by:

$$\begin{aligned} \sum_{k \in \mathcal{H}(k_c)} \Big[& \zeta_v E_v(k) + \zeta_{gas} F(k) + \zeta_{buy}(k) P_{buy}(k) - \zeta_{sell}(k) P_{sell}(k) \\ & + \zeta_m y_m(k) + \zeta_b \psi_b(k) \Big] - \zeta_{store}(k_c + 47) E_b(k_c + 47) + \zeta_\Lambda \Lambda \end{aligned} \quad (4.43)$$

where ζ are cost coefficients or penalty weights. The terms are the penalty for commitment violations, cost of fuel consumed, cost and revenue from power exchange with the macrogrid, microturbine startup costs, battery cycle costs, value of the terminal battery storage level, and the commitment deviation penalty, respectively. Energy left in the battery is valued since it can be sold or used in the future. Note that this terminal storage value is only used due to the finite horizon formulation, and neither it nor the

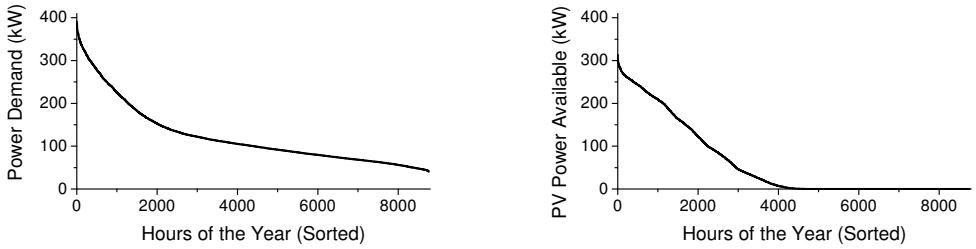

(a) (b)

Figure 4.2: Duration curves for aggregate (a) power demand and (b) PV power in the case study considered. Data obtained from Pecan Street Inc. Dataport.

commitment deviation penalty are included when calculating the realized cost.

4.4.7 Scheduling Formulations

The chance-constrained scheduling problem is the MILP:

$$\begin{aligned} &\text{Minimize} \quad (4.43) \\ &\text{Subject to:} \quad (4.4), (4.8)-(4.9), (4.11)-(4.14), (4.16)-(4.31), (4.39)-(4.42) \end{aligned}$$

In order to provide a consistent frame of reference for the results, two alternate scheduling formulations are used. One, referred to as the business-as-usual (BAU) case, does not require microgrid operators to make energy exchange commitments. This formulation will be used to evaluate the impact of the proposed market structure on the results. Since the BAU case cannot have commitment violations, the relevant constants and terms in the objective function are removed.

The other alternative, referred to as the deterministic case, requires microgrid operators to make energy exchange commitments, but does not incorporate consideration of the uncertainty into the scheduling optimization. In other words, (4.39)-(4.42) are removed from the problem. This approach will be used to evaluate the importance and effect of accounting for stochasticity during scheduling.

Table 4.2: Microturbine Model Parameters

P_m^{up} (kW)	30	$F_{m,var}$	2.7
P_m^{lo} (kW)	3	$F_{m,fix}$ (kW)	15.6
N_m	4	ζ_m (\$)	3

4.5 Case Study

A case study is considered for a microgrid serving a community of residential customers. A one year dataset of aggregate residential load and rooftop PV output is used to compare these different approaches to the scheduling problem. Recorded data of actual load and PV output in Austin, TX was obtained from the Pecan Street Inc. Dataport [2]. Duration curve representations of these datasets are shown in Fig. 4.2. The microturbine and battery sizes were chosen empirically based on the system load and the parameters are shown in Tables 4.2 and 4.3, respectively.

A time-of-use pricing scheme (shown in Table 4.4) is used for energy exchange with the macrogrid based on reported time-of-use energy tariffs for Austin Energy[3]. A constant natural gas price of 2.27 ¢/kWh is used. The commitment violation penalty rate, ζ_v, is taken to be 30.6 ¢/kWh (3x the on-peak electricity tariff). The commitment deviation penalty coefficient ζ_Λ is taken to be 100. The value of energy stored in the battery is based on the feed-in tariff after the optimization horizon:

$$\zeta_{store}(k) = \frac{\zeta_{sell}(k+1) + \zeta_{sell}(k+2) + \zeta_{sell}(k+3)}{3}$$

The results are analyzed as the two market parameters, schedule elasticity and schedule adaptability, are independently varied from 10-60 kWh. The MILP optimization problems are formulated in GAMS and solved with the CPLEX 12 solver to within a relative optimality gap of 1%. The realized values of second-stage variables are calculated in MATLAB. Total computation time for simulation of all three scheduling approaches is 90 minutes on a 2.67 GHz Intel Xeon W3520 with 4 GB RAM.

[2] `https://dataport.pecanstreet.org/`

[3] `http://en.openei.org/wiki/Utility_Rate_Database` (Accessed December 3, 2015)

Table 4.3: Battery Model Parameters

$E_{b,max}$ (kWh)	600	η_d	0.95
$E_{b,min}$ (kWh)	120	η_c	0.9
ζ_b ($)	60		

Table 4.4: Time-of-Use Pricing Scheme

Rate	Applicable Times	ζ_{buy} (¢/kWh)	ζ_{sell} (¢/kWh)
Off-Peak	10PM-6AM	4.34	0
Mid-Peak	6AM-10PM (except On-Peak)	7.68	3.57
On-Peak	Weekdays June-Sept., 2PM-8PM	10.19	6.07

4.5.1 Calculation of Realized Second Stage Variables

After each scheduling optimization is performed, the true values for demand and PV availability for the next hour are revealed and the second stage variables are calculated. To do so, the setpoints for the battery and microturbine are initially set at their scheduled values, the PV curtailment is set to 0, and the grid power is set as close to the scheduled value as possible without commitment violations. If demand exceeds generation, the dispatch of microturbines is increased first, then batteries, then the macrogrid. If generation exceeds demand, the dispatch of microturbines is decreased first, then batteries, then the macrogrid (until the energy exchange commitment would be violated), and finally PV power is curtailed. If there is still excessive generation, the contribution of the grid is decreased further. This strategy minimizes commitment violations and renewables curtailment. First-stage variables are not allowed to change from their scheduled values.

4.6 Results and Discussion

4.6.1 Power Exchange with the Macrogrid

Figs. 4.3 and 4.4 show the frequency and magnitude of realized commitment violations for both the deterministic and chance-constrained scheduling approaches. Considering

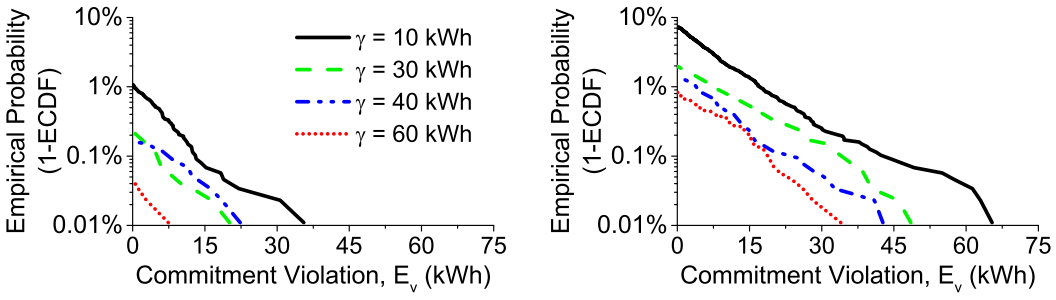

(a) Chance-constrained scheduling approach

(b) Deterministic scheduling approach

Figure 4.3: Complimentary empirical cumulative distribution function of commitment violations when schedule adpatability is 30 kWh.

uncertainty at the scheduling stage via the chance-constrained approach reduces the frequency of commitment violations by an order of magnitude versus the deterministic scheduling approach. Fig. 4.3 shows that increasing the schedule elasticity decreases the frequency and magnitude of violations since microgrid operators are given more freedom to deviate from commitments before penalties/violations are incurred. In Fig. 4.4 there is no clearly identifiable trend between schedule adaptability and commitment violations. As microgrid operators are given more freedom to establish a schedule which aggressively tracks renewable output, they are still able to meet their energy exchange commitments with a similar level of satisfaction. For practical purposes, the uncertainty in the residual load is equal to the schedule elasticity since commitment violations are infrequent (i.e. $\leq$1.5% of the time). The frequency and magnitude of commitment violations could be further reduced by incorporating flexible loads (in particular heating and air conditioning) into the scheduling problem.

Fig. 4.5 shows how the tuning of market parameters affects the residual load variability. In the BAU case, there is a large increase in this variability versus the unmodified power demand. This high variability significantly increases the ramping requirements on the macrogrid. The proposed market structure can be used to reduce or largely eliminate these high ramping requirements through a proper selection of the schedule elasticity and adaptability. For a sufficiently low schedule adaptability and elasticity, the distribution of step sizes approaches that of the unmodified power demand with the exception of a small number of larger steps when commitment violations are incurred

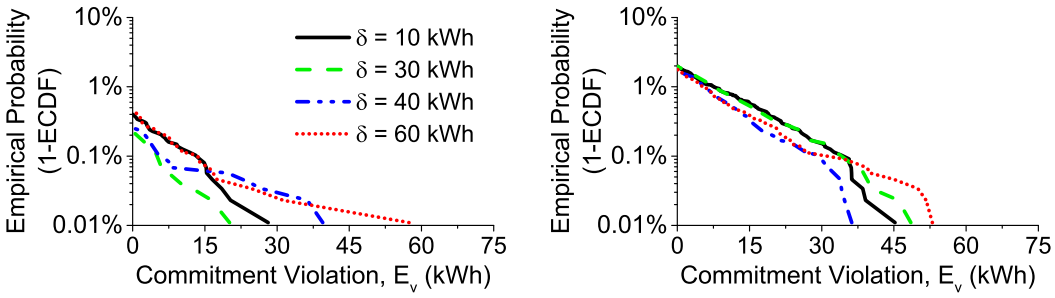

(a) Chance-constrained scheduling approach (b) Deterministic scheduling approach

Figure 4.4: Complimentary empirical cumulative distribution function of commitment violations when schedule elasticity is 30 kWh.

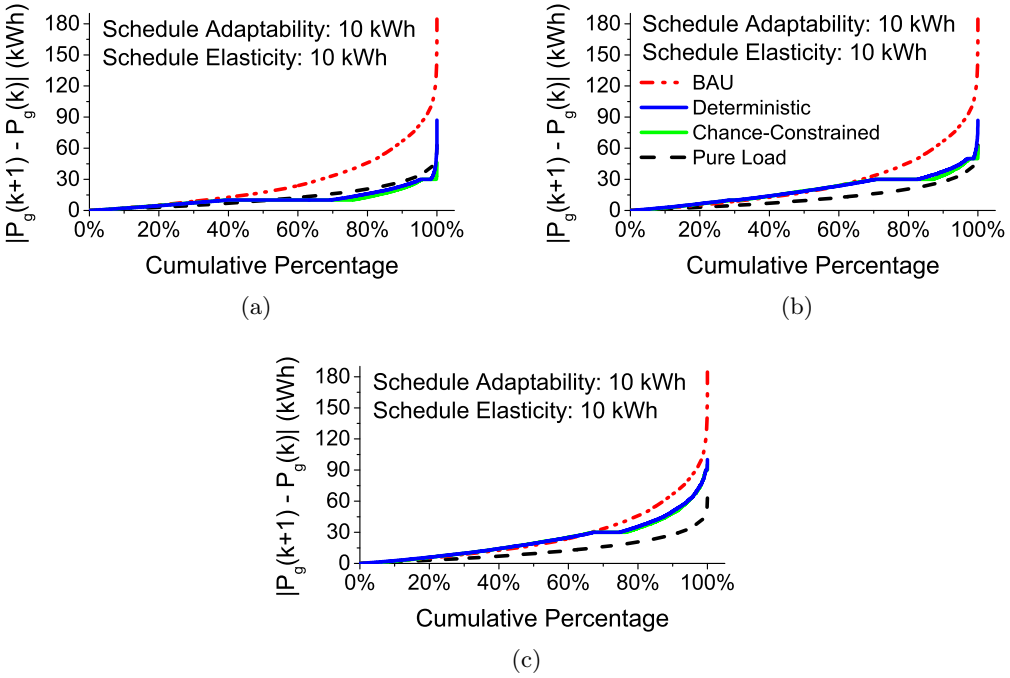

(a) (b)

(c)

Figure 4.5: Distribution of step sizes in energy exchange with the macrogrid for the unmodified load, load minus all available renewable power, chance-constrained scheduling results, and deterministic scheduling results. Load and PV data obtained from Pecan Street Inc. Dataport.

(see the sharp peak in Fig. 4.5a near 100%).

Fig. 4.6 shows how the tuning of market parameters affects the annual peak load.

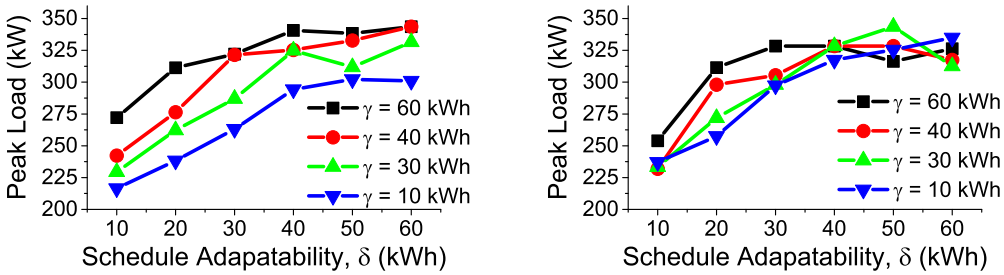

(a) Chance-constrained scheduling approach

(b) Deterministic scheduling approach

Figure 4.6: Annual peak load vs. market parameters.

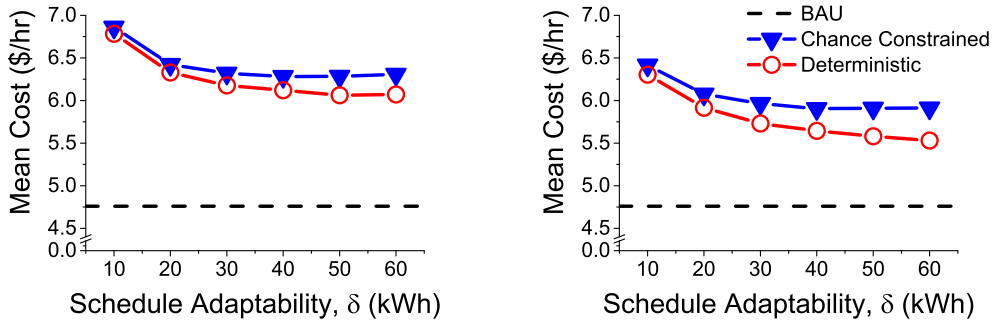

(a) Schedule elasticity = 10 kWh

(b) Schedule elasticity = 30 kWh

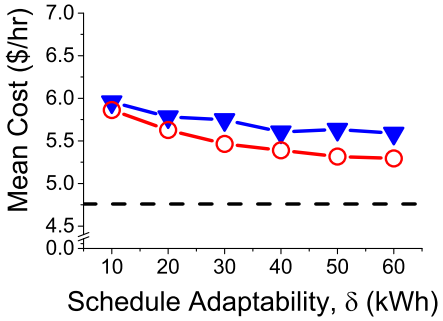

(c) Schedule elasticity = 60 kWh

Figure 4.7: Realized operating cost vs. schedule adaptability.

For the BAU case, the annual peak load is 358 kW. The peak load is lower under the proposed market structure over the entire parameter space investigated for both the chance-constrained and deterministic scheduling approaches. This peak load is

particularly reduced when the schedule adaptability is set very low (up to ∼30-40% reduction when $\delta = 10$ kWh). Varying the schedule elasticity is observed to have only a mild impact on these results. Annual peak load determines the generation capacity needed by the macrogrid, and reducing it helps to lower macrogrid energy costs.

4.6.2 Operating Cost

Fig. 4.7 shows the average microgrid operating cost as the two market parameters are changed. The cost in both chance-constrained and deterministic scheduling approaches is significantly higher than the BAU cost, though relaxing the market parameters reduces the cost. As schedule elasticity is decreased, microgrid operators are allowed less freedom to deviate from economically poor commitments that are made due to inaccurate load and renewables forecasts. In addition, commitment violation penalties increase as the elasticity is lowered. Finally, when the elasticity is low, the chance-constrained optimization must commit more microturbines even when they have low expected utilization because the macrogrid connection cannot supply much reserve capacity. The cost also decreases as the schedule adaptability is increased. This is largely due to the fact that a higher schedule adaptability allows microgrid operators to achieve a higher utilization of the freely available solar power, as will be shown in Section 4.6.3. This decrease in cost versus adaptability tapers off as the renewables utilization approaches 100 %. Finally, the operating cost is higher in the chance-constrained approach than the deterministic approach since the scheduling results are inherently more conservative in order to ensure that the probability of incurring commitment violations is very small. On average, the chance-constrained scheduling approach is 4% more expensive than the deterministic scheduling approach.

In addition to curtailment of renewables, the cost under the proposed market structure is high since flexibility is provided solely via microturbines and the battery. Microturbines are less electrically efficient and more costly than utility-provided power, but they may be more attractive when used for cogeneration. This was not considered in this work to maintain simplicity. In addition, the battery cycling cost is based on the replacement cost which is significant. The BAU case has a lower energy supply cost because it uses these units relatively infrequently and typically relies on the macrogrid connection for providing any needed balancing power. The relative cost depends on the

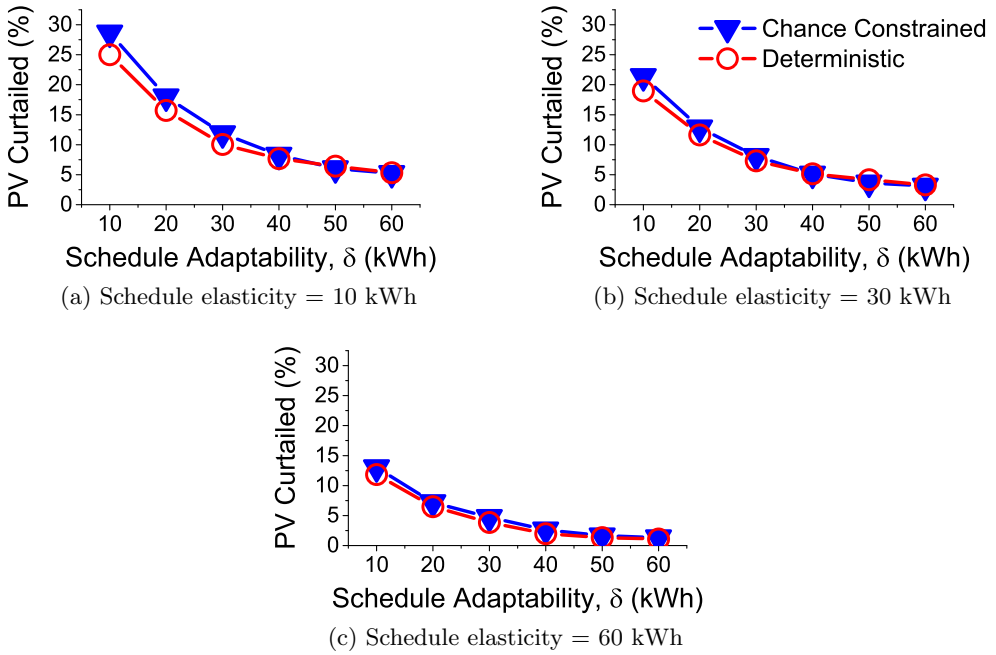

(a) Schedule elasticity = 10 kWh

(b) Schedule elasticity = 30 kWh

(c) Schedule elasticity = 60 kWh

Figure 4.8: Curtailed PV power vs. schedule adaptability.

case study specifics, but the incorporation of active loads is expected to significantly improve this trade-off between regulation and economic performance (e.g. heating and cooling loads can be shifted at little opportunity cost).

4.6.3 Utilization of Renewables

Fig. 4.8 shows the amount of available solar power curtailed. Curtailment can reach extreme values of >20% when energy exchange with the macrogrid is very tightly regulated. However, increasing the schedule elasticity and/or the schedule adaptability allows microgrid operators to achieve a higher utilization of renewables. Fig. 4.8a shows that, with a high schedule adaptability, microgrid operators are able to utilize over 95% of available PV power even when the schedule elasticity is low. As previously mentioned, the chance-constrained scheduling approach is inherently more conservative than the deterministic approach which results in more curtailment of PV power. However, this curtailment is at worst 3.7 percentage points higher than the deterministic case over the entire parameter space investigated. The renewables utilization under strict

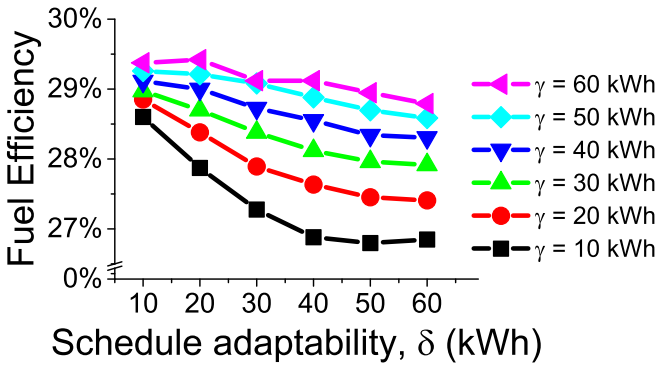

Figure 4.9: Local fuel efficiency for the chance-constrained scheduling approach.

market regulation could be improved by incorporating flexible loads into the scheduling and dispatch of the microgrid system as it would provide another potential use for the power that cannot be exported to the grid.

4.6.4 Local Fuel Efficiency

Fig. 4.9 shows the overall microturbine fuel efficiency achieved in the chance-constrained scheduling approach. As the schedule adaptability is increased at constant schedule elasticity, the average fuel efficiency decreases. Utilization of PV power increases with the adaptability, but this introduces more uncertainty into the power balance. This leads to more frequent operation of microturbines at low power setpoints to provide reserve capacity that can respond to stochasticity and a lower fuel efficiency. As the schedule elasticity increases, the fuel efficiency improves because the grid connection can respond more actively to realized stochasticity and there is less need for local reserve capacity. Furthermore, when the schedule elasticity is high, microturbines are less likely to need to be turned on due to a poor energy exchange commitment.

4.7 Conclusion

In this chapter, a novel market structure with constrained energy exchange is proposed to reduce the disruptive impact of microgrids on the macrogrid. A case study for a residential microgrid is used to show that the proposed market structure is able to significantly reduce the uncertainty and variability of the microgrid residual load. The

magnitude of this uncertainty and variability reduction depends on the choice of two tunable market parameters, the schedule elasticity and schedule adaptability. Under sufficiently tight energy exchange regulation, the macrogrid ramping requirements for serving the residual load are practically indistinguishable from serving the unmodified power demand. When stochasticity is incorporated into the microgrid scheduling problem via the proposed chance-constrained formulation, the empirical probability of exceeding the allowed elasticity (or equivalently, the probability of having any commitment violation) in a given hour is less than 1.5% for all the combinations of market parameters studied. Not accounting for stochasticity during scheduling resulted in an order of magnitude increase in the probability of incurring commitment violations.

There is a degradation in microgrid performance as the level of regulation increases. Most importantly, the operating cost and curtailment of available renewable power rise sharply under tight regulation. The fuel efficiency and environmental performance of the microgrid may also be negatively impacted by increasing regulation. These trends may limit the level of regulation that can be achieved without rendering microgrids economically infeasible. However, there is a range of market parameters where reasonable trade-offs between energy exchange regulation and microgrid performance is observed. The chance-constrained scheduling approach has slightly worse performance in these areas, but is significantly better at fulfilling energy exchange commitments. Finally, the cost of meeting energy exchange commitments was shown to be significant, but the incorporation of controllable loads and cogeneration into the scheduling and dispatch can be used to reduce this cost; this will be addressed in the next chapter.

4.8 Nomenclature

Table 4.5: Nomenclature - Sets/Indicies

k	Time periods	$\mathcal{H}(k)$	Planning horizon
$\mathcal{H}_1(k)$	Portion of planning horizon with commitments	$\mathcal{H}_2(k)$	Portion of planning horizon without commitments

Table 4.6: Nomenclature - Parameters

α	Confidence level	e_ℓ	Power load forecast error
γ	Schedule elasticity	e_s	Solar power forecast error
δ	Schedule adaptability	$E_{b,max}$	Maximum battery storage level
ζ_Λ	Commitment deviation cost	$E_{b,min}$	Minimum battery storage level
ζ_b	Battery cycle cost	E_{gc}	Energy exchange commitment
ζ_{buy}	Power purchase cost	$F_{m,fix}$	Microturbine fixed fuel consumption
ζ_{gas}	Natural gas cost	$F_{m,var}$	Microturbine marginal fuel consumption
ζ_m	Microturbine start up cost	N_m	Number of microturbines installed
ζ_{sell}	Feed-in tariff	P_ℓ	Forecasted power load
ζ_{store}	Battery storage value	$\hat{P}_\ell$	True power load
ζ_v	Commitment violation cost	$P_{m,lo}$	Minimum microturbine setpoint
η_c	Battery charging efficiency	$P_{m,up}$	Maximum microturbine setpoint
η_d	Battery discharging efficiency	P_s^{max}	Forecasted solar power available
σ_ℓ	Load error standard deviation	$\hat{P}_s^{max}$	True solar power available
σ_s	Solar error standard deviation	$P_{s,rated}$	Solar panel rated power

Table 4.7: Nomenclature - Binary Variables ($1 \implies$ True)

χ_b	Is battery charging	ψ_b	Is battery cycled

Table 4.8: Nomenclature - Integer Variables ($\in \{0, 1, 2, ...\}$)

x_m	Number of microturbines on	y_m	Number of microturbines started up

Table 4.9: Nomenclature - Continuous Variables

Λ	Commitment deviation	P_d	Planned power discharged
E_{gc}^{exp}	Expected exchange commitment	$\hat{P}_d$	True power discharged
E_v	Planned commitment violation	P_d^{max}	Maximum power discharged
$\hat{E}_v$	True commitment violation	P_g	Planned power exchange
E_b	Battery storage level	$\hat{P}_g$	True power exchange
F_m	Microturbine fuel usage	P_m	Planned microturbine power
P_{buy}	Planned power import	$\hat{P}_m$	True microturbine power
P_c	Planned power charged	P_s	Planned solar PV power
$\hat{P}_c$	True power charged	$\hat{P}_s$	True solar PV power
P_c^{max}	Maximum power charged	P_{sell}	Planned power export

CHAPTER 5

Scheduling and Supervisory Control for Cost Effective Load Shaping of Microgrids with Flexible Demands

5.1 Introduction

In the last chapter, a market/regulatory structure for microgrids which sought to address the issues of both variability and uncertainty in an intrinsic manner was proposed. Fundamentaly, this market structure explicitly limits both the uncertainty and variability burden placed on utility companies by their customers who choose to install distributed generation. This is achieved by requiring the residual load to lie close to day-ahead commitments made by the microgrid operator. The results in Chapter 4 show that a high level of regulatory performance can be achieved (i.e. residual load uncertainty and variability can be reduced as desired). However, this also results in a 20-45% increase in microgrid operating cost. This cost increase is primarily associated with enabling local flexibility via microturbines and a battery bank alone.

A key improvement made in this chapter is to directly consider controllable loads along with controllable generation and storage. By taking an integrated supply-side and demand-side focus, the flexibility inherent in controllable loads can be used to meet load shaping constraints at very little opportunity cost. In particular, space heating and

cooling demands (which constitute a large fraction of the energy demands of residential and commercial customers) are an attractive candidate since they are ubiquitous and can typically be shifted several hours with no impact on end-user comfort. Other authors have shown that model predictive control of heating/cooling systems for buildings can result in substantial energy or cost savings (i.e. in the case of time-varying electricity prices) by leveraging this inherent flexibility [113, 114]. Motivated by this, the model presented in Chapter 4 is extended to consider a controllable air conditioning (A/C) system and the relevant building temperature dynamics. Furthermore, in this chapter, a hierarchical control approach is formulated which considers not only the hourly scheduling of such a system, but also the real-time control.

Past works have highlighted the potential benefits of integrating controllable loads into microgrid power systems. Typically, these controllable loads have been used to improve the performance of the microgrid in the context of time-varying and uncertain market prices and/or end user demand. Past authors have considered cases where the controllable loads are shiftable [97, 115, 116], curtailable [117], flexible [79, 118, 119], or a combination thereof [81, 120]. They have shown that integrated supply and demand management leads to reduced energy supply cost, renewable curtailment, environmental impact, and peak demand. However, these controllable loads have typically been treated in a fairly abstracted/generalized manner. Exceptions do exist where a a specific, detailed controllable load is considered; for example, [118] considers a microgrid coupled with a flexible reverse osmosis desalination system. Others have also considered the integration of electric vehicles to serve as controllable storage/loads within a microgrid (e.g. [106, 121]). In this chapter, air conditioning is selected as a controllable load both due to its intrinsic flexibility and because it is already a widely used technology (i.e. unlike electric vehicles). Thus, the formulation developed is widely applicable, and the results presented serve as a good general indicator of the potential for demand management to enhance load shaping in microgrids.

From a technical perspective, the research in this chapter offers two important contributions:

- A method is proposed for effectively integrating economic optimization at different time scales for these microgrid energy systems.

- A detailed dynamic simulation of a microgrid is developed in the Simulink environment. This model is used to test the formulated supervisory controller, and it has been made available online.

The first is important as many works in literature focus on scheduling or control of microgrid systems at a single time scale, e.g. [78–80, 83–85, 87, 88, 91, 92, 95, 96, 98, 101, 102, 106, 115, 116, 119, 120]. In doing so, they risk missing degradation in performance of the control system due to poor coordination between decision making at different time scales (and over different prediction horizons). Furthermore, performance degradation may result from inherent plant-model mismatch between the optimization formulation and the true underlying dynamic system, or due to the discrete sampling time of the optimization-based decision making. The second technical contribution of this chapter helps to address this issue. The virtual microgrid model that has been made publicly available provides an open-source platform that can be used to test similar scheduling and supervisory control approaches. Thus, it enables researchers to more easily reproduce published work, and they can this virtual microgrid as needed.

5.2 Model Formulation

To demonstrate that the desired load-shaping can be achieved in a cost-effective manner, a microgrid supervisory control problem is formulated for the system shown in Figure 5.1. In the problem considered, several time scales naturally arise. In particular, a slow time scale on the order of hours-days is associated with the evolution of storage inventories (e.g. battery level), diurnal weather patterns, and the temperature dynamics of solid building elements (e.g. thick concrete floors and external walls). Moreover, energy exchange with the utility company must be coordinated on this time scale as dictated by the market structure that was described in Chapter 4. A fast time scale on the order of minutes-hours is associated with temperature dynamics of the indoor air and fluctuations in demand and weather (e.g. cloud coverage).[1]

Thus, to effectively manage storage inventory and market participation, a planning horizon of days is required. However, the control system must also update decisions

[1] An even faster time scale (on the order of seconds or less) is associated with setpoint tracking by the various distributed energy units. This time scale is not considered by the central/supervisory controller since established local control methods can be used for fast, offset-free tracking of these setpoints.

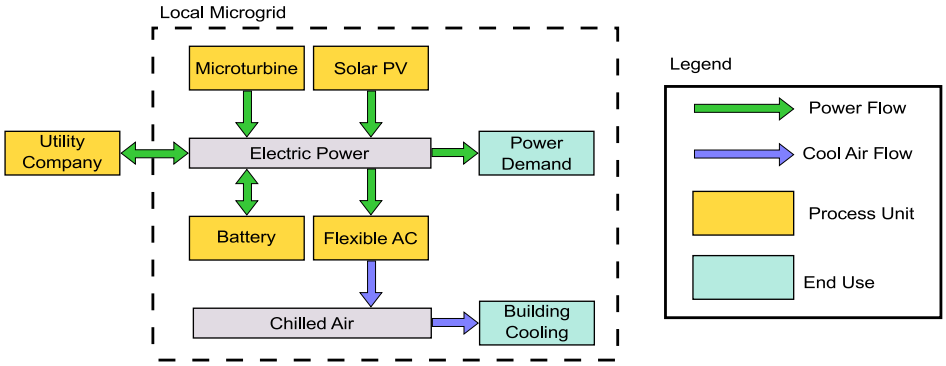

Figure 5.1: System considered.

frequently to respond to intra-hour stochasticity, efficiently utilize all available renewable energy, and prevent violating energy exchange commitments.

To effectively address this challenging control problem, a hierarchical approach is proposed where centralized decision making occurs at two time scales: the scheduling stage (which considers a time horizon of days) and the dispatch stage (which considers a time horizon of hours). The primary goal of the scheduling stage is to optimize the unit commitments (i.e. the discrete operating state of units), determine the trajectory for slowly evolving system states (e.g. average building temperature), and coordinate participation in the external power market. The primary goal of the dispatch layer is to optimize the setpoint trajectory for each unit in order to minimize the short-run operational cost, respond to disturbances, and keep the system on track to meet long-term goals (e.g. building temperature, external energy exchange). An overview of the information flow in this hierarchical scheme is shown in figure 5.2.

Receding horizon optimization is used for both the scheduling and dispatch problems. An economic cost is minimized at both time scales since intra-hour disturbances (which are only accounted for by the dispatch layer) can have a significant impact on the overall operating cost. Due to the longer time horizon and mixed integer nature of the scheduling problem, it utilizes a coarser temporal granularity and convex approximations for the process dynamics.

In the following subsections, the market structure is outlined, and the optimization problem is described. In the interest of readability and brevity, only key equations are highlighted in the main body of the chapter, and the full optimization formulations can

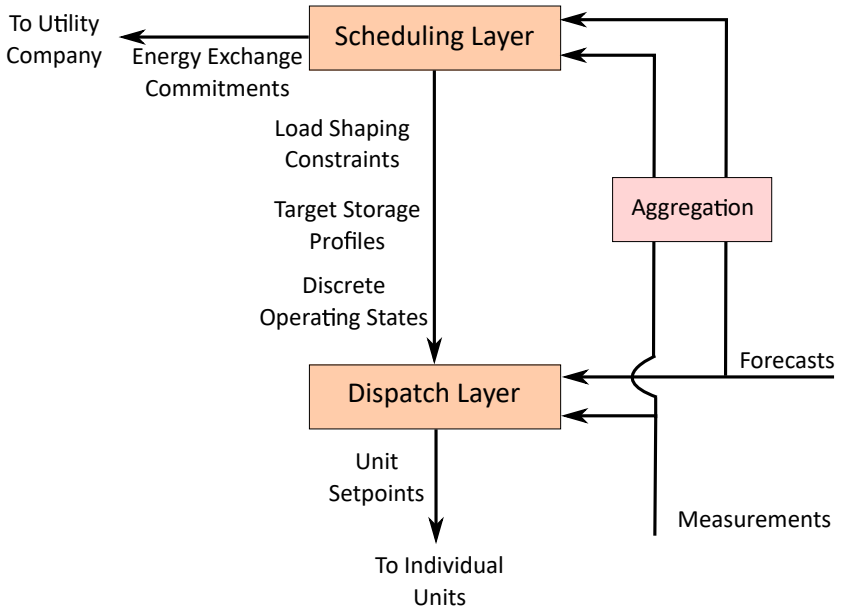

Figure 5.2: Overview of information flow in the proposed hierarchical control approach.

be found in Sections 5.8.1 and 5.8.2.

5.2.1 Market Structure

The market structure proposed in Chapter 4 is again used, so only a brief description is provided here. The presentation is modified slightly since some decision making (i.e. the dispatch layer) considers a finer temporal granularity than in Chapter 4.

Power is continuously exchanged with the utility company based on the difference between local generation and consumption. This power is metered over a series of *balancing periods* resulting in a net energy exchange over each balancing period:

$$E_g(h) = \int_{t \in h} P_g(t) dt \tag{5.1}$$

where h is a balancing period index, P_g is the power load (i.e. the instantaneous power exchange between the microgrid and utility company), and E_g is the net energy

exchange[2]. In a discrete time formulation, this is calculated as:

$$E_g(h) = \sum_{k \in h} P_g(k) \Delta_T \tag{5.2}$$

where Δ_T is the time period length in the discrete-time formulation. A balancing period of 1 hour is used (for example, net energy exchange would be metered over the period from 8 AM to 9 AM).

Recall that, the *uncertainty* in the energy exchange over each balancing period is explicitly limited by the market parameter called *schedule elasticity*:

$$-\gamma - E_v(h) \leq E_g(h) - E_{gc}(h) \leq \gamma + E_v(h) \tag{5.3}$$

where γ is the schedule elasticity parameter, E_v is a non-negative commitment violation which the microgrid operator will be penalized for, and E_{gc} is an energy exchange commitment. Also recall that, *variability* in the residual load profile is explicitly limited by limiting the hour-to-hour difference between commitments with a market parameter called *schedule adaptability*:

$$E_{gc}(h-1) - \delta \leq E_{gc}(h) \leq E_{gc}(h-1) + \delta \tag{5.4}$$

where δ is the schedule adaptability. Microgrid operators must provide this energy exchange commitment to the utility company 24 hours in advance. This gives utility companies sufficient time to incorporate the information into their scheduling and dispatch decisions. Importantly, microgrid energy demands will always be met, but fines are incurred for violating these restrictions (i.e. if $E_v(h) \neq 0$).

5.2.2 Microturbines

Microturbines generate power locally via combustion of natural gas. These units are controllable and are treated as indistinguishable in the optimization formulation. The aggregate power generated by microturbines is confined within some stable operating

[2]Note that in Chapter 4 no distinction was made between P_g and E_g since the decision-making and analysis was all done at a sampling time of 1 hour. This is no longer the case in this chapter.

range described by:

$$x_m(k)P_m^{lo} \leq P_m(k) \leq x_m(k)P_m^{up} \tag{5.5}$$

where x_m is the number of microturbines currently on, P_m is the total power output, and P_m^{lo} and P_m^{up} are the minimum and maximum setpoints for an individual microturbine. Importantly, x_m is a decision variable in the scheduling formulation, whereas it is treated as a fixed parameter in the dispatch formulation (based on the decisions made in the most recent scheduling iteration). This prevents the rapid on-off cycling of microturbines in response to short-term stochasticity.

The primary cost of utilizing these microturbines comes from the fuel consumption, which is taken to be an affine function of the power output:

$$F_m(k) = F_{m,var}P_m(k) + F_{m,fix}x_m(k) \tag{5.6}$$

where F_m is the fuel consumption, and $F_{m,var}$ and $F_{m,fix}$ are positive constants. By directly relating fuel consumption to power output (and leaving electrical efficiency implicitly defined), one does not introduce any non-convexities and still achieves an accurate representation of the performance at partial load [45].

In the scheduling formulation, an additional cost is accrued when turning on microturbines due to the wear-and-tear incurred in these events.

5.2.3 Photovoltaic Panel

Fixed-angle photovoltaic panels generate renewable power on-site. The available renewable power is a function of the weather only and is not impacted by the control decisions. This maximum available renewable power is computed before each optimization instance based on the current system state and available weather forecasts. However, the PV panels can be intentionally operated at sub-optimal conditions to use less than the maximum available power. Thus, the PV power is *curtailable* rather than controllable:

$$0 \leq P_s(k) \leq P_s^{max}(k) \tag{5.7}$$

where P_s^{max} is the weather-dependent renewable availability and P_s is the actual renewable power used. While not normally desirable, this curtailment of renewable power

may be necessary to avoid exporting too much power to the utility company and thereby incurring commitment violations.

5.2.4 Battery

A battery bank is used for electrical energy storage. In Chapter 4, the battery was modeled using a fixed cycle cost and constant efficiencies. In this chapter, the battery model is improved by penalizing charing and discharging of the batter (i.e. deep cycles are *de facto* more expensive than shallow cycles). Additionally, the battery efficiency is not explicitly calculated (much like the microturbine modeling). Instead, losses are imposed by calculating the energy lost to internal heat generation.

The change in the battery storage level is related to the apparent power and internal heat generation:

$$E_{b,max}\big(\xi_b(k) - \xi_b(k-1)\big) = \Delta_T\big(\eta_I P_c(k) - Q_c(k) - P_d(k)/\eta_I - Q_d(k)\big) \tag{5.8}$$

where $E_{b,max}$ is the rated battery storage capacity, ξ_b is the battery state of charge (SOC), η_I is the inverter efficiency, P_c is the power sent to the battery, P_d is the power withdrawn from the battery, and Q_c and Q_d are internal heat generation due to charging and discharging, respectively. Internal heat generation is related directly to the charging and discharging power:

$$Q_c(k) \geq \lambda_{c1} P_c(k)^2 \tag{5.9}$$

$$Q_d(k) \geq \lambda_{d1} P_d(k)^2 \tag{5.10}$$

where the λ parameters are positive, empirical constants. Thus, the *de facto* efficiency of the battery is lower if charging or discharging rapidly. In addition, the charging efficiency is known to be lower when the battery is nearly full. This can be captured by adding an additional inequality:

$$Q_c(k) \geq \lambda_{c2} P_c(k)^2 + \lambda_{c3} P_c(k) + \lambda_{c4} \xi_b(k) + \lambda_{c5} \tag{5.11}$$

where this new constraint is active when the battery SOC is close to 1. This modeling of internal heat generation also allows one to predict the battery electrolyte temperature

and prevent battery overheating which could cause irreversible damage. In the scheduling formulation, a binary variable, χ_b, is introduced so that simultaneous charging and discharging cannot be considered.

A storage value term is included in the objective function which rewards a high battery SOC at the end of the planning horizon. Moreover, a soft-tracking constraint is added to the dispatch problem:

$$\epsilon_b \geq \xi_b^{target} - \xi_b(k_f) \tag{5.12}$$

where ϵ_b is a storage shortfall which is penalized, k_f is the final period in the planning horizon, and ξ_b^{target} is a target storage level. This target storage level is used to prevent myopic closed-loop behavior due to the short planning horizon of the dispatch layer. The value of ξ_b^{target} is based on the storage trajectory in the solution of the scheduling problem[3]. Thus, the dispatch layer is able to deviate from the long-term storage trajectory (e.g. in response to realized disturbances), but is penalized for doing so because it may compromise the ability to meet energy exchange commitments in the future.

Finally, the dispatch problem also considers the battery *depth of charge* (DOC) in addition to the SOC. The DOC is the amount of energy accessible based on the charging/discharging history. In particular, the DOC will be lower than the SOC during prolonged periods of discharging. In the dispatch problem, the DOC is constrained to lie above a minimum value since the internal resistance of the battery will diverge as the DOC approaches 0. Similar considerations cannot be incorporated into the scheduling problem due to their non-convexity[4]. However, the dispatch layer is generally able to find a setpoint trajectory for the battery that satisfies other needs and does not violate this minimum DOC constraint.

5.2.5 Building Thermal Model

The building is modeled as a set of air conditioned thermal zones, a set of solid building elements (e.g. walls, floors, etc.), and a set of plenum spaces (where air is returned

[3] E.g., if the dispatch planning horizon ends at 9:34 AM, ξ_b^{target} is found by linearly interpolating between the optimal storage levels (as determined by the scheduling layer) at 9 AM and 10 AM.

[4] In addition the temporal resolution of the scheduling layer is quite coarse, so it is less likely that these constraints related to transient phenomena will be active.

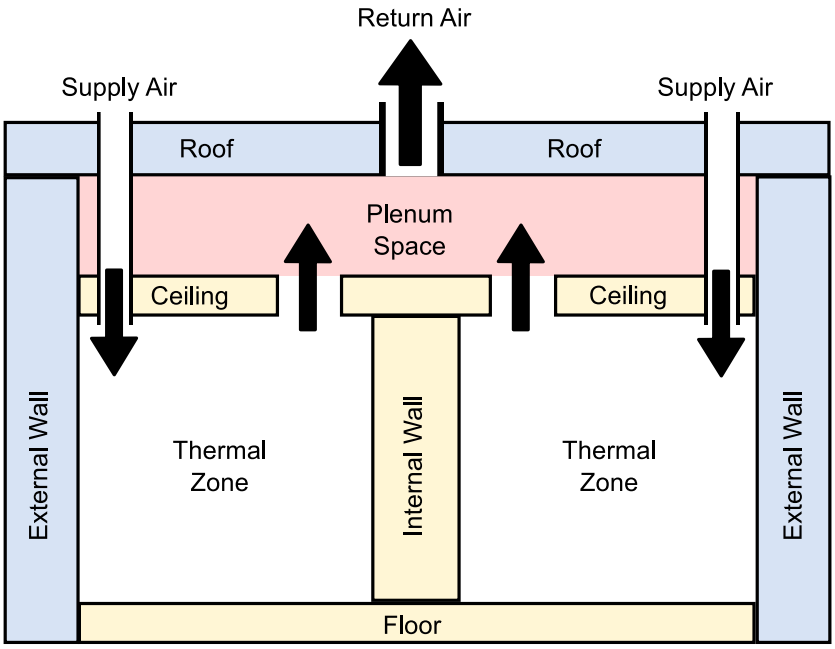

Figure 5.3: Sample building model. Internal building elements (e.g. internal walls, ceilings, etc.) are shown in light yellow, external building elements (i.e. external walls, roofs) are shown in blue, conditioned thermal zones are shown in white, and plenum spaces are shown in red. Black arrows indicate air flow for the ventillation system.

from the conditioned zones to the A/C system). A simple diagram of such a building model consisting of only two zones is shown in figure 5.3. The supply air is cooled to a constant temperature by the A/C system, and the flow rate of air to each zone is varied to regulate zone temperature. The air temperature in each zone should be:

- Between 21-24^{o}C during occupied hours (i.e. 8 AM - 6 PM)
- Between 18-27^{o}C during unoccupied hours

The air in each zone is assumed to be well-mixed. The temperature dynamics are then described by:

$$\begin{aligned} \rho C_p V_z \tfrac{dT_z}{dt} &= \rho C_p q_{leak,z}\big(T_{amb}(t) - T_z(t)\big) \\ &+ \textstyle\sum_e A_{z,e} h_{int}\big(T_e^{int}(t) - T_z(t)\big) \\ &+ \textstyle\sum_i A_{z,i} h_{int}\big(T_i(t) - T_z(t)\big) \\ &+ \textstyle\sum_w A_{z,w} U_w\big(T_{amb}(t) - T_z(t)\big) \\ &+ \textstyle\sum_w A_{z,w} H_w(t)\sigma_w \\ &+ Q_{gen,z}(t) + Q_{flow,z}(t) \end{aligned} \tag{5.13}$$

The first line describes enthalpy flow due to infiltration/exfiltration. The second and third line describe convective heat transfer with solid building elements. The fourth line describes heat transfer with the outdoor air via windows. The fifth line describes heat gain from solar radiation on the windows. The last line describes the internal heat generation within the zone and cooling power delivered by the ventilation of chilled air.

Similar ordinary differential equations (ODEs) are used to describe the temperature in plenum spaces:

$$\begin{aligned} \rho C_p V_{pl} \tfrac{dT_{pl}}{dt} &= \rho C_p q_{leak,pl}\big(T_{amb}(t) - T_{pl}(t)\big) \\ &+ \textstyle\sum_e A_{pl,e} h_{int}\big(T_e^{int}(t) - T_{pl}(t)\big) \\ &+ \textstyle\sum_i A_{pl,i} h_{int}\big(T_i(t) - T_{pl}(t)\big) \\ &+ Q_{flow,pl}(t) \end{aligned} \tag{5.14}$$

Note that there are no windows in plenum spaces, and the last line represents the flow of enthalpy from thermal zones to the plenum spaces due to the ventilation flow.

The enthalpy flow terms $Q_{flow,z}$ and $Q_{flow,p}$ are given by bilinear equations:

$$Q_{flow,z}(t) = q_{vent,z}(t)\rho C_p\big(T_{ac} - T_z(t)\big) \tag{5.15}$$

$$Q_{flow,pl}(t) = \sum_{z \in \mathcal{Z}_{pl}} q_{vent,z}(t)\rho C_p\big(T_z(t) - T_{pl}(t)\big) \tag{5.16}$$

where $q_{vent,z}$ is the ventilation rate of chilled air to each zone and $\mathcal{Z}_{pl}$ is the set of zones connected to plenum space pl. Each zone is connected to exactly one plenum.

The internal building elements are each assumed to be at uniform temperature. Their temperatures are described by:

$$\begin{aligned} M_i \tfrac{dT_i}{dt} &= \textstyle\sum_z A_{z,i} h_{int}\big(T_z(t) - T_i(t)\big) \\ &+ \textstyle\sum_{pl} A_{pl,i} h_{int}\big(T_{pl}(t) - T_i(t)\big) \end{aligned} \tag{5.17}$$

The external walls and roof have a significantly higher thermal resistance, and are exposed to much larger temperature differentials than internal building elements. Therefore, rather than a single uniform temperature, these external building elements are described in terms of an *internal*, *external*, and *bulk* temperature:

$$\begin{aligned} M_e^{int} \frac{dT_e^{int}}{dt} &= A_e U_{e,1}\big(T_e^{blk}(t) - T_e^{int}(t)\big) \\ &+ \sum_z A_{z,e} h_{int}\big(T_z(t) - T_e^{int}(t)\big) \\ &+ \sum_{pl} A_{pl,e} h_{int}\big(T_{pl}(t) - T_e^{int}(t)\big) \end{aligned} \tag{5.18}$$

$$\begin{aligned} M_e^{blk} \frac{dT_e^{blk}}{dt} &= A_e U_{e,1}\big(T_e^{int}(t) - T_e^{blk}(t)\big) \\ &+ A_e U_{e,2}\big(T_e^{ext}(t) - T_e^{blk}(t)\big) \end{aligned} \tag{5.19}$$

$$\begin{aligned} M_e^{ext} \frac{dT_e^{ext}}{dt} &= A_e U_{e,2}\big(T_e^{blk}(t) - T_e^{ext}(t)\big) \\ &+ A_e h_{ext}\big(T_{amb}(t) - T_e^{ext}(t)\big) \\ &+ A_e \sigma_e H_e(t) \end{aligned} \tag{5.20}$$

Equations (5.13)-(5.14) and (5.17)-(5.20) can be combined into:

$$\boldsymbol{M}\frac{d\boldsymbol{T}}{dt} = \boldsymbol{A}\boldsymbol{T}(t) + \boldsymbol{B}\boldsymbol{U}(t) \tag{5.21}$$

$$\boldsymbol{U}(t) = \big[\boldsymbol{Q_{flow}}(t)\ \ \boldsymbol{Q_{gen}}(t)\ \ \boldsymbol{H}(t)\ \ T_{amb}(t)\big]^T \tag{5.22}$$

where $\boldsymbol{T}$ is the vector of all building temperatures, $\boldsymbol{Q_{flow}}$ is the vector that collects all $Q_{flow,z}$ and $Q_{flow,pl}$, $\boldsymbol{Q_{gen}}$ is the vector of $Q_{gen,z}$ for all zones, $\boldsymbol{H}$ is the vector of solar radiation on all surfaces, and $\boldsymbol{M}$, $\boldsymbol{A}$, and $\boldsymbol{B}$ are appropriately defined matrices.

Then, the thermal model in the dispatch problem is given by the discretized ODEs using a zero-order hold approximation for the enthalpy flow terms:

$$\boldsymbol{T}(k+1) = \boldsymbol{A_d}\boldsymbol{T}(k) + \boldsymbol{B_d}\boldsymbol{U}(k) \tag{5.23}$$

$$Q_{flow,z}(k) = q_{vent,z}(k)\rho C_p\big(T_{ac} - T_z(k)\big) \tag{5.24}$$

$$Q_{flow,pl}(k) = \sum_{z\in\mathcal{Z}_{pl}} q_{vent,z}(k)\rho C_p\big(T_z(k) - T_{pl}(k)\big) \tag{5.25}$$

where,

$$\boldsymbol{A_d} = e^{\Delta_T \boldsymbol{M}^{-1}\boldsymbol{A}} \tag{5.26}$$

$$\boldsymbol{B_d} = \boldsymbol{A}^{-1}\boldsymbol{M}\big(e^{\Delta_T \boldsymbol{M}^{-1}\boldsymbol{A}} - \boldsymbol{I}\big)\boldsymbol{M}^{-1}\boldsymbol{B} \tag{5.27}$$

To reduce problem size at the scheduling stage, some aggregation is performed. In particular:

- All internal air (i.e. conditioned zones and plenum spaces) is assumed to be at a single uniform temperature.
- All internal building elements of the same type are considered indistinguishable (i.e. all internal walls are aggregated, all floors are aggregated, etc.)

Then, the reduced order thermal model is described in terms of similar discretized ODEs with the appropriate phenomena removed (e.g. the enthalpy flow from zones to plenum spaces is neglected since only an average indoor air temperature is considered). Furthermore, to preserve the convexity of the scheduling problem, Eq. (5.24) is replaced by:

$$Q_{flow}(k) = q^{tot}_{vent}(k)\rho C_p\big(T_{ac} - \bar{T}_z\big) \tag{5.28}$$

where q_{vent} is the total ventilation flow rate, and $\bar{T}_z$ is a nominal indoor temperature.

Finally, the weighted average building temperature is calculated as it represents an implicit form of storage (i.e. having the building colder will offset future power consumption by the A/C unit). Like battery storage level, the terminal building temperature is rewarded in the objective function. Moreover, a tracking constraint analogous to Equation (5.12) is included in the dispatch problem so that activities like pre-cooling of the building during the night can be coordinated.

5.2.6 Cooling System

A controllable A/C and ventilation system is used to deliver cool air to the building zones. The thermal cooling power needed to maintain the fixed air supply temperature is given by:

$$Q_{ac}(k) = \rho C_p q^{tot}_{vent}(k)\big(T_{mix}(k) - T_{ac}\big) \tag{5.29}$$

where T_{mix} is the inlet temperature, and Q_{ac} is the cooling duty of the A/C unit. The input air to the A/C unit is a mixture of the air returned via plenum spaces and outdoor air:

$$q^{tot}_{vent}(k)T_{mix}(k) = q^{tot}_{vent}(k)T_{amb}(k)\big(1 - f_r(k)\big) + \sum_{pl}\sum_{z\in\mathcal{Z}_{pl}} q_{vent,z}(k)T_{pl}(k)f_r(k) \tag{5.30}$$

where f_r is the fraction of return air that is recycled (i.e. chilled and sent back to the building). Fresh air from outside is used to supplement this recycled air if $f_r < 1$. Typically it is more energy efficient to recycle indoor air rather than using outdoor air. However, during rare occurrences it may be energetically favorable to use outdoor air (e.g. an unusually cold summer night). In addition, some minimum flow rate of fresh air is typically required during occupied hours for human health and safety purposes [122]:

$$q_{vent,z}(k)\big(1 - f_r(k)\big) \geq q^{min}_{fresh,z}(k) \tag{5.31}$$

where $q^{min}_{fresh,z}$ is the minimum flow rate of fresh air, which is taken to be 8.5 L/s-person during occupied hours.

Due to the aggregation in the scheduling problem, the cooling duty can be alternatively described by:

$$Q_{ac}(k) = \rho C_p q^{tot}_{fresh}(k)\big(T_{amb}(k) - T_{ac}\big) + \rho C_p q^{tot}_{recycle}(k)\big(\bar{T}_z - T_{ac}\big) \tag{5.32}$$

$$q^{tot}_{vent}(k) = q^{tot}_{fresh}(k) + q^{tot}_{recycle}(k) \tag{5.33}$$

$$q^{tot}_{fresh}(k) \geq \sum_z q^{min}_{fresh,z}(k) \tag{5.34}$$

where q^{tot}_{fresh} is the total flow rate of fresh air and $q^{tot}_{recycle}$ is the flow rate of recycled air. Again, a nominal indoor temperature (i.e. $\bar{T}_z$) has been used to avoid introducing

non-convex bilinearities into the scheduling problem.

The power consumption of the A/C unit is taken to be a quadratic function of the cooling duty:

$$P_{ac}(k) \geq \lambda_{ac,1} Q_{ac}(k)^2 + \lambda_{ac,2} Q_{ac}(k) \tag{5.35}$$

where P_{ac} is the electricity consumption, and the λ_{ac} coefficients are positive parameters. Similarly, the ventilation system is assumed to have a quadratic power consumption since higher flow rates will increase the pressure drop:

$$P_{vent}(k) \geq \lambda_{vent,1} q_{vent}^{tot}(k)^2 + \lambda_{vent,2} q_{vent}^{tot}(k) \tag{5.36}$$

where P_{vent} is the electricity consumption of the ventilation system, and λ_{vent} coefficients are positive parameters.

5.2.7 Incorporation of Uncertainty

The overall power generation, consumption, and import/export must be balanced:

$$P_m(k) + P_d(k) + P_s(k) + P_g(k) = P_\ell(k) + P_c(k) + P_{ac}(k) + P_{vent}(k) \tag{5.37}$$

In both the scheduling and dispatch formulations, this power balance is based on the *forecasted* renewable availability and power demands. These forecasts are assumed to be sufficiently accurate at the dispatch time scale because of the short prediction horizon. In contrast, the scheduling problem, which has a prediction horizon on the order of days, will have significant forecasting errors. Therefore, as in Chapter 4, a stochastic formulation is used in the scheduling layer to ensure that sufficient flexibility is built-in to the schedule to respond to disturbances. In particular, the chance-constrained energy balance, Eq. (5.38), is used. In this equation, α is a confidence level close to 1, and the variables denoted with a circumflex (e.g. $\hat{P_m}$) refer to the realized values after uncertainty has been revealed and recourse action has been taken.

$$Prob\left[\begin{array}{l|r} \hat{P_m}(k)+\hat{P_d}(k) + \hat{P_s}(k) + \hat{P_g}(k) & \hat{E_v}(k) \leq E_v(k) \\ \qquad = \hat{P_\ell}(k) + \hat{P_c}(k) + \hat{P_{ac}}(k) + \hat{P_{vent}}(k) & x_m(k),\ \chi_b(k) \end{array}\right] \geq \alpha \tag{5.38}$$

Recall that this constraint states that there must be a high probability of satisfying the power balance during real-time operations without updating discrete unit states or incurring unexpected commitment violations. Note that the time period length in the scheduling problem and the balancing period length are assumed to be equal.

By assuming a probability model for forecasting errors, one can obtain linear inequalities that ensure this chance constraint is satisfied. Equations (5.39) and (5.40) are obtained by assuming normally distributed forecasting errors for both power demand and solar availability.

$$\begin{aligned} P_m^{max}(k) + P_d^{max}(k) - P_{ac}^{min}(k) - P_{vent}^{min}(k) + E_{gc}(k) + \gamma + E_v(k) \\ \geq P_\ell(k) - P_s^{max}(k) + \Phi^{-1}\left(\frac{1+\alpha}{2}\right)\sqrt{\sigma_\ell^2(k) + \sigma_s^2(k)} \end{aligned} \tag{5.39}$$

$$\begin{aligned} P_m^{min}(k) - P_c^{max}(k) - P_{ac}^{max}(k) - P_{vent}^{max}(k) + E_{gc}(k) - \gamma - E_v(k) \\ \leq P_\ell(k) + \Phi^{-1}\left(\frac{1-\alpha}{2}\right)\sigma_\ell(k) \end{aligned} \tag{5.40}$$

In these equations, the maximum and minimum feasible contribution of each unit (e.g. $P_m^{max}(k)$ and $P_m^{min}(k)$) are based on the first-stage decisions (i.e. discrete operating states and energy exchange commitments) and the constraints related to each unit. In addition, $\Phi^{-1}(p)$ denotes the inverse cumulative distribution function of the standard normal evaluated at probability level p. More details of the transformation of this chance constraint can be found in Chapter 4. A confidence level of 95% is used in this work.

For time periods in the scheduling problem where energy exchange commitments have not yet been made (i.e. hours 25 and beyond of the planning horizon), auxiliary variables representing the expected commitments, E_{gc}^{exp}, are introduced in place of E_{gc}.

5.2.8 Optimization Formulations

The scheduling layer is ultimately formulated as a mixed integer quadratically constrained program with the objective function:

$$\begin{aligned} \text{minimize} \quad & \sum_k \Big[\quad \zeta_{buy}(k)E_{buy}(k) - \zeta_{sell}(k)E_{sell}(k) + \zeta_{gas}F_m(k) + \zeta_m y_m(k) \\ & \qquad +\zeta_c P_c(k) + \zeta_d P_d(k) + \zeta_v E_v(k) + \zeta_{comfort}T_v(k) \Big] \\ & - \quad \zeta_{store}(k_f)E_{b,max}\xi_b(k_f) + \zeta_{AC}(k_f)T_{bldg}(k_f) \end{aligned} \tag{5.41}$$

where ζ_{buy} and ζ_{sell} are the buying and selling price of electricity in each balancing period, ζ_{gas} is the cost of natural gas, ζ_{start} is the cost of starting up microturbines, y_m is the number of microturbines started up, ζ_c and ζ_d are the cost of utilizing the battery, ζ_v is the cost of commitment violations, $\zeta_{comfort}$ is the cost of comfort violations (i.e. indoor air temperature outside of the desired range), T_v is the magnitude of comfort violations, ζ_{store} and ζ_{AC} are the storage values for battery level and building temperature, and T_{bldg} is the weighted average building temperature. All of the cost cofficients, ζ, are non-negative. Note that:

$$E_{buy}(k) = \max\big(E_g(k), 0\big) \tag{5.42}$$

$$E_{sell}(k) = \max\big(-E_g(k), 0\big) \tag{5.43}$$

where these non-smooth operators can be moved to the constraints and replaced by linear inequalities assuming that $\zeta_{buy}(k) > \zeta_{sell}(k)\ \forall k$, which holds true in the case study.

The scheduling problem has a receding horizon of 48 hours and a sampling time of 1 hour. It is important to note that all the quadratic constraints within this scheduling problem are convex, so it is computationally tractable to solve the problem to global optimality. The scheduling decisions for the number of microturbines turned on, the energy exchange commitments, and the targets for battery level and building temperature are relayed to the dispatch layer.

The dispatch layer is ultimately formulated as a nonlinear program with the objective

function:

$$\begin{aligned} \text{minimize} \quad & \sum_{h} \Big[\quad \zeta_{buy}(h)E_{buy}(h) - \zeta_{sell}(h)E_{sell}(h) + \zeta_v E_v(h) \Big] \\ & +\Delta_T \sum_{k} \Big[\quad \zeta_{gas}F_m(k) + \zeta_{comfort}T_v(k) + \zeta_c P_c(k) + \zeta_d P_d(k) \Big] \\ & - \quad \zeta_{store}(k_f)C_b\big(\xi_b(k_f) - \tfrac{2}{3}\epsilon_b\big) \\ & + \quad \zeta_{AC}(k_f)\big(T_{bldg}(k_f) + \tfrac{2}{3}\epsilon_T\big) \end{aligned} \tag{5.44}$$

where ϵ_b and ϵ_T represent storage shortfalls (with respect to the long-term schedule) for battery level and building temperature. Unlike the scheduling problem, the balancing periods, h, and the time periods, k, are no longer interchangeable. Recall that to get the energy exchange in each balancing period, one can include Eq. (5.2) in the constraints. Again, note that all integer decisions are fixed by the scheduling layer, so no start up term appears in the objective.

The dispatch problem has a receding horizon of 2 hours and a sampling time of 2 minutes. This dispatch problem in non-convex, and it is only solved to local optimality since global optimality cannot be achieved in a practical time. The dispatch decisions for power generation levels (e.g. P_m) and ventilation rates to each zone are then broadcast to each unit within the microgrid. Each unit tracks their setpoint request using local control.

5.3 Dynamic System Model

A dynamic system model built in Simulink is used to implement and test the proposed control approach. This Simulink file has continuous-time dynamic models for each microgrid unit and the building temperatures. Each unit has some base control loops (e.g. based on PI control) to track setpoint requests and maintain local stability. The dynamic modeling and local control for each unit are briefly described here. This model is available on-line for those interested[5].

The microturbine model consists of a mechanical subsystem (i.e. compressor, combustion chamber, turbine, and recuperator) and an electrical subsystem (i.e. permanent

[5]Available at http://research.cems.umn.edu/daoutidis/software.php

magnet synchronous generator (PMSG)). The compressor, turbine, and recuperator are assumed to have constant isentropic eciencies. The combustor is assumed to be perfectly adiabatic with pressure loss factor of 4%. All gases are assumed to be ideal, and heat capacities and enthalpies are calculated on-line. The PMSG is modeled based on the work presented in [123] with a shaft viscous loss term added. Two PI controllers are used to track the power reference setpoint and regulate the rotor speed. Note that when multiple microturbines are operated, the total power production is divided evenly among them to minimize the potential impact of a sudden unit failure/outage.

The photovoltaic panel is modeled as a coupled thermal mass and electrical equivalent circuit. The model is based on the work presented in [124] with physical parameter based on values for a typical silicon solar cell. Several electrical properties in the equivalent circuit are temperature dependent. A perturb-and-observe controller is used to track the track the requested setpoint if curtailment is desired. In the case where no curtailment is desired, the controller instead performs maximum power point tracking.

The battery is also modeled as a coupled thermal mass and electrical equivalent circuit. The model is based on the work presented in [125] with physical parameter values based on a flooded lead-acid battery. Note that internal resistances within the battery depend on the current electrolyte temperature, battery SOC, and battery DOC. A local PI controller is used to track the requested setpoint.

The air in each thermal zone of the building is assumed to be well-mixed and uniform in temperature. If the zone temperature rises above the desired comfort range, the requested ventilation flow rate is increased automatically by the local control layer. This allows the real-time control layer to quickly reject disturbances and prevent thermal comfort violations without having to wait for the next dispatch instance. Plenum spaces are also modeled as well-mixed air volumes.

Internal building elements are modeled as lumped thermal masses. External walls and the roof are represented as 1-D finite element models of composite materials. The number of nodes in each layer of the composite walls are chosen such that the Biot number is ≤ 1.

A static model is used for the air conditioning and ventilation system. The pressure drop between the supply air to the return air is taken to be an affine function of the total ventilation rate. In addition, ventilation fans are assumed to have a total efficiency

of 55%. Finally, the coefficient of performance of the A/C unit is taken to be an affine function of the cooling duty.

5.3.1 Other Considerations

For simplicity, measurement noise is neglected within the simulation. In addition, the following system states (which are not typically directly measurable) are assumed to be perfectly estimated:

- Battery state of charge
- Battery electrolyte temperature
- Photovoltaic panel temperature
- Temperatures of the solid building elements (e.g. walls, floors, etc.)
- Air temperature within the plenum spaces

It is unlikely that a small estimation error for these states would lead to any significant degradation of the closed loop microgrid performance.

Finally, the observed difference between past forecasts and measured values is used to bias future forecasts. For example, for inflexible power demands:

$$\tau_\ell \frac{d\delta_\ell}{dt} + \delta_\ell(t) = \hat{P}_\ell(t) - \tilde{P}_\ell(t) \tag{5.45}$$

where $\tilde{P}_\ell$ is the original demand forecast, $\hat{P}_\ell$ is the observed demand, δ_ℓ is an estimated forecasting error, and τ_ℓ is a filter time constant. Forecasts for the future are then given as:

$$P_\ell(t) = \tilde{P}_\ell(t) + \delta_\ell(\mathcal{T}) e^{-\frac{t-\mathcal{T}}{\beta_\ell}} \quad \forall t \geq \mathcal{T} \tag{5.46}$$

where P_ℓ is the current forecast, $\mathcal{T}$ is the current time, and β_ℓ is a relaxation time. A similar approach is used for forecasting ambient temperature and solar radiation as described in Section 5.8.4.

Table 5.1: Case study market parameters

	Schedule Elasticity (kWh)	Schedule Adaptability (kWh)
Base Case	∞	∞
Case 1	10	10
Case 2	10	30
Case 3	30	10
Case 4	30	30

5.4 Case Study

A case study is considered for a microgrid serving a 5000 ft^2 office building in Minneapolis, MN. The performance of the proposed control approach is investigated at different levels of regulatory strictness. This regulatory strictness is modified by changing the tunable market parameters *schedule elasticity* and *schedule adaptability*. In particular, the cases considered are shown in Table 5.1. Note that the average power demand, including the controllable A/C and ventilation loads, is approximately 100 kW. Recall that a small value for schedule elasticity means strict regulation of residual load uncertainty, and a small value for schedule adaptability means strict regulation of residual load variability. A base case with no load shaping regulation is used as a basis for comparison.

In each case, a 9 day closed-loop simulation is performed, but the first 2 days are discarded as a burn-in period (because some initial energy exchange commitments and conditions must be specified). Weather data are drawn from the Typical Meterological Year 3 dataset [126]. The power demand forecast is shown in Fig. 5.4, and the weather forecasts are shown in Figs. 5.5 and 5.6.

A time-of-use pricing scheme (shown in Table 5.2) is used for energy exchanged with the utility company. The values assigned to the terminal battery level and building temperature are based on these electricity tariff values as shown in Table 5.3. All other cost coefficients are taken as constants and are shown in Table 5.4.

For the case study, the unit sizes in the microgrid system are:

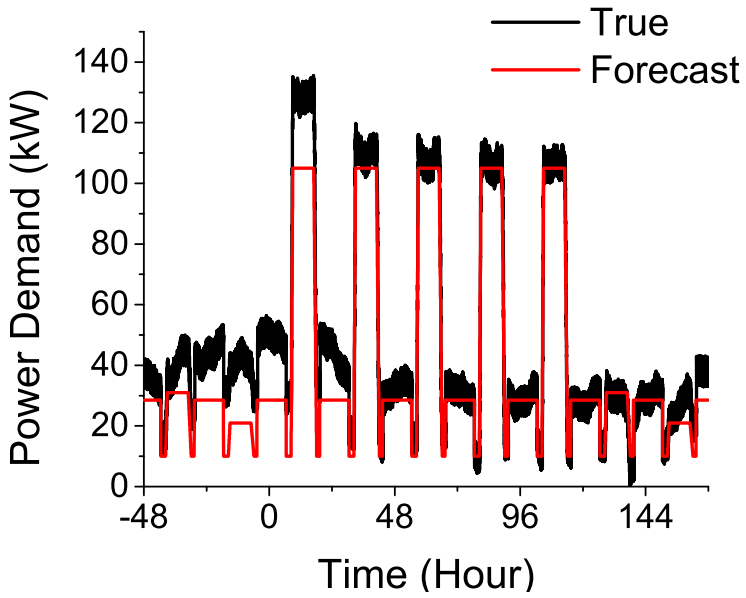

Figure 5.4: True and forecasted value for inflexible power demand.

Table 5.2: Time-of-Use Pricing Scheme

Rate	Applicable Times	ζ_{buy} (¢/kWh)	ζ_{sell} (¢/kWh)
Off-Peak	10PM-6AM	5	0
Mid-Peak	6AM-10PM (except On-Peak)	10	5
On-Peak	2PM-8PM (weekdays only)	15	7.5

- 3 microturbines with a rated power of 30 kW
- 1800 m^2 solar array[6]
- 300 kWh battery bank
- 85 ton A/C system[7]
- Maximum ventilation flow rate of 25 m^3/s

[6]Corresponds to a peak power of ∼175 kW
[7]Corresponds to a maximum cooling duty of ∼300 kW

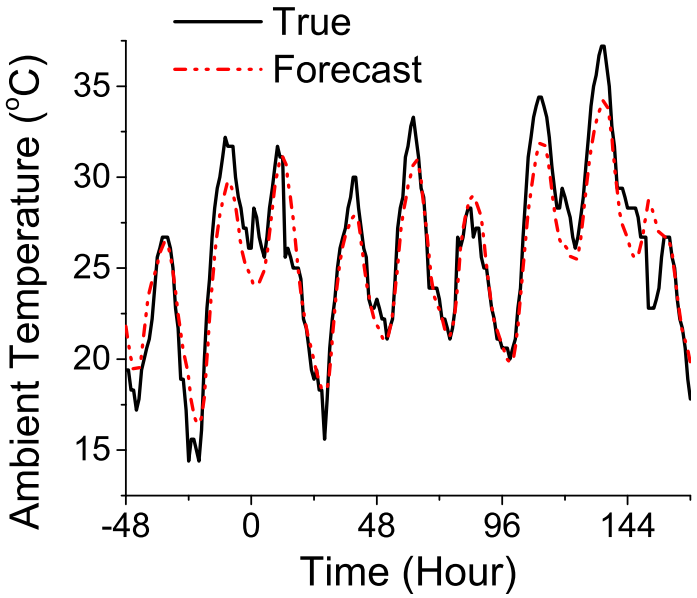

Figure 5.5: True and forecasted value for outdoor air temperature.

Table 5.3: Terminal Storage Values

Rate	Applicable Times	ζ_{store} (¢/kWh)	ζ_{AC} (¢/K)
Off-Peak	10PM-6AM	3.75	900
Mid-Peak	6AM-10PM (except On-Peak)	7.5	1800
On-Peak	2PM-8PM (weekdays only)	11.25	2700

Table 5.4: Constant Cost Values

Parameter	Value	Parameter	Value
ζ_{gas}	2.5 ¢/kWh	ζ_v	45 ¢/kWh
ζ_c	4 ¢/kWh	ζ_d	4 ¢/kWh
ζ_m	100 ¢	$\zeta_{comfort}$	3500 ¢/K

All other parameter values assumed in the case study are listed in Section 5.8.3. The scheduling and dispatch optimization problems are formulated in GAMS and solved with the CPLEX and IPOPT solvers, respectively.

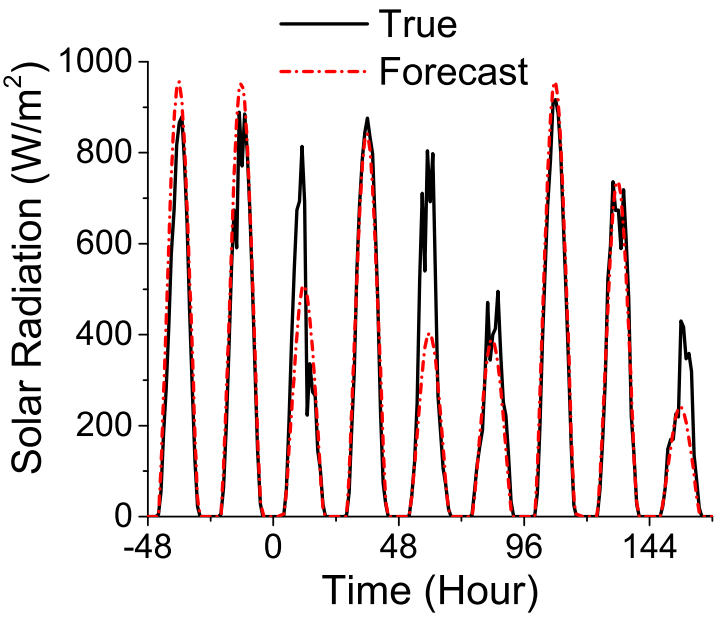

Figure 5.6: True and forecasted value for global solar radiation on a horizontal plane.

It is important to note that the results reported in the following section do not include cost accrued, commitment violations, etc. from the burn-in period.

5.5 Results

A high level of regulatory compliance is achieved in all cases. This is shown graphically in Figure 6.6 for Case 1. As evidenced by the figure, the realized energy exchange lies close to or within the allowed bounds at all times. Quantitative results for all cases are presented in Table 5.5. The number of commitment violations rises under stricter load shaping constraints (i.e. Case 1), but the cumulative magnitude of commitment violations is exceedingly small when compared to the net energy exchange in all cases. Therefore, the utility company is truly able to rely on the commitments provided at the day-ahead stage without having to worry about significant commitment violations during real-time operations.

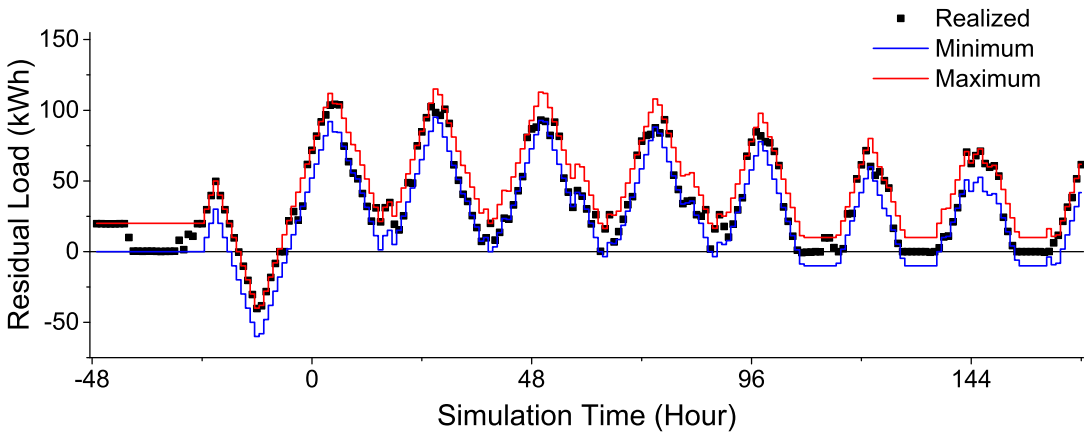

Figure 5.7: Microgrid residual load in Case 1 with maximum and minimum bounds based on the day-ahead commitments. Time less than zero indicates the burn-in period.

In addition, Table 5.5 presents two measures of residual load quality:

$$\text{Load Variability} = \frac{\sum_{h=1}^{167} \left| E_g(h) - E_g(h+1) \right|}{167} \tag{5.47}$$

$$\text{Load Factor} = \frac{\sum_{h=1}^{168} E_g(h)}{168 \cdot \max_h(E_g(h))} \tag{5.48}$$

The proposed market structure reduces load variability by 20-60% and increases load factor by up to 41%. As expected, the residual load profile is better behaved (i.e. easier for the utility company to serve) under tighter regulatory constraints. This can be see graphically in Figure 5.8 which compares the residual load profile in Cases 1 and 4 over a three-day period. The tighter restriction on variability (i.e. lower schedule adaptability) results in some smoothing of the load profile, e.g. in hours 30-36. The tighter restriction on uncertainty (i.e. lower schedule elasticity) results in less rapid, hour-to-hour fluctuations in energy exchange, e.g. in hours 59-69.

Table 5.6 shows the effect of these load shaping restrictions on the microgrid operating cost. Due to the high level of regulatory compliance achieved, the violation cost is very small in all cases. Under the proposed market structure, the fuel consumption

Table 5.5: Energy Exchange Results

	Case				
	Base	1	2	3	4
# of Commitment Violations	NA	16	11	4	2
Sum of Violations (kWh)	NA	5.8	4.5	1.2	0.3
Gross Imports (kWh)	7510	6750	7310	6980	7340
Gross Exports (kWh)	289	2.4	88	24	115
Load Variability (kW)	21.7	8.65	15.3	13.1	17.4
Load Factor	0.273	0.385	0.274	0.337	0.295

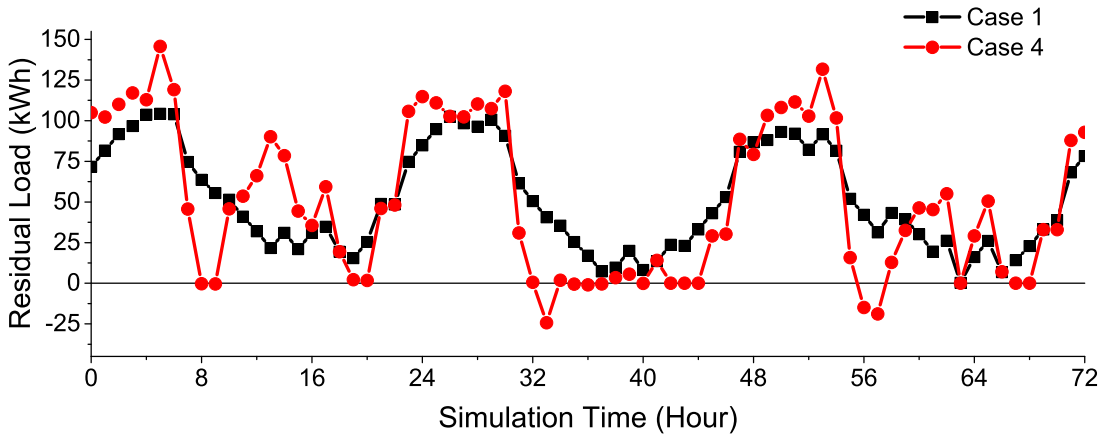

Figure 5.8: Comparison of residual load in Case 1 and Case 4 over first 3 days.

increases by ∼15-25% in order to smooth the residual load profile and ensure that generation capacity is on-line to respond to potential forecasting errors. The most significant increase in cost is associated with the battery unit. In the base case, the battery is hardly used due to its high cost, and excess power is instead sold to the utility company or used for pre-cooling of the building. In the cases with load shaping constraints, the battery is cycled approximately once per day as shown in Figure 5.9. Under tighter regulation the cycles are deeper, and thus the cost is higher. However, it should be noted that the overall cost compared to the base case is much more palatable than the results in Chapter 4, with Case 4 (relatively lenient regulation) ∼5% more expensive and Case 1 (strict regulation) only ∼11% more expensive. It should also be noted that,

Table 5.6: Economic Results

	Case				
	Base	1	2	3	4
Violation Cost ($/h)	NA	0.016	0.012	0.003	0.001
Energy Exchange Cost ($/h)	3.00	2.86	2.79	2.83	2.84
Fuel Cost ($/h)	1.10	1.38	1.36	1.29	1.24
Startup Cost ($/h)	0.089	0.089	0.095	0.089	0.089
Battery Cost ($/h)	0.03	0.35	0.32	0.25	0.26
Total Cost ($/h)	4.22	4.69	4.58	4.46	4.43

unlike in Chapter 4, there is negligable curtailment of available solar power (i.e. the curtailment is $\leq 0.65\%$ is all cases).

Cases 2 and 3 represent a trade-off between improvements in the residual load profile and microgrid operating cost. In Case 2 little improvement in the load variability and load factor are achieved, but the uncertainty in the residual load profile is reduced since energy exchange must lie very close to day ahead commitments. In Case 3, the improvement in load variability and load factor is similar to Case 1, but there is more uncertainty in the residual load profile since the schedule elasticity is relatively lenient. However, both Cases 2 and 3 are similar in cost to Case 4 which has lenient regulation of both uncertainty and variability. Thus, if reducing uncertainty is the primary concern of the utility company, market parameters like in Case 2 should be implemented. If instead reducing variability is the primary concern, market parameters like in Case 3 should be implemented. If reductions in both uncertainty and variability are desired, a situation like Case 1 can be pursued, but it will result in a $\sim$10% increase in microgrid operating cost.

In the absence of explicit public policy, utility companies could entice microgrid customers to participate in the proposed market structure by offering lower energy tariffs or other economic incentives to offset the increase in their operating cost. Hopefully, the reduced uncertainty and variability in the residual load profile will benefit utility companies more than enough to offset such incentives. However, consideration of the utility scheduling problem and resulting economics lie outside of the scope of this chapter.

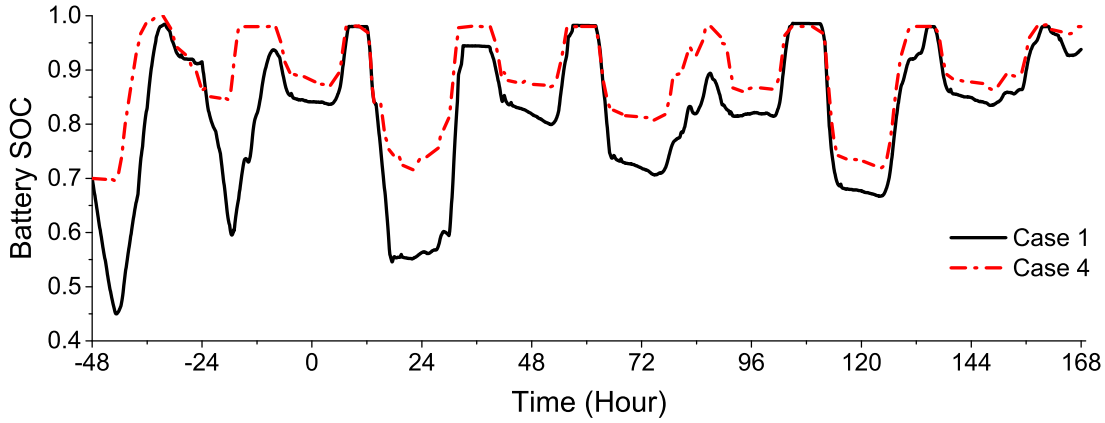

Figure 5.9: Battery state of charge in Case 1 and Case 4. Time less than zero indicates the burn-in period.

The control system is able to maintain acceptable indoor air temperature during dynamic operation as shown in Figure 5.10. This figure shows the average temperature in perimeter zones (i.e. those zones that contact at least 1 external wall) and core zones (i.e. zones that do not contact external walls). The building is typically precooled overnight to reduce the cooling demand over the following day. Then, during the middle of the day when power purchases are more expensive, the temperature is allowed to rise to the acceptable upper bound. Note that the core zones are generally kept colder than perimeter zones because any energy losses from these core zones will be to other areas of the building rather than to the external environment.

Figure 5.11 shows the weighted average temperature of the building (i.e. including the contribution of solid building elements like walls) in addition to the average zone air temperature. The building average temperature evolves on a slower time scale due to the large thermal inertia of elements like the concrete floors, and thus does not exhibit rapid fluctuations like the air temperature. Moreover, the times of Off-peak and On-peak pricing are shown shaded on the plot. Pre-cooling of the building is pursued during the periods of Off-peak pricing. In addition, more aggressive pre-cooling is pursued before weekdays since the expensive On-peak pricing will be in effect the following day. It is important to note that this intelligent emergent behavior is only enabled by the coupling of decision making across both the scheduling and dispatch layers, as

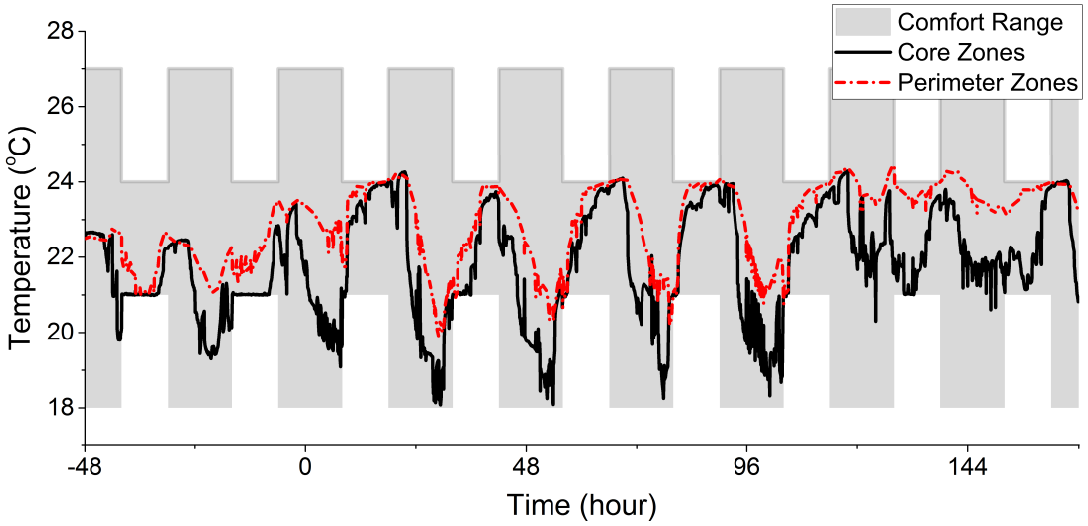

Figure 5.10: Average temperature in core zones and perimeter zones in Case 1. The shaded region indicates the target temperature range. Time less than zero indicates the burn-in period.

the dispatch planning horizon is only 2 hours. Thus, the dispatch layer only pursues aggressive pre-cooling in response to the long-term tracking targets communicated by the scheduling layer.

There are some violations of the desired temperature range due to the discrete sampling time of the central controller and the soft constraint approach used in the formulation. The frequency and magnitude of these temperature violations are shown in Figure 5.12. This figure shows that >95% of the time there no violations of the desired temperature bounds. Additionally, the temperature violation is $\leq 0.02^{o}$C for 99% of the time, and $\leq 0.6^{o}$C for 99.9% of the time. Therefore, occupants would be unlikely to notice these temperature violations due to their small magnitude and short duration. In addition, if stricter temperature compliance is desired, one could introduce a small back-off of the true temperature bounds in the optimization formulations. This is unlikely to significantly impact the operating cost achieved, but has not been specifically investigated since the temperature compliance is deemed satisfactory.

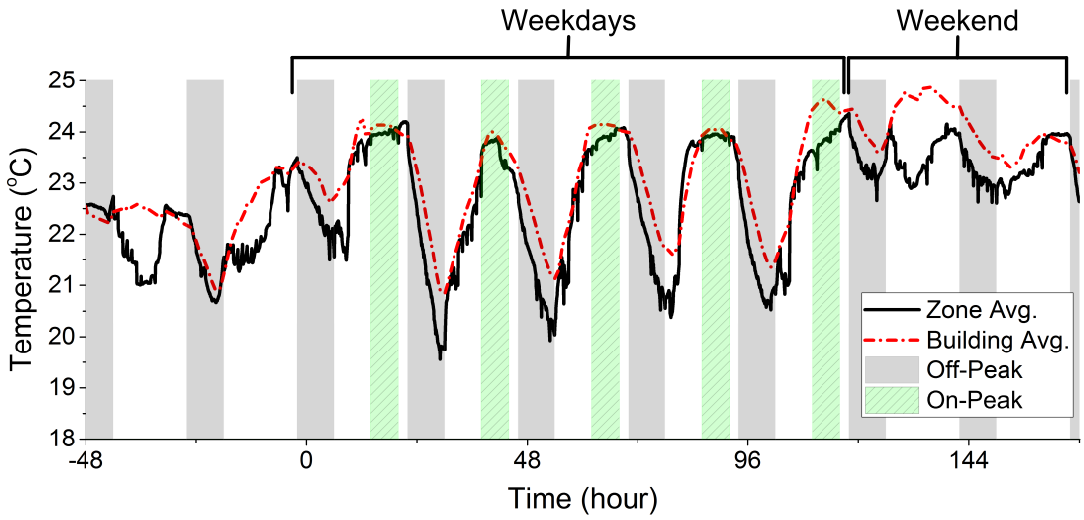

Figure 5.11: Zone average and total building average temperatures in Case 1. The shaded regions indicate times of On-Peak and Off-Peak pricing. Time less than zero indicates the burn-in period.

5.6 Conclusions

In this chapter, a scheduling/supervisory control framework is developed for a microgrid operating in a market structure designed to explicitly limit the uncertainty and variability in the residual load. The formulation presented specifically accounts for a controllable cooling load and the building temperature dynamics in order to meet these load shaping requirements in an economical manner. A case study is used to show that the proposed market structure results in specific, quantifiable improvements in the residual load profile that will reduce the burden placed on the utility company.

The cost associated with explicit electricity storage (i.e. batteries) is the largest contributor to the opportunity cost of this load shaping. However, by including flexible cooling in the formulation, the total microgrid operating cost is only 5-11% above the case with no load shaping regulations. This relatively small opportunity cost could potentially be offset by incentives or rebates offered by the utility company. Moreover, this load shaping activity does not come at the expense of thermal comfort for occupants as the indoor air is maintained within a designated temperature interval.

The proposed hierarchical control scheme effectively coordinates the decision making

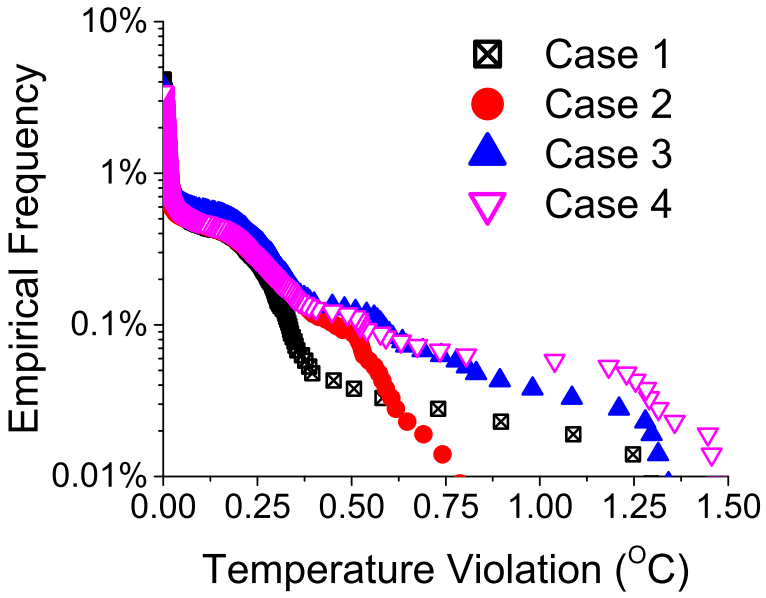

Figure 5.12: Frequency and magnitude of temperature violations.

at the scheduling and dispatch time scales to not only honor day-ahead commitments with a high level of satisfaction, but also to enable intelligent behavior such as aggressive pre-cooling of the building prior to peak electricity prices. In the next chapter, this approach is extended to a wider variety of customer-types and other seasons (e.g. winter where flexible heating loads can be leveraged rather than flexible cooling).

5.7 Nomenclature

Table 5.7: Nomenclature - Sets/Indicies

$e \in \mathcal{E}$	External Building Elements	$\mathcal{K}_h$	Time periods in balacing period h
h	Balancing periods	$pl \in \mathcal{P}$	Plenums
h_1	First balancing period in horizon	t	Time
h_f	Last balancing period in horizon	$\mathcal{T}$	Current time
$i \in \mathcal{I}$	Internal Building Elements	$w \in \mathcal{W}$	Windows
k	Time periods	$z \in \mathcal{Z}$	Zones
k_f	Final time period in horizon	$\mathcal{Z}_{pl}$	Zones connected to plenum pl

Table 5.8: Nomenclature - Parameters

α	Confidence level
β_ℓ	Load forecast relaxation time
β_s	Insolation forecast relaxation time
β_T	Temperature forecast relaxation time
δ	Schedule adaptability
δ_ℓ	Load forecast error
δ_s	Insolation forecast error
δ_T	Ambient temperature forecast error
Δ_T	Sampling time
η_I	Battery inverter efficiency
γ	Schedule elasticity
Γ_b	Battery DOC coefficient
$\lambda_{ac,1}$	A/C quadratic power cost
$\lambda_{ac,2}$	A/C linear power cost
$\lambda_{c1} - \lambda_{c5}$	Empirical coefficients for battery internal heat generation during battery charging
λ_{d1}	Empirical coefficient for battery internal heat generation during battery discharging
$\lambda_{vent,1}$	Ventilation quadratic power cost

Continued on next page

Table 5.8 – continued from previous page

$\lambda_{vent,2}$	Ventilation linear power cost
ρ	Air density
σ_ℓ	Power forecast std. dev.
σ_e	Solar gain coef. of e
σ_s	Solar forecast std. dev.
σ_w	Solar gain coef. of w
τ_b	Battery characteristic time
τ_ℓ	Load forecast filter time
τ_s	Insolation forecast filter time
τ_T	Temperature forecast filter time
ξ_b^{min}	Minimum battery SOC
ζ_{AC}	Value of building temperature
ζ_{buy}	Electricity import price
ζ_c	Battery charge cost
$\zeta_{comfort}$	Temperature violation price
ζ_d	Battery discharge cost
ζ_{gas}	Natrual gas price
ζ_m	Microturbine startup cost
ζ_{sell}	Electricity export price
ζ_{store}	Value of stored electricity
ζ_v	Commitment violation price
ξ_b^{target}	Target for terminal battery SOC
A_d	State matrix of thermal model
$A_{pl,e}$	Surface area between thermal elements pl and e
$A_{pl,i}$	Surface area between thermal elements pl and i
$A_{z,e}$	Surface area between thermal elements z and e
$A_{z,i}$	Surface area between thermal elements z and i
$A_{z,w}$	Surface area between thermal elements$z$ and w
A_b	Battery heat transfer area
A_e	Area of building element e

Continued on next page

Table 5.8 – continued from previous page

B_d	Input matrix of thermal model
C_p	Air heat capacity
D_b^{min}	Minimum battery DOC
$E_{b,max}$	Battery storage capacity
E_{gc}	Energy exchange commitment
E_g^0	Energy exchange so far in current balancing period
$F_{m,fix}$	No-load fuel consumption
$F_{m,var}$	Marginal fuel consumption
h_{int}	Convective heat transfer coefficient indoors
h_{ext}	Convective heat transfer coefficient outdoors
H_e	Solar radiation on element e
H	Solar radiation on a horizontal surface
$\tilde{H}$	Original forecast for solar radiation
$\tilde{H}^{avg}$	Filtered value for $\tilde{H}$
$\hat{H}$	Observed solar radiation
$\hat{H}^{avg}$	Filtered value for $\hat{H}$
H_w	Solar radiation on window w
L_h	Fraction of balancing period h which lies in the planning horizon
M_b	Battery thermal inertia
M_e^{int}, M_e^{blk}, M_e^{ext}	Thermal masses of element e (interior, bulk, and exterior, respectively)
M_i	Thermal mass of element i
N_m	Number of microturbines
P_ℓ	Forecasted inflexible power demand
$\tilde{P}_\ell$	Original forecast for inflexible power demand
$\hat{P}_\ell$	Realized power demand
P_m^{lo}	Minimum microturbine setpoint
P_m^{up}	Maximum microturbine setpoint
P_s^{max}	Available solar power

Continued on next page

Table 5.8 – continued from previous page

Q_{ac}^{rated}	Rated cooling duty of the A/C
$Q_{gen,z}$	Internal heat generation
$q_{leak,pl}$	Plenum infiltration flow
$q_{leak,z}$	Zone infiltration flow
q_{vent}^{up}	Maximum ventilation flow rate
$q_{fresh,z}^{min}$	Minimum flow rate of fresh air to zone z
T_{ac}	Supply air temperature
T_{air}^{max}	Maximum desired zone temperature
T_{air}^{min}	Minimum desired zone temperature
T_{amb}	Forecasted ambient temperature
$\tilde{T}_{amb}$	Original forecast for ambient temperature
$\hat{T}_{amb}$	Observed ambient temperature
T_b^{max}	Maximum battery temperature
T_{bldg}^{target}	Terminal building temp. target
T_{ref}	Reference temperature
$\bar{T}_z$	Nominal indoor air temperature
$U_{e,1}$, $U_{e,2}$	Internal heat transfer coefficient (interior-to-bulk and bulk-to-exterior, respectively)
U_b	Battery overall heat transfer coefficient
U_w	Window overall heat transfer coefficient
V_{pl}	Plenum volume
V_z	Zone Volume

Table 5.9: Nomenclature - Binary Variables ($1 \implies$ True)

χ_b	Is battery charging

Table 5.10: Nomenclature - Integer Variables ($\in \{0, 1, 2, ...\}$)

x_m	Number of microturbines on	y_m	Number of microturbines started up
z_m	Number of microturbines shut down		

Table 5.11: Nomenclature - Continuous Variables

ϵ_b	Battery storage shortfall
ϵ_T	Building temperature shortfall
ξ_b	Battery state of charge
$\xi_b^{aux1}, \xi_b^{aux2}$	Auxiliary battery SOC variable
D_b	Battery depth of charge
E_{buy}	Energy import from utility
E_g	Energy exchange with utility
E_{gc}^{exp}	Expected exchange commitment
E_{sell}	Energy export to utility
E_v	Commitment violation
$\hat{E}_v$	Realized commitment violation
f_r	Fraction of recycled air
F_m	Fuel consumption
P_{ac}	A/C power consumption
$\hat{P}_{ac}$	Realized A/C power consumption
P_{ac}^{max}	Maximum feasible A/C power
P_{ac}^{min}	Minimum feasible A/C power
P_b^{avg}	Average battery power
P_c	Battery charge power
$\hat{P}_c$	Realized battery charging power
P_c^{max}	Maximum feasible charge power
P_d	Battery discharge power
$\hat{P}_d$	Realized battery discharging power
P_d^{max}	Maximum feasible discharge power
P_g	Utility power exchange
$\hat{P}_g$	Realized power exchange
P_m	Microturbine power
$\hat{P}_m$	Realized microturbine power
P_m^{max}	Maximum feasible microturbine power

Continued on next page

Table 5.11 – continued from previous page

P_m^{min}	Minimum feasible microturbine power
P_s	Solar power used
$\hat{P}_s$	Realized solar power
P_{vent}	Ventilation power consumption
$\hat{P}_{vent}$	Realized ventilation power
P_{vent}^{max}	Maximum feasible ventilation power
P_{vent}^{min}	Minimum feasible ventilation power
q_{fresh}^{aux1}, q_{fresh}^{aux2}	Auxiliary fresh air flow
q_{fresh}^{tot}	Fresh air flow rate
$q_{recycle}^{aux1}$, $q_{recycle}^{aux2}$	Auxiliary recycle air flow
$q_{recycle}^{tot}$	Recycle air flow rate
q_{vent}^{aux1}, q_{vent}^{aux2}	Auxiliary ventilation rate
q_{vent}^{tot}	Total ventilation flow rate
$q_{vent,z}$	Ventilation flow rate to zone z
Q_{ac}	A/C cooling duty
Q_{ac}^{max}	Maximum feasible cooling duty
Q_{ac}^{min}	Minimum feasible cooling duty
Q_c	Battery charge heat
Q_c^{max}	Maximum feasible battery charge heat
Q_d	Battery discharge heat
Q_d^{max}	Maximum feasible battery discharge heat
Q_{flow}^{aux1}, Q_{flow}^{aux2}	Auxiliary enthalpy flow
Q_{flow}	Enthalpy flow from ventilation
$Q_{flow,pl}$	Enthalpy flow to plenum
$\boldsymbol{Q}_{flow,\mathcal{P}}$	Row vector of all $Q_{flow,pl}$
$Q_{flow,z}$	Enthalpy flow to zones
$\boldsymbol{Q}_{flow,\mathcal{Z}}$	Row vector of all $Q_{flow,z}$
T_b	Battery temperature
T_{bldg}	Average temperature of building
$T_e^{int}, T_e^{blk}, T_e^{ext}$	Temperature of element e (interior, bulk, exterior)

Continued on next page

Table 5.11 – continued from previous page

$\boldsymbol{T}_{\mathcal{E}}$	Row vector of all T_e
T_i	Temperature of element i
$\boldsymbol{T}_{\mathcal{I}}$	Row vector of all T_i
T_{pl}	Plenum temperature
$\boldsymbol{T}_{\mathcal{P}}$	Row vector of all T_{pl}
T_v	Temperature violation
T_z	Zone Temperature
$\boldsymbol{T}_{\mathcal{Z}}$	Row vector of all T_z

5.8 Supporting Information

5.8.1 Scheduling Layer Formulation

Because a time period length of 1 hour is used, a conversion factor is not shown when converting between energy (in units of kWh) and power (in units of kW).

$$\begin{aligned}\text{minimize} \quad & \textstyle\sum_k \Big[\zeta_{buy}(k)E_{buy}(k) - \zeta_{sell}(k)E_{sell}(k) + \zeta_{gas}F_m(k) + \zeta_m y_m(k) \\ & \qquad +\zeta_c P_c(k) + \zeta_d P_d(k) + \zeta_v E_v(k) + \zeta_{comfort}T_v(k)\Big] \\ & -\zeta_{store}(k_f)E_{b,max}\xi_b(k_f) + \zeta_{AC}(k_f)T_{bldg}(k_f)\end{aligned}$$

subject to:

$$P_m(k) + P_d(k) + P_s(k) + P_g(k) = P_\ell(k) + P_c(k) + P_{ac}(k) + P_{vent}(k) \qquad \forall k$$

$$\begin{aligned}P_m^{max}(k) + P_d^{max}(k) + E_{gc}(k) + \gamma + E_v(k) - P_{ac}^{min} - P_{vent}^{min}(k) & \\ \geq P_\ell(k) - P_s^{max} + +1.96\sqrt{\sigma_\ell^2(k) + \sigma_s^2(k)} & \qquad \forall k \leq k_{24}\end{aligned}$$

$$\begin{aligned}P_m^{max}(k) + P_d^{max}(k) + E_{gc}^{exp}(k) + \gamma + E_v(k) - P_{ac}^{min} - P_{vent}^{min}(k) & \\ \geq P_\ell(k) - P_s^{max} + 1.96\sqrt{\sigma_\ell^2(k) + \sigma_s^2(k)} & \qquad \forall k > k_{24}\end{aligned}$$

$$P_m^{min}(k) - P_c^{max}(k) + E_{gc}(k) - \gamma - E_v(k) - P_{ac}^{max} - P_{vent}^{max}(k) \leq P_\ell(k) - 1.96\sigma_\ell(k) \qquad \forall k \leq k_{24}$$

$$P_m^{min}(k) - P_c^{max}(k) + E_{gc}^{exp}(k) - \gamma - E_v(k) - P_{ac}^{max} - P_{vent}^{max}(k) \leq P_\ell(k) - 1.96\sigma_\ell(k) \qquad \forall k > k_{24}$$

Market Constraints

$$E_{buy}(k) - E_{sell}(k) = P_g(k) \qquad \forall k$$

$$-\gamma - E_v(k) \leq P_g(k) - E_{gc}(k) \leq \gamma + E_v(k) \qquad \forall k \leq k_{24}$$

$$-\gamma - E_v(k) \leq P_g(k) - E_{gc}^{exp}(k) \leq \gamma + E_v(k) \qquad \forall k > k_{24}$$

$$E_{gc}(k_{24}) - \delta \leq E_{gc}^{exp}(k_{25}) \leq E_{gc}(k_{24}) + \delta$$

$$E_{gc}^{exp}(k-1) - \delta \leq E_{gc}^{exp}(k) \leq E_{gc}^{exp}(k-1) + \delta \qquad \forall k > k_{25}$$

$$E_{gc}^{exp}(k_{25}) = P_g(k_{25})$$

Solar Constraints

$$P_s(k) \leq P_s^{max}(k) \qquad \forall k$$

Microturbine Constraints

$$P_m^{max}(k) = x_m(k) P_m^{up} \qquad \forall k$$

$$P_m^{min}(k) = x_m(k) P_m^{lo} \qquad \forall k$$

$$P_m^{min}(k) \leq P_m(k) \leq P_m^{max}(k) \qquad \forall k$$

$$F_m(k) = F_{m,var} P_m(k) + F_{m,fix} x_m(k) \qquad \forall k$$

$$x_m(k) = x_m(k-1) + y_m(k) - z_m(k) \qquad \forall k$$

Battery Constraints

$$E_{b,max}\big(\xi_b(k) - \xi_b(k-1)\big) = \Delta_T\big(\eta_I P_c(k) - Q_c(k) - P_d(k)/\eta_I - Q_d(k)\big) \qquad \forall k$$

$$T_b(k) = T_b(k-1) + \Delta_T \frac{U_b A_b\big(T_{ref} - T_b(k)\big) + Q_c(k) + Q_d(k)}{M_b} \qquad \forall k$$

$$T_b(k) \leq T_b^{max} \qquad \forall k$$

$$Q_c(k) \geq \lambda_{c1} P_c(k)^2 \qquad \forall k$$

$$Q_d(k) \geq \lambda_{d1} P_d(k)^2 \qquad \forall k$$

$$Q_c(k) \geq \lambda_{c2} P_c(k)^2 + \lambda_{c3} P_c(k) + \lambda_{c4} \xi_b(k) + \lambda_{c5} \qquad \forall k$$

$$P_c(k) \leq P_c^{max}(k) \qquad \forall k$$

$$P_d(k) \leq P_d^{max}(k) \qquad \forall k$$

$$E_{b,max}\big(\xi_b^{aux1}(k) - \xi_b(k-1)\big) = \Delta_T\big(\eta_I P_c^{max}(k) - Q_c^{max}(k)\big) \qquad \forall k$$

$$E_{b,max}\big(\xi_b^{aux2}(k) - \xi_b(k-1)\big) = \Delta_T\big(- P_d^{max}(k)/\eta_I - Q_d^{max}(k)\big) \qquad \forall k$$

$$T_b^{max} \geq T_b(k-1) + \Delta_T \frac{U_b A_b\big(T_{ref} - T_b^{max}\big) + Q_c^{max}(k) + Q_d^{max}(k)}{M_b} \qquad \forall k$$

$$Q_c^{max}(k) \geq \lambda_{c1} P_c^{max}(k)^2 \qquad \forall k$$

$$Q_d^{max}(k) \geq \lambda_{d1} P_d^{max}(k)^2 \qquad \forall k$$

$$Q_c^{max}(k) \geq \lambda_{c2} P_c^{max}(k)^2 + \lambda_{c3} P_c^{max}(k) + \lambda_{c4} \xi_b^{aux1}(k) + \lambda_{c5} \qquad \forall k$$

$$P_c^{max}(k) \leq 0.4(1 - \chi_b(k)) C_b/\eta_I \qquad \forall k$$

$$P_d^{max}(k) \leq 0.4 \chi_b(k) C_b \eta_I \qquad \forall k$$

$$\xi_b^{min} \leq \xi_b(k) \leq 1 \qquad \forall k$$

$$\xi_b^{min} \leq \xi_b^{aux1}(k) \leq 1 \qquad \forall k$$

$$\xi_b^{min} \leq \xi_b^{aux2}(k) \leq 1 \qquad \forall k$$

Temperature Dynamics

$$\boldsymbol{T}(k) = A_d \boldsymbol{T}(k-1) + B_d \boldsymbol{U}(k) \qquad \forall k$$

$$\boldsymbol{T}(k) = [T_{air}(k) \;\; \boldsymbol{T}_{\mathcal{I}}(k) \;\; \boldsymbol{T}_{\mathcal{E}}(k)]^T$$

$$\boldsymbol{U}(k) = [Q_{flow}(k) \;\; Q_{gen}(k) \;\; \boldsymbol{H}(k) \;\; T_{amb}(k)]^T$$

$$T_{air}^{min}(k) - T_v(k) \leq T_{air}(k) \leq T_{air}^{max}(k) + T_v(k) \qquad \forall k$$

$$T_{bldg}(k) = \frac{\big(\sum_z \rho C_p V_z + \sum_{pl} \rho C_p V_{pl}\big) T_{air}(k) + \sum_i M_i T_i(k)}{\sum_z \rho C_p V_z + \sum_{pl} \rho C_p V_{pl} + \sum_i M_i + \sum_e \big(M_e^{int} + M_e^{blk} + M_e^{ext}\big)} + \frac{\sum_e \big(M_e^{int} T_e^{int}(k) + M_e^{blk} T_e^{blk}(k) + M_e^{ext} T_e^{ext}(k)\big)}{\sum_z \rho C_p V_z + \sum_{pl} \rho C_p V_{pl} + \sum_i M_i + \sum_e \big(M_e^{int} + M_e^{blk} + M_e^{ext}\big)} \qquad \forall k$$

HVAC Constraints

$$q_{vent}^{tot}(k) = q_{recycle}^{tot}(k) + q_{fresh}^{tot}(k) \qquad \forall k$$

$$q_{fresh}^{tot}(k) \geq \sum_{z} q_{fresh,z}^{min}(k) \qquad \forall k$$

$$Q_{flow}(k) = q_{vent}^{tot}(k)\rho C_p\big(T_{ac} - \bar{T}_z\big) \qquad \forall k$$

$$Q_{ac}(k) = \rho C_p q_{fresh}^{tot}(k)\big(T_{amb}(k) - T_{ac}\big) + \rho C_p q_{recycle}^{tot}(k)\big(\bar{T}_z - T_{ac}\big) \qquad \forall k$$

$$P_{ac}(k) \geq \lambda_{ac,1} Q_{ac}(k)^2 + \lambda_{ac,2} Q_{ac}(k) \qquad \forall k$$

$$P_{vent}(k) \geq \lambda_{vent,1} q_{vent}^{tot}(k)^2 + \lambda_{vent,2} q_{vent}^{tot}(k) \qquad \forall k$$

$$q_{vent}^{tot}(k) \leq q_{vent}^{up} \qquad \forall k$$

Auxiliary HVAC Equations Set 1 (Used to bound P_{ac}^{max}, P_{vent}^{max})

$$T_{air}^{min}(k) - T_v(k) \leq T_{air}^{aux1}(k) \leq T_{air}^{max}(k) + T_v(k) \qquad \forall k$$

$$\boldsymbol{T}^{aux1}(k) = A_d \boldsymbol{T}(k-1) + B_d \boldsymbol{U}^{aux1}(k) \qquad \forall k$$

$$\boldsymbol{U}^{aux1}(k) = [Q_{flow}^{aux1}(k) \;\; Q_{gen}(k) \;\; \boldsymbol{H}(k) \;\; T_{amb}(k)]^T$$

$$q_{vent}^{aux1}(k) = q_{recycle}^{aux1}(k) + q_{fresh}^{aux1}(k) \qquad \forall k$$

$$q_{vent}^{aux1}(k) \leq q_{vent}^{up} \qquad \forall k$$

$$q_{fresh}^{aux1}(k) \geq \sum_{z} q_{fresh,z}^{min}(k) \qquad \forall k$$

$$Q_{flow}^{aux1}(k) = q_{vent}^{aux1}(k)\rho C_p\big(T_{ac} - \bar{T}_z\big) \qquad \forall k$$

$$Q_{ac}^{max}(k) = \rho C_p q_{fresh}^{aux1}(k)\big(T_{amb}(k) - T_{ac}\big) + \rho C_p q_{recycle}^{aux1}(k)\big(\bar{T}_z - T_{ac}\big) \qquad \forall k$$

$$P_{ac}^{max}(k) = \lambda_{ac,1} Q_{ac}^{rated} Q_{ac}^{max}(k) + \lambda_{ac,2} Q_{ac}^{max}(k) \qquad \forall k$$

$$P_{vent}^{max}(k) = \lambda_{vent,1} q_{vent}^{up} q_{vent}^{aux1}(k) + \lambda_{vent,2} q_{vent}^{aux1}(k) \qquad \forall k$$

Auxiliary HVAC Equations Set 2 (Used to bound P_{ac}^{min}, P_{vent}^{min})

$$T_{air}^{min}(k) - T_v(k) \leq T_{air}^{aux2}(k) \leq T_{air}^{max}(k) + T_v(k) \qquad \forall k$$

$$\boldsymbol{T}^{aux2}(k) = A_d \boldsymbol{T}(k-1) + B_d \boldsymbol{U}^{aux2}(k) \qquad \forall k$$

$$\boldsymbol{U}^{aux2}(k) = [Q_{flow}^{aux2}(k) \;\; Q_{gen}(k) \;\; \boldsymbol{H}(k) \;\; T_{amb}(k)]^T$$

$$q_{vent}^{aux2}(k) = q_{recycle}^{aux2}(k) + q_{fresh}^{aux2}(k) \qquad \forall k$$

$$q_{vent}^{aux2}(k) \leq q_{vent}^{up} \qquad \forall k$$

$$q_{fresh}^{aux2}(k) \geq \sum_{z} q_{fresh,z}^{min}(k) \qquad \forall k$$

$$Q_{flow}^{aux2}(k) = q_{vent}^{aux2}(k)\rho C_p\big(T_{ac} - \bar{T}_z\big) \qquad \forall k$$

$$Q_{ac}^{min}(k) = \rho C_p q_{fresh}^{aux2}(k)\big(T_{amb}(k) - T_{ac}\big) + \rho C_p q_{recycle}^{aux2}(k)\big(\bar{T}_z - T_{ac}\big) \qquad \forall k$$

$$P_{ac}^{min}(k) \geq \lambda_{ac,1} Q_{ac}^{min}(k)^2 + \lambda_{ac,2} Q_{ac}^{min}(k) \qquad \forall k$$

$$P_{vent}^{min}(k) \geq \lambda_{vent,1} q_{vent}^{aux2}(k)^2 + \lambda_{vent,2} q_{vent}^{aux2}(k) \qquad \forall k$$

Non-negativity Constraints

$$P_m(k),\, P_s(k),\, P_d(k),\, P_c(k),\, P_{ac}(k),\, P_{vent}(k),\, Q_{ac}(k),\, Q_{ac}^{min}(k) \geq 0 \qquad \forall k$$

$$P_{ac}^{max}(k),\, P_{vent}^{min}(k),\, P_{vent}^{max}(k),\, F_m(k),\, Q_c(k),\, Q_d(k),\, P_c^{max}(k),\, P_d^{max}(k) \geq 0 \qquad \forall k$$

$$E_v(k),\, E_{buy}(k),\, E_{sell}(k),\, Q_c^{max}(k),\, Q_d^{max}(k),\, q_{fresh}^{tot}(k),\, q_{recycle}^{tot}(k) \geq 0 \qquad \forall k$$

$$T_v(k),\, Q_{ac}^{max}(k),\, P_{ac}^{min}(k),\, q_{fresh}^{aux1}(k),\, q_{fresh}^{aux2}(k),\, q_{recycle}^{aux1}(k),\, q_{recycle}^{aux2}(k) \geq 0 \qquad \forall k$$

Integrality Constraints

$$x_m(k),\, y_m(k),\, z_m(k) \in \{0, 1, ..., N_m\} \qquad \forall k$$

$$\chi_b(k) \in \{0, 1\} \qquad \forall k$$

5.8.2 Dispatch Layer Formulation

$$\begin{aligned}\text{minimize} \quad & \sum_{h=h_1}^{h_3}\Big[\zeta_{buy}(h)E_{buy}(h) - \zeta_{sell}(h)E_{sell}(h) + \zeta_v E_v(h)\Big] \\ & +\Delta_T \sum_{k=k_1}^{k_f}\Big[\zeta_{gas}F_m(k) + \zeta_{comfort}T_v(k) + \zeta_c P_c(k) + \zeta_d P_d(k)\Big] \\ & -\zeta_{store}(k_f)E_{b,max}\big(\xi_b(k_f) - \tfrac{2}{3}\epsilon_b\big) + \zeta_{AC}(k_f)\big(T_{bldg}(k_f) + \tfrac{2}{3}\epsilon_T\big)\end{aligned}$$

subject to:

$$P_m(k) + P_d(k) + P_s(k) + P_g(k) = P_\ell(k) + P_c(k) + P_{ac}(k) + P_{vent}(k) \qquad \forall k$$

Market Constraints

$$E_{buy}(h) - E_{sell}(h) = E_g(h) \qquad \forall h$$

$$E_g(h_1) = E_g^0 + \Delta_T \sum_{k\in\mathcal{K}_{h_1}} P_g(k)$$

$$E_g(h) = \Delta_T \sum_{k\in\mathcal{K}_h} P_g(k) \qquad \forall h \neq h_1$$

$$-\gamma - E_v(h) \leq E_g(h) - E_{gc}(h) \leq \gamma + E_v(h) \qquad \forall h \neq h_3$$

$$-\gamma - E_v(h_3) \leq E_g(h_3) - L_{h_3}E_{gc}(h_3) \leq \gamma + E_v(h_3)$$

Solar Constraints

$$P_s(k) \leq P_s^{max}(k) \qquad \forall k$$

Microturbine Constraints

$$x_m(k)P_m^{lo} \leq P_m(k) \leq x_m(k)P_m^{up} \qquad \forall k$$

$$F_m(k) = F_{m,var}P_m(k) + F_{m,fix}x_m(k) \qquad \forall k$$

Battery Constraints

$$E_{b,max}\big(\xi_b(k) - \xi_b(k-1)\big) = \Delta_T\big(\eta_I P_c(k) - Q_c(k) - P_d(k)/\eta_I - Q_d(k)\big) \qquad \forall k$$

$$T_b(k) = T_b(k-1) + \Delta_T\frac{U_b A_b\big(T_{ref} - T_b(k)\big) + Q_c(k) + Q_d(k)}{M_b} \qquad \forall k$$

$$Q_c(k) \geq \lambda_{c1} P_c(k)^2 \qquad \forall k$$

$$Q_d(k) \geq \lambda_{d1} P_d(k)^2 \qquad \forall k$$

$$Q_c(k) \geq \lambda_{c2} P_c(k)^2 + \lambda_{c3} P_c(k) + \lambda_{c4} \xi_b(k) + \lambda_{c5} \qquad \forall k$$

$$P_b^{avg}(k) = P_b^{avg}(k-1) e^{-\Delta_T/\tau_b} + \big(P_d(k) - P_c(k)\big)\big(1 - e^{-\Delta_T/\tau_b}\big) \qquad \forall k$$

$$D_b(k)\big(1 - \Gamma_b P_b^{avg}(k)\big) = -\Gamma_b P_b^{avg}(k) + \xi_b(k) \qquad \forall k$$

$$\epsilon_b \geq \xi_b^{target} - \xi_b(k_f)$$

$$P_c(k) \leq 0.5 E_{b,max} \qquad \forall k$$

$$P_d(k) \leq 0.5 E_{b,max} \qquad \forall k$$

$$\xi_b^{min} \leq \xi_b(k) \leq 1 \qquad \forall k$$

$$D_b(k) \geq D_b^{min} \qquad \forall k$$

$$T_b(k) \leq T_b^{max} \qquad \forall k$$

Temperature Dynamics

$$\boldsymbol{T}(k) = A_d \boldsymbol{T}(k-1) + B_d \boldsymbol{U}(k) \qquad \forall k$$

$$\boldsymbol{T}(k) = [\boldsymbol{T}_{\mathcal{Z}}(k)\ \ \boldsymbol{T}_{\mathcal{P}}(k)\ \ \boldsymbol{T}_{\mathcal{I}}(k)\ \ \boldsymbol{T}_{\mathcal{E}}(k)]^T \qquad \forall k$$

$$\boldsymbol{U}(k) = [\boldsymbol{Q}_{flow,\mathcal{Z}}(k)\ \ \boldsymbol{Q}_{flow,\mathcal{P}}(k)\ \ \boldsymbol{H}(k)\ \ T_{amb}(k)]^T \qquad \forall k$$

$$T_{air}^{min}(k) - T_v(k) \leq T_z(k) \leq T_{air}^{max}(k) + T_v(k) \qquad \forall k, z$$

$$T_{bldg}(k) = \frac{\sum_z \rho C_p V_z T_z(k) + \sum_{pl} \rho C_p V_{pl} T_{pl}(k) + \sum_i M_i T_i(k)}{\sum_z \rho C_p V_z + \sum_{pl} \rho C_p V_{pl} + \sum_i M_i + \sum_e \left(M_e^{int} + M_e^{blk} + M_e^{ext}\right)} + \frac{\sum_e \left(M_e^{int} T_e^{int}(k) + M_e^{blk} T_e^{blk}(k) + M_e^{ext} T_e^{ext}(k)\right)}{\sum_z \rho C_p V_z + \sum_{pl} \rho C_p V_{pl} + \sum_i M_i + \sum_e \left(M_e^{int} + M_e^{blk} + M_e^{ext}\right)} \qquad \forall k$$

$$\epsilon_T \geq T_{bldg}(k_f) - T_{bldg}^{target}$$

HVAC Constraints

$$q_{vent}^{tot}(k) = \sum_z q_{vent,z}(k) \qquad \forall k$$

$$q_{vent,z}(k)\big(1 - f_r(k)\big) \geq q_{fresh,z}^{min}(k) \qquad \forall k, z$$

$$Q_{flow,z}(k) = q_{vent,z}(k) \rho C_p \big(T_{ac} - T_z(k)\big) \qquad \forall k, z$$

$$Q_{flow,pl}(k) = \sum_{z \in \mathcal{Z}_{pl}} q_{vent,z}(k) \rho C_p \Big(T_z(k) - T_{pl}(k) \Big) \qquad \forall k, pl$$

$$Q_{ac}(k) = \rho C_p \Big[q^{tot}_{vent}(k) T_{amb}(k) \big(1 - f_r(k)\big) + \sum_{pl} \sum_{z \in \mathcal{Z}_{pl}} q_{vent,z}(k) T_{pl}(k) f_r(k) - q^{tot}_{vent}(k) T_{AC} \big) \Big] \qquad \forall k$$

$$P_{ac}(k) \geq \lambda_{ac,1} Q_{ac}(k)^2 + \lambda_{ac,2} Q_{ac}(k) \qquad \forall k$$

$$P_{vent}(k) \geq \lambda_{vent,1} q_{vent}(k)^2 + \lambda_{vent,2} q_{vent}(k) \qquad \forall k$$

$$0 \leq f_r(k) \leq 1 \qquad \forall k$$

$$q^{tot}_{vent}(k) \leq q^{up}_{vent} \qquad \forall k$$

Non-negativity Constraints

$$E_v(h),\ E_{buy}(h),\ E_{sell}(h) \geq 0 \qquad \forall h$$

$$P_m(k),\ P_s(k),\ P_d(k),\ P_c(k),\ P_{ac}(k),\ T_v(k) \geq 0 \qquad \forall k$$

$$P_{vent}(k),\ Q_{ac}(k),\ F_m(k),\ Q_c(k),\ Q_d(k) \geq 0 \qquad \forall k$$

$$q_{vent,z}(k) \geq 0 \qquad \forall k, z$$

$$\epsilon_b,\ \epsilon_T \geq 0$$

5.8.3 Case Study Parameter Values

In the case study presented, sets associated with the building have the following sizes:

$$z \in \mathcal{Z} = \{z_1, z_2, ..., z_{15}\}$$
$$pl \in \mathcal{P} = \{pl_1, pl_2, pl_3\}$$
$$i \in \mathcal{I} = \{i_1, i_2, ..., i_{42}\}$$
$$e \in \mathcal{E} = \{e_1, e_2, ..., e_5\}$$
$$w \in \mathcal{W} = \{w_1, w_2, w_3, w_4\}$$

Note that $\{i_1, i_2, ..., i_{24}\}$ represent the internal walls, $\{i_{25}, i_{26}, ..., i_{39}\}$ represent the drop ceilings, and $\{i_{40}, i_{41}, i_{42}\}$ represent the concrete floors.

In addition, the connection between zones and plenum spaces is given by:

$$\mathcal{Z}_{pl_1} = \{z_1, z_2, z_3, z_4, z_5\}$$
$$\mathcal{Z}_{pl_2} = \{z_6, z_7, z_8, z_9, z_{10}\}$$
$$\mathcal{Z}_{pl_3} = \{z_{11}, z_{12}, z_{13}, z_{14}, z_{15}\}$$

Table 5.12: Scalar Case Study Values

α	0.95	$E_{b,max}$	300 kWh
Δ_T (scheduling)	3600 s	$F_{m,fix}$	11.9 kW
Δ_T (dispatch)	120 s	$F_{m,var}$	3.72
η_I	0.95	h_{int}	15 W/m^2-K
λ_{c1}	1.28E-03 kW^{-1}	h_{ext}	20 W/m^2-K
λ_{c2}	4.36E-05 kW^{-1}	N_m	3
λ_{c3}	0.234	M_b	16,200 kJ/K
λ_{c4}	21.1	P_m^{lo}	3 kW
λ_{c5}	-22.06	P_m^{up}	30 kW
λ_{d1}	2.38E-03 kW^{-1}	Q_{ac}^{rated}	300 kW
$\lambda_{ac,1}$	2.75E-04 kW^{-1}	q_{vent}^{up}	25 m^3/s
$\lambda_{ac,2}$	0.2841	T_{ac}	286 K
$\lambda_{vent,1}$	0.0436 kW-s^2/m^6	T_{air}^{max} (occupied)	297.15 K
$\lambda_{vent,2}$	0.1382 kW-s/m^2	T_{air}^{max} (unoccupied)	300.15 K
Γ_b	0.007 kW^{-1}	T_{air}^{min} (occupied)	294.15 K
ρ	1.225 kg/m^3	T_{air}^{min} (unoccupied)	291.15 K
σ_w	0.39	T_{ref}	297 K
τ_b	5000 s	T_b^{max}	308 K
ξ_b^{min}	0.2	$\bar{T}_z$	297.15 K
A_b	14 m^2	U_b	16 W/m^2-K
C_p	1 kJ/kg-K	U_w	3.24 W/m^2-K
D_b^{min}	0.1		

$$V_{\mathcal{Z}} = \begin{bmatrix} 1100 \\ 1100 \\ 641 \\ 641 \\ 1100 \\ 1100 \\ 1100 \\ 641 \\ 641 \\ 1100 \\ 1100 \\ 1100 \\ 641 \\ 641 \\ 1100 \end{bmatrix} \left[\mathrm{m}^3\right] \qquad V_{\mathcal{P}} = \begin{bmatrix} 2083 \\ 2083 \\ 2083 \end{bmatrix} \left[\mathrm{m}^3\right]$$

$$M_{\mathcal{E}}^{int} = \begin{bmatrix} 6120 \\ 6120 \\ 4080 \\ 4080 \\ 253264 \end{bmatrix} \left[\frac{\mathrm{kJ}}{\mathrm{K}}\right] \qquad M_{\mathcal{E}}^{blk} = \begin{bmatrix} 1544 \\ 1544 \\ 1029 \\ 1029 \\ 80511 \end{bmatrix} \left[\frac{\mathrm{kJ}}{\mathrm{K}}\right] \qquad M_{\mathcal{E}}^{ext} = \begin{bmatrix} 13840 \\ 13840 \\ 9227 \\ 9227 \\ 23892 \end{bmatrix} \left[\frac{\mathrm{kJ}}{\mathrm{K}}\right]$$

$$A_{\mathcal{E}} = \begin{bmatrix} 420 \\ 420 \\ 280 \\ 280 \\ 1667 \end{bmatrix} \left[\mathrm{m}^2\right] \qquad \sigma_{\mathcal{E}} = \begin{bmatrix} 0.6 \\ 0.6 \\ 0.6 \\ 0.6 \\ 0.7 \end{bmatrix} \qquad U_{\mathcal{E},1} = \begin{bmatrix} 0.465 \\ 0.465 \\ 0.465 \\ 0.465 \\ 7.090 \end{bmatrix} \left[\frac{\mathrm{W}}{\mathrm{m}^2\text{-K}}\right]$$

$$U_{\mathcal{E},2} = \begin{bmatrix} 0.852 \\ 0.852 \\ 0.852 \\ 0.852 \\ 0.385 \end{bmatrix} \left[\frac{\text{W}}{\text{m}^2\text{-K}}\right]$$

$$A_{\mathcal{Z},\mathcal{E}} = \begin{bmatrix} 77.5 & 0 & 0 & 0 & 0 \\ 0 & 77.5 & 0 & 0 & 0 \\ 0 & 0 & 51.7 & 0 & 0 \\ 0 & 0 & 0 & 51.7 & 0 \\ 0 & 0 & 0 & 0 & 0 \\ 77.5 & 0 & 0 & 0 & 0 \\ 0 & 77.5 & 0 & 0 & 0 \\ 0 & 0 & 51.7 & 0 & 0 \\ 0 & 0 & 0 & 51.7 & 0 \\ 0 & 0 & 0 & 0 & 0 \\ 77.5 & 0 & 0 & 0 & 0 \\ 0 & 77.5 & 0 & 0 & 0 \\ 0 & 0 & 51.7 & 0 & 0 \\ 0 & 0 & 0 & 51.7 & 0 \\ 0 & 0 & 0 & 0 & 0 \end{bmatrix} \left[\text{m}^2\right]$$

$$A_{\mathcal{Z},\mathcal{W}} = \begin{bmatrix} 60 & 0 & 0 & 0 \\ 0 & 60 & 0 & 0 \\ 0 & 0 & 40 & 0 \\ 0 & 0 & 0 & 40 \\ 0 & 0 & 0 & 0 \\ 60 & 0 & 0 & 0 \\ 0 & 60 & 0 & 0 \\ 0 & 0 & 40 & 0 \\ 0 & 0 & 0 & 40 \\ 0 & 0 & 0 & 0 \\ 60 & 0 & 0 & 0 \\ 0 & 60 & 0 & 0 \\ 0 & 0 & 40 & 0 \\ 0 & 0 & 0 & 40 \\ 0 & 0 & 0 & 0 \end{bmatrix} \quad [\mathrm{m}^2]$$

$$A_{\mathcal{P},\mathcal{E}} = \begin{bmatrix} 62.5 & 62.5 & 41.7 & 41.7 & 0 \\ 62.5 & 62.5 & 41.7 & 41.7 & 0 \\ 62.5 & 62.5 & 41.7 & 41.7 & 2198 \end{bmatrix} \quad [\mathrm{m}^2]$$

$$M_{\mathcal{I}} = \begin{bmatrix} 1815 \\ 1815 \\ 807 \\ 807 \\ 856 \\ 856 \\ 856 \\ 856 \\ 1815 \\ 1815 \\ 807 \\ 807 \\ 856 \\ 856 \\ 856 \\ 856 \\ 1815 \\ 1815 \\ 807 \\ 807 \\ 856 \\ 856 \\ 856 \\ 856 \\ 4280 \\ 4280 \\ 2497 \\ 2497 \\ 4280 \\ 4280 \\ 4280 \\ 2497 \\ 2497 \\ 4280 \\ 4280 \\ 4280 \\ 2497 \\ 2497 \\ 4280 \\ 333333 \\ 333333 \\ 333333 \end{bmatrix} \left[\frac{\mathrm{kJ}}{\mathrm{K}}\right] \qquad A_{\mathcal{P},\mathcal{I}} = \begin{bmatrix} 0 & 0 & 0 \\ 400 & 0 & 0 \\ 400 & 0 & 0 \\ 233 & 0 & 0 \\ 233 & 0 & 0 \\ 400 & 0 & 0 \\ 0 & 400 & 0 \\ 0 & 400 & 0 \\ 0 & 233 & 0 \\ 0 & 233 & 0 \\ 0 & 400 & 0 \\ 0 & 0 & 400 \\ 0 & 0 & 400 \\ 0 & 0 & 233 \\ 0 & 0 & 233 \\ 0 & 0 & 400 \\ 0 & 0 & 0 \\ 2198 & 0 & 0 \\ 0 & 2198 & 0 \end{bmatrix}^T \left[\mathrm{m}^2\right]$$

$$A_{\mathcal{Z},\mathcal{I}} = \begin{bmatrix}
82.5 & 0 & 0 & 0 & 82.5 & 0 & 0 & 0 & 0 & 0 & 0 & 0 & 0 & 0 & 0 \\
0 & 82.5 & 0 & 0 & 82.5 & 0 & 0 & 0 & 0 & 0 & 0 & 0 & 0 & 0 & 0 \\
0 & 0 & 36.7 & 0 & 36.7 & 0 & 0 & 0 & 0 & 0 & 0 & 0 & 0 & 0 & 0 \\
0 & 0 & 0 & 36.7 & 36.7 & 0 & 0 & 0 & 0 & 0 & 0 & 0 & 0 & 0 & 0 \\
0 & 38.9 & 0 & 38.9 & 0 & 0 & 0 & 0 & 0 & 0 & 0 & 0 & 0 & 0 & 0 \\
38.9 & 0 & 0 & 38.9 & 0 & 0 & 0 & 0 & 0 & 0 & 0 & 0 & 0 & 0 & 0 \\
38.9 & 0 & 38.9 & 0 & 0 & 0 & 0 & 0 & 0 & 0 & 0 & 0 & 0 & 0 & 0 \\
0 & 38.9 & 38.9 & 0 & 0 & 0 & 0 & 0 & 0 & 0 & 0 & 0 & 0 & 0 & 0 \\
0 & 0 & 0 & 0 & 0 & 82.5 & 0 & 0 & 0 & 82.5 & 0 & 0 & 0 & 0 & 0 \\
0 & 0 & 0 & 0 & 0 & 0 & 82.5 & 0 & 0 & 82.5 & 0 & 0 & 0 & 0 & 0 \\
0 & 0 & 0 & 0 & 0 & 0 & 0 & 36.7 & 0 & 36.7 & 0 & 0 & 0 & 0 & 0 \\
0 & 0 & 0 & 0 & 0 & 0 & 0 & 0 & 36.7 & 36.7 & 0 & 0 & 0 & 0 & 0 \\
0 & 0 & 0 & 0 & 0 & 0 & 38.9 & 0 & 38.9 & 0 & 0 & 0 & 0 & 0 & 0 \\
0 & 0 & 0 & 0 & 0 & 38.9 & 0 & 0 & 38.9 & 0 & 0 & 0 & 0 & 0 & 0 \\
0 & 0 & 0 & 0 & 0 & 38.9 & 0 & 38.9 & 0 & 0 & 0 & 0 & 0 & 0 & 0 \\
0 & 0 & 0 & 0 & 0 & 0 & 38.9 & 38.9 & 0 & 0 & 0 & 0 & 0 & 0 & 0 \\
0 & 0 & 0 & 0 & 0 & 0 & 0 & 0 & 0 & 0 & 82.5 & 0 & 0 & 0 & 82.5 \\
0 & 0 & 0 & 0 & 0 & 0 & 0 & 0 & 0 & 0 & 0 & 82.5 & 0 & 0 & 82.5 \\
0 & 0 & 0 & 0 & 0 & 0 & 0 & 0 & 0 & 0 & 0 & 0 & 36.7 & 0 & 36.7 \\
0 & 0 & 0 & 0 & 0 & 0 & 0 & 0 & 0 & 0 & 0 & 0 & 0 & 36.7 & 36.7 \\
0 & 0 & 0 & 0 & 0 & 0 & 0 & 0 & 0 & 0 & 0 & 38.9 & 0 & 38.9 & 0 \\
0 & 0 & 0 & 0 & 0 & 0 & 0 & 0 & 0 & 0 & 38.9 & 0 & 0 & 38.9 & 0 \\
0 & 0 & 0 & 0 & 0 & 0 & 0 & 0 & 0 & 0 & 38.9 & 0 & 38.9 & 0 & 0 \\
0 & 0 & 0 & 0 & 0 & 0 & 0 & 0 & 0 & 0 & 0 & 38.9 & 38.9 & 0 & 0 \\
400 & 0 & 0 & 0 & 0 & 0 & 0 & 0 & 0 & 0 & 0 & 0 & 0 & 0 & 0 \\
0 & 400 & 0 & 0 & 0 & 0 & 0 & 0 & 0 & 0 & 0 & 0 & 0 & 0 & 0 \\
0 & 0 & 233 & 0 & 0 & 0 & 0 & 0 & 0 & 0 & 0 & 0 & 0 & 0 & 0 \\
0 & 0 & 0 & 233 & 0 & 0 & 0 & 0 & 0 & 0 & 0 & 0 & 0 & 0 & 0 \\
0 & 0 & 0 & 0 & 400 & 0 & 0 & 0 & 0 & 0 & 0 & 0 & 0 & 0 & 0 \\
0 & 0 & 0 & 0 & 0 & 400 & 0 & 0 & 0 & 0 & 0 & 0 & 0 & 0 & 0 \\
0 & 0 & 0 & 0 & 0 & 0 & 400 & 0 & 0 & 0 & 0 & 0 & 0 & 0 & 0 \\
0 & 0 & 0 & 0 & 0 & 0 & 0 & 233 & 0 & 0 & 0 & 0 & 0 & 0 & 0 \\
0 & 0 & 0 & 0 & 0 & 0 & 0 & 0 & 233 & 0 & 0 & 0 & 0 & 0 & 0 \\
0 & 0 & 0 & 0 & 0 & 0 & 0 & 0 & 0 & 400 & 0 & 0 & 0 & 0 & 0 \\
0 & 0 & 0 & 0 & 0 & 0 & 0 & 0 & 0 & 0 & 400 & 0 & 0 & 0 & 0 \\
0 & 0 & 0 & 0 & 0 & 0 & 0 & 0 & 0 & 0 & 0 & 400 & 0 & 0 & 0 \\
0 & 0 & 0 & 0 & 0 & 0 & 0 & 0 & 0 & 0 & 0 & 0 & 233 & 0 & 0 \\
0 & 0 & 0 & 0 & 0 & 0 & 0 & 0 & 0 & 0 & 0 & 0 & 0 & 233 & 0 \\
0 & 0 & 0 & 0 & 0 & 0 & 0 & 0 & 0 & 0 & 0 & 0 & 0 & 0 & 400 \\
400 & 400 & 233 & 233 & 400 & 0 & 0 & 0 & 0 & 0 & 0 & 0 & 0 & 0 & 0 \\
0 & 0 & 0 & 0 & 0 & 400 & 400 & 233 & 233 & 400 & 0 & 0 & 0 & 0 & 0 \\
0 & 0 & 0 & 0 & 0 & 0 & 0 & 0 & 0 & 0 & 400 & 400 & 233 & 233 & 400
\end{bmatrix}^T$$

$$\left[\mathrm{m}^2\right]$$

Some other case study values are calculated using algebraic relationships.

The required fresh air flow rate is taken as:

$$q^{min}_{fresh,z}(k) = \begin{cases} V_z 2e^{-4}\mathrm{s}^{-1} & \text{Weekday 9 AM - 6 PM} \\ V_z 4e^{-5}\mathrm{s}^{-1} & \text{Saturday 9 AM - 6 PM} \\ V_z 2e^{-5}\mathrm{s}^{-1} & \text{Sunday 9 AM - 6 PM} \\ 0 & \text{Else} \end{cases}$$

The infiltration rates are calculated as a function of contact area with external walls and the roof:

$$q_{leak,z} = 0.001\frac{\mathrm{m}}{\mathrm{s}}\sum_e A_{z,e}$$
$$q_{leak,pl} = 0.001\frac{\mathrm{m}}{\mathrm{s}}\sum_e A_{pl,e}$$

The incident solar radiation (insolation) on all surfaces is calculated based on the insolation on a horizontal plane, a.k.a. global horizontal insolation (GHI), the extraterrestrial radiation (ETR), and the solar geometry:

$$\psi(t) = \frac{GHI(t)}{ETR(t)}$$

$$f_{diff}(t) = \begin{cases} 1.02 - 0.248\psi(t) & \psi(t) \leq 0.3 \\ 1.45 - 1.67\psi(t) & 0.3 < \psi(t) \leq 0.78 \\ 0.147 & \psi > 0.78 \end{cases}$$

$$DHI(t) = GHI(t) f_{diff}(t)$$

$$DNI(t) = \frac{GHI(t)\big(1 - f_{diff}(t)\big)}{\sin\big(\omega(t)\big)}$$

$$H_e(t) = DNI(t)\cos\big(\phi_e(t)\big) + DHI(t)\frac{1+\cos\big(\theta_e\big)}{2} + GHI(t)\frac{A\Big(1-\cos\big(\theta_e\big)\Big)}{2}$$

$$H_w(t) = DNI(t)\cos\big(\phi_w(t)\big) + DHI(t)\frac{1+\cos\big(\theta_w\big)}{2} + GHI(t)\frac{A\Big(1-\cos\big(\theta_w\big)\Big)}{2}$$

$$H_s(t) = DNI(t)\cos\big(\phi_s(t)\big) + DHI(t)\frac{1+\cos\big(\theta_s\big)}{2} + GHI(t)\frac{A\Big(1-\cos\big(\theta_s\big)\Big)}{2}$$

where ψ is a clearness index; f_{diff} is the diffuse fraction; DHI is the diffuse horizontal insolation; DNI is the direct solar insolation; ω is the solar elevation angle; A is the ground albedo; H_e, H_w, H_s are solar insolation values on building surfaces, windows, and the PV panels, receptively; ϕ_e, ϕ_w, ϕ_s are the angle of incidence between direct solar radiation and these surfaces; and θ_e, θ_w, θ_s are the angle between these surfaces and the horizontal plane (i.e. their tilt angle).

Note that the ETR and ω are easy to find/calculate given a latitude, longitude, and the date/time. The ground albedo is assumed to 0.2. The tilt angles are:

$$\theta_{\mathcal{E}} = \begin{bmatrix} 90^o \\ 90^o \\ 90^o \\ 90^o \\ 0^o \end{bmatrix} \quad \theta_{\mathcal{W}} = \begin{bmatrix} 90^o \\ 90^o \\ 90^o \\ 90^o \end{bmatrix} \quad \theta_s = 44.9^o$$

I.e. there are 4 vertical walls and a horizontal roof, the windows are all vertical, and the solar panels are tilted equal to the latitude. In addition, to calculate the incidence angles, the azimuth of the surfaces are needed. The walls (i.e. $\{e_1, e_2, e_3, e_4\}$) face directly East, West, South, and North, respectively. The windows follow the same pattern. The PV panels are South-facing. Then, one can again use known solar geometry to find the angle of incidence. Obviously a higher degree of accuracy could be obtained using measured data for all of these surfaces, but this provides a simple, straight-forward approach that can be used for case studies where only GHI is available.

The available solar power is calculated as a function of solar radiation and panel

temperature:

$$T_s(k) = T_s(k-1) + \Delta_T \frac{h_{ext}\big(T_{amb}(k) - T_s(k)\big) + 0.3H_s(k)}{8.33 \text{ kJ/K-m}^2} \qquad \forall k$$

$$P_s^{max}(k) = P_s^{rated} \frac{H_s(k)}{1000 \text{ W/m}^2}\left(1 - 0.005\big(T_s(k) - 25^o\text{C}\big)\right) \qquad \forall k$$

where T_s is the solar panel temperature, and P_s^{rated} is the rated panel power output (200 kW). Note that these equations do not depend at all on the optimization decision variables, and can be calculated *a priori*.

For the scheduling layer, forecast uncertainties depend on the forecasted values and the look-ahead time:

$$\sigma_\ell(k) = P_\ell(k)\left(0.2 + 0.015\frac{k-k_c}{47}\right) \qquad \forall k \geq k_c$$

$$\sigma_s(k) = \min\left(P_s^{rated}\left(0.17 + 0.05\frac{k-k_c}{47}\right), \frac{P_s^{max}(k)}{3}\right) \qquad \forall k \geq k_c$$

where k_c is the current time period.

5.8.4 Online Forecast Updates

The observed values for power demand, ambient temperature, and solar radiation are used to update future forecasts by estimating some forecast errors, δ_ℓ, δ_T, and δ_s, respectively:

$$\tau_\ell \frac{d\delta_\ell}{dt} + \delta_\ell(t) = \hat{P}_\ell(t) - \tilde{P}_\ell(t) \tag{5.49}$$

$$\tau_T \frac{d\delta_T}{dt} + \delta_T(t) = \hat{T}_{amb}(t) - \tilde{T}_{amb}(t) \tag{5.50}$$

$$\tau_s \frac{d\hat{H}^{avg}}{dt} + \hat{H}^{avg}(t) = \hat{H}(t) \tag{5.51}$$

$$\tau_s \frac{d\tilde{H}^{avg}}{dt} + \tilde{H}^{avg}(t) = \tilde{H}(t) \tag{5.52}$$

$$\delta_s(t) = \frac{max\big(\hat{H}^{avg}(t),\, 50\, W/m^2\big)}{max\big(\tilde{H}^{avg}(t),\, 50\, W/m^2\big)} \tag{5.53}$$

Note that δ_ℓ and δ_T refer to an absolute deviation, whereas δ_s refers to a fraction deviation. This method is used for solar radiation is used since the solar clearness fraction tends to be relatively stable whereas absolute solar radiation has a very strong diurnal pattern. Moreover, this approach for solar power prevents forecasting of negative solar radiation and does not alter the predicted sunrise/sunset times. The solar terms are saturated at 50 W/m^2 so that small deviations around sunrise and sunset do not have an overly pronounced impact on the forecast. The filter time constants τ_ℓ, τ_T, and τ_s are selected as 10 minutes, 1 hour, and 1 hour, respectively.

Future forecasts are then given by:

$$P_\ell(t) = \tilde{P}_\ell(t) + \delta_\ell(\mathcal{T}) e^{-\frac{t-\mathcal{T}}{\beta_\ell}} \qquad \forall t \geq \mathcal{T} \tag{5.54}$$

$$T_{amb}(t) = \tilde{T}_{amb}(t) + \delta_\ell(\mathcal{T}) e^{-\frac{t-\mathcal{T})}{\beta_T}} \qquad \forall t \geq \mathcal{T} \tag{5.55}$$

$$H(t) = \tilde{H}(t)\left(1 + \big(\delta_s(\mathcal{T}) - 1\big) e^{-\frac{t-\mathcal{T}}{\beta_S}}\right) \qquad \forall t \geq \mathcal{T} \tag{5.56}$$

where the current time is denoted as $\mathcal{T}$. The values of β_T and β_s are taken to be 10 hours and 3 hours, respectively. The value of β_ℓ is taken to be ∞. In essence, the forecasting error for power demand is assumed to persist indefinitely, whereas the weather terms are assumed to decay back to the original, long-term forecast with some characteristic times β_T and β_s. This approach is used since the original power forecast is just based on a typical load profile, but the weather forecasts would come from a physics-based weather model which should accurately predict the long-term trends over the next several days.

CHAPTER 6

Energy Management and Load Shaping for Commercial Microgrids Coupled with Flexible Building Environmental Control

6.1 Introduction

In Chapter 5, load shaping regulation was achieved by incorportating flexible cooling loads into the microgrid scheduling and control problem. In particular, a case study for a 5,000 m^2 office building located in Minneapolis, MN over a 1 week period in the summer was examined. Conceivably this approach might work well only for the particular case study chosen (e.g. works well in the summer when cooling demand is high but poorly in other seasons). In this chapter, the formulation and analysis is extended to consider several different commercial load shapes and other seasons, i.e. fall (when cooling loads are much milder) and winter (when heating loads are also present). This chapter provides important insights about how well this commercial microgrid paradigm can be used to absorb the stochasticity and variability of on-site renewable generation, and highlights what potential limitations might exist.

The primary contributions of this chapter are an extension of the formulation from Chapter 5 to consider process units and thermal dynamics associated with space heating, formulation of a more generic building model that can represent a wide variety of end

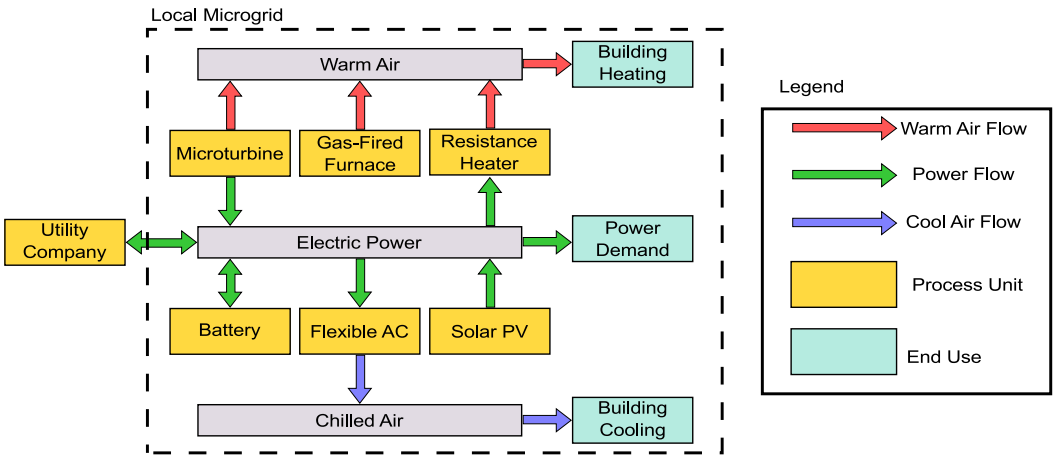

Figure 6.1: Energy flow diagram of the microgrid system considered.

users, and analysis of an extended case study across a diverse group of commercial load shapes and seasons. In Section 6.2 the optimization model used in scheduling and supervisory control is formulated. A brief description of the underlying real-time, dynamic system is also provided. In Section 6.3, a case study over multiple commercial load shapes and seasons is described. Finally, specific results and overall conclusions from this case study are showcased in Sections 6.4 and 6.5, respectively.

6.2 Model Formulation

A microgrid scheduling and supervisory control problem is formulated for the system shown in Figure 6.1. This supervisory controller seeks to regulate the indoor air temperature and the net power flow between the microgrid system and the external utility. In this problem, a fast time scale (on the order of minutes) is associated with stochastic fluctuations in weather and loads, and with the dynamics of building air temperatures (which can be changed relatively rapidly by the HVAC system). A slower time scale (on the order of hours) is associated with the battery storage level, slow temperature dynamics (i.e. those of walls and floors), and the natural diurnal patterns of occupancy and weather. Moreover, the supervisory controller needs to coordinate local power generation and consumption such that the hourly energy exchange with the external utility lies within a specific interval as dictated by the proposed market structure.

Thus, the centralized decision making is divided into an hourly scheduling problem and a more frequent economic dispatch problem. The hourly scheduling problem dictates long-term goals for energy exchange, storage levels, and building average temperatures. The economic dispatch problem responds to realized conditions and optimizes unit setpoints to minimize operating cost and keep the system on track to meet long-term goals. The decision making at both time scales is based on economic model predictive control (E-MPC). The scheduling problem considers a relatively coarse temporal granularity and discrete decisions such as on/off states, but utilizes some approximations for non-convex terms. In contrast, the dispatch problem fixes all discrete decisions based on the most recent scheduling iteration, but considers inherent process non-convexities and employs a finer temporal granularity in the problem formulation.

Since the proposed market structure has been discussed in more detail in Chapters 4 and 5, it is only briefly restated in Section 6.2.1. Then, the system model used in the E-MPC is formulated. This model is an extension of the one presented in Chapter 5, with the primary addition being consideration of building heating instead of just cooling.

6.2.1 Market Structure

The same market structure from Chapters 4 and 5 is considered again. Recall that unlike existing demand response schemes, the utility company is provided with specific information about the residual load from each microgrid 24 hours ahead of time. The mathematical formulation is again briefly summarized here.

The energy exchange between the microgrid and the external utility is metered over a series of balancing periods, where each balancing period is taken to be 1 hour (e.g. net energy exchange would be metered over the period from 8 AM to 9AM):

$$E_g(h) = \sum_{k \in h} P_g(k) \Delta_T \tag{6.1}$$

where h is a balancing period index, k is a discrete time index, P_g is the power flow between the microgrid and the utility, Δ_T is the sampling time, and E_g is the metered

energy exchange. The energy exchange is expected to lie close to some previously established commitment, as constrained by a market parameter called *schedule elasticity*:

$$-\gamma - E_v(h) \leq E_g(h) - E_{gc}(h) \leq \gamma + E_v(h) \tag{6.2}$$

where E_{gc} is an energy exchange commitment, γ is the schedule elasticity (i.e. the allowed uncertainty in the residual load), and E_v is a non-negative commitment violation. The microgrid incurs steep fines if this commitment violation is non-zero.

In addition, adjacent commitments are required to lie close to each other, as constrained by a market parameter called *schedule adaptability*:

$$E_{gc}(h-1) - \delta \leq E_{gc}(h) \leq E_{gc}(h-1) + \delta \tag{6.3}$$

where δ is the schedule adaptability (i.e. the allowed variability in the residual load). These energy exchange commitments are dictated by the microgrid, but they must be communicated to the utility company at least 24 hours before the start of the relevant balancing period.

6.2.2 Microturbines

Microturbines serve as a source of controllable local power generation, and energy can be recovered from their exhaust to help in space heating. Microturbines of the same model type are treated as indistinguishable in the model formulation, and, for simplicity, only a single type is considered (though this assumption could easily be relaxed). The aggregate power output of microturbines is then given by:

$$x_m(k)P_m^{lo}(k) \leq P_m(k) \leq x_m(k)P_m^{up} \tag{6.4}$$

where x_m is the number on, P_m^{lo} and P_m^{up} are the maximum and minimum operating setpoints, and P_m is the power output. The waste heat recovery is then given by:

$$Q_m(k) \leq \lambda_{m,var}P_m(k) + \lambda_{m,fix}x_m(k) \tag{6.5}$$

where $\lambda_{m,var}$ and $\lambda_{m,fix}$ are positive coefficients, and Q_m is the heat recovered for use in space heating of the building.

The fuel source of the microturbines is taken as natural gas, with a consumption rate given by:

$$F_m(k) = F_{m,var}P_m(k) + F_{m,fix}x_m(k) \tag{6.6}$$

where F_m is the fuel consumption rate, and $F_{m,var}$ and $F_{m,fix}$ are positive constants.

The number of active microturbines, i.e. x_m, is treated as a decision variable in the hourly scheduling problem, but is taken as a parameter in the dispatch problem. This not only prevents the introduction of discrete variables into the non-convex dispatch problem, but also prevents rapid on-off cycling of microturbines in response to short-term stochasticity.

6.2.3 Photovoltaic Panel

A photovoltaic array (PV) generates on-site renewable power. The available renewable power is a function of the weather only, and can be calculated before each optimization instance based on the current weather forecasts. The PV power is *curtailable* if desired, i.e. the total available power does not have to be used:

$$0 \leq P_s(k) \leq P_s^{max}(k) \tag{6.7}$$

where P_s^{max} is the renewable availability, and P_s is the actual PV power used. In general, PV curtailment will only be used to avoid exporting too much power to the utility and incurring commitment violations.

6.2.4 Battery

A battery bank is used for storing and later dispatching electrical energy. The battery storage dynamics are described by:

$$E_{b,max}\big(\xi_b(k) - \xi_b(k-1)\big) = \Delta_T\big(\eta_I P_c(k) - P_d(k)/\eta_I - Q_c(k) - Q_d(k)\big) \tag{6.8}$$

where $E_{b,max}$ is the battery storage capacity, ξ_b is the battery state of charge (SOC), η_I is the inverter efficiency, P_c and P_d are the charging and discharging power (respectively)

measured at the battery terminals, and Q_c and Q_d are the internal heat generation due to charging and discharging (respectively).

The internal heat generation terms are described in the same way as Chapter 5:

$$Q_d(k) \geq \kappa_{d1} P_d(k)^2 \tag{6.9}$$

$$Q_c(k) \geq \kappa_{c1} P_c(k)^2 \tag{6.10}$$

$$Q_c(k) \geq \kappa_{c2} P_c(k)^2 + \kappa_{c3} P_c(k) + \kappa_{c4} \xi_b(k) - \kappa_{c5} \tag{6.11}$$

The battery temperature is constrained to lie below some maximum operating temperature to prevent damage and excessive degradation.

Additional constraints are added to the dispatch formulation which ensure that a minimum battery depth of charge is not exceeded, and which penalize under-charging the battery (i.e. having a terminal storage level below the value requested by the hourly scheduling). More details on these can be found in Chapter 5.

6.2.5 Building Thermal Model

The building thermal model consists of a set of zones (i.e. air volumes), interior furnishings, interior solid building elements (e.g. internal walls), and exterior solid building elements (i.e. external walls and roofs). Unlike in Chapter 5, no explicit distinction is made between occupiable zones and plenum spaces in this chapter, and thermal dynamics of interior furnishings are considered. This is done to facilitate a more general building model.

The temperature dynamics of zones are described by:

$$\begin{aligned} \rho C_p V_z \tfrac{dT_z}{dt} = \; & \textstyle\sum_f A_{z,f} h_{z,f} \big(T_f(t) - T_z(t)\big) \\ & + \textstyle\sum_i A_{z,i} h_{z,i} \big(T_i(t) - T_z(t)\big) \\ & + \textstyle\sum_e A_{z,e} h_{z,e} \big(T_e^{int}(t) - T_z(t)\big) \\ & + \textstyle\sum_w A_{z,w} U_w \big(T_{amb}(t) - T_z(t)\big) \\ & + \textstyle\sum_w A_{z,w} \sigma_w H_w(t) \\ & + \rho C_p q_{leak,z} \big(T_{amb}(t) - T_z(t)\big) \\ & + Q_{gen,z}(t) + Q_{HVAC,z}(t) \end{aligned} \tag{6.12}$$

The first three lines on the right-hand side describe convective heat transfer with other thermal elements. Note that, different from the formulation in Chapter 5, the convective heat transfer coefficient inside the building is no longer uniform. This allows the model to capture the impact of materials like carpeting which can impede heat transfer but have negligible thermal mass. The fourth and fifth line describe heat transfer and direct solar gain via windows. The sixth line describes heat loss due to infiltration/exfiltration. The final line describes the heat gain due to internal generation within the zone and heat gain/loss due to HVAC system. This HVAC term is the heat gain/lost due to forced ventilation plus heat gain from the heating system:

$$Q_{HVAC,z}(t) = Q_{flow,z}(t) + Q_{heat,z}(t) \tag{6.13}$$

The temperature dynamics of furnishings are described by:

$$M_f \frac{dT_f}{dt} = \sum_z A_{z,f} h_{z,f} \big(T_z(t) - T_f(t)\big) \tag{6.14}$$

It is worthwhile to note that each furnishing element will contact exactly one zone.

The temperature dynamics of interior solid building elements are described by:

$$\begin{aligned} M_i \tfrac{dT_i}{dt} &= \sum_z A_{z,i} h_{z,i} \big(T_z(t) - T_i(t)\big) \\ &\quad + A_{g,i} U_{g,i} \big(T_{amb}(t) - T_i(t)\big) \end{aligned} \tag{6.15}$$

Note that building elements like the slab or underground walls (which contact the soil, but not ambient air) are treated as interior building elements. These elements have some slow rate of heat transfer with the environment governed by the contact area with the soil, $A_{g,i}$, and an overall heat transfer coefficient, $U_{g,i}$.

The exterior solid building elements directly contact the ambient air on one side. As before, they are described in terms of a *interior*, *exterior*, and *bulk* temperature:

$$\begin{aligned} M_e^{int} \tfrac{dT_e^{int}}{dt} &= \sum_z A_{z,e} h_{z,e} \big(T_z(t) - T_e^{int}(t)\big) \\ &\quad + A_e U_{e,1} \big(T_e^{blk}(t) - T_e^{int}(t)\big) \end{aligned} \tag{6.16}$$

$$\begin{aligned} M_e^{blk}\tfrac{dT_e^{blk}}{dt} &= A_e U_{e,1}\big(T_e^{int}(t) - T_e^{blk}(t)\big) \\ &\quad + A_e U_{e,2}\big(T_e^{ext}(t) - T_e^{blk}(t)\big) \end{aligned} \tag{6.17}$$

$$\begin{aligned} M_e^{ext}\tfrac{dT_e^{ext}}{dt} &= A_e U_{e,2}\big(T_e^{blk}(t) - T_e^{ext}(t)\big) \\ &\quad + A_e h_{ext}\big(T_{amb}(t) - T_e^{ext}(t)\big) \\ &\quad + A_e \sigma_e H_e(t) \end{aligned} \tag{6.18}$$

The heat gain/loss term in (6.12) is a bilinear function of the ventilation flow rate and the zone temperatures:

$$Q_{flow,z}(t) = \rho C_p \left[q_{vent,z}\big(T_{ac} - T_z(t)\big) + \sum_{z' \in \mathcal{C}_z} q_{vent,z'}\big(T_{z'}(t) - T_z(t)\big) \right] \tag{6.19}$$

where $\mathcal{C}_z$ is the subset of zones which feed air to zone z. As an example, consider Figure 6.2. In this example, $\mathcal{C}_{z_1} = \emptyset$, $\mathcal{C}_{z_2} = \emptyset$, and $\mathcal{C}_{z_3} = \{z_1, z_2\}$. In addition, note that zone z_3 in this example cannot receive supply air directly from the A/C unit (i.e. $q_{vent,z_3} := 0$).

The affine temperature dynamics in (6.12)-(6.18) can be summarized as the continuous-time linear system:

$$\frac{d\boldsymbol{T}}{dt} = \boldsymbol{A}\boldsymbol{T}(t) + \boldsymbol{B}\boldsymbol{U}(t) \tag{6.20}$$

with the stacked temperature vector, $\boldsymbol{T}$, and appropriately defined matrices $\boldsymbol{A}$ and $\boldsymbol{B}$. The $Q_{HVAC,z}$ terms are treated as exogenous inputs (i.e. included in $\boldsymbol{U}$). Then, the

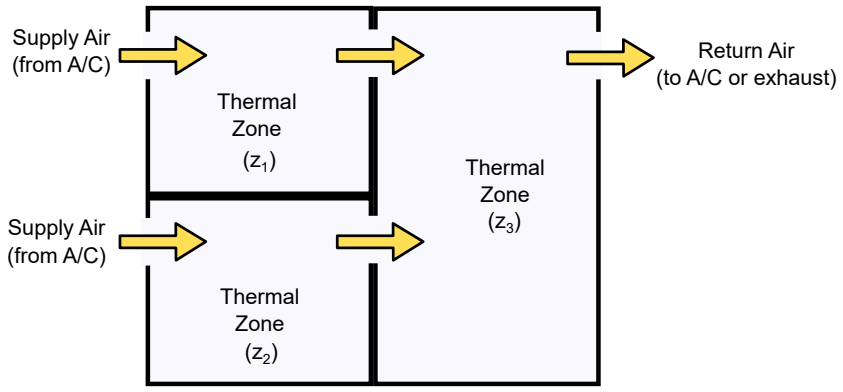

Figure 6.2: Illustrative thermal model example.

temperature dynamics are given at the discrete sampling time by:

$$\boldsymbol{T}(k) = \boldsymbol{A_d}\boldsymbol{T}(k-1) + \boldsymbol{B_d}\boldsymbol{U}(k) \tag{6.21}$$

$$\boldsymbol{A_d} = e^{\Delta_T \boldsymbol{A}} \tag{6.22}$$

$$\boldsymbol{B_d} = \boldsymbol{A}^{-1}\left(e^{\Delta_T \boldsymbol{A}} - \boldsymbol{I}\right)\boldsymbol{B} \tag{6.23}$$

$$\tag{6.24}$$

with the bilinear terms treated with a zero-order hold approximation

$$Q_{flow,z}(k) = \rho C_p \left[q_{vent,z}\big(T_{ac} - T_z(k)\big) + \sum_{z' \in \mathcal{C}_z} q_{vent,z'}\big(T_{z'}(k) - T_z(k)\big) \right] \tag{6.25}$$

This transformation to discrete-time $\boldsymbol{A_d}$ and $\boldsymbol{B_d}$ results in very dense matrices (i.e. there are no zero elements), though many elements remain exceedingly small. To improve computational tractability of the optimization problem, some terms are neglected. In particular, terms introduced by this discrete time transformation with a sufficiently small magnitude (e.g. $< 10^{-3}$) are eliminated.

6.2.6 HVAC System

The heating, ventilation, and air conditioning (HVAC) system supplies space heating and cooling to the building zones in order to regulate the temperature to some desired range. In particular, the supervisory controller should regulate the indoor air temperature to be:

- 21-24^{o}C during occupied hours
- 18-27^{o}C during unoccupied hours

Note that in this chapter, the occupied hours vary among the different buildings types considered. The ventilation system supplies chilled air at a constant temperature to cool zones. In addition, an independent heating system (e.g. a system of hot water radiators) can supply heat to the zones.

The total ventilation rate is given by:

$$q_{vent}^{tot}(k) = \sum_{z \in \mathcal{Z}_v} q_{vent,z}(k) \tag{6.26}$$

where q_{vent}^{tot} is the ventilation flow rate and $\mathcal{Z}_v$ is the subset of zones which have air supplied to them directly by the HVAC system. Recall that some zones do not receive ventilation directly from the HVAC system:

$$q_{vent,z}(k) := 0 \qquad \forall z \notin \mathcal{Z}_v \tag{6.27}$$

Returning to the earlier example in Figure 6.2, $\mathcal{Z}_v = \{z_1, z_2\}$, and $z_3 \notin \mathcal{Z}_v$.

The cooling duty of the A/C unit is a function of the inlet temperature and the total ventilation rate:

$$Q_{ac}(k) = \rho C_p q_{vent}^{tot}(k)\big(T_{mix}(k) - T_{ac}\big) \tag{6.28}$$

where Q_{ac} is the cooling duty, T_{mix} is the inlet temperature to the HVAC system, and T_{ac} is the supply air temperature. The inlet air is a mixture of recycled building air and fresh air from outside. The inlet temperature is then given by:

$$\begin{aligned} q_{vent}^{tot}(k)T_{mix}(k) =& q_{fresh}^{tot}(k)T_{amb}(k) \\ &+ f_r(k) \sum_{z \in \mathcal{Z}_r} \left[\big(q_{vent,z}(k) + \sum_{z' \in \mathcal{C}_z} q_{vent,z'}(k)\big) T_z(k) \right] \end{aligned} \tag{6.29}$$

$$q_{vent}^{tot}(k) = q_{fresh}^{tot}(k) + f_r(k) \sum_{z \in \mathcal{Z}_r} \left[q_{vent,z}(k) + \sum_{z' \in \mathcal{C}_z} q_{vent,z'}(k) \right] \tag{6.30}$$

where q_{fresh}^{tot} is the flow rate of fresh air to the building, $\mathcal{Z}_r$ is the subset of zones which can recycle air to the HVAC system[1], and f_r is the fraction of air recycled. During occupied hours, adequate fresh air must be supplied to the building zones, as described by:

$$q_{fresh}^{tot}(k) q_{vent,z}(k) \geq q_{fresh,z}^{min}(k) q_{vent}^{tot}(k) \tag{6.31}$$

[1]Some building zones, such as kitchens and medical spaces, cannot recycle their air and must vent it all directly outside. Additionally, some other zones not return directly to the HVAC unit, e.g. zones z_1 and z_2 in Figure 6.2.

where $q^{min}_{fresh,z}$ is a parameter which characterizes the minimum fresh air flow rate to zone z.

The cooling-duty is supplied by an A/C unit with a parasitic power consumption described by:

$$P_{ac}(k) = \lambda_{ac,1} Q_{ac}(k)^2 + \lambda_{ac,2} Q_{ac}(k) \tag{6.32}$$

In addition, the parasitic power of the fans in the ventilation system is described by:

$$P_{vent}(k) = \lambda_{vent,1} q^{tot}_{vent}(k)^2 + \lambda_{vent,2} q^{tot}_{vent}(k) \tag{6.33}$$

The heating-duty is supplied by a combination of waste heat recovery, resistive heating, and dedicated natural gas heating:

$$\sum_z Q_{heat,z}(k) = Q_m(k) + Q_r(k) + Q_n(k) \tag{6.34}$$

where Q_r is the heat supplied by an electric resistive heater, and Q_n is heat supplied via a traditional gas-fired furnace. Obviously, using resistive heating leads to coincident parasitic power consumption:

$$P_r(k) = Q_r(k)/\eta_r \tag{6.35}$$

Similarly, natural gas heating has coincident fuel usage:

$$F_n(k) = Q_n(k)/\eta_n \tag{6.36}$$

The efficiency of gas-fired heating and resistive heating are taken to be 85% and 90%, respectively.

During seasons when heating is not needed (e.g. the Summer) the terms and equations related to space heating can be removed from the optimization formulation to reduce the problem size. Note that cooling is generally needed for some zones throughout the year (i.e. zones that lie within the core of the building and do not contact any external building elements).

Some changes are made to the thermal model and HVAC model to preserve convexity and reduce computational complexity in the scheduling formulation. In particular, a reduced thermal model is used by aggregating thermal elements of the same type, and a

nominal indoor temperature is assumed in calculating cooling duties and enthalpy flow terms. This approach is described in more detail in Chapter 5. The only significant difference is that not all indoor air is aggregated into a single, lumped temperature. Instead, the zones are divided into 2 categories based on the ratio of window and external element contact area to zone volume, i.e.:

$$\frac{\sum_{e} A_{z,e} + 10 \sum_{w} A_{z,w}}{V_z}$$

A factor of 10 is used for window area since heat transfer via windows is much higher than via external walls or roofs. Zones in which this characteristic ratio is high will generally need heating during the winter, while zones in which this characteristic ratio is low or zero will generally need cooling even during the winter. Aggregating all air into a single element would therefore underestimate both heating and cooling needs in the winter months.

6.2.7 Energy Balances

The energy balances from Chapter 5 are updated to reflect the new terms (i.e. the power consumption of the resistive heater):

$$P_m(k) + P_d(k) + P_s(k) + P_g(k) = P_\ell(k) + P_c(k) + P_{ac}(k) + P_r(k) + P_{vent}(k) \quad (6.37)$$

$$Prob\left[\begin{array}{l} \hat{P}_m(k) + \hat{P}_d(k) + \hat{P}_s(k) + \hat{P}_g(k) = \\ \qquad \hat{P}_\ell(k) + \hat{P}_c(k) + \hat{P}_{ac}(k) + \hat{P}_r(k) + \hat{P}_{vent}(k) \end{array} \middle| \begin{array}{l} \hat{E}_v(k) \leq E_v(k) \\ x_m(k),\ \chi_b(k) \end{array} \right] \geq \alpha \quad (6.38)$$

where again variables denoted with a circumflex (e.g. $\hat{P}_m$) refer to the realized values after uncertainty has been revealed and recourse actions have been taken.

As in Chapters 4 and 5, a set of linear inequalities are derived which guarantee the chance constraints can be satisfied:

$$\begin{aligned} P_m^{max}(k) + P_d^{max}(k) - P_{ac}^{min}(k) - P_{vent}^{min}(k) - P_r^{min}(k) + E_{gc}(k) + \gamma + E_v(k) \\ \geq P_\ell(k) - P_s^{max}(k) + \Phi^{-1}\left(\frac{1+\alpha}{2}\right)\sqrt{\sigma_\ell^2(k) + \sigma_s^2(k)} \end{aligned} \quad (6.39)$$

$$P_m^{min}(k) - P_c^{max}(k) - P_{ac}^{max}(k) - P_{vent}^{max}(k) + P_r^{max}(k) + E_{gc}(k) - \gamma - E_v(k) \leq P_\ell(k) + \Phi^{-1}\left(\frac{1-\alpha}{2}\right)\sigma_\ell(k) \quad (6.40)$$

where $\Phi^{-1}(p)$ denotes the inverse cumulative distribution function of the standard normal distribution at probability level p. The auxiliary variables on the left hand side (e.g. P_m^{max} and P_m^{min}) specify the maximum and minimum energy generation/consumption of each unit. Some auxiliary variables are constrained based on first-stage decisions (i.e. the on/off state microturbines, the charge/discharge state of the battery, and energy exchange commitments). Auxiliary variables are also constrained based on the path constraints of state variables (e.g. zone temperatures and battery level) and the relevant system dynamics. For example, P_{ac}^{min} should be sufficient to ensure the maximum zone temperature is not exceeded. The full set of constraints related to these auxiliary variables can be seen in the optimization formulations shown in Section 6.7.1. Note that normally distributed forecasting errors are assumed in this work[2].

6.2.8 Objective Functions

The scheduling layer is ultimately formulated as a mixed integer quadratically constrained program with the objective function:

$$\begin{aligned} \text{minimize} \quad \sum_k \Big[& \zeta_{buy}(k)E_{buy}(k) - \zeta_{sell}(k)E_{sell}(k) + \zeta_{gas}\big(F_m(k) + F_n(k)\big) \\ & + \zeta_m y_m(k) + \zeta_c P_c(k) + \zeta_d P_d(k) + \zeta_{comfort} T_v(k) \\ & + \zeta_v E_v(k) \Big] - \zeta_{store}(k_f) E_{b,max} \xi_b(k_f) + \zeta_{temp}(k_f) T_{bldg}(k_f) \end{aligned} \quad (6.41)$$

where a term for fuel consumption by the natural gas heater has been added. In addition, the coefficient for the terminal building temperature (ζ_{temp}) now also depends on the season. For example, in the summer it is advantageous to have the building cold (i.e. $\zeta_{temp} > 0$) to offset future A/C needs, but this is not the case in the winter. The scheduling problem has a receding horizon of 48 hours and a sampling time of 1 hour. It is important to note that all the quadratic constraints within this scheduling problem

[2]This assumption could easily be relaxed as the stochastic parameters appear affinely in the chance constraint. Thus, one only needs to evaluate the cumulative distribution function of the stochastic terms $P_\ell(k)$ and $P_\ell(k) - P_s^{max}(k)$ at the appropriate probability levels.

are convex, so it is computationally tractable to solve the problem to global optimality. The scheduling decisions for the number of microturbines turned on, the energy exchange commitments, and the targets for battery level and building temperature are relayed to the dispatch layer.

The dispatch layer is ultimately formulated as a nonlinear program with the objective function:

$$\begin{aligned} \text{minimize} \quad & \textstyle\sum_h \Big[\zeta_{buy}(h)E_{buy}(h) - \zeta_{sell}(h)E_{sell}(h) + \zeta_v E_v(h) \Big] \\ & + \Delta_T \textstyle\sum_k \Big[\zeta_{gas}\big(F_m(k) + F_n(k)\big) + \zeta_{comfort}T_v(k) + \zeta_c P_c(k) \\ & \qquad + \zeta_d P_d(k) \Big] - \zeta_{store}(k_f)C_b\big(\xi_b(k_f) - \tfrac{2}{3}\epsilon_b\big) \\ & + \quad \zeta_{temp}(k_f)T_{bldg}(k_f) + \zeta_{track}(k_f)\epsilon_T \end{aligned} \tag{6.42}$$

The dispatch problem has a receding horizon of 2 hours and a sampling time of 2 minutes. This dispatch problem in non-convex, and it is only solved to local optimality since global optimality cannot be achieved in a practical time. The dispatch decisions for power generation levels (e.g. P_m) and ventilation rates to each zone are then broadcast to each unit within the microgrid. Each unit tracks their setpoint request using local control.

6.2.9 Dynamic System Model

A continuous-time, dynamic system model built in Simulink is used to implement and test the proposed control approach. In particular, this model is an extension of the one used in Chapter 5. New units corresponding to the heaters and a heat exchanger for waste heat recovery from the microturbine exhaust are added.

For simplicity, the resistive and natural gas heaters are modeled as static energy conversion units with a constant efficiency. The heat recovery unit is modeled as a dynamic heat exchanger. A controllable damper varies the fraction of the microturbine exhaust flow which is sent the heat recovery unit in order to regulate the amount of heat supplied. This split fraction can be set to use all available microturbine exhaust during the winter unless the building is at risk of overheating (i.e. exceeding the maximum desired temperature). During appropriate seasons (e.g. summer) these heaters and heat

recovery unit can be left out of the model to improve simulation speed. For a description of the modeling of other process units, see Section 5.3.

6.3 Case Study

A case study is used to showcase that this proposed approach is able to effectively mitigate uncertainty and variability in the residual load at little opportunity cost across a range of commercial buildings. In particular, we will focus on the following commercial building types:

- Office space
- Education
- Mercantile
- Health care

Together, these building types account for over 50% of the electricity consumption of commercial buildings [127]. Moreover, they exhibit significant differences in their load shapes on daily, weekly, and seasonal times scales. Thus, they provide a relevant and interesting test set for examining the effectiveness of the proposed control approach. In our case study, these general commercial building types are represented by:

- A 5,000 m^2 office building
- A 6,871 m^2 school building
- A 2,500 m^2 stand-alone retail store
- A 22,436 m^2 hospital

The U.S. Department of Energy reference commercial reference buildings were used as a starting point for modeling [128]. The non-HVAC power demands and total internal heat generation for each building type are shown in Figures 6.3. Note that these values are assumed to have no seasonal dependence (while the *total* power demand including HVAC loads will have a significant seasonal dependence). The layout of thermal zones in each building is shown in Section 6.7.3.

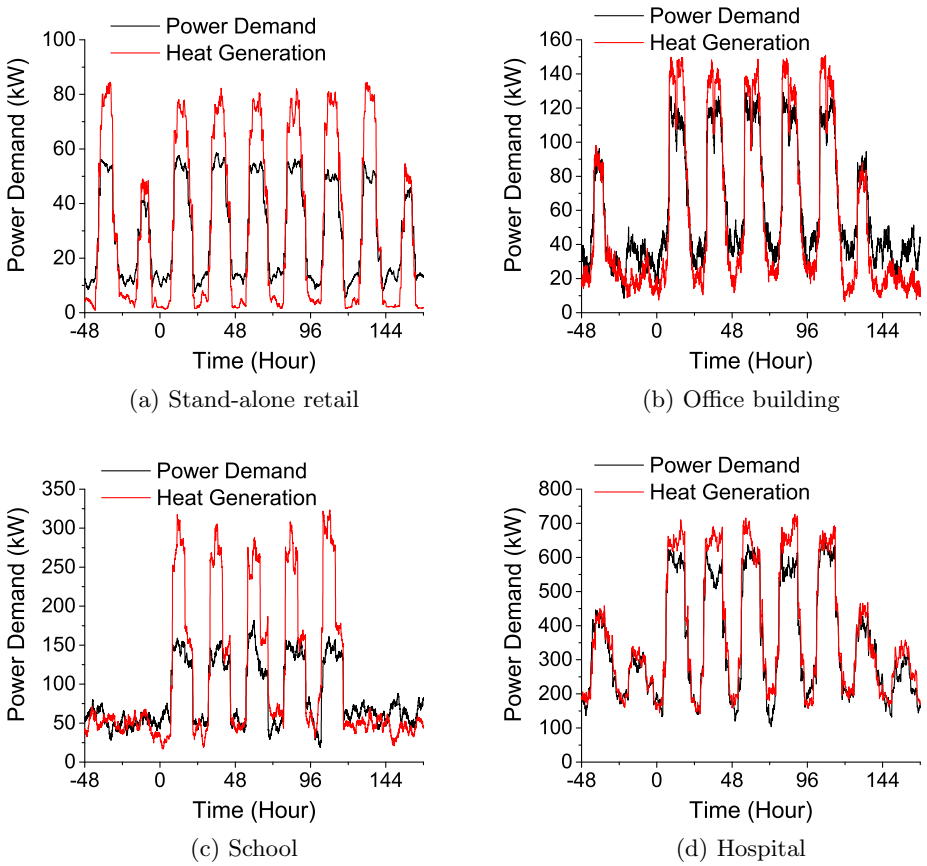

(a) Stand-alone retail

(b) Office building

(c) School

(d) Hospital

Figure 6.3: Power demand and heat generation profiles for each customer type.

The performance of this control approach is studied in a winter period, a summer period, and a shoulder period (when temperature values are less extreme, i.e. fall). In each case, a 9-day closed-loop simulation is performed, but the results from the first 48 hours are discarded as a burn-in period. The weather inputs, i.e. solar global horizontal irradiance (GHI) and ambient temperature are taken from the Typical Meteorological Year 3 data[3] for Minneapolis, MN. The date ranges used are:

- Summer period: July 12th-20th
- Shoulder period: September 10th-18th

[3]Accessible at http://rredc.nrel.gov/solar/old_data/nsrdb/1991-2005/tmy3/

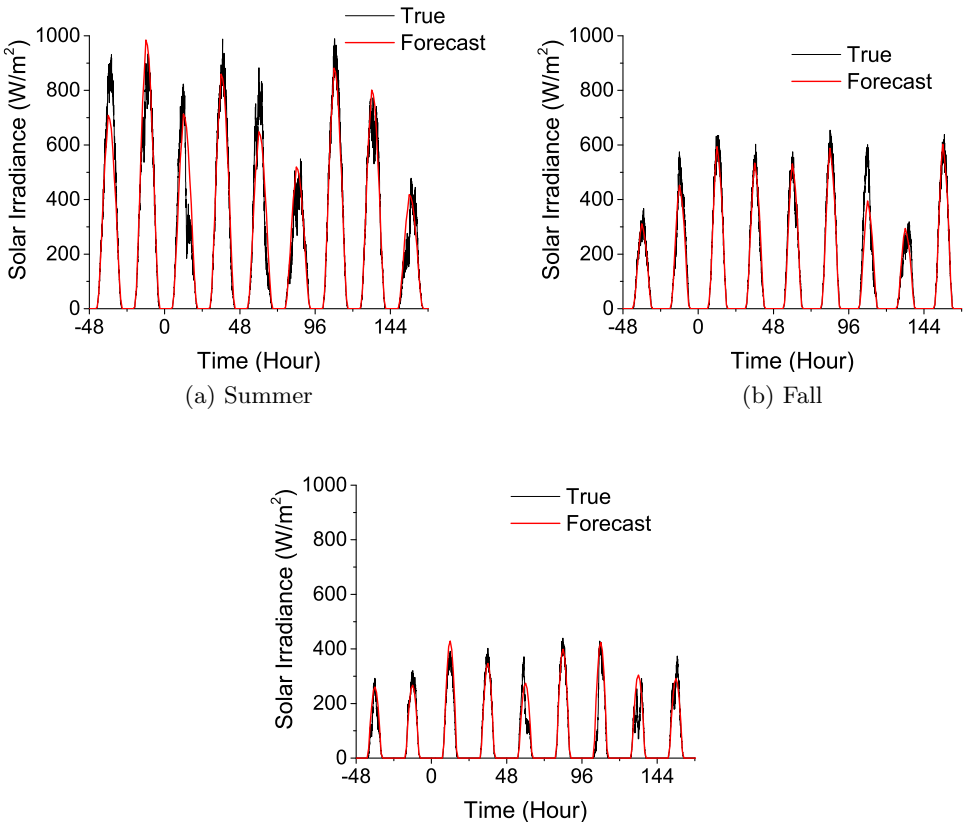

(a) Summer

(b) Fall

(c) Winter

Figure 6.4: Solar radiation profiles and forecasts for each season.

- Winter period: January 7th-15th

White noise was added to the GHI signal to simulate more realistic, noisy data. Solar radiation on other surfaces (e.g. walls, inclined solar panels, etc.) are calculated based on the GHI. Noise was not added to the temperature data as the natural thermal dynamics of the system would damp them out regardless. The GHI values and forecasts for each season are shown in Figure 6.4.

For each building type, the schedule elasticity and schedule adaptability values are scaled based on the average energy demands. The exact values are shown in Table 6.1. To facilitate a fair comparison, a base case is considered for all building types and seasons where no regulatory/load shaping constraints are imposed on the microgrid (i.e.

Table 6.1: Market Parameters

	Retail	Office	School	Hospital
Schedule Elasticity (kWh)	6	10	20	57.5
Schedule Adaptability (kWh)	6	10	20	57.5

Table 6.2: Unit sizing

	Retail	Office	School	Hospital
Number of microturbines	3	3	3	3
Rated microturbine power (kW)	4	7	15	40
Rated PV power (kW)	100	200	313	1150
Battery capacity (kWh)	150	300	470	1725
A/C capacity (tons)	35	65	100	375
Resistive heater capacity (kW)	10	20	31	115
Furnace capacity (kW)	122.5	225	350	700

schedule elasticity and adaptability are taken as ∞). This base case is used to scale results where appropriate. For example, the cost of energy supply increases with the building size, so a relative cost is defined:

$$\text{Relative Cost} = \frac{\text{Cost}}{(\text{Cost})_{\text{Base Case}}} \tag{6.43}$$

The sizing of local process units is also scaled according to the characteristic building energy demands as shown in Table 6.2. Note that the installed capacity of dispatchable generation (i.e. microturbines) has been reduced by a factor of $\sim$3 compared to Chapter 5. This was done to analyze what impact this reduction in dispatchable capacity might have on the load shaping ability of the microgrid. Other details on the case study parameter values are provided in Section 6.7.4.

6.4 Results

The overall cost of energy supply in each case is shown in Table 6.3. The breakdown of the different cost factors is shown in Figure 6.5. As mentioned, the values are scaled by

Table 6.3: Energy supply cost (relative to base case).

	Retail	Office	School	Hospital
Summer	1.27	1.14	1.43	1.14
Fall	1.18	1.15	1.22	1.04
Winter	1.21	1.36	1.27	1.41

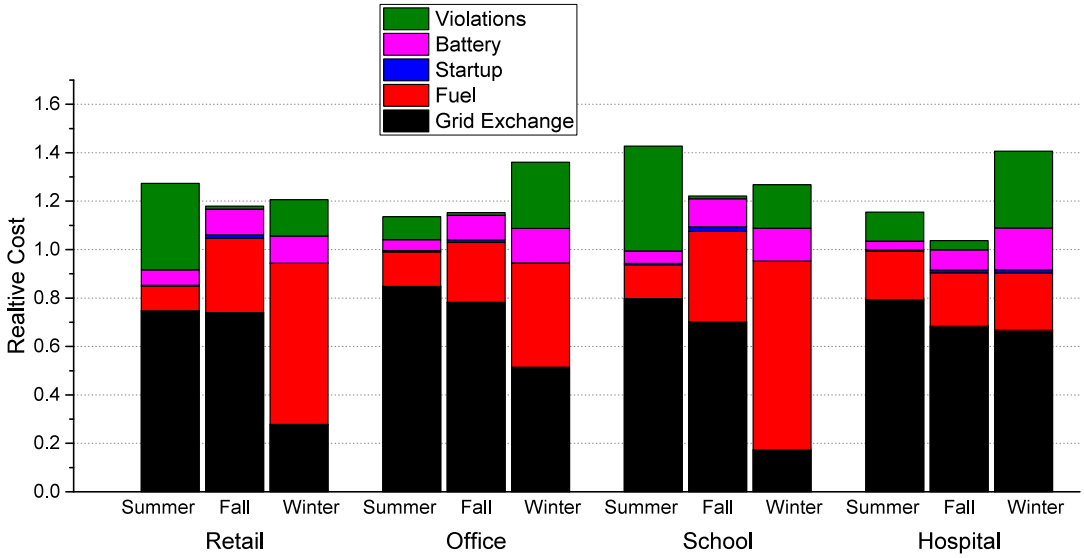

Figure 6.5: Breakdown of cost factors in each scenario. Values are shown in terms of relative cost (i.e. scaled by the total cost in the base case).

the base case in which no no load shaping restrictions are imposed. In most cases, the cost is ∼15-25% higher than the base case. Comparing the cost of the office building in the summer to the results from Chapter 5, reducing the installed capacity of dispatchable generation by a factor of ∼3 has only caused the relative cost to rise from 1.11 to 1.14.

In the winter, the cost is largely dominated by the fuel cost (i.e. to supply the gas-fired furnace and the microturbines which cogenerate both heat and power). An exception to this trend is the hospital. The hospital has a higher level of power consumption and occupancy during off-peak hours (i.e. overnight) compared to the other load shapes considered. Thus, it has a relatively high level of internal heat generation during the night/weekends, and less need for the furnace and microturbines to supply space heating. Furthermore, the hospital is a large building, so the rate of heat loss to

Table 6.4: Cumulative commitment violations (kWh). The value in parenthesis shows this cumulative commitment violations scaled by the allowed elasticity to facilitate easier comparison among the load shapes.

	Retail	Office	School	Hospital
Summer	563 (94)	222 (22.2)	2,180 (109)	1,460 (25.3)
Fall	6.5 (1.1)	16 (1.6)	16.9 (0.9)	289 (5.0)
Winter	171 (28.5)	444 (44.4)	625 (31.2)	2,440 (42.4)

the environment is slow compared to a small building like the stand-alone retail store (due to the scaling between building surface area and volume). In the summer, the cost is dominated by the cost of imported power. Although more solar power is available during the summer, it is not enough to offset the overall increase in power demands due to the high cooling loads, and more power must be imported. The fall season represents a balance between these two cases. Space heating needs are negligible (or non-existent) so less fuel is used, but the cooling loads are also lower so less power tends to be imported.

The magnitude of incurred commitment violations in each case is shown in Table 6.4. To aid in comparison among the cases with different energy demand magnitudes, a normalized value (i.e. scaled by the allowed elasticity) is also shown in parenthesis. The magnitude of commitment violations is higher in the summer and winter seasons as compared to the fall. In the winter, space cooling only accounts for a small fraction of the energy usage, and space heating is achieved primarily by using natural gas rather than electricity as a primary energy source. Thus, the flexible HVAC system is less effective at enabling load shaping and commitment violations occur more frequently. In the fall, the inherent flexibility in the air conditions/cooling system can be effectively leveraged to mitigate renewable and demand uncertainty. In summer, cooling loads are very high, and the HVAC system is less able to engage in flexible operation (i.e. the system may need to be operated continuously to prevent temperatures from rising too high).

The residual load profile for each load shape over the summer season is shown in Figure 6.6. Note that realized values outside of the maximum/minimum bounds indicate commitment violations. A similar shape to the residual load profile is seen among all

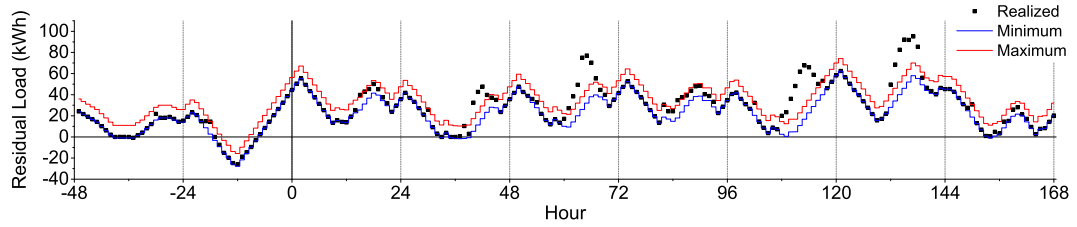

(a) Retail

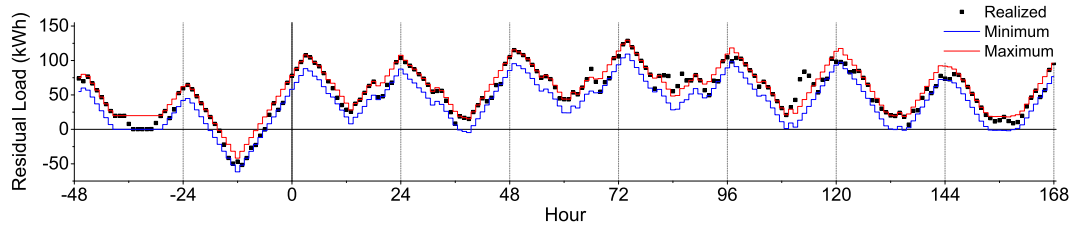

(b) Office

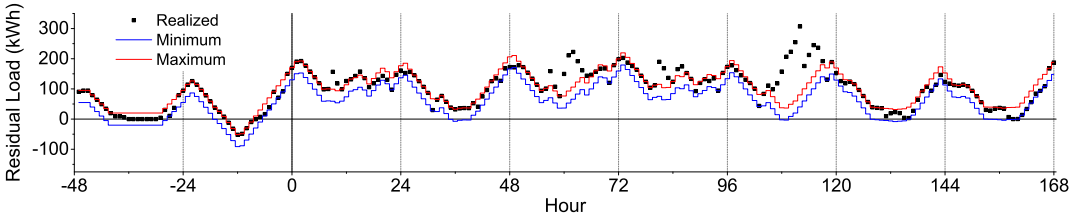

(c) School

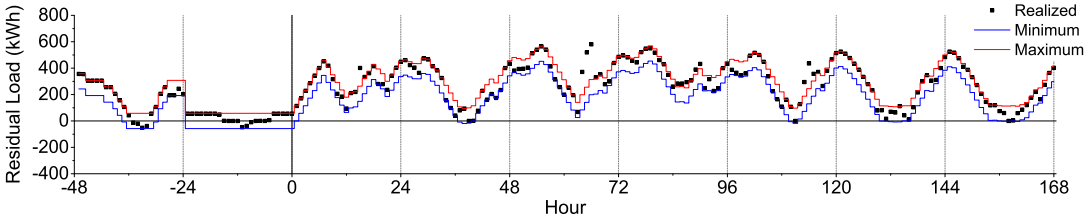

(d) Hospital

Figure 6.6: Residual load profile for each load shape in the summer season. Maximum and minimum bounds result from the day-ahead commitments.

4 systems. In particular, the energy imports are higher during the evening hours and overnight when the electricity prices are lower. During the middle of the day, less power is purchased from the utility company due to the combined effect of high prices and the availability of solar power. Sale/export of power to the utility company is generally rare, and tends to only occur on the weekends when local power demand is very low.

Table 6.5: Characteristic time scales for heat losses in each building in units of hours.

Retail	Office	School	Hospital
5.1	8.6	5.8	12.0

As evidenced by both Table 6.4 and Figure 6.6, the systems with the office building and hospital have a level of commitment violations that is 4-5x lower than the other cases in the summer season. This is in part due to the difference in the time scale for heat loss to the environment among the different buildings considered. A characteristic time scale for heat losses in each building can be calculated as:

$$\frac{M_{bldg}}{\sum_{e} A_e h_{ext} + \sum_{w} \sum_{z} A_{z,w} U_w + \sum_{i} A_{g,i} U_{g,i}}$$

where M_{bldg} is the total thermal mass of the building given by:

$$M_{bldg} = \sum_{z} \rho C_p V_z + \sum_{f} M_f + \sum_{i} M_i + \sum_{e} \left(M_e^{int} + M_e^{blk} + M_e^{ext} \right)$$

The values of this characteristic time for each building considered are shown in Table 6.5. As shown by this table, the retail building and school have a significantly lower characteristic time (i.e. heat losses to the environment occur faster). Thus, their effective thermal storage is akin to a leaky battery, and the load shaping performance is worse (i.e. more commitment violations are incurred). In particular, due to the higher rate of losses to the environment, less pre-cooling of the building is observed during closed-loop operations, and so flexibility is not available to mitigate forecasting errors. This can be seen in Figure 6.7 which compares the temperature profiles during the summer season. In summer, the office building is pre-cooled to a larger extent compared to both the school and retail buildings. Typically the office is pre-cooled overnight to a building average temperature of $\sim 21^o$C as compared to $\sim 23^o$C and $\sim 22^o$C for the retail building and school, respectively. The control system elects not to pre-cool these buildings as much since more of this stored energy would be lost (and it is therefore economically inefficient). Furthermore, the office heats up slower over the daytime hours, so flexible operation of the A/C unit can still be achieved during the

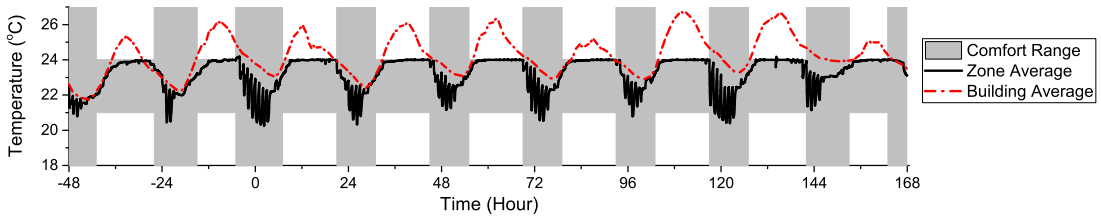

(a) Retail

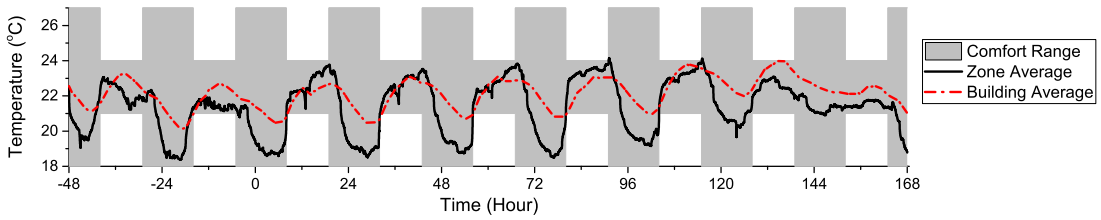

(b) Office

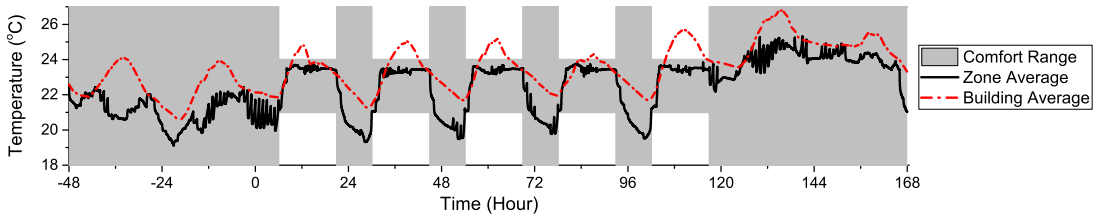

(c) School

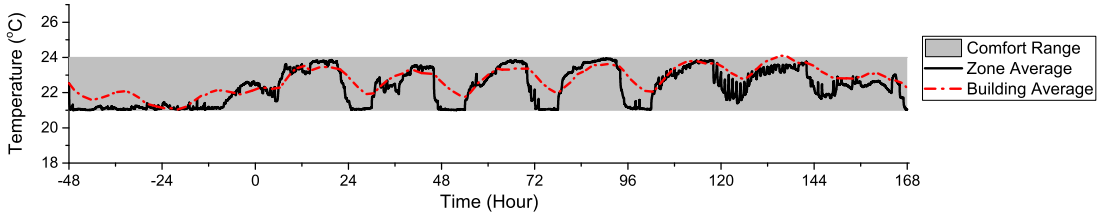

(d) Hospital

Figure 6.7: Temperature profiles for each load shape in the summer season. The comfort range varies by load shape due to the differences in occupancy patterns.

later afternoon/evening hours when the school and retail building incur commitment violations.

The retail building has a fast characteristic time for heat losses due to its smaller size (i.e. in terms of square footage). In general, the volume of the building will scale with the total square footage of the building raised to a power of 1.5, whereas the area

for heat loss to the environment will scale linearly. Therefore, a larger building will have a more attractive ratio of volume (and thus thermal inertia) to surface area for heat loss, and so will perform better at the required load shaping. The school building, despite its relatively large square footage, also has a high specific surface area due to its layout with 3 separate wings (see the layouts in Section 6.7.3). Therefore, it also performs poorly at load shaping in the summer.

The hospital is assumed to be occupied at all hours, so deep pre-cooling of the building zones is not allowed. However, by keeping the air temperature close to the lower bound during the night hours, the average building temperature can still be brought quite low. In addition, the hospital has a slow rate of heat exchange with the surroundings due to its large volume-to-surface area ratio. Combined, these effects allow for sufficient shifting of thermal loads, and a relatively low magnitude of commitment violations.

Figure 6.8 shows the residual load profile of the office building in each season. The overall profile is similar in each season. In particular, energy imports are higher during the overnight period when electricity is inexpensive. In the fall and winter the difference between the peaks and valleys in the residual load profile are less extreme. Thus, a tightening of the allowed schedule adaptability would likely primarily impact the cost during the summer season. Export of power to the utility company is more common during the fall and winter seasons since less power is needed locally for cooling. During the winter season a small amount of power is sometimes exported around noon on weekdays, but overall these exports occur midday on the weekends. The utility company could redistribute this energy to serve nearby residential customers which have higher loads on the weekend. Similar trends are observed for the other load shapes considered.

Figure 6.9 shows the temperature profiles of the office building in each season. Similar closed-loop behavior is seen in the summer and fall where pre-cooling of the building is done overnight. In the fall, very deep levels of pre-cooling can be achieved on cold nights (e.g. around hours 50 and 75) since freely available cold air can be sent directly to the building zones (i.e. power is only needed for the ventilation and not for chilling of the air). In the winter, the building is building cools overnight due to heat loss to the environment. The building heats somewhat during the daytime hours due to the high level of internal heat generation from occupants and electricity consumption, but

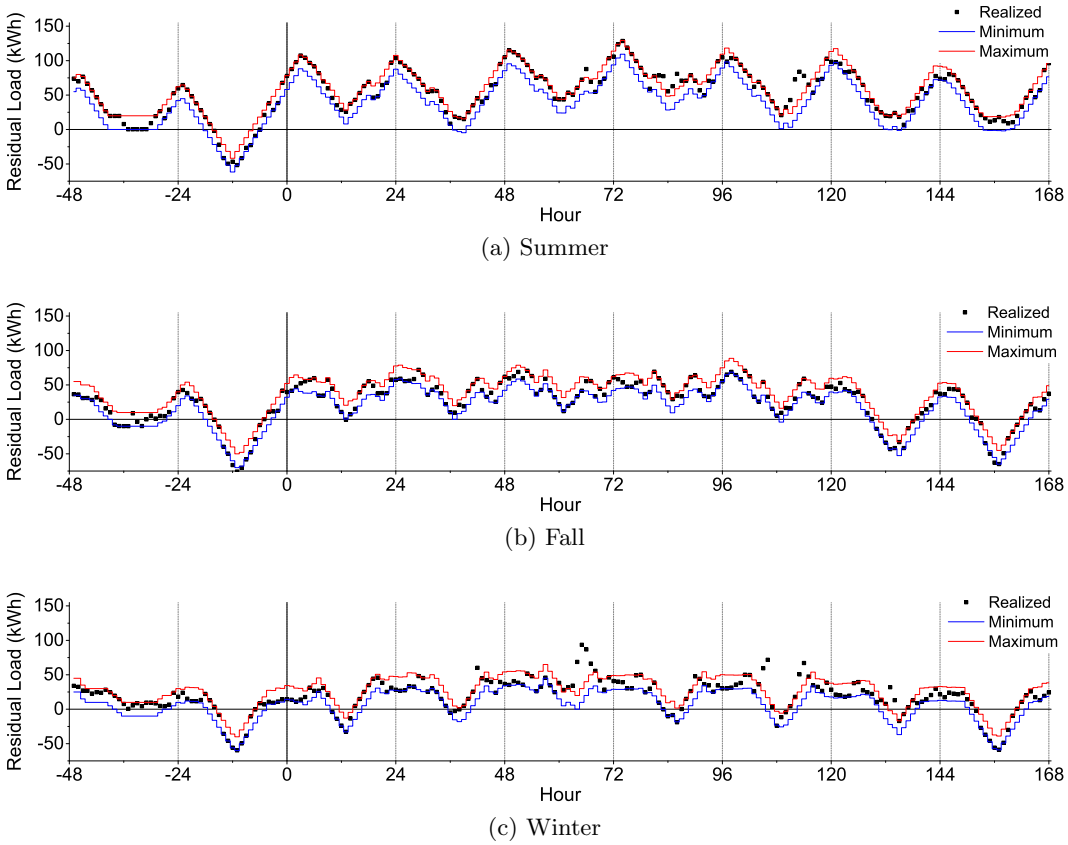

(a) Summer

(b) Fall

(c) Winter

Figure 6.8: Residual load profile for the office building in each season. Maximum and minimum bounds result from the day-ahead commitments.

the upper comfort bound is never approached. Similar trends are observed for the other buildings considered. In all cases, satisfactory indoor air temperatures are maintained.

Table 6.6 shows the load factor (defined in the same way as Chapter 5) in each case. The load factor is substantially increased in all cases by +20-80% relative to the base case. In some cases, the improvement in load factor is strongly season-dependent. For buildings with a fast characterisitc time scale for heat loss, this improvement is modest in the summer (i.e. since the HVAC system must be operated more consistently to keep the building cool). However, in the fall and winter, overall power demand is lower (i.e. little to no energy must be spent in cooling), and cogeneration technologies are favored since significant space heating is needed. In the base case, the average energy imports are very low in these seasons, leading to a small load factor. A dramatic improvement

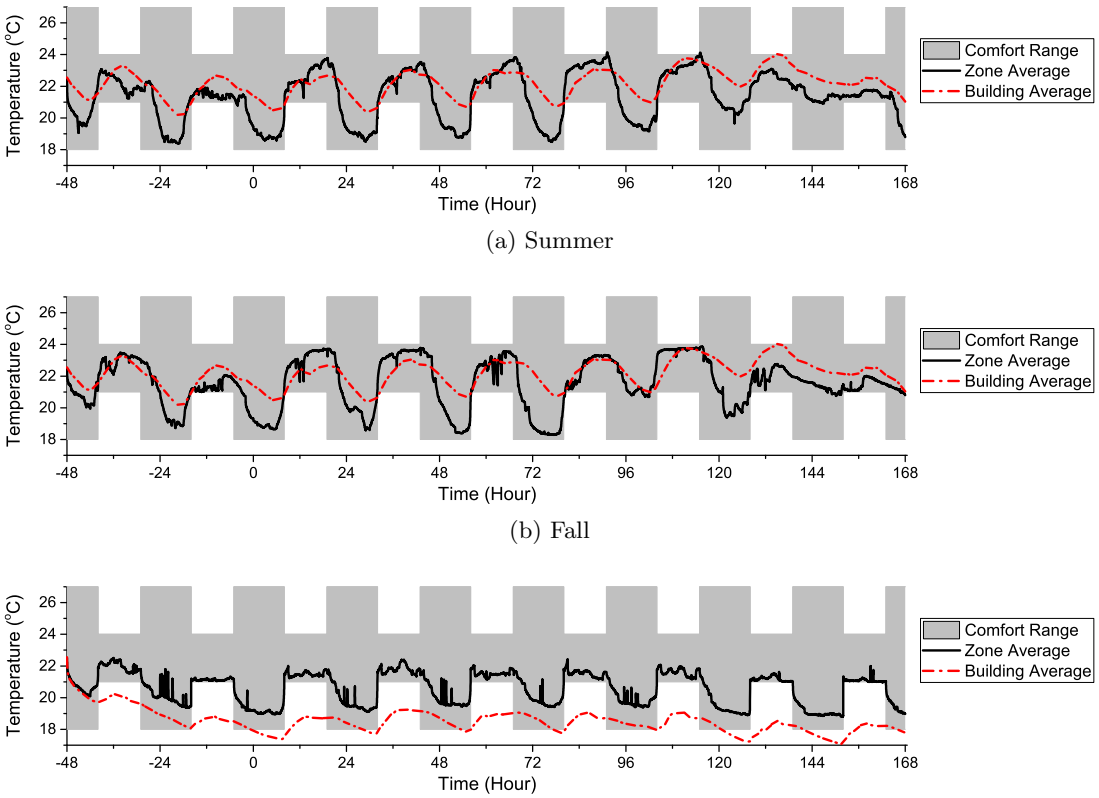

(a) Summer

(b) Fall

(c) Winter

Figure 6.9: Temperature profiles for the office building in each season.

is then seen when the proposed market structure is implemented.

For buildings with a long characteristic time scale for heat transfer with the environment (i.e. the office and hospital), the improvement in the load factor is fairly uniform across all seasons. Such buildings still utilize a significant amount of space cooling in the winter, and technologies which cogenerate heat and power are less attractive. Thus, imported power remains a larger fraction of total energy supply throughout the year, and the load factor is relatively stable across seasons.

Table 6.7 shows that the load variability (defined the same way as in Chapter 5) is also improved (i.e. variability is decreased). Unlike load factor, this improvement is fairly uniform across all load shapes and seasons at a ∼30-45% reduction in hour-to-hour variability. Obviously this can be tuned through a proper selection of the schedule adaptability parameter.

Table 6.6: Mean load factor. The value in parenthesis shows the improvement relative to the base case.

	Retail	Office	School	Hospital
Summer	0.354 (+44%)	0.496 (+23%)	0.387 (+20%)	0.524 (+45%)
Fall	0.356 (+81%)	0.445 (+54%)	0.294 (+58%)	0.358 (+22%)
Winter	0.227 (+82%)	0.243 (+44%)	0.131 (+60%)	0.381 (+34%)

Table 6.7: Load variability in units of kW. The value in parenthesis shows the change relative to the base case.

	Retail	Office	School	Hospital
Summer	6.51 (-27%)	9.38 (-52%)	21.6 (-56%)	60.9 (-42%)
Fall	4.33 (-38%)	9.75 (-38%)	17.3 (-35%)	53.2 (-30%)
Winter	5.30 (-41%)	9.98 (-42%)	18.0 (-46%)	52.5 (-44%)

Finally, utilization of available renewable power is shown in Table 6.8. As shown, practically all of the available solar power is used in every cases. Thus, unlike the results in Chapter 4 curtailment of renewable power is not needed because the supervisory controller is leveraging the flexible operation of the HVAC system.

6.5 Conclusions

In this chapter, a scheduling/supervisory control framework is developed for microgrids that can be used to explicitly limit the uncertainty and variability in the residual load throughout the year. The formulation presented uses flexible heating and cooling loads to help address load shaping needs. A case study utilizing multiple different commercial load shapes shows a substantial improvement in both the load factor and load variability are observed in all seasons.

For appropriate building types, this load shaping only results in a $\sim$15% increase in microgrid operating cost for most of the year. The level of commitment violations is relatively high during the winter since little space cooling is needed, and the space heating loads are not as effective for electric load shaping. In particular, space heating is dominated by gas-based technologies (i.e. the furnace and microturbines). If space

Table 6.8: Utilization of available solar power.

	Retail	Office	School	Hospital
Summer	100%	100%	100%	100%
Fall	98.8%	98.9%	98.8%	98.4%
Winter	100%	100%	100%	99.0%

heating were instead based on an electric furnace or heat pump, load shaping results (i.e. in terms of commitment violations) should be similar in both summer and winter. Such heating systems are more common in warmer climates, but can also be implemented in cold climates (e.g. via a ground-source heat pump).

Buildings with a high specific surface area exhibit higher load shaping costs during summer since pre-cooling is less economically attractive (i.e. a significant amount of energy leaks out to the environment) and is less effective (i.e. even when pre-cooled, the building heats up faster). Similar high costs are not observed during the fall and winter seasons since cooling loads are much lower. These challenges can be addressed at the project planning stage if the building and microgrid are co-designed by rationally selecting the building layout, or by selecting building materials which enable better insulation. The system could also be augmented with cold thermal storage units (e.g. at the project planning state or later via a retrofit) to further enhance the shifting of cooling loads. The use of thermal storage units could similarly improve the economic performance of buildings which are always occupied (i.e. the hospital) by allowing for better shifting of thermal loads. Such approaches were not addressed in this chapter in order to maintain simplicity in the formulation and comparability among the systems considered.

In all cases, similar closed-loop behavior is observed across different building types and in different seasons. Importantly, this indicates that these microgrid systems will behave predictably from the utility company perspective. In addition, rational behavior emerges during the closed-loop operation, such as pre-cooling the building in response to low electricity prices or cold ambient temperatures.

6.6 Nomenclature

Table 6.9: Nomenclature - Sets/Indicies

$\mathcal{C}_z \subset \mathcal{Z}$	Zones upstream from zone z	t	Time
$e \in \mathcal{E}$	External Building Elements	$\mathcal{T}$	Current time
$f \in \mathcal{F}$	Interior furnishings	$w \in \mathcal{W}$	Windows
h	Balancing periods	$z \in \mathcal{Z}$	Zones
h_1	First balancing period in horizon	$\mathcal{Z}_1 \subset \mathcal{Z}$	Zones aggregated into group 1
h_f	Last balancing period in horizon	$\mathcal{Z}_2 \subset \mathcal{Z}$	Zones aggregated into group 2
$i \in \mathcal{I}$	Internal Building Elements	$\mathcal{Z}_v \subset \mathcal{Z}$	Set of zones which are directly
k	Time periods		ventilated by the HVAC system
k_f	Final time period in horizon	$\mathcal{Z}_r \subset \mathcal{Z}$	Set of zones which may return
$\mathcal{K}_h$	Time periods in balacing period h		air to the HVAC system

Table 6.10: Nomenclature - Parameters

α	Confidence level
β_ℓ	Load forecast relaxation time
β_s	Insolation forecast relaxation time
β_T	Temperature forecast relaxation time
δ	Schedule adaptability
δ_ℓ	Load forecast error
δ_s	Insolation forecast error
δ_T	Ambient temperature forecast error
Δ_T	Sampling time
η_I	Battery inverter efficiency
η_n	Furnace efficiency
η_r	Resistive heater efficiency
γ	Schedule elasticity
Γ_b	Battery DOC coefficient
$\lambda_{ac,1}$	A/C quadratic power cost
$\lambda_{ac,2}$	A/C linear power cost

Continued on next page

Table 6.10 – continued from previous page

$\lambda_{c1} - \lambda_{c5}$	Empirical coefficients for battery internal heat generation during battery charging
λ_{d1}	Empirical coefficient for battery internal heat generation during battery discharging
$\lambda_{m,var}$	Marginal waste heat availability
$\lambda_{m,fix}$	No-load waste heat availability
$\lambda_{vent,1}$	Ventilation quadratic power cost
$\lambda_{vent,2}$	Ventilation linear power cost
ρ	Air density
σ_ℓ	Power forecast standard deviation
σ_e	Solar gain coefficient of e
σ_s	Solar forecast standard deviation
σ_w	Solar gain coefficient of w
τ_b	Battery characteristic time
τ_ℓ	Load forecast filter time
τ_s	Insolation forecast filter time
τ_T	Temperature forecast filter time
ξ_b^{min}	Minimum battery SOC
ζ_{buy}	Electricity import price
ζ_c	Battery charge cost
$\zeta_{comfort}$	Temperature violation price
ζ_d	Battery discharge cost
ζ_{gas}	Natrual gas price
ζ_m	Microturbine startup cost
ζ_{sell}	Electricity export price
ζ_{store}	Value of stored electricity
ζ_{temp}	Value of building temperature
ζ_{track}	Value of tracking scheduled temperature
ζ_v	Commitment violation price
ξ_b^{target}	Target for terminal battery SOC

Continued on next page

Table 6.10 – continued from previous page

A_d	State matrix of thermal model
$A_{g,i}$	Surface area between thermal element i and soil
$A_{z,e}$	Surface area between thermal elements z and e
$A_{z,f}$	Surface area between thermal elements z and f
$A_{z,i}$	Surface area between thermal elements z and i
$A_{z,w}$	Surface area between thermal elements$z$ and w
A_b	Battery heat transfer area
A_e	Area of building element e
B_d	Input matrix of thermal model
C_p	Air heat capacity
D_b^{min}	Minimum battery DOC
$E_{b,max}$	Battery storage capacity
E_{gc}	Energy exchange commitment
E_g^0	Energy exchange so far in current balancing period
$F_{m,fix}$	No-load fuel consumption
$F_{m,var}$	Marginal fuel consumption
h_{ext}	Convective heat transfer coefficient outdoors
$h_{z,f}$	Convective heat transfer coefficient between z and f
$h_{z,e}$	Convective heat transfer coefficient between z and e
$h_{z,i}$	Convective heat transfer coefficient between z and i
H_e	Solar radiation on element e
H	Solar radiation on a horizontal surface
$\tilde{H}$	Original forecast for solar radiation
$\tilde{H}^{avg}$	Filtered value for $\tilde{H}$
$\hat{H}$	Observed solar radiation
$\hat{H}^{avg}$	Filtered value for $\hat{H}$
H_w	Solar radiation on window w
L_h	Fraction of balancing period h which lies in the planning horizon
M_b	Battery thermal inertia

Continued on next page

Table 6.10 – continued from previous page

M_e^{int}, M_e^{blk}, M_e^{ext}	Thermal masses of element e (interior, bulk, and exterior, respectively)
M_f	Thermal mass of furnishing element f
M_i	Thermal mass of element i
N_m	Number of microturbines
P_ℓ	Forecasted inflexible power demand
$\tilde{P}_\ell$	Original forecast for inflexible power demand
$\hat{P}_\ell$	Realized power demand
P_m^{lo}	Minimum microturbine setpoint
P_m^{up}	Maximum microturbine setpoint
P_s^{max}	Available solar power
Q_{ac}^{rated}	Rated cooling duty of the A/C
$Q_{gen,1}$, $Q_{gen,2}$	Internal heat generation (in aggregated scheduling model)
$Q_{gen,z}$	Internal heat generation
$q_{leak,z}$	Zone infiltration flow
Q_n^{up}	Maximum setpoint of the resistive heater
Q_r^{up}	Maximum furnace heating duty
q_{vent}^{up}	Maximum ventilation flow rate
$q_{fresh,z}^{min}$	Minimum flow rate of fresh air to zone z
T_{ac}	Supply air temperature
T_{air}^{max}	Maximum desired zone temperature
T_{air}^{min}	Minimum desired zone temperature
T_{amb}	Forecasted ambient temperature
$\tilde{T}_{amb}$	Original forecast for ambient temperature
$\hat{T}_{amb}$	Observed ambient temperature
T_b^{max}	Maximum battery temperature
T_{bldg}^{target}	Terminal building temp. target
T_{ref}	Reference temperature
$\bar{T}_z$	Nominal indoor air temperature

Continued on next page

Table 6.10 – continued from previous page

$U_{e,1}$, $U_{e,2}$	Internal heat transfer coefficient (interior-to-bulk and bulk-to-exterior, respectively)
U_b	Battery overall heat transfer coefficient
$U_{g,i}$	Overall heat transfer from i through the ground to ambient surroundings
U_w	Window overall heat transfer coefficient
V_z	Zone Volume

Table 6.11: Nomenclature - Binary Variables ($1 \implies$ True)

χ_b	Is battery charging

Table 6.12: Nomenclature - Integer Variables ($\in \{0, 1, 2, ...\}$)

x_m	Number of microturbines on	y_m	Number of microturbines started up
z_m	Number of microturbines shut down		

Table 6.13: Nomenclature - Continuous Variables

ϵ_b	Battery storage shortfall
ϵ_T	Building temperature shortfall
ξ_b	Battery state of charge
$\xi_b^{aux1}, \xi_b^{aux2}$	Auxiliary battery SOC variable
D_b	Battery depth of charge
E_{buy}	Energy import from utility
E_g	Energy exchange with utility
E_{gc}^{exp}	Expected exchange commitment
E_{sell}	Energy export to utility
E_v	Commitment violation
$\hat{E}_v$	Realized commitment violation
f_r	Fraction of recycled air

Continued on next page

Table 6.13 – continued from previous page

F_m	Microturbine fuel consumption
F_n	Furnace fuel consumption
P_{ac}	A/C power consumption
$\hat{P}_{ac}$	Realized A/C power consumption
P_{ac}^{max}	Maximum feasible A/C power
P_{ac}^{min}	Minimum feasible A/C power
P_b^{avg}	Average battery power
P_c	Battery charge power
$\hat{P}_c$	Realized battery charging power
P_c^{max}	Maximum feasible charge power
P_d	Battery discharge power
$\hat{P}_d$	Realized battery discharging power
P_d^{max}	Maximum feasible discharge power
P_g	Utility power exchange
$\hat{P}_g$	Realized power exchange
P_m	Microturbine power
$\hat{P}_m$	Realized microturbine power
P_m^{max}	Maximum feasible microturbine power
P_m^{min}	Minimum feasible microturbine power
P_s	Solar power used
$\hat{P}_s$	Realized solar power
P_r	Restive heater power consumption
$\hat{P}_r$	Realized restive heater power
P_r^{max}	Maximum feasible resistive heater power
P_r^{min}	Minimum feasible resistive heater power
P_{vent}	Ventilation power consumption
$\hat{P}_{vent}$	Realized ventilation power
P_{vent}^{max}	Maximum feasible ventilation power
P_{vent}^{min}	Minimum feasible ventilation power
$q_{fresh,1}$, $q_{fresh,2}$	Fresh air flow rate (in aggregated scheduling model)

Continued on next page

Table 6.13 – continued from previous page

$q^{aux1}_{fresh,1}$, $q^{aux2}_{fresh,1}$	Auxiliary fresh air flow for group $\mathcal{Z}_1$
$q^{aux1}_{fresh,2}$, $q^{aux2}_{fresh,2}$	Auxiliary fresh air flow for group $\mathcal{Z}_2$
q^{tot}_{fresh}	Total fresh air flow rate
$q_{recycle,1}$, $q_{recycle,2}$	Recycle air flow rates (in aggregated scheduling model)
$q^{aux1}_{recycle,1}$, $q^{aux2}_{recycle,1}$	Auxiliary recycle air flow for group $\mathcal{Z}_1$
$q^{aux1}_{recycle,2}$, $q^{aux2}_{recycle,2}$	Auxiliary recycle air flow for group $\mathcal{Z}_2$
$q^{aux1}_{vent,1}$, $q^{aux2}_{vent,1}$	Auxiliary ventilation rate for group $\mathcal{Z}_1$
$q^{aux1}_{vent,2}$, $q^{aux2}_{vent,2}$	Auxiliary ventilation rate for group $\mathcal{Z}_2$
$q_{vent,1}$, $q_{vent,2}$	Ventilation flow rates (in aggregated scheduling model)
q^{tot}_{vent}	Total ventilation flow rate
$q_{vent,z}$	Ventilation flow rate to zone z
Q_{ac}	A/C cooling duty
Q^{max}_{ac}	Maximum feasible cooling duty
Q^{min}_{ac}	Minimum feasible cooling duty
Q_c	Battery charge heat
Q^{max}_c	Maximum feasible battery charge heat
Q_d	Battery discharge heat
Q^{max}_d	Maximum feasible battery discharge heat
$Q_{flow,1}$, $Q_{flow,2}$	Enthalpy flow from ventilation (in aggregated scheduling model)
$Q^{aux1}_{flow,1}$, $Q^{aux2}_{flow,1}$	Auxiliary enthalpy flow for group $\mathcal{Z}_1$
$Q^{aux1}_{flow,2}$, $Q^{aux2}_{flow,2}$	Auxiliary enthalpy flow for group $\mathcal{Z}_2$
$Q_{flow,z}$	Enthalpy flow to zones
$Q_{heat,1}$, $Q_{heat,2}$	Zone heating (in aggregated scheduling model)
$Q^{aux1}_{heat,1}$, $Q^{aux2}_{heat,1}$	Auxiliary zone heating for group $\mathcal{Z}_1$
$Q^{aux1}_{heat,2}$, $Q^{aux2}_{heat,2}$	Auxiliary zone heating for group $\mathcal{Z}_2$
$Q_{heat,z}$	Zone heating

Continued on next page

Table 6.13 – continued from previous page

$Q_{HVAC,1}$, $Q_{HVAC,2}$	Net heating/cooling due to HVAC system (in aggregated scheduling model)
$Q^{aux1}_{HVAC,1}$, $Q^{aux2}_{HVAC,1}$	Auxiliary heating/cooling from HVAC system for group $\mathcal{Z}_1$
$Q^{aux1}_{HVAC,2}$, $Q^{aux2}_{HVAC,2}$	Auxiliary heating/cooling from HVAC system for group $\mathcal{Z}_2$
$Q_{HVAC,z}$	Net heating/cooling due to HVAC system
$\boldsymbol{Q}_{HVAC,\mathcal{Z}}$	Row vector of all $Q_{HVAC,z}$
Q_m	Microturbine waste heat recovered
Q^{aux1}_m, Q^{aux2}_m	Auxiliary waste heat recovery
Q_n	Furnace heat output
Q^{aux1}_n, Q^{aux2}_n	Auxiliary furnace heat output
Q_r	Resistive heater output
Q^{aux1}_r, Q^{aux2}_r	Auxiliary resistive heater output
$T_{air,1}$, $T_{air,2}$	Lumped indoor air temperatures (used in scheduling)
$T^{aux1}_{air,1}$, $T^{aux1}_{air,2}$	Auxiliary lumped indoor air temperatures
$T^{aux2}_{air,1}$, $T^{aux2}_{air,2}$	Auxiliary lumped indoor air temperatures
T_b	Battery temperature
T_{bldg}	Average temperature of building
$T^{int}_e, T^{blk}_e, T^{ext}_e$	Temperature of element e (interior, bulk, exterior)
$\boldsymbol{T}_{\mathcal{E}}$	Row vector of all T_e
T_f	Furnishing temperature
$\boldsymbol{T}_{\mathcal{F}}$	Row vector of all T_f
T_i	Temperature of element i
$\boldsymbol{T}_{\mathcal{I}}$	Row vector of all T_i
T_v	Temperature violation
T_z	Zone Temperature
$\boldsymbol{T}_{\mathcal{Z}}$	Row vector of all T_z

6.7 Supporting Information

6.7.1 Scheduling Layer Formulation

Because a time period length of 1 hour is used, a conversion factor is not shown when converting between energy (in units of kWh) and power (in units of kW).

$$\begin{aligned}\text{minimize} \quad \sum_k \Big[& \zeta_{buy}(k)E_{buy}(k) - \zeta_{sell}(k)E_{sell}(k) + \zeta_{gas}\big(F_m(k) + F_n(k)\big) \\ & + \zeta_m y_m(k) + \zeta_c P_c(k) + \zeta_d P_d(k) + \zeta_{comfort} T_v(k) \\ & + \zeta_v E_v(k) \Big] - \zeta_{store}(k_f) E_{b,max} \xi_b(k_f) + \zeta_{temp}(k_f) T_{bldg}(k_f)\end{aligned}$$

subject to:

$$P_m(k) + P_d(k) + P_s(k) + P_g(k) = P_\ell(k) + P_c(k) + P_{ac}(k) + P_{vent}(k) + P_r(k) \qquad \forall k$$

$$\begin{aligned}P_m^{max}(k) + P_d^{max}(k) + E_{gc}(k) + \gamma + E_v(k) - P_{ac}^{min} - P_{vent}^{min}(k) - P_r^{min}(k) & \\ \geq P_\ell(k) - P_s^{max} + +1.96\sqrt{\sigma_\ell^2(k) + \sigma_s^2(k)} & \quad \forall k \leq k_{24}\end{aligned}$$

$$\begin{aligned}P_m^{max}(k) + P_d^{max}(k) + E_{gc}^{exp}(k) + \gamma + E_v(k) - P_{ac}^{min} - P_{vent}^{min}(k) - P_r^{min}(k) & \\ \geq P_\ell(k) - P_s^{max} + 1.96\sqrt{\sigma_\ell^2(k) + \sigma_s^2(k)} & \quad \forall k > k_{24}\end{aligned}$$

$$\begin{aligned}P_m^{min}(k) - P_c^{max}(k) + E_{gc}(k) - \gamma - E_v(k) - P_{ac}^{max} - P_{vent}^{max}(k) - P_r^{max}(k) & \\ \leq P_\ell(k) - 1.96\sigma_\ell(k) & \quad \forall k \leq k_{24}\end{aligned}$$

$$\begin{aligned}P_m^{min}(k) - P_c^{max}(k) + E_{gc}^{exp}(k) - \gamma - E_v(k) - P_{ac}^{max} - P_{vent}^{max}(k) - P_r^{max}(k) & \\ \leq P_\ell(k) - 1.96\sigma_\ell(k) & \quad \forall k > k_{24}\end{aligned}$$

Market Constraints

$$E_{buy}(k) - E_{sell}(k) = P_g(k) \qquad \forall k$$

$$-\gamma - E_v(k) \leq P_g(k) - E_{gc}(k) \leq \gamma + E_v(k) \qquad \forall k \leq k_{24}$$

$$-\gamma - E_v(k) \leq P_g(k) - E_{gc}^{exp}(k) \leq \gamma + E_v(k) \qquad \forall k > k_{24}$$

$$E_{gc}(k_{24}) - \delta \leq E_{gc}^{exp}(k_{25}) \leq E_{gc}(k_{24}) + \delta$$

$$E_{gc}^{exp}(k-1) - \delta \leq E_{gc}^{exp}(k) \leq E_{gc}^{exp}(k-1) + \delta \qquad \forall k > k_{25}$$

$$E_{gc}^{exp}(k_{25}) = P_g(k_{25})$$

Solar Constraints

$$P_s(k) \leq P_s^{max}(k) \qquad \forall k$$

Microturbine Constraints

$$P_m^{max}(k) = x_m(k) P_m^{up} \qquad \forall k$$

$$P_m^{min}(k) = x_m(k) P_m^{lo} \qquad \forall k$$

$$P_m^{min}(k) \leq P_m(k) \leq P_m^{max}(k) \qquad \forall k$$

$$F_m(k) = F_{m,var} P_m(k) + F_{m,fix} x_m(k) \qquad \forall k$$

$$x_m(k) = x_m(k-1) + y_m(k) - z_m(k) \qquad \forall k$$

$$Q_m(k) \leq \lambda_{m,var} P_m(k) + \lambda_{m,fix} x_m(k) \qquad \forall k$$

Battery Constraints

$$E_{b,max}\big(\xi_b(k) - \xi_b(k-1)\big) = \Delta_T\big(\eta_I P_c(k) - Q_c(k) - P_d(k)/\eta_I - Q_d(k)\big) \qquad \forall k$$

$$T_b(k) = T_b(k-1) + \Delta_T \frac{U_b A_b\big(T_{ref} - T_b(k)\big) + Q_c(k) + Q_d(k)}{M_b} \qquad \forall k$$

$$T_b(k) \leq T_b^{max} \qquad \forall k$$

$$Q_c(k) \geq \lambda_{c1} P_c(k)^2 \qquad \forall k$$

$$Q_d(k) \geq \lambda_{d1} P_d(k)^2 \qquad \forall k$$

$$Q_c(k) \geq \lambda_{c2} P_c(k)^2 + \lambda_{c3} P_c(k) + \lambda_{c4} \xi_b(k) + \lambda_{c5} \qquad \forall k$$

$$P_c(k) \leq P_c^{max}(k) \qquad \forall k$$

$$P_d(k) \leq P_d^{max}(k) \qquad \forall k$$

$$E_{b,max}\big(\xi_b^{aux1}(k) - \xi_b(k-1)\big) = \Delta_T\big(\eta_I P_c^{max}(k) - Q_c^{max}(k)\big) \qquad \forall k$$

$$E_{b,max}\big(\xi_b^{aux2}(k) - \xi_b(k-1)\big) = \Delta_T\big(-P_d^{max}(k)/\eta_I - Q_d^{max}(k)\big) \qquad \forall k$$

$$T_b^{max} \geq T_b(k-1) + \Delta_T \frac{U_b A_b\big(T_{ref} - T_b^{max}\big) + Q_c^{max}(k) + Q_d^{max}(k)}{M_b} \qquad \forall k$$

$$Q_c^{max}(k) \geq \lambda_{c1} P_c^{max}(k)^2 \qquad \forall k$$

$$Q_d^{max}(k) \geq \lambda_{d1} P_d^{max}(k)^2 \qquad \forall k$$

$$Q_c^{max}(k) \geq \lambda_{c2} P_c^{max}(k)^2 + \lambda_{c3} P_c^{max}(k) + \lambda_{c4} \xi_b^{aux1}(k) + \lambda_{c5} \qquad \forall k$$

$$P_c^{max}(k) \leq 0.4(1 - \chi_b(k)) C_b / \eta_I \qquad \forall k$$

$$P_d^{max}(k) \leq 0.4 \chi_b(k) C_b \eta_I \qquad \forall k$$

$$\xi_b^{min} \leq \xi_b(k) \leq 1 \qquad \forall k$$

$$\xi_b^{min} \leq \xi_b^{aux1}(k) \leq 1 \qquad \forall k$$

$$\xi_b^{min} \leq \xi_b^{aux2}(k) \leq 1 \qquad \forall k$$

Temperature Dynamics

$$\boldsymbol{T}(k) = A_d \boldsymbol{T}(k-1) + B_d \boldsymbol{U}(k) \qquad \forall k$$

$$\boldsymbol{T}(k) = [T_{air,1}(k) \;\; T_{air,2}(k) \;\; \boldsymbol{T}_{\mathcal{F}}(k) \;\; \boldsymbol{T}_{\mathcal{I}}(k) \;\; \boldsymbol{T}_{\mathcal{E}}(k)]^T$$

$$\boldsymbol{U}(k) = [Q_{HVAC,1}(k) \;\; Q_{HVAC,2}(k) \;\; Q_{gen,1}(k) \;\; Q_{gen,2}(k) \;\; \boldsymbol{H}(k) \;\; T_{amb}(k)]^T$$

$$T_{air}^{min}(k) - T_v(k) \leq T_{air,1}(k) \leq T_{air}^{max}(k) + T_v(k) \qquad \forall k$$

$$T_{air}^{min}(k) - T_v(k) \leq T_{air,2}(k) \leq T_{air}^{max}(k) + T_v(k) \qquad \forall k$$

$$T_{bldg}(k) = \frac{\sum\limits_{z \in \mathcal{Z}_1} \rho C_p V_z T_{air,1}(k) + \sum\limits_{z \in \mathcal{Z}_2} \rho C_p V_z T_{air,2}(k) + \sum\limits_f M_f T_f(k)}{\sum\limits_z \rho C_p V_z + \sum\limits_f M_f + \sum\limits_i M_i + \sum\limits_e \left(M_e^{int} + M_e^{blk} + M_e^{ext} \right)} \qquad \forall k$$
$$+ \frac{\sum\limits_i M_i T_i(k) + \sum\limits_e \left(M_e^{int} T_e^{int}(k) + M_e^{blk} T_e^{blk}(k) + M_e^{ext} T_e^{ext}(k) \right)}{\sum\limits_z \rho C_p V_z + \sum\limits_f M_f + \sum\limits_i M_i + \sum\limits_e \left(M_e^{int} + M_e^{blk} + M_e^{ext} \right)}$$

$$Q_{HVAC,1}(k) = Q_{flow,1}(k) + Q_{heat,1}(k) \qquad \forall k$$

$$Q_{HVAC,2}(k) = Q_{flow,2}(k) + Q_{heat,2}(k) \qquad \forall k$$

HVAC Constraints

$$q_{vent,1}(k) = q_{recycle,1}(k) + q_{fresh,1}(k) \qquad \forall k$$

$$q_{vent,2}(k) = q_{recycle,2}(k) + q_{fresh,2}(k) \qquad \forall k$$

$$q_{fresh,1}(k) \geq \sum_{z \in \mathcal{Z}_1} q^{min}_{fresh,z}(k) \qquad \forall k$$

$$q_{fresh,2}(k) \geq \sum_{z \in \mathcal{Z}_2} q^{min}_{fresh,z}(k) \qquad \forall k$$

$$Q_{flow,1}(k) = q_{vent,1}(k)\rho C_p\big(T_{ac} - \bar{T}_z\big) \qquad \forall k$$

$$Q_{flow,2}(k) = q_{vent,2}(k)\rho C_p\big(T_{ac} - \bar{T}_z\big) \qquad \forall k$$

$$\begin{aligned} Q_{ac}(k) \geq & \rho C_p\big(q_{fresh,1}(k) + q_{fresh,2}(k)\big)\big(T_{amb}(k) - T_{ac}\big) \\ & + \rho C_p\big(q_{recycle,1}(k) + q_{recycle,2}(k)\big)\big(\bar{T}_z - T_{ac}\big) \end{aligned} \qquad \forall k$$

$$P_{ac}(k) \geq \lambda_{ac,1} Q_{ac}(k)^2 + \lambda_{ac,2} Q_{ac}(k) \qquad \forall k$$

$$P_{vent}(k) \geq \lambda_{vent,1}\big(q_{vent,1}(k) + q_{vent,2}(k)\big)^2 + \lambda_{vent,2}\big(q_{vent,1}(k) + q_{vent,2}(k)\big) \qquad \forall k$$

$$Q_{heat,1}(k) + Q_{heat,2}(k) = Q_m(k) + Q_r(k) + Q_n(k) \qquad \forall k$$

$$F_n(k) = Q_n(k)/\eta_n(k) \qquad \forall k$$

$$P_r(k) = Q_r(k)/\eta_r(k) \qquad \forall k$$

$$q_{vent,1}(k) + q_{vent,2}(k) \leq q^{up}_{vent} \qquad \forall k$$

$$Q_r(k) \leq Q^{up}_r \qquad \forall k$$

$$Q_n(k) \leq Q^{up}_n \qquad \forall k$$

Auxiliary HVAC Equations Set 1 (Used to bound P^{max}_{ac}, P^{max}_{vent}, P^{max}_r)

$$T^{min}_{air}(k) - T_v(k) \leq T^{aux1}_{air,1}(k) \leq T^{max}_{air}(k) + T_v(k) \qquad \forall k$$

$$T^{min}_{air}(k) - T_v(k) \leq T^{aux1}_{air,2}(k) \leq T^{max}_{air}(k) + T_v(k) \qquad \forall k$$

$$\boldsymbol{T}^{aux1}(k) = A_d \boldsymbol{T}(k-1) + B_d \boldsymbol{U}^{aux1}(k) \qquad \forall k$$

$$\boldsymbol{U}^{aux1}(k) = [Q^{aux1}_{HVAC,1}(k)\ \ Q^{aux1}_{HVAC,2}(k)\ \ Q_{gen,1}(k)\ \ Q_{gen,2}(k)\ \ \boldsymbol{H}(k)\ \ T_{amb}(k)]^T$$

$$Q^{aux1}_{HVAC,1}(k) = Q^{aux1}_{flow,1}(k) + Q^{aux1}_{heat,1}(k) \qquad \forall k$$

$$Q^{aux1}_{HVAC,2}(k) = Q^{aux1}_{flow,2}(k) + Q^{aux1}_{heat,2}(k) \qquad \forall k$$

$$q^{aux1}_{vent,1}(k) = q^{aux1}_{recycle,1}(k) + q^{aux1}_{fresh,1}(k) \qquad \forall k$$

$$q^{aux1}_{vent,2}(k) = q^{aux1}_{recycle,2}(k) + q^{aux1}_{fresh,2}(k) \qquad \forall k$$

$$q^{aux1}_{fresh,1}(k) \geq \sum_{z \in \mathcal{Z}_1} q^{min}_{fresh,z}(k) \qquad \forall k$$

$$q^{aux1}_{fresh,2}(k) \geq \sum_{z\in\mathcal{Z}_2} q^{min}_{fresh,z}(k) \qquad \forall k$$

$$Q^{aux1}_{flow,1}(k) = q^{aux1}_{vent,1}(k)\rho C_p\big(T_{ac} - \bar{T}_z\big) \qquad \forall k$$

$$Q^{aux1}_{flow,2}(k) = q^{aux1}_{vent,2}(k)\rho C_p\big(T_{ac} - \bar{T}_z\big) \qquad \forall k$$

$$\begin{aligned} Q^{max}_{ac}(k) \geq & \rho C_p\big(q^{aux1}_{fresh,1}(k) + q^{aux1}_{fresh,2}(k)\big)\big(T_{amb}(k) - T_{ac}\big) \\ & + \rho C_p\big(q^{aux1}_{recycle,1}(k) + q^{aux1}_{recycle,2}(k)\big)\big(\bar{T}_z - T_{ac}\big) \end{aligned} \qquad \forall k$$

$$P^{max}_{ac}(k) \geq \lambda_{ac,1}Q^{max}_{ac}(k)^2 + \lambda_{ac,2}Q^{max}_{ac}(k) \qquad \forall k$$

$$P^{max}_{vent}(k) \geq \lambda_{vent,1}\big(q^{aux1}_{vent,1}(k) + q^{aux1}_{vent,2}(k)\big)^2 + \lambda_{vent,2}\big(q^{aux1}_{vent,1}(k) + q^{aux1}_{vent,2}(k)\big) \qquad \forall k$$

$$q^{aux1}_{vent,1}(k) + q^{aux1}_{vent,2}(k) \leq q^{up}_{vent} \qquad \forall k$$

$$Q^{aux1}_{heat,1}(k) + Q^{aux1}_{heat,2}(k) = Q^{aux1}_{m}(k) + Q^{aux1}_{r}(k) + Q^{aux1}_{n}(k) \qquad \forall k$$

$$P^{max}_{r} = Q^{aux1}_{r}(k)/\eta_r \qquad \forall k$$

$$Q^{aux1}_{m} \leq \lambda_{m,var}x_m(k)P^{up}_{m} + \lambda_{m,fix}x_m(k) \qquad \forall k$$

$$Q^{aux1}_{r}(k) \leq Q^{up}_{r} \qquad \forall k$$

$$Q^{aux1}_{n}(k) \leq Q^{up}_{n} \qquad \forall k$$

Auxiliary HVAC Equations Set 2 (Used to bound P^{min}_{ac}, P^{min}_{vent}, P^{min}_{r})

$$T^{min}_{air}(k) - T_v(k) \leq T^{aux2}_{air,1}(k) \leq T^{max}_{air}(k) + T_v(k) \qquad \forall k$$

$$T^{min}_{air}(k) - T_v(k) \leq T^{aux2}_{air,2}(k) \leq T^{max}_{air}(k) + T_v(k) \qquad \forall k$$

$$\boldsymbol{T}^{aux2}(k) = A_d\boldsymbol{T}(k-1) + B_d\boldsymbol{U}^{aux2}(k) \qquad \forall k$$

$$\boldsymbol{U}^{aux2}(k) = [Q^{aux2}_{HVAC,1}(k)\ \ Q^{aux2}_{HVAC,2}(k)\ \ Q_{gen,1}(k)\ \ Q_{gen,2}(k)\ \ \boldsymbol{H}(k)\ \ T_{amb}(k)]^T$$

$$Q^{aux2}_{HVAC,1}(k) = Q^{aux2}_{flow,1}(k) + Q^{aux2}_{heat,1}(k) \qquad \forall k$$

$$Q^{aux2}_{HVAC,2}(k) = Q^{aux2}_{flow,2}(k) + Q^{aux2}_{heat,2}(k) \qquad \forall k$$

$$q^{aux2}_{vent,1}(k) = q^{aux2}_{recycle,1}(k) + q^{aux2}_{fresh,1}(k) \qquad \forall k$$

$$q^{aux2}_{vent,2}(k) = q^{aux2}_{recycle,2}(k) + q^{aux2}_{fresh,2}(k) \qquad \forall k$$

$$q^{aux2}_{fresh,1}(k) \geq \sum_{z\in\mathcal{Z}_1} q^{min}_{fresh,z}(k) \qquad \forall k$$

$$q^{aux2}_{fresh,2}(k) \geq \sum_{z\in\mathcal{Z}_2} q^{min}_{fresh,z}(k) \qquad \forall k$$

$$Q^{aux2}_{flow,1}(k) = q^{aux2}_{vent,1}(k)\rho C_p\big(T_{ac} - \bar{T}_z\big) \qquad \forall k$$

$$Q^{aux2}_{flow,2}(k) = q^{aux2}_{vent,2}(k)\rho C_p\big(T_{ac} - \bar{T}_z\big) \qquad \forall k$$

$$\begin{aligned} Q^{min}_{ac}(k) \geq & \rho C_p\big(q^{aux2}_{fresh,1}(k) + q^{aux2}_{fresh,2}(k)\big)\big(T_{amb}(k) - T_{ac}\big) \\ & + \rho C_p\big(q^{aux2}_{recycle,1}(k) + q^{aux2}_{recycle,2}(k)\big)\big(\bar{T}_z - T_{ac}\big) \end{aligned} \qquad \forall k$$

$$P^{min}_{ac}(k) \geq \lambda_{ac,1}Q^{min}_{ac}(k)^2 + \lambda_{ac,2}Q^{min}_{ac}(k) \qquad \forall k$$

$$P^{min}_{vent}(k) \geq \lambda_{vent,1}\big(q^{aux2}_{vent,1}(k) + q^{aux2}_{vent,2}(k)\big)^2 + \lambda_{vent,2}\big(q^{aux2}_{vent,1}(k) + q^{aux2}_{vent,2}(k)\big) \qquad \forall k$$

$$q^{aux2}_{vent,1}(k) + q^{aux2}_{vent,2}(k) \leq q^{up}_{vent} \qquad \forall k$$

$$Q^{aux2}_{heat,1}(k) + Q^{aux2}_{heat,2}(k) = Q^{aux2}_{m}(k) + Q^{aux2}_{r}(k) + Q^{aux2}_{n}(k) \qquad \forall k$$

$$P^{max}_{r} = Q^{aux2}_{r}(k)/\eta_r \qquad \forall k$$

$$Q^{aux2}_{m} \leq \lambda_{m,var}x_m(k)P^{lo}_{m} + \lambda_{m,fix}x_m(k) \qquad \forall$$

$$Q^{aux2}_{r}(k) \leq Q^{up}_{r} \qquad \forall k$$

$$Q^{aux2}_{n}(k) \leq Q^{up}_{n} \qquad \forall k$$

Non-negativity Constraints

$$P_m(k),\, P_s(k),\, P_d(k),\, P_c(k),\, P_{ac}(k),\, P_{vent}(k),\, P^{min}_{ac}(k),\, Q_{ac}(k),\, Q^{min}_{ac} \geq 0 \qquad \forall k$$

$$P^{max}_{ac}(k),\, P^{min}_{vent}(k),\, P^{max}_{vent}(k),\, F_m(k),\, Q_c(k),\, Q_d(k),\, P^{max}_{c}(k),\, P^{max}_{d}(k) \geq 0 \qquad \forall k$$

$$E_v(k),\, E_{buy}(k),\, E_{sell}(k),\, Q^{max}_{c}(k),\, Q^{max}_{d}(k),\, q_{fresh,1}(k),\, q_{fresh,2}(k) \geq 0 \qquad \forall k$$

$$q_{recycle,1}(k),\, q_{recycle,2}(k),\, q^{aux1}_{fresh,1}(k),\, q^{aux2}_{fresh,1}(k),\, q^{aux1}_{recycle,1}(k),\, q^{aux2}_{recycle,1}(k) \geq 0 \qquad \forall k$$

$$q^{aux1}_{fresh,2}(k),\, q^{aux2}_{fresh,2}(k),\, q^{aux1}_{recycle,2}(k),\, q^{aux2}_{recycle,2}(k),\, T_v(k)),\, Q^{max}_{ac} \geq 0 \qquad \forall k$$

Integrality Constraints

$$x_m(k),\, y_m(k),\, z_m(k) \in \{0, 1, ..., N_m\} \qquad \forall k$$

$$\chi_b(k) \in \{0, 1\} \qquad \forall k$$

6.7.2 Dispatch Layer Formulation

$$\begin{aligned}\text{minimize} \quad & \textstyle\sum_h \Big[\zeta_{buy}(h)E_{buy}(h) - \zeta_{sell}(h)E_{sell}(h) + \zeta_v E_v(h) \Big] \\ & + \Delta_T \textstyle\sum_k \Big[\zeta_{gas}\big(F_m(k) + F_n(k)\big) + \zeta_{comfort}T_v(k) + \zeta_c P_c(k) \\ & \qquad + \zeta_d P_d(k) \Big] - \zeta_{store}(k_f)C_b\big(\xi_b(k_f) - \tfrac{2}{3}\epsilon_b\big) \\ & + \quad \zeta_{temp}(k_f)T_{bldg}(k_f) + \zeta_{track}(k_f)\epsilon_T\end{aligned}$$

subject to:

$$P_m(k) + P_d(k) + P_s(k) + P_g(k) = P_\ell(k) + P_c(k) + P_{ac}(k) + P_{vent}(k) + P_r(k) \qquad \forall k$$

Market Constraints

$$E_{buy}(h) - E_{sell}(h) = E_g(h) \qquad \forall h$$

$$E_g(h_1) = E_g^0 + \Delta_T \sum_{k \in \mathcal{K}_{h_1}} P_g(k)$$

$$E_g(h) = \Delta_T \sum_{k \in \mathcal{K}_h} P_g(k) \qquad \forall h \neq h_1$$

$$-\gamma - E_v(h) \leq E_g(h) - E_{gc}(h) \leq \gamma + E_v(h) \qquad \forall h \neq h_3$$

$$-\gamma - E_v(h_3) \leq E_g(h_3) - L_{h_3}E_{gc}(h_3) \leq \gamma + E_v(h_3)$$

Solar Constraints

$$P_s(k) \leq P_s^{max}(k) \qquad \forall k$$

Microturbine Constraints

$$x_m(k)P_m^{lo} \leq P_m(k) \leq x_m(k)P_m^{up} \qquad \forall k$$

$$F_m(k) = F_{m,var}P_m(k) + F_{m,fix}x_m(k) \qquad \forall k$$

$$Q_m(k) \leq \lambda_{m,var}P_m(k) + \lambda_{m,fix}x_m(k) \qquad \forall k$$

Battery Constraints

$$E_{b,max}\big(\xi_b(k)-\xi_b(k-1)\big)=\Delta_T\big(\eta_I P_c(k)-Q_c(k)-P_d(k)/\eta_I-Q_d(k)\big) \qquad \forall k$$

$$T_b(k)=T_b(k-1)+\Delta_T\frac{U_bA_b\big(T_{ref}-T_b(k)\big)+Q_c(k)+Q_d(k)}{M_b} \qquad \forall k$$

$$Q_c(k)\geq\lambda_{c1}P_c(k)^2 \qquad \forall k$$

$$Q_d(k)\geq\lambda_{d1}P_d(k)^2 \qquad \forall k$$

$$Q_c(k)\geq\lambda_{c2}P_c(k)^2+\lambda_{c3}P_c(k)+\lambda_{c4}\xi_b(k)+\lambda_{c5} \qquad \forall k$$

$$P_b^{avg}(k)=P_b^{avg}(k-1)e^{-\Delta_T/\tau_b}+\big(P_d(k)-P_c(k)\big)\big(1-e^{-\Delta_T/\tau_b}\big) \qquad \forall k$$

$$D_b(k)\big(1-\Gamma_bP_b^{avg}(k)\big)=-\Gamma_bP_b^{avg}(k)+\xi_b(k) \qquad \forall k$$

$$\epsilon_b\geq\xi_b^{target}-\xi_b(k_f)$$

$$P_c(k)\leq 0.5E_{b,max} \qquad \forall k$$

$$P_d(k)\leq 0.5E_{b,max} \qquad \forall k$$

$$\xi_b^{min}\leq\xi_b(k)\leq 1 \qquad \forall k$$

$$D_b(k)\geq D_b^{min} \qquad \forall k$$

$$T_b(k)\leq T_b^{max} \qquad \forall k$$

Temperature Dynamics

$$\boldsymbol{T}(k)=A_d\boldsymbol{T}(k-1)+B_d\boldsymbol{U}(k) \qquad \forall k$$

$$\boldsymbol{T}(k)=[\boldsymbol{T}_{\mathcal{Z}}(k)\ \ \boldsymbol{T}_{\mathcal{F}}(k)\ \ \boldsymbol{T}_{\mathcal{I}}(k)\ \ \boldsymbol{T}_{\mathcal{E}}(k)]^T \qquad \forall k$$

$$\boldsymbol{U}(k)=[\boldsymbol{Q}_{HVAC,\mathcal{Z}}(k)\ \ \boldsymbol{Q}_{gen,\mathcal{Z}}(k)\ \ \boldsymbol{H}(k)\ \ T_{amb}(k)]^T \qquad \forall k$$

$$T_{air}^{min}(k)-T_v(k)\leq T_z(k)\leq T_{air}^{max}(k)+T_v(k) \qquad \forall k, z\in\mathcal{Z}_v$$

$$T_{bldg}(k)=\frac{\sum\limits_z\rho C_pV_zT_z(k)+\sum\limits_f M_fT_f(k)+\sum\limits_i M_iT_i(k)}{\sum\limits_z\rho C_pV_z+\sum\limits_f M_f+\sum\limits_i M_i+\sum\limits_e\big(M_e^{int}+M_e^{blk}+M_e^{ext}\big)} + \frac{\sum\limits_e\big(M_e^{int}T_e^{int}(k)+M_e^{blk}T_e^{blk}(k)+M_e^{ext}T_e^{ext}(k)\big)}{\sum\limits_z\rho C_pV_z+\sum\limits_f M_f+\sum\limits_i M_i+\sum\limits_e\big(M_e^{int}+M_e^{blk}+M_e^{ext}\big)} \qquad \forall k$$

$$\epsilon_T\geq T_{bldg}(k_f)-T_{bldg}^{target}$$

HVAC Constraints

$$Q_{HVAC,z}(k) = Q_{flow,z}(k) + Q_{heat,z}(k) \qquad \forall k, z$$

$$q^{tot}_{vent}(k) = \sum_{z \in \mathcal{Z}_v} q_{vent,z}(k) \qquad \forall k$$

$$q_{vent,z}(k)\big(1 - f_r(k)\big) \geq q^{min}_{fresh,z}(k) \qquad \forall k, z$$

$$q^{tot}_{vent}(k) = q^{tot}_{fresh}(k) + f_r(k) \sum_{z \in \mathcal{Z}_r} \left[\big(q_{vent,z}(k) + \sum_{z' \in \mathcal{C}_z} q_{vent,z'}(k)\big) \right] \qquad \forall k$$

$$Q_{flow,z}(k) = \rho C_p \left[q_{vent,z}\big(T_{ac} - T_z(t)\big) + \sum_{z' \in \mathcal{C}_z} q_{vent,z'}\big(T_{z'}(t) - T_z(t)\big) \right] \qquad \forall k, z$$

$$\begin{aligned} Q_{ac}(k) \geq \rho C_p \Big[& q^{tot}_{fresh}(k) T_{amb}(k) - q^{tot}_{vent}(k) T_{AC} \\ & + f_r(k) \sum_{z \in \mathcal{Z}_r} \big(q_{vent,z}(k) + \sum_{z' \in \mathcal{C}_z} q_{vent,z'}(k)\big) T_z(k) \Big] \end{aligned} \qquad \forall k$$

$$P_{ac}(k) \geq \lambda_{ac,1} Q_{ac}(k)^2 + \lambda_{ac,2} Q_{ac}(k) \qquad \forall k$$

$$P_{vent}(k) \geq \lambda_{vent,1} q^{tot}_{vent}(k)^2 + \lambda_{vent,2} q^{tot}_{vent}(k) \qquad \forall k$$

$$\sum_z Q_{heat,z}(k) = Q_r(k) + Q_n(k) + Q_m(k) \qquad \forall k$$

$$P_r(k) = Q_r(k)/\eta_r \qquad \forall k$$

$$F_n(k) = Q_n(k)/\eta_n \qquad \forall k$$

$$0 \leq f_r(k) \leq 1 \qquad \forall k$$

$$q^{tot}_{vent}(k) \leq q^{up}_{vent} \qquad \forall k$$

$$Q_r(k) \leq Q^{up}_r(k) \qquad \forall k$$

$$Q_n(k) \leq Q^{up}_n(k) \qquad \forall k$$

Non-negativity Constraints

$$E_v(h),\ E_{buy}(h),\ E_{sell}(h) \geq 0 \qquad \forall h$$

$$P_m(k),\ P_s(k),\ P_d(k),\ P_c(k),\ P_{ac}(k),\ T_v(k) \geq 0 \qquad \forall k$$

$$P_{vent}(k),\ Q_{ac}(k),\ F_m(k),\ Q_c(k),\ Q_d(k) \geq 0 \qquad \forall k$$

$$q_{vent,z}(k) \geq 0 \qquad \forall k, z$$

$$\epsilon_b,\ \epsilon_T \geq 0$$

6.7.3 Building Layouts

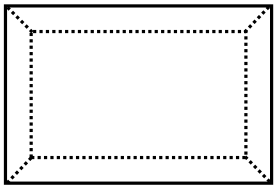

Figure 6.10: Office building layout.

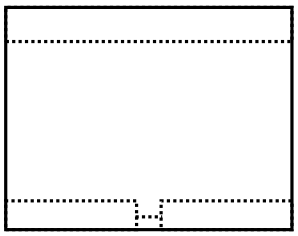

Figure 6.11: Stand-alone retail building layout.

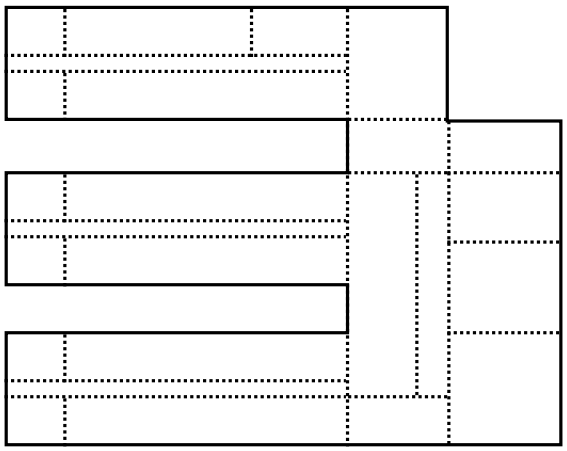

Figure 6.12: School building layout.

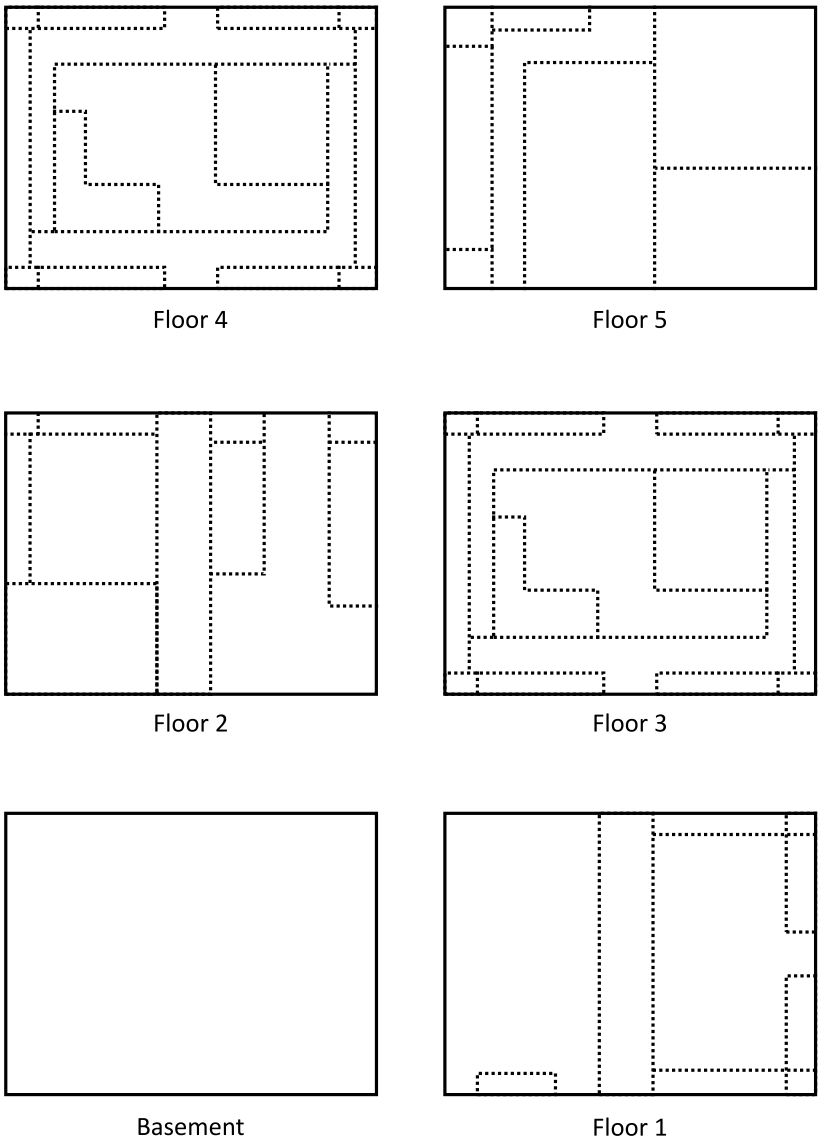

Figure 6.13: Hospital building layout.

6.7.4 Case Study Parameter Values

$$\zeta_{temp}(k) = \begin{cases} 1.5e^{-7} M_{bldg} \zeta_{buy}(k) & \text{Summer} \\ 0 & \text{Fall} \\ 0 & \text{Winter} \end{cases}$$

Table 6.14: Scalar Case Study Values

α	0.95	ζ_c	4 ¢/kWh
β_ℓ	10 h	ζ_d	4 ¢/kWh
β_s	3 h	ζ_{gas}	2.5 ¢/kWh
β_T	10 h	ζ_v	45 ¢/kWh
Δ_T (scheduling)	3600 s	C_p	1 kJ/kg-K
Δ_T (dispatch)	120 s	D_b^{min}	0.1
η_I	0.95	h_{ext}	20 W/m^2-K
η_n	0.85	T_{ac}	286 K
η_r	0.9	T_{air}^{max} (occupied)	297.15 K
ρ	1.225 kg/m^3	T_{air}^{max} (unoccupied)	300.15 K
σ_e (external walls)	0.6	T_{air}^{min} (occupied)	294.15 K
σ_e (roofs)	0.7	T_{air}^{min} (unoccupied)	291.15 K
σ_w (skylights)	0.33	T_b^{max}	308 K
σ_w (other windows)	0.39	T_{ref}	297 K
τ_b	5000 s	$\bar{T}_z$	297.15 K
τ_ℓ	10 min	U_b	16 W/m^2-K
τ_s	1 h	U_w (skylights)	0.05 W/m^2-K
τ_T	1 h	U_w (other windows)	3.24 W/m^2-K
ξ_b^{min}	0.2		

$$\zeta_{track}(k) = \begin{cases} 1e^{-7} M_{bldg} \zeta_{buy}(k) & \text{Summer} \\ 1e^{-7} M_{bldg} \zeta_{buy}(k) & \text{Fall} \\ 2.67e^{-7} M_{bldg} \zeta_{gas} & \text{Winter} \end{cases}$$

$$\zeta_{comfort} = 3e^{-6} M_{bldg}$$

For the scheduling layer, forecast uncertainties depend on the forecasted values and the look-ahead time:

$$\sigma_\ell(k) = P_\ell(k) \left(0.1 + 0.1 \frac{k - k_c}{47}\right) \qquad \forall k \geq k_c$$

Table 6.15: Time-of-Use Values

Rate	Applicable Times	ζ_{buy} (¢/kWh)	ζ_{sell} (¢/kWh)	ζ_{store} (¢/kWh)
Off-Peak	10PM-6AM	5	0	3.75
Mid-Peak	6AM-10PM (except On-Peak)	10	5	7.5
On-Peak	2PM-8PM (weekdays only)	15	7.5	11.25

$$\sigma_s(k) = \min\left(P_s^{rated}\left(0.1 + 0.22\frac{k-k_c}{47}\right), \frac{P_s^{max}(k)}{3}\right) \qquad \forall k_c \leq k \leq k_c + 26$$

$$\sigma_s(k) = \min\left(0.22 \cdot P_s^{rated}, \frac{P_s^{max}(k)}{3}\right) \qquad \forall k \geq k_c + 27$$

where k_c is the current time period.

The US Department of Energy (DOE) commercial reference building model files[4] were used to develop the building thermal models. In particular, Version 1.4_7.2 New Construction buildings files were considered. These files contain the information regarding building layouts necessary to find:

- Zone footprint area (A_z) and zone volumes (V_z)
- Contact area between zones, internal building elements, external building elements, windows, and the ground ($A_{z,i}$, $A_{z,e}$, $A_{z,w}$, and $A_{g,i}$)
- Size of internal and external building elements (A_i and A_e, respectively)

These values are not reproduced here due to the large size of the vectors and matrices. These files also describe nominal building occupancy profiles which are used to determine fresh air requirements (i.e. $q_{fresh,z}^{min}$). The fresh air required is calculated as:

$$q_{fresh,z}^{min}(k) = O_z(k) \cdot 10\frac{\text{L}}{\text{s-person}}$$

where O_z is the expected occupancy (in persons) of zone z. The office occupancy profile is modified somewhat to be closer to the one used in Chapter 5:

[4]Available from `https://energy.gov/eere/buildings/commercial-reference-buildings`. Accessed on 1 February 2017.

Office Building, Saturday

$$\frac{O_z(k)}{O_z^{max}} = \begin{cases} 0 & \text{12 AM - 8 AM} \\ 0.03 & \text{8 AM - 9 AM} \\ 0.2 & \text{9 AM - 5 PM} \\ 0.17 & \text{5 PM - 6 PM} \\ 0.0025 & \text{6 PM - 7 PM} \\ 0 & \text{7 PM - 12 AM} \end{cases} \qquad \forall z \in \mathcal{Z}_v$$

Office Building, Sunday

$$\frac{O_z(k)}{O_z^{max}} = \begin{cases} 0 & \text{12 AM - 8 AM} \\ 0.025 & \text{8 AM - 9 AM} \\ 0.1 & \text{9 AM - 5 PM} \\ 0.075 & \text{5 PM - 6 PM} \\ 0 & \text{6 PM - 12 AM} \end{cases} \qquad \forall z \in \mathcal{Z}_v$$

Office Building, Weekday

$$\frac{O_z(k)}{O_z^{max}} = \begin{cases} 0 & \text{12 AM - 8 AM} \\ 0.225 & \text{8 AM - 9 AM} \\ 1 & \text{9 AM - 5 PM} \\ 0.775 & \text{5 PM - 6 PM} \\ 0.05 & \text{6 PM - 7 PM} \\ 0 & \text{7 PM - 12 AM} \end{cases} \qquad \forall z \in \mathcal{Z}_v$$

The infiltration flow is proportional to the contact area with windows and external building elements:

$$q_{leak,z} = 3.02e^{-4} \frac{\text{m}^3}{\text{s-m}^2} \left(\sum_w A_{z,w} + \sum_e A_{z,e} \right) \qquad \forall z \in \mathcal{Z}$$

Each ventilated zone is associated with some interior furnishings (i.e. z_1 is associated

with f_1, z_2 is associated with f_2, etc.). The contact area for heat transfer is given as:

$$A_{z_i,f_j} = A_z \delta_{ij} \qquad \forall z_i \in \mathcal{Z}_v,\ f_j \in \mathcal{F}$$

where δ_{ij} is the Kronecker delta function. The furnishing thermal mass is then given by:

$$M_f = 98 \frac{\text{kJ}}{\text{K-m}^2} \sum_z A_{z,f} \qquad \forall f \in \mathcal{F}$$

The thermal mass of interior building elements is given by:

$$M_i = \begin{cases} A_i \cdot 4.90 \frac{\text{kJ}}{\text{K-m}^2} & \text{If drop ceiling} \\ A_i \cdot 16.5 \frac{\text{kJ}}{\text{K-m}^2} & \text{If interior wall} \\ A_i \cdot 381 \frac{\text{kJ}}{\text{K-m}^2} & \text{If basement wall} \\ A_i \cdot 190 \frac{\text{kJ}}{\text{K-m}^2} & \text{If floor/slab} \end{cases} \qquad \forall i \in \mathcal{I}$$

The thermal mass of exterior building elements is given by:

$$M_e^{int} = \begin{cases} A_e \cdot 3.17 \frac{\text{kJ}}{\text{K-m}^2} & \text{If exterior wall} \\ A_e \cdot 135 \frac{\text{kJ}}{\text{K-m}^2} & \text{If roof} \end{cases} \qquad \forall e \in \mathcal{E}$$

$$M_e^{blk} = \begin{cases} A_e \cdot 17.5 \frac{\text{kJ}}{\text{K-m}^2} & \text{If exterior wall} \\ A_e \cdot 56.3 \frac{\text{kJ}}{\text{K-m}^2} & \text{If roof} \end{cases} \qquad \forall e \in \mathcal{E}$$

$$M_e^{ext} = \begin{cases} A_e \cdot 12.1 \frac{\text{kJ}}{\text{K-m}^2} & \text{If exterior wall} \\ A_e \cdot 28 \frac{\text{kJ}}{\text{K-m}^2} & \text{If roof} \end{cases} \qquad \forall e \in \mathcal{E}$$

Heat transfer through the exterior building elements is described by:

$$U_{e,1} = \begin{cases} 0.427 \frac{\text{W}}{\text{K-m}^2} & \text{If exterior wall} \\ 3.0 \frac{\text{W}}{\text{K-m}^2} & \text{If roof} \end{cases} \qquad \forall e \in \mathcal{E}$$

$$U_{e,2} = \begin{cases} 0.786 \frac{\text{W}}{\text{K-m}^2} & \text{If exterior wall} \\ 0.267 \frac{\text{W}}{\text{K-m}^2} & \text{If roof} \end{cases} \qquad \forall e \in \mathcal{E}$$

The heat transfer between zones and other thermal elements (i.e. $h_{z,f}$, $h_{z,i}$, and $h_{z,e}$) is generally taken to be 5 W/m^2-K. The only exception is the top-side of floors in the school, office, and hospital (except the basement floor), where the convection coefficient is instead taken to be 2.4 W/m^2-K. This is done to capture the thermal resistance of materials like carpeting.

The heat transfer coefficient via the ground, $U_{g,i}$, is calculated as:

$$U_{g,i} = \frac{1}{c_1 d_i + c_2} \qquad \text{for underground walls} \tag{6.44}$$

$$U_{g,i} = \frac{P_i F}{A_{g,i}} \qquad \text{for slabs on grade} \tag{6.45}$$

$$U_{g,i} = \frac{1}{\frac{A_{g,i}}{P_i F} + c_1 d_i + c_2} \qquad \text{for underground (i.e. basement) floors} \tag{6.46}$$

where P_i is the perimeter length of element i, d_i is the average depth below the ground of element i, and c_1, c_2, and F are constant parameters taken as:

$$c_1 = 0.3479 \frac{\text{m-K}}{\text{W}} \tag{6.47}$$

$$c_2 = 0.0601 \frac{\text{m}^2\text{-K}}{\text{W}} \tag{6.48}$$

$$F = 1.22 \frac{\text{W}}{\text{m-K}} \tag{6.49}$$

Table 6.16: Load-Shape Dependent Values

Parameter	Retail	Office	School	Hospital
$\lambda_{ac,1}$ (kW^{-1})	6.79E-4	3.65E-4	2.38E-4	6.34E-5
$\lambda_{ac,2}$	0.2841	0.2841	0.2841	0.2841
λ_{c1} (kW^{-1})	2.6E-3	1.28E-3	8.17E-4	2.23E-4
λ_{c2} (kW^{-1})	8.72E-5	4.36E-5	2.78E-5	7.58E-6
λ_{c3}	0.234	0.234	0.234	0.234
λ_{c4}	10.6	21.1	33.1	121
λ_{c5}	-11.0	-22.1	-34.6	-127
λ_{d1} (kW^{-1})	4.8E-3	2.38E-3	1.5E-3	4.14E-4
$\lambda_{m,fix}$ (kW)	0.37	0.74	1.16	4.22
$\lambda_{m,var}$	1.45	1.45	1.45	1.45
$\lambda_{vent,1}$ ($kW\text{-}s^2/m^6$)	0.0727	0.0436	0.0291	0.0075
$\lambda_{vent,2}$ ($kW\text{-}s/m^2$)	0.1382	0.1382	0.1382	0.1382
Γ_b(kW^{-1})	0.014	0.007	0.0045	0.0012
A_b (m^2)	8.8	14.0	18.9	45.0
$E_{b,max}$ (kWh)	150	300	470	1725
$F_{m,fix}$ (kW)	1.2	2.4	3.8	13.7
$F_{m,var}$	3.2	3.2	3.2	3.2
q_{vent}^{up} (m^3/s)	15	25	37.5	145
Q_{ac}^{rated} (kW)	123	229	352	1,320
M_b (kJ/K)	8,100	16,200	25,380	93,150
N_m	3	3	3	3
P_m^{lo} (kW)	0.35	0.75	1.1	5.75
P_m^{up} (kW)	3.5	7	11	57.5
Q_n^{up} (kW)	122.5	225	350	700
Q_r^{up} (kW)	10	20	31	115

CHAPTER 7

Conclusion and Future Directions

7.1 Conclusions

The research presented in this thesis tackles several challenges related to the integration of distributed power production into the current infrastructure. Process Systems Engineering techniques are used to address these challenges in a systematic manner.

In Chapters 2 and 3, mixed integer linear optimization is used to address optimal microgrid design and technology selection. These chapters present a general formulation for this design optimization and then show how it can be used as a valuable tool for analysis simply by slightly changing constraints or input data. In Chapter 2 this is used to compare the impact of different policy scenarios on the optimal design. The results show that adoption of distributed renewables is best enabled by reducing their cost (i.e. either instantaneously via tax incentives or over the long term by investing in research and development). It is also shown that achieving 20-40% autonomy via cogeneration units is a relatively low-regret microgrid design choice. In essence, the performance of this microgrid design is not unduly impacted by potential policy changes, and this system design can be retrofitted later with added renewables capacity in order to further reduce environmental impact or in response to a drop in their price.

In Chapter 3, optimization is used to explore the impact of geographic location and load shape on microgrid design. The results further support the widespread value of a microgrid design based primarily on a combination of local cogeneration and import of power from the macrogrid. Results from both Chapters 2 and 3 indicate that relying solely on local power generation is undesirable/expensive except in a few niche cases. The results from Chapter 3 are further used to develop a surrogate model which is used to identify underlying trends and provide quantitative predictions of key design metrics.

Chapters 4, 5, and 6 explore the use of Economic Model Predictive Control to enable microgrids to interact with the existing electrical infrastructure in a non-disruptive manner. In Chapter 4, a novel market structure is proposed which explicitly requires this non-disruptive interaction. Then, an EMPC formulation is derived based on chance constrained optimization for scheduling of an electric-only microgrid. The level of regulatory compliance is shown to be very high: commitment violations occur $\leq 1\%$ of the time. In addition, annual peak loads are reduced by up to 30%, and the hour-to-hour variability in the residual load can be explicitly controlled by a selection of tunable market parameters. However, enabling this load shaping increased the microgrid operating cost by 20-45% due to lower fuel efficiency, renewable curtailment, and the cost of utilizing battery storage.

In Chapter 5 and 6 this cost of load shaping is addressed by returning to a microgrid system which supplies both power and some form of thermal energy (i.e. space cooling in Chapter 5 and both space cooling and space heating in Chapter 6). A hierarchical supervisory control structure is formulated in Chapter 5 which considers the building thermal dynamics and decision making at multiple time scales. This supervisory controller is able to simultaneously regulate energy exchange with the utility company and ensure comfortable indoor air temperature. In Chapter 6 this approach is extended to consider other seasons and load shapes. By coupling power supply and building temperature management, load shaping can be carried out with as little as $10 - 15\%$ increase in cost, and the curtailment of available renewable power is essentially eliminated. This small increase in operating cost could be offset by changes in the electricity tariffs since these microgrids are now behaving as almost ideal customers.

The research presented in this thesis shows how the techniques from Process Systems Engineering can be used to identify and address issues related to distributed power

integration. However, there still several open questions and future directions that require further investigation.

7.2 Future Directions

7.2.1 Operation of Non-Commercial Systems

The microgrid operation work presented in Chapters 5 and 6 relied on utilizing flexible heating and cooling loads in order to mitigate the stochasticity inherent in energy demands and renewable availability. The case studies presented focused on commercial buildings because these building types typically have well-defined environmental regulation goals (i.e. to ensure a comfortable working environment). In certain cases, there may even be legal obligations or specifications in a lease that explicitly define allowable temperature. Moreover, heating and cooling is typically achieved via a forced ventilation system.

Residential buildings, on the other hand, do not have such strict requirements on environmental conditions, and occupants are more likely to use alternative methods (e.g. opening a window) to regulate air temperature. However, residential loads have other sources of flexible demand that are insignificant or not present in many commercial buildings. For example, water heating and refrigeration can be significant sources of electricity demand that are ubiquitously present throughout the year and shiftable (as long as appropriate temperatures are maintained) [129]. In addition, emerging technologies, such as schedulable smart appliances and plug-in vehicles, offer new opportunities for flexible loads. These could also be supplemented by active measures; for example, a text notification could be sent to customers in danger of incurring commitment violations so they have an opportunity to turn off lights and appliances. For residential microgrids, this combination of alternative flexible loads and active measures could be used to meet the load shaping regulations of the proposed market/regulatory structure like HVAC loads were used for commercial microgrids.

Microgrids could also be coupled with small-scale distributed chemicals and/or fuels production systems. These chemical processes can enable system flexibility by taking advantage of low-cost liquid storage vessels. Thus, some combination of traditional electrical storage (e.g. batteries) and inherent process flexibility could be used to comply

with the load shaping regulations of the proposed market structure. Further process integration could also be achieved by allowing conversion of chemicals/fuels back into electricity (e.g. via a fuel cell) in an emergency. Some preliminary work on this idea of distributed generation of power, fuels, and chemicals can be found in [130].

A study of the extension of the proposed scheduling and supervisory control to these other cases would further improve our understanding of how end users can effectively mitigate the disruptive impact of on-site distributed generation, and it would provide valuable insights about what mix of active and passive measures are useful for achieving these goals.

7.2.2 Development of Rich Simulation Testbed

As part of the work in Chapters 5 and 6, a dynamic microgrid model was developed in Simulink. The Simulink file was made available on the internet to facilitate reproduction and further research efforts. This work could be extended to incorporate a much larger library of DER units for use in dynamic simulation studies. In particular, the models developed focused on capturing dynamic phenomena on the time-scale of seconds or more. Thus, they are useful for similar studies on the scheduling, supervisory control, and energy production coordination of a microgrid.

Furthering developing an open-source modeling library and simulation platform for microgrids is useful as many current works in literature do not study the implementation of the proposed central/supervisory control in a continuous-time system. In doing so, one risks overestimating the performance because they do not have effects from plant-model mismatch or degradation in performance due to the discrete sampling time of the central controller. Thus, a virtual library of high fidelity DER models in an appropriate simulation testbed would be useful to the research community at large as it would allow for more accurate analysis of performance, easier reproduction by other authors, and easier comparison among studies carried out in a consistent framework.

7.2.3 On-Line Model Identification

Unit models for individual DER units are necessary for the Model Predictive Control framework used in Chapters 4, 5, and 6. Researchers are able to develop these unit

models based on open-loop simulation of high-fidelity dyanmic models, teting of experimental equipment, or first-principles arguments. In reality, microgrid operators will need to develop such models for their own individual DER units. This task is complicated because the majority of end users may not possess the necessary technical skills to perform the model identification themselves. Manufacturers are not fully able to address this need either since there will be inevitable variances between the performance of individual units based on imperfections in manufacturing, aging, and local environmental conditions.

On-line model identification at the supervisory layer could be used to identify these models during closed loop operations. Because the dispatch of the various units is inherently dynamic (i.e. due to varying energy demands and renewable availability), there may be sufficient excitation present in closed loop operation of a microgrid system to enable automated model identification. This could be supplemented by limited model identification experiments as needed. Developing a methodology to perform this model identification during closed-loop operations would enable any consumer to utilize this sophisticated MPC framework for microgrid operations without a deep level of technical expertise. Moreover, the supervisory layer could continue to refine the unit models over time to adapt to changing conditions (e.g. changes in the performance of an individual unit due to aging/wear).

7.2.4 Integration of Design and Non-Disruptive Operations

The microgrid design and technology selection research presented in Chapters 2 and 3 used modeling assumptions based on how microgrids and distributed generation are currently treated in marketplace. However, it would valuable to revisit this design problem in light of the proposed market/regulator structure and results from Chapters 4, 5, and 6. With the knowledge gained from these studies, one could analyze microgrid design not only with the nominal energy supply cost in mind, but also seeking to enable future operational flexibility so that load shaping is easily achievable. In particular, based on the results form Chapters 5 and 6, it would be interesting to consider the co-design of a microgrid, building layout, and building environmental controls with the thought of combined control of microgrid units and the HVAC system in mind. Obviously, this does not make sense for existing buildings which are considering investing

in microgrids, but could provide interesting insights about future directions for low-carbon intesity neighborhoods or districts.

A study on the design of microgrids for economic performance and non-disruptive operations would further improve the understanding of the strengths and weaknesses of various DER technologies, and could provide new insights about synergies that can be developed between these technologies. At a fundamental level these answers are of interest even if the proposed market structure is never widely implemented. For example, this underlying concept of intentionally building flexibility into the system design would enable microgrid energy systems to more effectively participate in a dynamic market environment (e.g. with real-time electricity prices), or could enable microgrids to offer more ancillary services (such as interruptible load capacity) to the power market.

7.2.5 Quantification of Operational Benefits to Utilities

The results presented in Chapters 4, 5, and 6 show that by tapping into the inherent flexibility of energy loads (i.e. HVAC loads were considered) end users can incorporate deep penetrations of on-site renewables while simultaneously reducing residual load variability and uncertainty. However, the analysis was done entirely from the end-user perspective. Thus, the results presented some quantitative properties of the residual load, but could not offer a financial analysis of what impact this has on the utility company operating cost. A study in this respect is ultimately needed to definitively quantify the economic benefits of this load shaping for utility companies. Moreover, this study could investigate how best to incorporate the information provided by microgrid operators (i.e. their energy exchange commitments) into the scheduling and control decisions of the utility company. This study can also be extended to compare different market structures for microgrids to identify the benefits and challenges each has in terms of utility operations.

7.2.6 Applications to Utility Expansion Planning

Another problem that Process Systems Engineering can be used to address is the long-term expansion planning of the utility/macrogrid infrastructure with regards to uncertainties in distributed generation adoption. These expansion activities (e.g. the

permitting and construction of traditional power plant) have long lead times and high investment costs. Obviously the task of economically making investments and ensuring the future reliability of the macrogrid becomes particularly challenging due to uncertainties in how much distributed generation will be adopted and how it will impact the day-to-day operations of the larger power system. A study on how stochastic formulations from the PSE field can be used to help address this problem would be useful. In particular, this study could also yield information about how changing the roles and responsibilities of microgrid users (e.g. by changing market structures) can either help to mitigate or exacerbate investment risks associated with this expansion planning problem.

Bibliography

[1] P. Wilkinson, K. R. Smith, S. Beevers, C. Tonne, and T. Oreszczyn, "Energy, energy efficiency, and the built environment," *Lancet*, vol. 370, no. 9593, pp. 1175–1187, 2007.

[2] N. Apergis and J. E. Payne, "A dynamic panel study of economic development and the electricity consumption-growth nexus," *Energy Economics*, vol. 33, no. 5, pp. 770–781, 2011.

[3] "The Quadrennial Technology Review," tech. rep., US Department of Energy, 2015.

[4] "Failure to Act: Closing the Infrastructure Investment Gap for Americas Economic Future," tech. rep., American Society of Civil Engineers, 2016.

[5] "Quadrennial Energy Review: Second Installment," tech. rep., US Department of Energy, 2017.

[6] "Energy Roadmap 2050." European Commission, 2011.

[7] "Annual energy outlook 2017: with projections to 2050," tech. rep., US Energy Information Administration, 2017.

[8] American Society of Civil Engineers, "2017 Infrastructure Report Card." Available from `http://www.infrastructurereportcard.org/wp-content/uploads/2017/01/Energy-Final.pdf`. Accessed on 31 March 2017.

[9] "Actual and planned transmission investment by investor-owned utilities (2009 – 2018)." Edison Electric Institute, 2015.

[10] "Ten-year network development plan 2016." European Network of Transmission System Operators for Electricity, 2016.

[11] "The smart grid: An introduction," tech. rep., US Department of Energy, 2008.

[12] H. Farhangi, "The path of the smart grid," *IEEE Power and Energy Magazine*, vol. 8, no. 1, 2010.

[13] California ISO, "What the duck curve tells us about managing a green grid." Available from `https://www.caiso.com/Documents/FlexibleResourcesHelpRenewables_FastFacts.pdf`. Accessed on 31 March 2017.

[14] M. Zachar, M. Trifkovic, and P. Daoutidis, "Policy effects on microgrid economics, technology selection, and environmental impact," *Computers and Chemical Engineering*, vol. 84, pp. 364–375, 2015.

[15] M. Zachar and P. Daoutidis, "Understanding and predicting the impact of location and load on microgrid design," *Energy*, vol. 90, pp. 1005–1023, 2015.

[16] M. Zachar and P. Daoutidis, "Microgrid/macrogrid energy exchange: A novel market structure and stochastic scheduling," *IEEE Transactions on Smart Grid*, vol. 8, no. 1, pp. 178–189, 2017.

[17] G. Pepermans, J. Driesen, D. Haeseldonckx, R. Belmans, and W. D'haeseleer, "Distributed generation: definition, benefits and issues," *Energy Policy*, vol. 33, no. 6, pp. 787–798, 2005.

[18] R. H. Lasseter, "Microgrids and distributed generation," *Journal of Energy Engineering*, vol. 133, no. 3, pp. 144–149, 2007.

[19] R. Lasseter, A. Akhil, C. Marnay, J. Stephens, J. Dagle, R. Guttromson, A. Meliopoulous, R. Yinger, and J. Eto, "The CERTS microgrid concept," tech. rep., Consortium for Electric Reliability Technology Solutions, 2002.

[20] M. Deshmukh and S. Deshmukh, "Modeling of hybrid renewable energy systems," *Renewable and Sustainable Energy Reviews*, vol. 12, no. 1, pp. 235–249, 2008.

[21] M. A. Delucchi and M. Z. Jacobson, "Providing all global energy with wind, water, and solar power, part II: Reliability, system and transmission costs, and policies," *Energy Policy*, vol. 39, no. 3, pp. 1170–1190, 2011.

[22] P. Dondi, D. Bayoumi, C. Haederli, D. Julian, and M. Suter, "Network integration of distributed power generation," *Journal of Power Sources*, vol. 106, no. 1-2, pp. 1–9, 2002.

[23] O. Hafez and K. Bhattacharya, "Optimal planning and design of a renewable energy based supply system for microgrids," *Renewable Energy*, vol. 45, pp. 7–15, 2012.

[24] A. Hawkes and M. Leach, "Modelling high level system design and unit commitment for a microgrid," *Applied Energy*, vol. 86, no. 7-8, pp. 1253–1265, 2009.

[25] A. Kashefi Kaviani, G. Riahy, and S. Kouhsari, "Optimal design of a reliable hydrogen-based stand-alone wind/PV generating system, considering component outages," *Renewable Energy*, vol. 34, no. 11, pp. 2380–2390, 2009.

[26] A. S. Siddiqui, C. Marnay, J. L. Edwards, R. Firestone, S. Ghosh, and M. Stadler, "Effects of carbon tax on microgrid combined heat and power adoption," *Journal of Energy Engineering*, vol. 131, no. 1, pp. 2–25, 2005.

[27] E. Mehleri, H. Sarimveis, N. Markatos, and L. Papageorgiou, "Optimal design and operation of distributed energy systems," in *Computer Aided Chemical Engineering*, vol. 29, pp. 1713–1717, 2011.

[28] R. Dufo-López and J. L. Bernal-Agustín, "Multi-objective design of PV-wind-diesel-hydrogen-battery systems," *Renewable Energy*, vol. 33, no. 12, pp. 2559–2572, 2008.

[29] R. Yokoyama and K. Ito, "Optimal operational planning method for cogeneration systems with thermal storage by the decomposition method," in *Transactions of the Japan Society of Mechanical Engineers Series C*, pp. 1817–1823, 1993.

[30] R. Yokoyama, K. Ito, and Y. Yuasa, "Multiobjective optimal unit sizing of hybrid power generation systems utilizing photovoltaic and wind energy," *Journal of Solar Energy Engineering*, vol. 116, pp. 167–173, 1994.

[31] W. Kellogg, M. Nehrir, G. Venkataramanan, and V. Gerez, "Generation unit sizing and cost analysis for stand-alone wind, photovoltaic, and hybrid wind/PV systems," *IEEE Transactions on Energy Conversion*, vol. 13, no. 1, pp. 70–75, 1998.

[32] R. Chedid and Y. Saliba, "Optimization and control of autonomous renewable energy systems," *International Journal of Energy Research*, vol. 20, no. 7, pp. 609–624, 1996.

[33] P. Liu, E. N. Pistikopoulos, and Z. Li, "An energy systems engineering approach to the optimal design of energy systems in commercial buildings," *Energy Policy*, vol. 38, no. 8, pp. 4224 – 4231, 2010.

[34] H. Ren and W. Gao, "A MILP model for integrated plan and evaluation of distributed energy systems," *Applied Energy*, vol. 87, pp. 1001–1014, 2010.

[35] E. Koutroulis, D. Kolokotsa, A. Potirakis, and K. Kalaitzakis, "Methodology for optimal sizing of stand-alone photovoltaic/wind-generator systems using genetic algorithms," *Solar Energy*, vol. 80, pp. 1072–1088, 2006.

[36] H. Borhanazad, S. Mekhilef, V. G. Ganapathy, M. Modiri-Delshad, and A. Mirtaheri, "Optimization of micro-grid system using MOPSO," *Renewable Energy*, vol. 71, pp. 295 – 306, 2014.

[37] G. Dalton, D. Lockington, and T. Baldock, "Feasibility analysis of stand-alone renewable energy supply options for a large hotel," *Renewable Energy*, vol. 33, no. 7, pp. 1475–1490, 2008.

[38] Z. Zhou, J. Zhang, P. Liu, Z. Li, M. C. Georgiadis, and E. N. Pistikopoulos, "A two-stage stochastic programming model for the optimal design of distributed energy systems," *Applied Energy*, vol. 103, pp. 135–144, 2013.

[39] Y. Cai, G. Huang, Z. Yang, Q. Lin, and Q. Tan, "Community-scale renewable energy systems planning under uncertainty - an interval chance-constrained programming approach," *Renewable and Sustainable Energy Reviews*, vol. 13, no. 4, pp. 721–735, 2009.

[40] M. Rivarolo, A. Greco, and A. Massardo, "Thermo-economic optimization of the impact of renewable generators on poly-generation smart-grids including hot thermal storage," *Energy Conversion and Management*, vol. 65, pp. 75–83, 2013.

[41] M. L. Ferrari, M. Pascenti, A. Sorce, A. Traverso, and A. F. Massardo, "Real-time tool for management of smart polygeneration grids including thermal energy storage," *Applied Energy*, vol. 130, pp. 670–678, 2014.

[42] "Business Energy Investment Tax Credit." 26 USC §48, 2015.

[43] "The emissions gap report: are the Copenhagen Accord pledges sufficient to limit global warming to 2^oC or 1.5^oC? A preliminary assessment," tech. rep., United Nations Environment Programme, 2010.

[44] "2013 distributed wind market report," tech. rep., US Department of Energy, 2013.

[45] "Technology characterization - microturbines," tech. rep., US Environmental Protection Agency, 2015.

[46] J. C. Ho, K. J. Chua, and S. K. Chou, "Performance study of a microturbine system for cogeneration application," *Renewable Energy*, vol. 29, no. 7, pp. 1121–1133, 2004.

[47] H. Yang, W. Zhou, L. Lu, and Z. Fang, "Optimal sizing method for stand-alone hybrid solarwind system with LPSP technology by using genetic algorithm," *Solar Energy*, vol. 82, no. 4, pp. 354–367, 2008.

[48] I. Hadjipaschalis, A. Poullikkas, and V. Efthimiou, "Overview of current and future energy storage technologies for electric power applications," *Renewable and Sustainable Energy Reviews*, vol. 13, no. 6-7, pp. 1513–1522, 2009.

[49] "WMO greenhouse gas bulletin: the state of greenhouse gases in the atmosphere based on global observations through 2012," tech. rep., World Meterological Organization, Atmospheric Environment Research Division, 2013.

[50] US Energy Information Administration, "Electric power monthly (March 2013)." Available from: https://www.eia.gov/electricity/monthly/.

[51] "Clean Energy Act 2011." Act No. 131, Paliament of the Commonwealth of Australia, 2011.

[52] "Climate Protection Act." S. 332, 133th U.S. Congress, 1st Sess, 2013.

[53] "Pathways to deep decarbonization: interm 2014 report," tech. rep., The Deep Decarbonization Pathways Project, 2014.

[54] "Annual energy outlook 2014: with projections to 2040," tech. rep., US Energy Information Administration, 2014.

[55] S. Yoshida, K. Ito, and R. Yokoyama, "Sensitivity analysis in structure optimization of energy supply systems for a hospital," *Energy Conversion and Management*, vol. 48, no. 11, pp. 2836–2843, 2007.

[56] W. Jiang-Jiang, Z. Chun-Fa, and J. You-Yin, "Multi-criteria analysis of combined cooling, heating and power systems in different climate zones in China," *Applied Energy*, vol. 87, no. 4, pp. 1247 – 1259, 2010.

[57] H. Ren, W. Zhou, and W. Gao, "Optimal option of distributed energy systems for building complexes in different climate zones in china," *Applied Energy*, vol. 91, no. 1, pp. 156–165, 2012.

[58] S. Wilcox and W. Marion, *Users manual for TMY3 data sets*. National Renewable Energy Laboratory Golden, CO, 2008.

[59] Capstone Microturbine Co., "Product catalog." Available from: http://www.capstoneturbine.com, 2010.

[60] G. Tamizhmani, L. Ji, Y. Tang, L. Petacci, and C. Osterwald, "Photovoltaic module thermal/wind performance: long-term monitoring and model development for energy rating," in *NCPV and Solar Program Review Meeting*, pp. 936–939, 2003.

[61] D. Feldman, G. Barbose, R. Margolis, R. Wiser, N. Darghouth, and A. Goodrich, "Photovoltaic (PV) Pricing Trends: Historical, Recent, and Near-Term Projections," tech. rep., US Department of Energy, 2012.

[62] D. J. MacKay, *Bayesian methods for adaptive models*. PhD thesis, California Institute of Technology, 1992.

[63] National Renewable Energy Lab, "Homer - the micropower optimization model." Available from: http://www.homerenergy.com/HOMER_legacy.html.

[64] Natural Resources Canada, "Retscreen." Available from: http://www.retscreen.net.

[65] "Annual energy outlook 2016," tech. rep., US Energy Information Administration, Washington, DC, USA, 2016.

[66] A. A. Bayod-Rújula, "Future development of the electricity systems with distributed generation," *Energy*, vol. 34, no. 3, pp. 377–383, 2009.

[67] N. Troy, E. Denny, and M. O'Malley, "Base-load cycling on a system with significant wind penetration," *IEEE Transactions on Power Systems*, vol. 25, no. 2, pp. 1088–1097, 2010.

[68] A. S. Brouwer, M. van den Broek, A. Seebregts, and A. Faaij, "Impacts of large-scale intermittent renewable energy sources on electricity systems, and how these can be modeled," *Renewable and Sustainable Energy Reviews*, vol. 33, pp. 443–466, 2014.

[69] A. S. Brouwer, M. van den Broek, A. Seebregts, and A. Faaij, "Operational flexibility and economics of power plants in future low-carbon power systems," *Applied Energy*, vol. 156, pp. 107–128, 2015.

[70] J.-B. Rosenkranz, C. B. Martinez-Anido, and B.-M. Hodge, "Analyzing the impact of solar power on multi-hourly thermal generator ramping," in *2016 IEEE Green Technologies Conference (GreenTech)*, pp. 153–158, 2016.

[71] K. Kim, F. Yang, V. M. Zavala, and A. A. Chien, "Data centers as dispatchable loads to harness stranded power," *IEEE Transactions on Sustainable Energy*, vol. 8, no. 1, pp. 208–218, 2017.

[72] C. Zhao and Y. Guan, "Unified stochastic and robust unit commitment," *IEEE Transactions on Power Systems*, vol. 28, no. 3, pp. 3353–3361, 2013.

[73] H. Gangammanavar, S. Sen, and V. M. Zavala, "Stochastic optimization of subhourly economic dispatch with wind energy," *IEEE Transactions on Power Systems*, vol. 31, no. 2, pp. 949–959, 2016.

[74] A. J. Lamadrid and T. Mount, "Ancillary services in systems with high penetrations of renewable energy sources, the case of ramping," *Energy Economics*, vol. 34, no. 6, pp. 1959–1971, 2012.

[75] M. Soshinskaya, W. H. Crijns-Graus, J. M. Guerrero, and J. C. Vasquez, "Microgrids: Experiences, barriers and success factors," *Renewable and Sustainable Energy Reviews*, vol. 40, pp. 659–672, 2014.

[76] A. K. Basu, S. Chowdhury, S. Chowdhury, and S. Paul, "Microgrids: Energy management by strategic deployment of DERsa comprehensive survey," *Renewable and Sustainable Energy Reviews*, vol. 15, no. 9, pp. 4348–4356, 2011.

[77] G. Cardoso, M. Stadler, A. Siddiqui, C. Marnay, N. DeForest, A. Barbosa-Póvoa, and P. Ferrão, "Microgrid reliability modeling and battery scheduling using stochastic linear programming," *Electric Power Systems Research*, vol. 103, pp. 61–69, 2013.

[78] J. Silvente, G. M. Kopanos, and A. Espuña, "A rolling horizon stochastic programming framework for the energy supply and demand management in microgrids," in *Computer Aided Chemical Engineering*, vol. 37, pp. 2321–2326, 2015.

[79] M. Alipour, B. Mohammadi-Ivatloo, and K. Zare, "Stochastic scheduling of renewable and CHP-based microgrids," *IEEE Transactions on Industrial Informatics*, vol. 11, no. 5, pp. 1049–1058, 2015.

[80] Y. Zhang, N. Gatsis, and G. B. Giannakis, "Robust energy management for microgrids with high-penetration renewables," *IEEE Transactions on Sustainable Energy*, vol. 4, no. 4, pp. 944–953, 2013.

[81] D. T. Nguyen and L. B. Le, "Risk-constrained profit maximization for microgrid aggregators with demand response," *IEEE Transactions on Smart Grid*, vol. 6, no. 1, pp. 135–146, 2015.

[82] G. Liu, Y. Xu, and K. Tomsovic, "Bidding strategy for microgrid in day-ahead market based on hybrid stochastic/robust optimization," *IEEE Transactions on Smart Grid*, vol. 7, no. 1, pp. 227–237, 2016.

[83] Z. Yang, R. Wu, J. Yang, K. Long, and P. You, "Economical operation of microgrid with various devices via distributed optimization," *IEEE Transactions on Smart Grid*, vol. 7, no. 2, pp. 857–866, 2015.

[84] R. Wang, P. Wang, and G. Xiao, "A robust optimization approach for energy generation scheduling in microgrids," *Energy Conversion and Management*, vol. 106, pp. 597–607, 2015.

[85] P. Velarde, L. Valverde, J. Maestre, C. Ocampo-Martinez, and C. Bordons, "On the comparison of stochastic model predictive control strategies applied to a hydrogen-based microgrid," *Journal of Power Sources*, vol. 343, pp. 161–173, 2017.

[86] M. Trifkovic, M. Sheikhzadeh, K. Nigim, and P. Daoutidis, "Modeling and control of a renewable hybrid energy system with hydrogen storage," *IEEE Transactions on Control Systems Technology*, vol. 22, no. 1, pp. 169–179, 2014.

[87] S. A. Pourmousavi, M. H. Nehrir, C. M. Colson, and C. Wang, "Real-time energy management of a stand-alone hybrid wind-microturbine energy system using particle swarm optimization," *IEEE Transactions on Sustainable Energy*, vol. 1, no. 3, pp. 193–201, 2010.

[88] A. Sobu and G. Wu, "Dynamic optimal schedule management method for microgrid system considering forecast errors of renewable power generations," in *Proceedings of the 2012 IEEE International Conference on Power System Technology*, pp. 1–6, 2012.

[89] M. Trifkovic, W. A. Marvin, P. Daoutidis, and M. Sheikhzadeh, "Dynamic real-time optimization and control of a hybrid energy system," *AIChE Journal*, vol. 60, no. 7, pp. 2546–2556, 2014.

[90] R. Palma-Behnke, C. Benavides, F. Lanas, B. Severino, L. Reyes, J. Llanos, and D. Saez, "A microgrid energy management system based on the rolling horizon strategy," *IEEE Transactions on Smart Grid*, vol. 4, no. 2, pp. 996–1006, 2013.

[91] H. Morais, P. Kádár, P. Faria, Z. A. Vale, and H. Khodr, "Optimal scheduling of a renewable micro-grid in an isolated load area using mixed-integer linear programming," *Renewable Energy*, vol. 35, no. 1, pp. 151–156, 2010.

[92] A. M. Z. Alabedin, E. F. El-Saadany, and M. M. A. Salama, "Generation scheduling in microgrids under uncertainties in power generation," in *Proceedings of the IEEE Electrical Power and Energy Conference*, pp. 133–138, 2012.

[93] Z. Wang, B. Chen, J. Wang, and J. Kim, "Decentralized energy management system for networked microgrids in grid-connected and islanded modes," *IEEE Transactions on Smart Grid*, vol. 7, no. 2, pp. 1097–1105, 2015.

[94] M. Hosseinzadeh and F. R. Salmasi, "Robust optimal power management system for a hybrid AC/DC micro-grid," *IEEE Transactions on Sustainable Energy*, vol. 6, no. 3, pp. 675–687, 2015.

[95] Y. Riffonneau, S. Bacha, F. Barruel, and S. Ploix, "Optimal power flow management for grid connected PV systems with batteries," *IEEE Transactions on Sustainable Energy*, vol. 2, no. 3, pp. 309–320, 2011.

[96] G. M. Kopanos, M. C. Georgiadis, and E. N. Pistikopoulos, "Energy production planning of a network of micro combined heat and power generators," *Applied Energy*, vol. 102, pp. 1522–1534, 2013.

[97] J. Silvente, A. M. Aguirre, M. a. Zamarripa, C. a. Méndez, M. Graells, and A. Espuña, "Improved time representation model for the simultaneous energy supply and demand management in microgrids," *Energy*, vol. 87, pp. 615–627, 2015.

[98] A. G. Tsikalakis and N. D. Hatziargyriou, "Centralized control for optimizing microgrids operation," *IEEE Transactions on Energy Conversion*, vol. 23, pp. 241–248, 2008.

[99] L. Jiang and S. Low, "Real-time demand response with uncertain renewable energy in smart grid," in *49th Annual Allerton Conference on Communication, Control, and Computing*, pp. 1334–1341, 2011.

[100] B. Fanzeres, A. Street, and L. A. Barroso, "Contracting strategies for renewable generators: A hybrid stochastic and robust optimization approach," *IEEE Transactions on Power Systems*, vol. 30, no. 4, pp. 1825–1837, 2015.

[101] T. Logenthiran, D. Srinivasan, A. M. Khambadkone, and H. N. Aung, "Multiagent system for real-time operation of a microgrid in real-time digital simulator," *IEEE Transactions on Smart Grid*, vol. 3, no. 2, pp. 925–933, 2012.

[102] E. Kuznetsova, Y.-F. Li, C. Ruiz, and E. Zio, "An integrated framework of agent-based modelling and robust optimization for microgrid energy management," *Applied Energy*, vol. 129, pp. 70–88, 2014.

[103] I. Atzeni, L. G. Ordonez, G. Scutari, D. P. Palomar, and J. R. Fonollosa, "Noncooperative day-ahead bidding strategies for demand-side expected cost minimization with real-time adjustments: A GNEP approach," *IEEE Transactions on Signal Processing*, vol. 62, no. 9, pp. 2397–2412, 2014.

[104] R. Deng, Z. Yang, J. Chen, and M.-Y. Chow, "Load scheduling with price uncertainty and temporally-coupled constraints in smart grids," *IEEE Transactions on Power Systems*, vol. 29, no. 6, pp. 2823–2834, 2014.

[105] M. C. Caramanis, E. Goldis, P. A. Ruiz, and A. Rudkevich, "Power market reform in the presence of flexible schedulable distributed loads. new bid rules, equilibrium and tractability issues," in *2012 50th Annual Allerton Conference on Communication, Control, and Computing*, pp. 1089–1096, 2012.

[106] T. Wang, D. O'Neill, and H. Kamath, "Dynamic control and optimization of distributed energy resources in a microgrid," *IEEE Transactions on Smart Grid*, vol. 6, no. 6, pp. 2884–2894, 2015.

[107] H. Kim and M. Thottan, "A two-stage market model for microgrid power transactions via aggregators," *Bell Labs Technical Journal*, vol. 16, no. 3, pp. 101–107, 2011.

[108] K. Nolde and M. Morari, "Electrical load tracking scheduling of a steel plant," *Computers & Chemical Engineering*, vol. 34, no. 11, pp. 1899–1903, 2010.

[109] R. Bo and F. Li, "Probabilistic LMP forecasting considering load uncertainty," *IEEE Transactions on Power Systems*, vol. 24, no. 3, pp. 1279–1289, 2009.

[110] H.-T. Yang, C.-M. Huang, Y.-C. Huang, and Y.-S. Pai, "A weather-based hybrid method for 1-day ahead hourly forecasting of PV power output," *IEEE Transactions on Sustainable Energy*, vol. 5, no. 3, pp. 917–926, 2014.

[111] J. Llanos, D. Saez, R. Palma-Behnke, A. Nunez, and G. Jimenez-Estevez, "Load profile generator and load forecasting for a renewable based microgrid using self organizing maps and neural networks," in *The 2012 International Joint Conference on Neural Networks*, 2012.

[112] L. A. Fernandez-Jimenez, A. Muñoz-Jimenez, A. Falces, M. Mendoza-Villena, E. Garcia-Garrido, P. M. Lara-Santillan, E. Zorzano-Alba, and P. J. Zorzano-Santamaria, "Short-term power forecasting system for photovoltaic plants," *Renewable Energy*, vol. 44, pp. 311–317, 2012.

[113] C. R. Touretzky and M. Baldea, "Nonlinear model reduction and model predictive control of residential buildings with energy recovery," *Journal of Process Control*, vol. 24, no. 6, pp. 723–739, 2014.

[114] Y. Ma, J. Matusko, and F. Borrelli, "Stochastic model predictive control for building HVAC systems: Complexity and conservatism," *IEEE Transactions on Control Systems Technology*, vol. 23, no. 1, pp. 101–116, 2015.

[115] J. Silvente, G. M. Kopanos, E. N. Pistikopoulos, and A. Espuña, "A rolling horizon optimization framework for the simultaneous energy supply and demand planning in microgrids," *Applied Energy*, vol. 155, pp. 485–501, 2015.

[116] D. Zhang, N. Shah, and L. G. Papageorgiou, "Efficient energy consumption and operation management in a smart building with microgrid," *Energy Conversion and Management*, vol. 74, pp. 209–222, 2013.

[117] A. Parisio, E. Rikos, and L. Glielmo, "Stochastic model predictive control for economic/environmental operation management of microgrids: An experimental case study," *Journal of Process Control*, vol. 43, pp. 24–37, 2016.

[118] W. Qi, J. Liu, and P. D. Christofides, "A distributed control framework for smart grid development: Energy/water system optimal operation and electric grid integration," *Journal of Process Control*, vol. 21, no. 10, pp. 1504–1516, 2011.

[119] M. Alipour, K. Zare, and B. Mohammadi-Ivatloo, "Short-term scheduling of combined heat and power generation units in the presence of demand response programs," *Energy*, vol. 71, pp. 289–301, 2014.

[120] Y. Zhang, T. Zhang, R. Wang, Y. Liu, and B. Guo, "Optimal operation of a smart residential microgrid based on model predictive control by considering uncertainties and storage impacts," *Solar Energy*, vol. 122, pp. 1052–1065, 2015.

[121] Y. Guo, J. Xiong, S. Xu, and W. Su, "Two-stage economic operation of microgrid-like electric vehicle parking deck," *IEEE Transactions on Smart Grid*, vol. 7, no. 3, pp. 1703–1712, 2016.

[122] "ANSI/ASHRAE standard 62.1-2007," *American Society of Heating, Refrigerating and Air-Conditioning Engineers, Inc., Atlanta, GA*, 2007.

[123] F. A. Mohamed, *Microgrid Modelling and Online Management.* PhD thesis, Helsinki University of Technology, 2008.

[124] S. Liu and R. Dougal, "Dynamic multiphysics model for solar array," *IEEE Transactions on Energy Conversion*, vol. 17, no. 2, pp. 285–294, 2002.

[125] M. Ceraolo, "New dynamical models of lead-acid batteries," *IEEE Transactions on Power Systems*, vol. 15, no. 4, pp. 1184–1190, 2000.

[126] S. Wilcox and W. Marion, *Users manual for TMY3 data sets*. National Renewable Energy Laboratory Golden, CO, 2008.

[127] "Commercial Buildings Energy Consumption Survey." US Energy Information Administration, 2012.

[128] "U.S. Department of Energy Commercial Reference Buildings of the National Building Stock," tech. rep., US Department of Energy, 2011.

[129] "Residential Energy Consumption Survey." US Energy Information Administration, 2015.

[130] A. Allman, M. Zachar, and P. Daoutidis, "Distributed chemicals and electricity production with regulated energy exchange," in *Proceedings of Foundations of Computer-Automated Process Operations/Chemical Process Control 2017*, 2017.

APPENDIX A

Glossary and Acronyms

A.1 Glossary

- **Curtailable** – A load or generation term which can be reduced if desired.
- **Distributed Energy Resource** – A process unit which provides distributed generation or distributed storage.
- **Distributed Generation** – The generation of power using small scale units close to the point of ultimate consumption (typically on-site).
- **Distributed Storage** – The storage of energy using small scale units close to the point of ultimate consumption (typically on-site).
- **Dispatchable** – A process unit which can up and down regulated at will.
- **Insolation** – The solar irradiance on a surface (i.e. the name comes from incident solar radiation)
- **Load Factor** – The ratio of the peak power demand to the average power demand.
- **Load Shape** – The profile of energy demand over time.

- **Macrogrid** – The large, interconnected network of power plants, power transmission and distribution infrastructure, and customers. This system spans wide geographic regions (e.g. multiple U.S. states) and consists of many independent parties (e.g. generation companies, system operators, etc.).
- **Microgrid** – A small power system which uses distributed generation and storage units to supply local energy demands.
- **Prosumer** – An end user who both produces and consumes electricity.
- **Residual Load** – The demand of a microgrid customer that is supplied by the utility company rather than via local generation. Note that this residual load can be negative, which indicates the utility is absorbing/buying excess power from the microgrid.
- **Schedule Adaptability** – The maximum hour-to-hour difference between energy exchange commitments in the proposed market structure used in Chapters 4, 5, and 6.
- **Schedule Elasticity** – The maximum difference between the energy exchange commitment and realized energy exchange before fines are incurred in the proposed market structure used in Chapters 4, 5, and 6.

A.2 Acronyms

Table A.1: Acronyms

Acronym	Meaning
A/C	Air Conditioning
ANN	Artificial Neural Network
CCHP	Combined Cooling, Heat, and Power
CHP	Combined Heat and Power
CV	Coefficient of Variation
DER	Distributed Energy Resource (i.e. distributed generation/storage unit)

Continued on next page

Table A.1 – continued from previous page

Acronym	Meaning
DG	Distributed Generation
E-MPC	Economic Model Predictive Control
GAMS	Generic Algebraic Modeling System (an optimization software)
GHG	Greenhouse Gas
HVAC	Heating, Ventilation, and Air Conditioning
MILP	Mixed Integer Linear Program
MIQCP	Mixed Integer Quadratically Constrained Program
MPC	Model Predictive Control
NLP	Nonlinear Program
ODE	Ordinary Differential Equation
PMSG	Permanent Magnet Synchronous Generator
PV	Photovoltaics
R&D	Research and Development

A.3 Piecewise Linearization

Piecewise linearization is a method of approximating a continuous nonlinear function with a set of connected linear line segments. An example of this is shown in Fig. A.1.

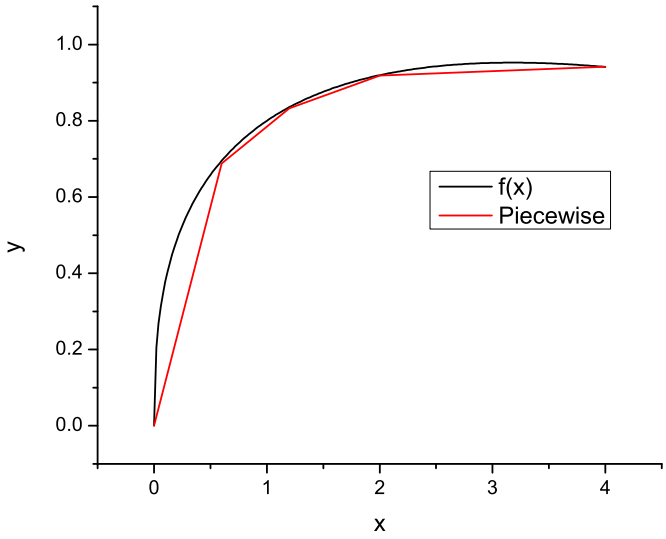

Figure A.1: Piecewise linear approximation for nonlinear function y=f(x)

In order to approximate a nonlinear function f(x), first define a set of points $\{(a_1, b_1)$, (a_2, b_2),... ,$(a_n, b_n)\}$ that lie on f(x):

$$b_i = f(a_i) \qquad \forall i = 1, ..., n$$

Then, define a set of linear functions $\{g_1(x), g_2(x), ..., g_{i-1}(x)\}$:

$$g_i(x) = m_i x + c_i \qquad \forall i = 1, ..., n-1$$

where m_i and c_i are defined as:

$$m_i = \frac{b_{i+1} - b_i}{a_{i+1} - a_i} \qquad \forall i = 1, ..., n-1$$

$$c_i = \frac{a_{i+1}b_i - a_i b_{i+1}}{a_{i+1} - a_i} \qquad \forall i = 1, ..., n-1$$

This set of linear functions then has the properties that:

$$\begin{aligned} f(a_1) &= g_1(a_1) \\ f(a_i) = g_{i-1}(a_i) &= g_i(a_i) \qquad \forall i = 2, ..., n-1 \\ f(a_n) &= g_{n-1}(a_n) \end{aligned}$$

And we can define the piecewise linear approximation, $\tilde{f}(x)$ as:

$$\tilde{f}(x) = \begin{cases} g_1(x), & a_1 \leq x < a_2 \\ g_2(x), & a_2 \leq x < a_3 \\ \vdots & \vdots \\ g_i(x), & a_i \leq x < a_{i+1} \\ \vdots & \vdots \\ g_{n-1}(x), & a_{i-1} \leq x \leq a_n \end{cases}$$

This could be represented in a MILP format as:

$$\begin{aligned} & a_i z_i \leq x_i \leq a_{i+1} z_i && \forall i = 1, ..., n-1 \\ & x = \sum_{i=1}^{n-1} x_i \\ & \tilde{f} = \sum_{i=1}^{n-1} m_i x_i + \sum_{i=1}^{n-1} c_i y_i \\ & \sum_{i=1}^{n-1} z_i \leq 1 \\ & z_i \in \{0, 1\} && \forall i = 1, ..., n-1 \end{aligned}$$

Note that this formulation allows for $z_i = 0 \ \ \forall i$, which results in $x = 0$ and $\tilde{f} = 0$. This would be helpful for the sizing problem as it allows the system to not include a unit.